Seismic Response and Design of Steel Multi-Tiered Eccentrically Braced Frames

by

Abolfazl Ashrafi

A thesis submitted in partial fulfillment of the requirements for the degree of

Doctor of Philososphy

in

Structural Engineering

Department of Civil and Environmental Engineering

University of Alberta

Abstract

Multi-tiered braced frames are commonly used as the lateral load-resisting system of tall single-storey buildings or tall storeys of multi-storey buildings. This framing system divides the frame or storey height into multiple bracing panels, resulting in more economical member sizes and practical connections. Although multi-tiered concentrically braced frames are preferred in practice, multi-tiered eccentrically braced frames (MT-EBFs) offer an alternative solution in high seismic regions due to their high ductility, stable and reliable yielding mechanism, and architectural versatility. Despite extensive research studies conducted to examine the seismic response of and develop design requirements for multi-tiered concentrically braced frames, there is limited research on the seismic performance of steel MT-EBFs. Furthermore, there exist no special design requirements for MT-EBFs given that there are several concerns associated with the stability response of their unbraced intermediate links and columns. Due to the lack of background research, the current edition of the Canadian steel design standard, CSA S16-19, does not recognize MT-EBFs as ductile EBF. This Ph.D. research project aims to improve understanding of the behaviour of MT-EBFs under seismic loads and develop new analysis and design requirements to improve their seismic stability of MT-EBFs with emphasis on their link beams and columns.

A set of prototype MT-EBFs part of an industrial building is selected and used to perform a numerical parametric study by varying the frame height, tier height ratio, number of tiers, link lateral bracing condition, and flexural rigidity of the brace-to-beam connections. The frames are designed as per 2019 CSA S16 assuming shear yielding mechanism in their links. Nonlinear response history analyses are then performed to evaluate their global and local response and quantify seismic-induced demands in the intermediate beams, braces, and columns as well as inelastic link rotation. The continuum-based numerical model of a two-tiered EBF with continuous I-section links and three-

and four-tiered EBFs with continuous built-up tubular links are developed and used to further evaluate the seismic response of MT-EBFs taking into consideration out-of-plane and torsional response of the links and columns. The results of the dynamic analyses performed on the MT-EBFs not specifically designed for the multi-tier response confirm that intermediate links had a tendency to buckle out-of-plane because of the loss of stiffness after shear yielding and the absence of out-of-plane bracing, which results in appreciable out-of-plane flexural bending on the columns. Moreover, progressive yielding of the links until full plastic mechanism develops causes non-uniform distribution of inelastic lateral deformation along the frame height, where the largest inelastic deformation tends to occur in the tier with the largest design shear to shear strength ratio. This response imposes in-plane flexural bending in the columns. MT-EBF columns subjected to in-plane and out-of-plane bending together with a large axial compression force caused by gravity and seismic loads are prone to buckling. Seismic analysis and design requirements are developed for two-tiered EBFs with continuous wide-flange links, and three- and four-tiered EBFs with continuous built-up tubular link beams. The requirements for two-tiered frames make use of intermediate beams to limit out-of-plane deformation of diagonal braces, torsionally brace the link beam in the intermediate level using diagonal braces, take advantage of column flexural stiffness and strength to brace the intermediate beam out-of-plane, estimate and account for column in-plane bending demands, and limit the inelastic link rotation. The proposed guidelines for three- and four-tiered EBFs with continuous built-up tubular links involve requirements to laterally brace diagonal braces and intermediate beams, requirements to verify inelastic link rotation at each tier, and requirements to verify the strength and stability of columns under the combined axial force plus in-plane and out-of-plane flexural demands. Nonlinear dynamic analyses are conducted to validate the proposed requirements, which confirm that the improved MT-EBFs can better distribute the inelastic lateral

deformation between tiers, experience lower inelastic link rotations in their links, and undergo limited out-of-plane response in their intermediate beams. Furthermore, column in-plane and out-of-plane flexural demands are properly predicted by the proposed methods.

Preface

This Ph.D. thesis is an original work conducted by Abolfazl Ashrafi. This research was part of my collaboration with Dr. Ali Imanpour, the research supervisor at the University of Alberta. The following chapters have been previously published/ in preparation for publication based on this thesis:

Chapter 3 is based on the published paper titled **Ashrafi A., Imanpour A., "Seismic response of steel multi-tiered eccentrically braced frames,"** ***Journal of Construction Steel Research, 2021***.

Chapter 4 will be submitted as **Ashrafi A., Imanpour A.*, "Analysis and Design Methods for Two-Tiered Steel Eccentrically Braced Frames with Continuous Wide Flange Links,"*** to a journal with minor modifications.

Chapter 5 will be submitted as ***Ashrafi A., Imanpour A., "Seismic Analysis and Design of Three- and Four-Tiered Eccentrically Braced Frames,"*** to a journal with minor modifications.

Part of this study has been published and presented:

- Ashrafi A., Imanpour A., "Seismic Response of Steel Multi-Tiered Eccentrically Braced Frames," *12th Canadian Conference on Earthquake Engineering,* 2019.
- Ashrafi A., Imanpour A., "Analytical Assessment of the Seismic Performance of the Two-Tiered Eccentrically Braced Frames," *12th Pacific Structural Steel Conference,* 2019.

Acknowledgements

I would like to express my sincere gratitude to my supervisor, Dr. Ali Imanpour, for his invaluable guidance, support, and encouragement throughout my research project. I would also like to thank my friends and coworkers at the Steel Centre for their insightful comments and helpful discussions. Besides my supervisor, I would like to thank my supervisory committee members, Dr. Robert Driver, Dr. Douglas Tomlinson and Dr. Roger Cheng for their constructive feedback toward my research. I would also like to thank my Ph.D. defence examiners, Dr. Carlos 'Lobo' Cruz Noguez and Dr. Tony Yang.

I would like to extend my thanks to Dr. Poulad Daneshvar for his input in ground motion scaling, and Dr. Morteza Dehghani, Prof. Taichiro Okazaki of Hokkaido University, and Dr. Yasaman Balazadeh Minouei for sharing the test data. The inputs from Robert Tremblay, Mehrak Razavi, Brett Morgan, and Trevor Whitney are highly appreciated.

I would like to acknowledge the financial support provided by the Natural Science and Engineering Research Council of Canada (NSERC), the Canadian Institute of Steel Construction (2019 Kulak Scholarship), and the Department of Civil and Environmental Engineering at the University of Alberta. Without their funding, this research project would not have been possible.

Last but not least, I would also like to thank my partner, Parisa, and my family for their perpetual love and support, which helped me stay motivated and focused throughout this project.

Table of Contents

List of Tables

List of Figures

List of Symbols

A, A_g	Gross cross-sectional area
A_w	Shear area of the section
b_f	Width of flange
C_f	Axial compression demand
C_r	Design axial compressive strength
d	Depth of the section
e	The length of the link
E	Elastic modulus of steel
F_y	Yielidng stress of steel
G	Shear modulus of steel
h	Total frame height
h_i	Heigh of Tier i
I_E	Importance factor for seismic load calculation
K	effective length factor
L	Span length
L_{ob}	Outer beam length
M_{fx}	Column design out-of-plane moment demand

M_{fy} Column design in-plane moment demand

M_p Plastic moment of section

M_{px} Plastic moment of section about its strong-axis

M_{py} Plastic moment of section about its weak-axis

M_v Higher mode effect factor

R_d Ductility-related force modification factor

R_o Overstrength-related force modification factor

R_{sh} Strain hardening parameter

R_y Ratio of expected yield stress to nominal yield stress

T Fundamental period of the frame

t_f Thickness of the flange

t_w Thickness of the web (wide-flange sections)

V Design base shear

V_f Shear force in the link

V_p Unfactored shear strength of the section

V_r Factored shear strength of the link

w Web thickness (tubular sections)

Z Plastic modulus of the section

β Coefficient for bending in beam-columns

γ_i Tier i link rotation

$\emptyset$ Resistance factor

δ_i Tier i displacement

δ_e Elastic storey displacement

θ_i Tier i drift ratio

List of Abbreviations

AISC	Americal Institute of Steel Construction
ASTM	American Society for Testing and Materials
bc	Bottom column
br	Brace
CBF	Concentrically braced frame
CSA	Canadian Standards Association
DCF	Drift concentration factor
DCR	Demand-to-capacity ratio
EBF	Eccentrically braced frame
HSS	Hollow structural section
DOF	Degree-of-freedom
FEM	Finite Element Model
GPa	Gigapascal
kN	Kilonewton
LHS	Left-hand side
LTB	Lateral-torsional buckling
MPa	Megapasacal

MT-BF	Multi-tiered braced frame
MT-BRBF	Multi-tiered buckling-restraint frame
MT-CBF	Multi-tiered concentrically braced frame
MT-EBF	multi-tiered eccentrically braced frame
NBCC	National Building Code of Canada
NLRHA	Nonlinear response history analysis
ob	Outer beam
OpenSees	Open System for Earthquake Engineering Simulation
RHS	Right-hand side
tc	Top column
W-shape	Wide-flange section

Chapter 1. Introduction

1.1 Background

Steel eccentrically braced frames (EBFs) are commonly used as the lateral load-resisting system of building structures in high seismic areas. EBFs consist of vertical trusses attached with link beams, which are designed to dissipate seismic-input energy through yielding in shear, flexure, or a combination of both. This framing system combines the high ductility of moment-resisting frames (MRFs) and the high lateral stiffness of chevron concentrically braced frames (CBFs). Compared with their concentric counterparts, EBFs with interior links offer large openings and walkways through braced bays, resulting in more flexibility in the architectural design.

Tall single-storey steel buildings are extensively used in North America to house convention centres, sports facilities, warehouses, chemical plants, or industrial buildings. In such buildings, multi-tiered braced frames (MT-BFs) typically serve as the lateral load-resisting system, in which the frame height between the ground and roof levels is divided into multiple bracing panels (or tiers) because the application of a single braced panel with long and large braces is neither practical nor economical. Figure 1-1a shows a four-tiered concentrically braced frame example. In MT-BFs, shorter braces are used, resulting in a smaller cross-section; additionally, the column in-plane buckling length is reduced by intermediate struts that provide lateral bracing in the plane of the frame, permitting smaller column sections. Although multi-tiered concentrically braced frames (MT-CBFs) are often preferred in practice, multi-tiered eccentrically braced frames (MT-EBFs) can offer a viable solution in regions of high seismicity because of the high ductility and stable inelastic response of the yielding mechanism in their link beams. A schematic of a two-tiered EBF is shown in Figure 1-1b. MT-EBFs with continuous wide-flange beams have been used in the

retrofit of Richmond-San Rafael Bridge piers [1] and those with continuous built-up tubular sections have been used in the staircases of steel buildings in Vancouver, British Columbia [2].

In MT-EBFs, hollow structural sections (HSSs) or wide-flange (W-shape) sections are typically used as braces. If they are used in single-storey buildings, the columns are commonly selected from wide-flange sections and are preferably oriented so that out-of-plane bending due to wind acts about the section strong axis. Therefore, the full frame height is taken as the out-of-plane buckling length because the columns are not braced in the out-of-plane direction. However, they are assumed to be braced in the plane of the frame for the in-plane buckling mode.

Although multi-tiered and multi-storey EBFs have similar appearances, they differ in various aspects. In single-storey MT-EBFs, most of the structure's mass is concentrated at the roof level, creating a single-degree-of-freedom system, whereas multi-storey structures embody a multi-degrees-of-freedom system because the structural mass is distributed almost uniformly along the frame height. MT-EBF columns also lack out-of-plane bracing at intermediate tier levels, reducing their out-of-plane buckling capacity and amplifying second-order effects out-of-plane, which may result in column out-of-plane instability. Finally, out-of-plane bracing of intermediate links may not be easily and practically achieved because of the lack of floor diaphragms, which may negatively impact the stability of the intermediate links.

(a)

(b)

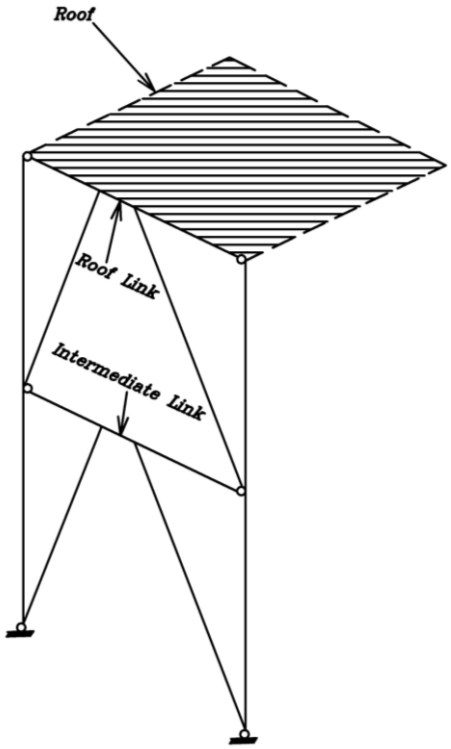

Figure 1-1. (a) Four-tiered concentrically braced frame in an industrial building; (b) Schematic of a two-tiered eccentrically braced frame.

North American steel design standards, including the Canadian steel design standard (CSA S16 [3]) and the United States (US) Seismic Provisions for Structural Steel Buildings (AISC 341 [4]), have special design provisions for the design of MT-CBFs under seismic loading; however, CSA S16-19 does not recognize MT-EBFs as a ductile eccentrically braced frame unless justified by rational analysis, and MT-EBFs are not addressed in 2022 Seismic Provisions for Structural Steel Buildings, AISC 341-22 [4]. The main reason for such provisions in Canada and the US is the lack of supporting research on the seismic response of MT-EBFs, in particular the stability response of intermediate links and columns and design methods addressing concerns with their seismic stability. Motivated by this need, this research seeks to establish an understanding of the seismic response of steel MT-EBFs through structural analysis methods, mechanics principles, and advanced numerical simulations, with an emphasis on the stability of links and columns.

Additionally, new design guidelines are proposed in the context of the Canadian design standard to improve the seismic stability response of such frames.

1.2 Problem Statement

A survey of past studies on eccentrically braced frames reveals that no research has been conducted on the seismic response of steel MT-EBFs. However, several concerns have been raised by the engineering community and code developers in Canada and US regarding their seismic behaviour, namely stability of intermediate links, stability of columns, and excessive inelastic deformation in the tier that yields first, which produces large inelastic link rotation.

1.2.1 Link Stability

Past research studies on the seismic response of EBFs with continuous I-shaped link beams [5–8] show that out-of-plane bracing is required at the ends of the link beam to prevent both lateral-torsional buckling (LTB) of the beam and out-of-plane displacement of brace end nodes. A small out-of-plane eccentricity in the compression-acting brace can produce considerable lateral and torsional demands in the EBF beam and trigger beam out-of-plane instability [9], given that the link undergoes a large inelastic deformation due to shear or flexural yielding. This response can be exacerbated by the loss of flexural stiffness because of plastic hinging of the link and fairly significant yielding in the outer beam adjacent to the link [7, 8]. Beam out-of-plane instability, if it develops, can prevent the frame from achieving the anticipated seismic response. To address these concerns, CSA S16 requires lateral out-of-plane bracing at both ends of the link in EBF structures as shown in Figure 1-2a. However, this requirement is not necessary for tubular link sections because of their inherent large torsional and out-of-plane stiffness. In multi-storey EBFs, lateral bracing can be achieved with the aid of floor slabs or secondary beams framing into the EBF bay (Figure 1-2a). However, such bracing may not be easily established for the intermediate

links of MT-EBFs, which can compromise the link stability condition (Figure 1-2b) and in turn, column stability. I-shape links without lateral support can experience excessive out-of-plane deformations because of the out-of-plane components of the brace or outer beam axial force, creating out-of-plane demands on the link beam.

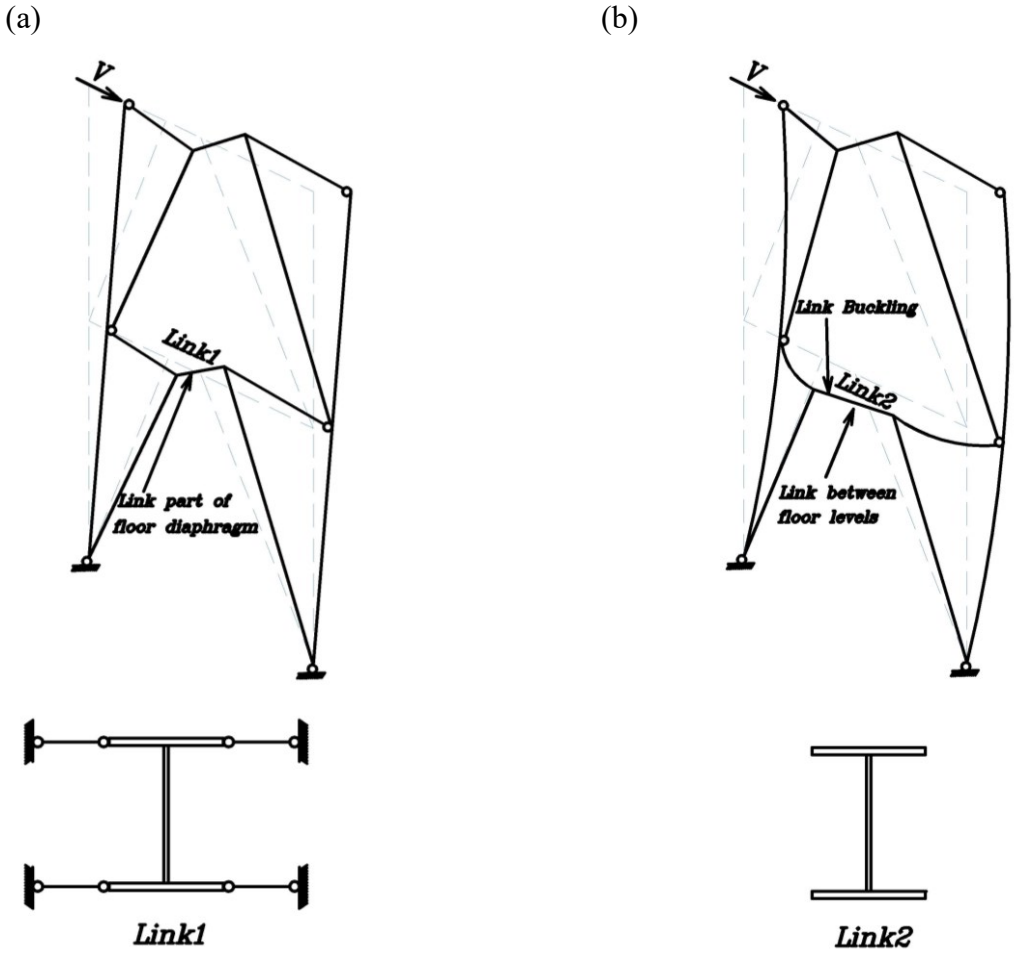

Figure 1-2. Anticipated lateral response of eccentrically braced frame (EBF) structures: (a) Two-storey EBF with links laterally braced; (b) Two-tiered EBF with intermediate link unbraced.

1.2.2 Column Stability and Demands

MT-EBF columns are subjected to an axial force in combination with in-plane and out-of-plane flexural bending. The axial force is induced by gravity loads and the tension or compression force developed by the inelastic response of links. Column in-plane moments are produced through a

delay in link yielding (i.e., progressive yielding) and/or link instability. The delay in link yielding is expected in MT-EBFs because of variations in the link material properties, geometry (length or area), boundary conditions, or demand-to-capacity ratios [10–18]. When link yielding develops in one of the tiers before others (e.g., Tier 1 in Figure 1-3a), lateral frame deformation tends to be distributed unevenly along the frame height, creating a kink in the column (Figure 1-3a), which translates to in-plane bending. The second source of column in-plane bending is the link out-of-plane instability, which reduces the stiffness of the link and, in turn, the respective tier; this results in non-uniform distribution of frame lateral deformation, which imposes in-plane flexural bending in the column segments adjacent to the tier where the link buckled (Figure 1-3b).

Column out-of-plane bending is induced by out-of-plane deformation in intermediate links lacking lateral supports and/or link out-of-plane instability. Because the columns lack out-of-plane support between the ground and roof levels, link out-of-plane deformation in the presence of out-of-plane initial geometric out-of-straightness can produce bending in the columns, as shown in Figure 1-4a. Although column axial forces are well understood and reflected in design standards, bending moment demands have not yet been quantified.

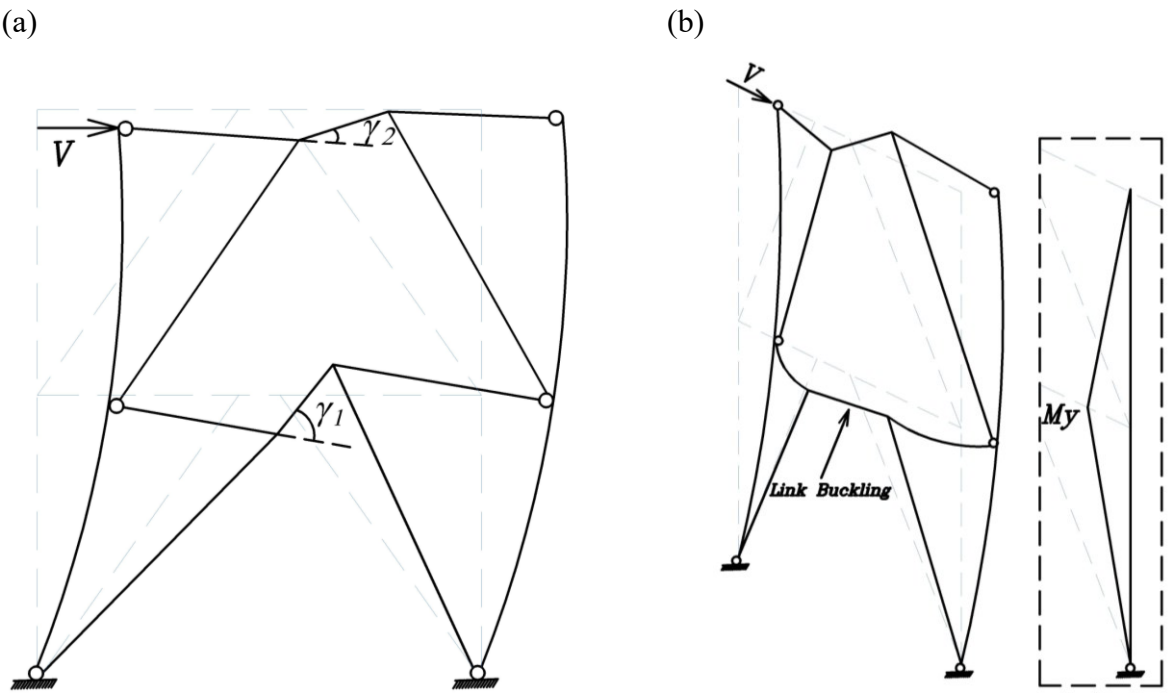

Figure 1-3. Anticipated lateral response of multi-tier eccentrically braced frames producing in-plane bending in the columns: (a) Non-uniform tier deformation; (b) Intermediate link out-of-plane buckling.

Excessive out-of-plane deformation of the link or out-of-plane buckling of the intermediate beam may result in large out-of-plane bending in the MT-EBF columns (Figure 1-4a) that lack out-of-plane lateral bracing between the base and roof levels. This out-of-plane bending combined with a large axial compression force and in-plane bending can lead to yielding of the column at the locations where the combined effects are the largest, e.g., intermediate beam level or mid-height of the first tier. Plastic hinge forming in the column can reduce flexural stiffness of the columns and eventually trigger in-plane or out-of-plane buckling (Figure 1-4b).

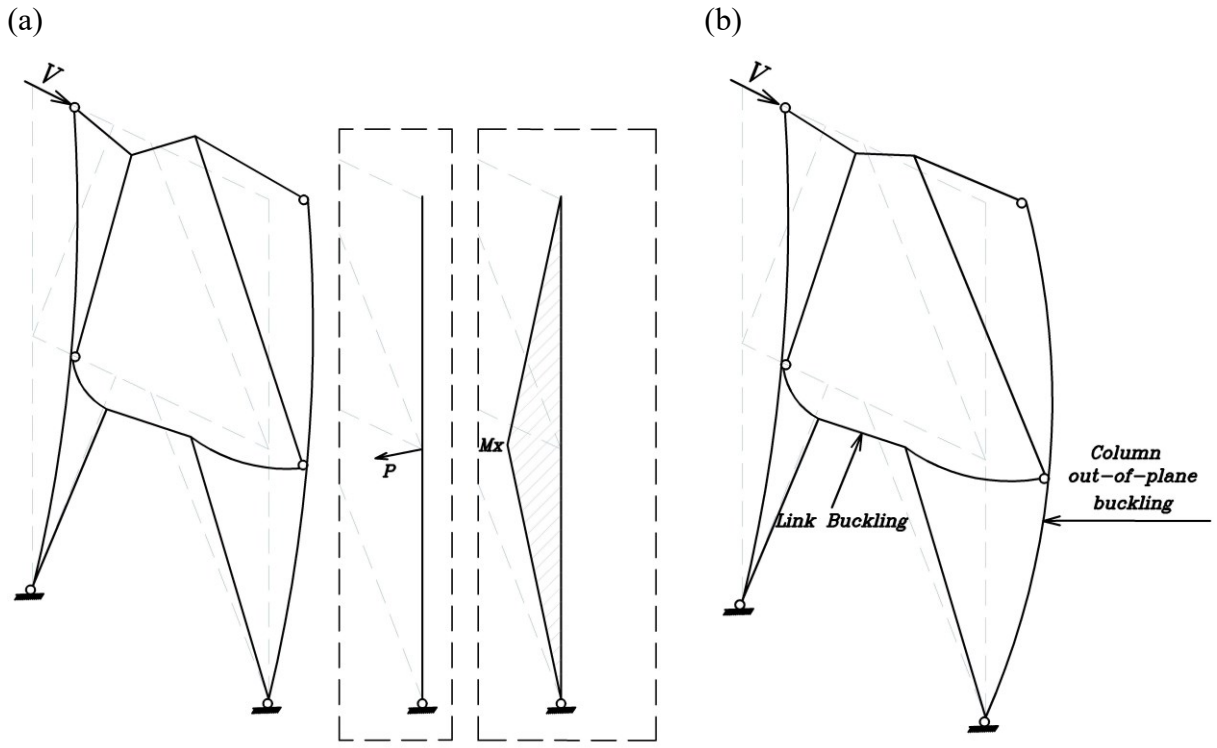

Figure 1-4. Anticipated lateral response of multi-tier eccentrically braced frames: (a) Column out-of-plane bending moment from link buckling; (b) Column out-of-plane buckling.

1.2.3 Excessive Inelastic Link Rotation

Progressive yielding of MT-EBF links, when the frame reaches full plastic mechanism, may create excessive inelastic rotation (e.g., > 0.08 rad in shear links) in the link that yields first (e.g., Tier 1 link in Figure 1-3a) and that experiences greater lateral deformation than other links in the frame. Such large inelastic rotations could fracture the link or adjacent connections [10, 19–24].

1.3 Research Objectives

The general objectives of this Ph.D. research project are to develop a better understanding of the global and local behaviour of MT-EBFs under seismic loading and to propose analysis and design requirements to improve seismic stability of MT-EBFs links and columns; specifically, stability design requirements for intermediate links and stability and strength requirements for columns

when the frame reaches its anticipated yielding mechanism. MT-EBFs that are part of single-storey steel buildings (e.g., industrial buildings) are studied here.

The specific objectives of this research study (Objectives **O1–8)** are as follows:

O1: To understand MT-EBF seismic response and examine the stability of the link and columns under static and dynamic loads using a computationally-efficient fibre-based numerical model of MT-EBFs.

O2: To examine the global and local seismic response of MT-EBFs, in particular, the influence of brace-to-beam and beam-to-column connections on the frame performance using a three-dimensional continuum-based finite element model of MT-EBFs.

O3: To identify parameters influencing the seismic response of MT-EBFs, specifically link out-of-plane deformation and column stability.

O4: To investigate alternatives to conventional lateral bracing systems for the intermediate links.

O5: To evaluate the seismic-induced demands in outer beams due to link and brace out-of-plane deformation.

O6: To quantify the seismic-induced demands in columns due to link progressive yielding and link and brace out-of-plane deformation.

O7: To assess the extent of non-uniform lateral deformation along the frame height due to link progressive yielding.

O8: To propose and validate analysis and design requirements for the intermediate links, intermediate outer beams, and columns in the framework of CSA S16.

1.4 Research Methodology

The following eight steps (**M1–8**) were completed to accomplish the objectives of this research (referred to in the brackets):

M1 (Literature review): An extensive survey of the past numerical and experimental studies was conducted to understand the seismic behaviour of steel EBFs, multi-tiered braced frames, steel wide-flange columns, cyclic behaviour of wide-flange and tubular links, and numerical modelling of links [**O1–8**].

M2 (EBF design): MT-EBFs in this project were designed in accordance with multi-storey EBF provisions of CSA S16-19 [3] assuming intermediate links are braced out-of-plane (referred to as Standard EBFs in this thesis) unless specified otherwise as in Chapters 4 and 5 (referred to as Improved EBFs in this thesis). Several geometric parameters, including the tier height ratio (i.e., the height of the first tier over the second tier), the number of tiers, total frame height, and the flexural rigidity of the brace-to-beam connections, were selected to develop the parametric study matrix. The ductility- and overstrength-related modification factors (R_d and R_o) of the prototype frames were adopted from 2015 National Building Code of Canada, NBCC [25] for the conventional EBF system [**O1–3, O8**].

M3 (Earthquake ground motion selection and scaling): A set of ground motion accelerations was selected and scaled in accordance with the Commentary J of 2015 NBC [25]. The scaling was performed to match, on average, the 2015 NBC design response spectra for the selected location of the building [**O1–2, O5–8**].

M4 (Response evaluation using fibre-based model): A nonlinear fibre-based numerical model of MT-EBFs was developed in the Open System for Earthquake Engineering Simulation (*OpenSees*) program [26]. Special attention was given to the nonlinear behaviour and buckling response of braces, columns, outer beams, and link beams. Nonlinear dynamic analyses of the

seismic response of the prototype frames designed in **M2** were used to assess the influential design parameters on the seismic response of MT-EBFs [**O1, O3–7**].

M5 (Response evaluation using continuum finite element model): A continuum-based finite element (CFE) model of MT-EBFs was developed in the ABAQUS finite element program [27] to evaluate the local and global response of two-tiered EBFs with continuous wide-flange links and three-tiered EBFs with continuous built-up tubular links, with an emphasis on the stability response of their links and columns when full plastic mechanism is achieved (e.g., lateral-torsional buckling mode of failure of the link beam). In this model, the braced frame connections were explicitly modelled. The CFE model of two frames selected using the fibre-based numerical model of **M4** was constructed because of the high computational cost of such models. The results obtained from these simulations were used to evaluate and quantify the seismic-induced demands in link beams (continuous wide-flange link beams and continuous built-up tubular link beams), their respective outer beams and columns, and their inelastic link rotation [**O2–3, O5–7**].

M6 (Design guideline development): The results obtained from numerical simulations, together with engineering mechanics principles and structural analysis methods, were used to propose seismic analysis and design requirements for two-tiered EBFs with continuous wide-flange link beams and three- and four-tiered EBFs with continuous built-up tubular link beams. For each set of frames, the following specific guidelines were proposed [**O8**]:

- **M6i (Design guideline for two-tiered EBFs with continuous wide-flange link beams):** Out-of-plane stiffness of the intermediate beam was used to brace intersecting diagonal braces. Out-of-plane stiffness of the diagonal braces was used to torsionally brace the link beam in the intermediate levels. Strong-axis stiffness of the column was employed to brace

the intermediate beam out-of-plane. The out-of-plane flexural bending moment demand of the intermediate beam and in-plane flexural bending demand of the columns were estimated. Column weak-axis flexural stiffness was utilized to control inelastic rotation of the critical tier (the tier with the largest design shear to shear strength ratio) link.

- **M6ii (Design guideline for three- and four-tiered EBFs continuous built-up tubular link beams):** Minimum strength and stiffness requirements were proposed for the intermediate beams to provide out-of-plane bracing for the diagonal braces connected to intermediate beams. Minimum stiffness and strength requirements were developed for the column bracing the intermediate beams out-of-plane. Column in-plane flexural bending from progressive link yielding was estimated. Column in-plane flexural stiffness was utilized to control link inelastic rotation in the critical tier.

M7 (Validation of design method): The proposed requirements were validated using static and dynamic nonlinear analyses with a focus on the stability and seismic demands of links and columns [**O8**].

M8 (Design of experimental test program): A full-scale test program was designed to verify the concerns associated with the seismic stability of steel MT-EBFs and experimentally validate the proposed design guidelines. Three two-tiered EBF specimens were designed using CSA S16 seismic provisions and those proposed in this study. Notably, the experimental test program was not conducted in this project because of a change to the project scope, and will be performed in future [**O8**].

1.5 Organization of Report

This Ph.D. thesis consists of six chapters and three appendices:

Chapter 1 contains the introduction and background information.

Chapter 2 is a review of past studies on the cyclic performance of the EBF system, multi-tiered braced frames, seismic design of EBFs, seismic response of steel wide-flange columns, and numerical modelling of EBF structures [**M1**].

Chapter 3 presents the seismic response of a set of nine MT-EBFs ranging from two to five tiers. This chapter has been published in the *Journal of Construction Steel Research* titled "Seismic Response of Steel Multi-tiered Eccentrically Braced Frames." [**M1–4**]

Chapter 4 describes the analysis and design procedures proposed for two-tiered EBFs with continuous wide-flange links in the framework of CSA S16. This chapter will be submitted to a journal titled "Analysis and Design Methods for Improved Stability of Two-Tiered Steel Eccentrically Braced Frames with Continuous Wide Flange Links." [**M1–2, M5–7**]

Chapter 5 presents the investigation of the seismic response of three- and four-tiered EBF with continuous built-up tubular links. Analysis and design guidelines are proposed for three- and four-tiered EBFs with continuous built-up tubular links in the framework of CSA S16. This chapter will be submitted to a journal titled "Seismic Analysis and Design of Three- and Four-Tiered Eccentrically Braced Frames with Continuous Built-up Tubular Links." [**M1–2, M5–7**]

Chapter 6 summarizes the key findings and limitations of this study, along with the recommendations for future studies.

Appendices A to C present the design of the experimental test program for the response evaluation of steel MT-EBFs, including the design of three full-scale two-tiered EBF specimens, the associated experimental setup, and structural drawings of the specimens [**M2**, **M8**].

Chapter 2. Literature Review

Steel eccentrically braced frames (EBFs) can be defined as a hybrid structural system that benefits from the large stiffness of concentrically braced frames (CBFs) and the high ductility of moment resisting frames (MRFs). In a well-designed EBF, the link behaves as a structural fuse, which dissipates the seismic-input energy. Bracing configuration, link length, and link cross-sectional properties are the key factors that control the design of EBFs. As required by the capacity design principle, the link is designed to resist the seismic design forces, and all other members are designed to withstand the link resistance. This section presents a review of the cyclic behaviour of wide-flange and tubular links, seismic response of multi-tiered braced frames, seismic design of EBFs, seismic response of steel wide-flange columns, and numerical modelling of EBFs.

2.1 Seismic Response of EBFs

Different configurations of EBFs are illustrated in Figure 2-1. The common types of EBF configurations are shown in Figure 2-1a, where the link beam falls between the end of braces. This configuration also benefits from the low axial force in the link. The arrangement in Figure 2-1b is typically used in narrow bays and requires a moment link-to-column connection to avoid instability. The EBF configuration shown in Figure 2-1c is expected to experience lower link rotation demands under a given frame drift than other configurations [9]. In all three configurations, keeping the angle between the brace and the link more than 40° is preferable [9]. This recommendation by Popov and Engelhardt [9] is intended to limit the axial force in the beam segment outside the link, thus avoiding potential strength and stability problems. It is also recommended to avoid configurations leading to high axial force in the link beam [9] to minimize link instability concerns.

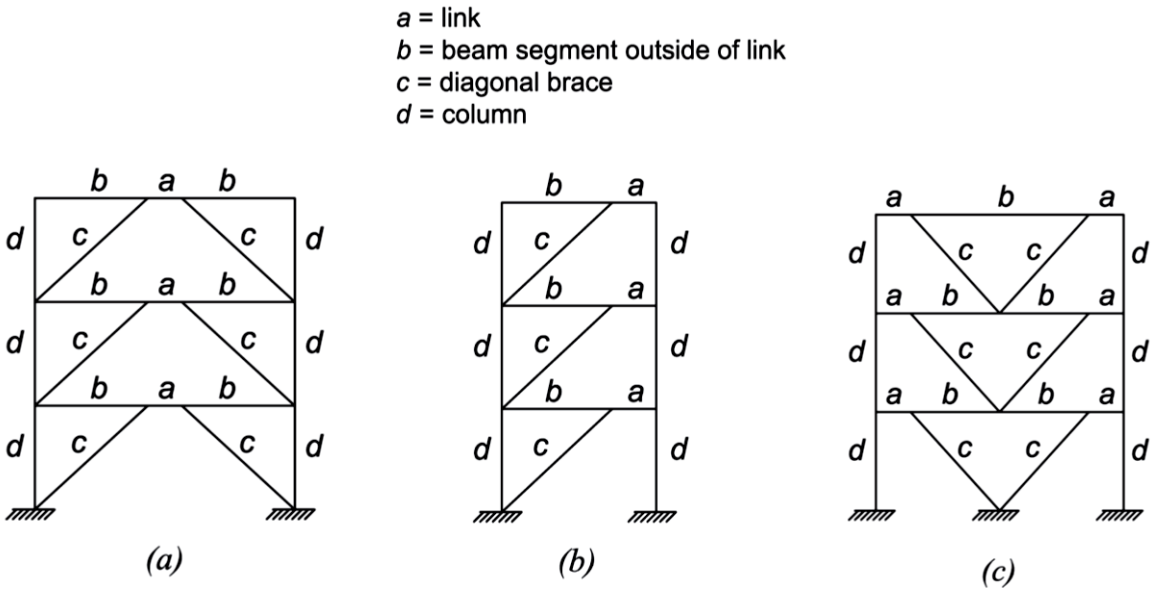

Figure 2-1. Typical eccentrically braced frame configurations [4].

The link length e has a considerable impact on the lateral stiffness of the frame. Figure 2-2 depicts the variation in the frame lateral stiffness for different e/L values, where e is the link length and L is the span length (Figure 2-2a) or half of the span length (Figure 2-2b). Here, $e = 0$ represents a CBF with the largest stiffness and $e = L$ represents an MRF with the lowest stiffness. As shown, for $e/L > 0.5$, the frame loses little stiffness; however, for $e/L < 0.5$, the stiffness changes considerably [28]. Overall, a higher frame stiffness is attained with a shorter link; however, as discussed later, the rotation demand in shorter links will be increased, which may control the link length. Furthermore, the link length cannot be shorter than the beam depth to ensure uniform yielding of the link and minimize stress concentration.

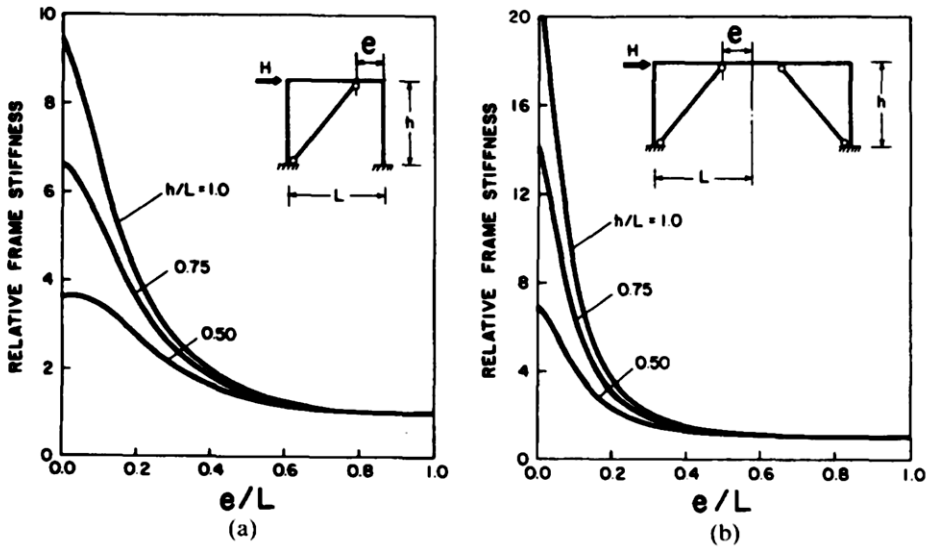

Figure 2-2. Variations of the lateral stiffness with e/L for two configurations: (a) L is the span length; (b) L is half of the span length [28].

In addition to affecting frame lateral stiffness, link length also influences the frame lateral strength. Figure 2-3 shows the variations in the frame lateral capacity, P_u, normalized by $2M_p/h$ (representative of an MRF strength) with e/L for two different span lengths, where M_p is the plastic moment capacity of the beam and h is the storey height. Elastic–perfectly plastic behaviour was assumed for the material in this comparison. In this plot, the frame sections are assumed to be constant as the link length varies. The frame strength increases considerably as the link length decreases, to reach its maximum capacity; this is representative of the full shear yielding of the link [29].

As a result, EBFs with short links are preferred in design because they provide higher stiffness and strength, which are the key design parameters when resisting lateral seismic loads.

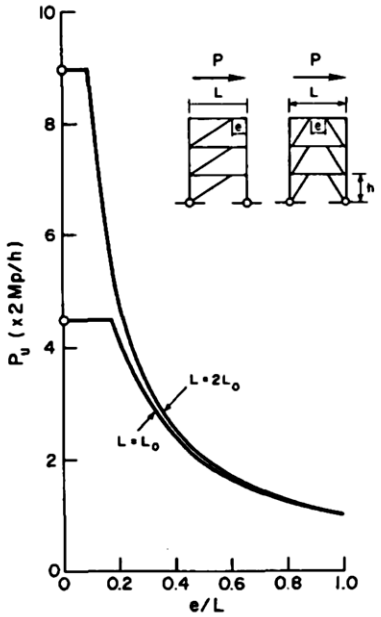

Figure 2-3. Variations of the frame lateral strength with e/L for two eccentrically braced frame configurations [29].

2.2 Link Cyclic Behaviour

The cyclic response of isolated link beams has been investigated by Hjelmstad and Popov [28] on a link subjected to a constant shear force with equal end moments and no axial force. A quasi-static load was applied as an increasing relative end displacement. The authors reported severe web buckling after the initiation of shear yielding in the unstiffened (i.e., without web stiffeners) specimens. This behaviour decreased the energy dissipation and ductility capacity of the link, causing a pinched hysteretic response, as depicted in Figure 2-4a. The specimen with the stiffened web showed substantial improvement in the cyclic response of the link (Figure 2-4b). The hysteretic response of this specimen remained stable over a considerable number of cycles without strength degradation. This specimen achieved large inelastic rotation, indicating a large energy dissipating capacity. Other researchers [10, 30] confirmed the stable hysteretic behaviour of shear link, exhibiting shear yielding under cyclic loadings.

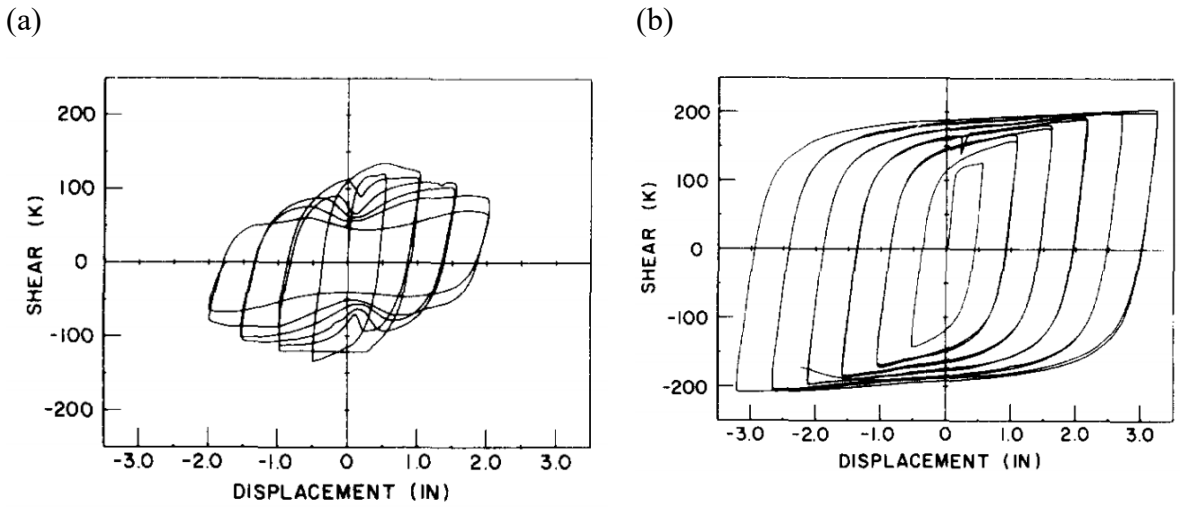

Figure 2-4. The hysteretic response of: (a) Unstiffened link; (b) Stiffened link [28].

Early experimental tests, mostly on A36 steel, conducted by Popov and his colleagues [9, 31] suggest a shear overstrength factor of 1.5 in the shear links because of strain hardening, which is still used implicitly in the current seismic design provisions [3, 4]. Okazaki and Engelhardt [10] reported the results of 37 link specimens that were constructed on W-shapes of ASTM A992 steel. The links were found to exhibit an overstrength factor ranging from 1.05 to 1.62, with an average of 1.35. Yigitosy et al. [32] showed that a single value for the overstrength factor of 1.5 was matched primarily with shear links and was overly conservative for longer links. Shear links with thick flanges can exhibit a higher overstrength factor because the shear forces carried by flanges are neglected [33, 34]. Experimental tests conducted by Berman and Bruneau on built-up tubular short links suggested 11% higher strain hardening [35]. The experimental data also indicate that for short links, the interaction between bending moment M and the shear force V can be neglected. Kasai and Popov [31] argued that because of the warping at the end of the links, stress distribution happens, allowing the web to carry more bending moments at the end regions. Additionally, shear strain hardening occurs in the link, leading to added strength without considerable loss of link global stiffness.

In an idealized case where no strain hardening exists (i.e., elastic–perfectly plastic material) and where M and V act independently without any interaction, a link length of $e = 2M_p/V_p$ is the boundary between the shear link and moment link. In this equation, M_p is the plastic bending moment, and Vp is the plastic shear capacity of the cross-section. If the overstrength factor of 1.5 for the probable shear strength and the limitation of 1.2Mp on the link end bending moments—suggested by Kasai and Popov [31] to prevent low cycle fatigue weld failure connecting the link flanges to the end plate—is accounted for, the shear link length becomes:

$$e \leq 2(1.2M_p/1.5V_p)=1.6M_p/V_p \quad (2\text{-}1)$$

Therefore, in order to achieve a shear link, a link design is recommended that complies with Eq. (2-1) [9].

Lateral torsional buckling (LTB) of links consisting of W-shape sections results in detrimental effects on the inelastic cyclic response of the link. The restraint against LTB can prevent the link out-of-plane displacement and twist, resulting in a stable cyclic behaviour. Additionally, the lateral bracing holds the braces in the plane of the frame, preventing the compression brace from imposing a twist in the link [9]. Hjelmstad and Lee [7] examined the lateral bracing effect on the propped cantilever beams under cyclic loads. They investigated the effect of lateral bracing on either the top or bottom flange with stocky and slender braces and found that the energy dissipation capacity of the beams that were laterally unbraced and partially braced against lateral torsional movement was smaller than of the laterally braced beams. Also, the traditional rules for the design of lateral bracing (2%–2.5% of the squash load of the compression flange) were not adequate because of the brace buckling occurred in one of the specimens, and 5% was proposed instead. Hjelmstad and Popov [36] reported that no lateral bracing was required for very short links if the link had adequate torsional resistance. Lateral bracing is required for both the top and bottom flange according to the

current seismic design provisions [3, 4]. The concrete slab may provide support for the top flange [8, 37], but the bottom flange requires lateral bracing using secondary beams or designated bracing systems. Full-depth stiffeners can also mitigate LTB, although the primary purpose of the stiffener is to increase the shear capacity of the beam web [8, 9]. Engelhardt and Popov [8] examined the effect of the brace-to-beam connection on the stability of the beam segment outside of the link and showed that the flexural-fixed connection decreased the bending moment demand on the beam outside of the link, resulting in a more stable behaviour.

Berman and Bruneau [30, 35, 38] investigated the cyclic behaviour of welded hollow rectangular sections (i.e., tubular) as the link beam because it has high torsional stiffness and is less susceptible to LTB. One of the common applications of HSSs is in bridge piers and towers where lateral supports cannot easily be provided. The results indicated that the tubular sections had satisfied the link rotation capacities originally specified for wide-flange sections if the proposed compactness ratios for the web and flanges were met.

Links with shear yielding mechanism are preferable in seismic design because they offer a more stable and reliable energy dissipation capacity. Shear yielding develops in the web along the link length—because the link is under a constant shear force, as shown in Figure 2-8b—with a limited yielding in the flanges. The reinforced web, along with the nearly elastic flanges, forms a tension field in the web resulting in a stable cyclic behaviour [5, 9]. Additionally, the plasticity is distributed in the large area of the web, whereas in moment links, flexural plastic hinges form at the two ends of the link with large strains concentrated locally on the flanges at two ends within a small length of the link.

2.3 Link Rotation

In seismic applications, link rotational demands need to be controlled through the frame collapse mechanism, as shown in Figure 2-5 for two EBF configurations. The hatched area in the figure is to define shear yielding and the potential collapse mechanism of the frame. The link rotation angle depends on the brace configuration, geometry of the frame, and the storey drift, as follows:

$$\gamma = L\theta/e \tag{2-1}$$

where θ is the storey drift. The link rotation for the two configurations shown in Figure 2-5 is the same as given in Eq. (2-2), but it is multiplied by 0.5 for the frame of Figure 2-1c.

The link rotation demand has an inverse relationship with e/L, as shown in Figure 2-6. For very short links, the rotation demand increases drastically.

Past experimental test results show that shear links can maintain larger link rotation without degradation of the strength [39]. This finding is also reflected in CSA S16 with a link rotation limit of 0.08 rad for shear links versus a link rotation limit of 0.02 for moment links.

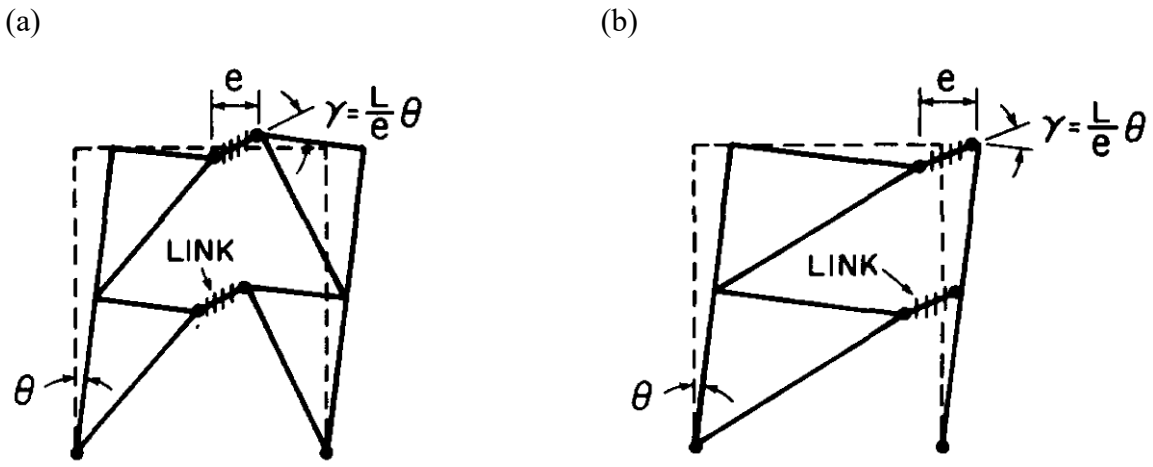

Figure 2-5. Frame collapse mechanism: (a) Chevron configuration; (b) Diagonal configuration [9].

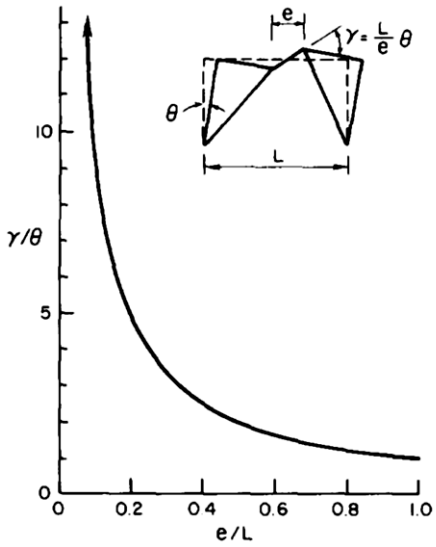

Figure 2-6. Variation of link rotation demand with *e*/*L* [9].

2.4 Seismic Design of EBFs

The shear force in EBF links can be determined under seismic design forces using a free-body diagram of the frame (e.g., a two-tiered EBF is shown in Figure 2-7). Using the moment equilibrium about point A and taking advantage of symmetry, the link design force V_{link} can be determined as follows:

$$V_{link} = V_s(h/2L) \quad (2\text{-}2)$$

where V_s is the storey shear force and h and L are the total frame height and frame span, respectively.

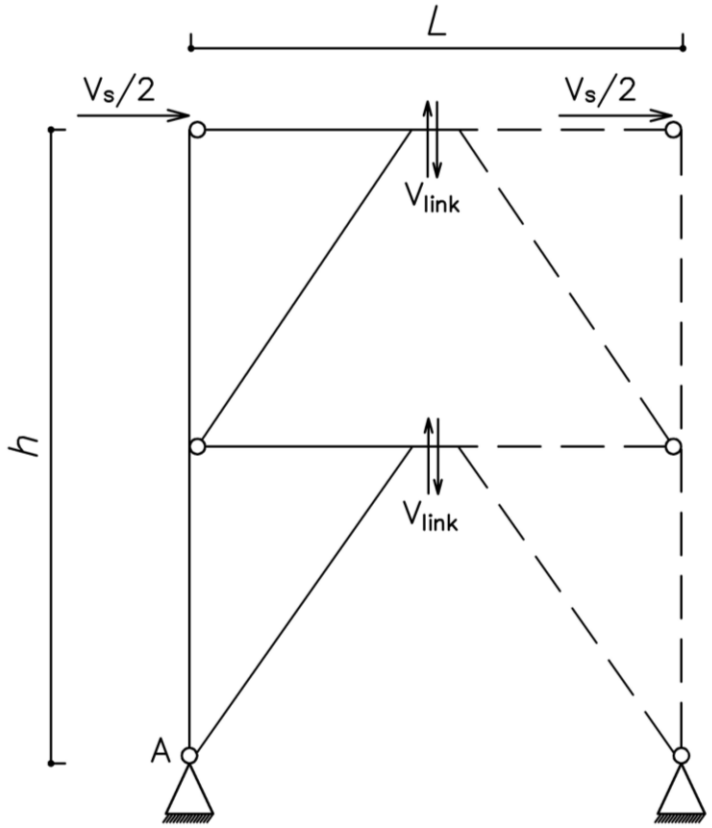

Figure 2-7. Link design force for a two-tiered eccentrically braced frame.

Once shear in the link is determined, the shear force V, bending moment M, and axial force P diagrams of the beam can be obtained using static equilibrium, as shown in Figure 2-8a. The link end moment can be obtained as follows:

$$M_{end} = V_{end}\, e/2 \quad (2\text{-}3)$$

where V_{end} and M_{end} are the shear force and bending moment at the link ends, and e is the link length. For short links, shear plastic hinging is expected because of the short moment arm, whereas large bending is developed at the link ends in long links, causing flexural plastic hinging at two

ends. The seismic response of these two types of links differs significantly. There is an intermediate-range of length in which a significant amount of shear and flexural yielding occurs [9].

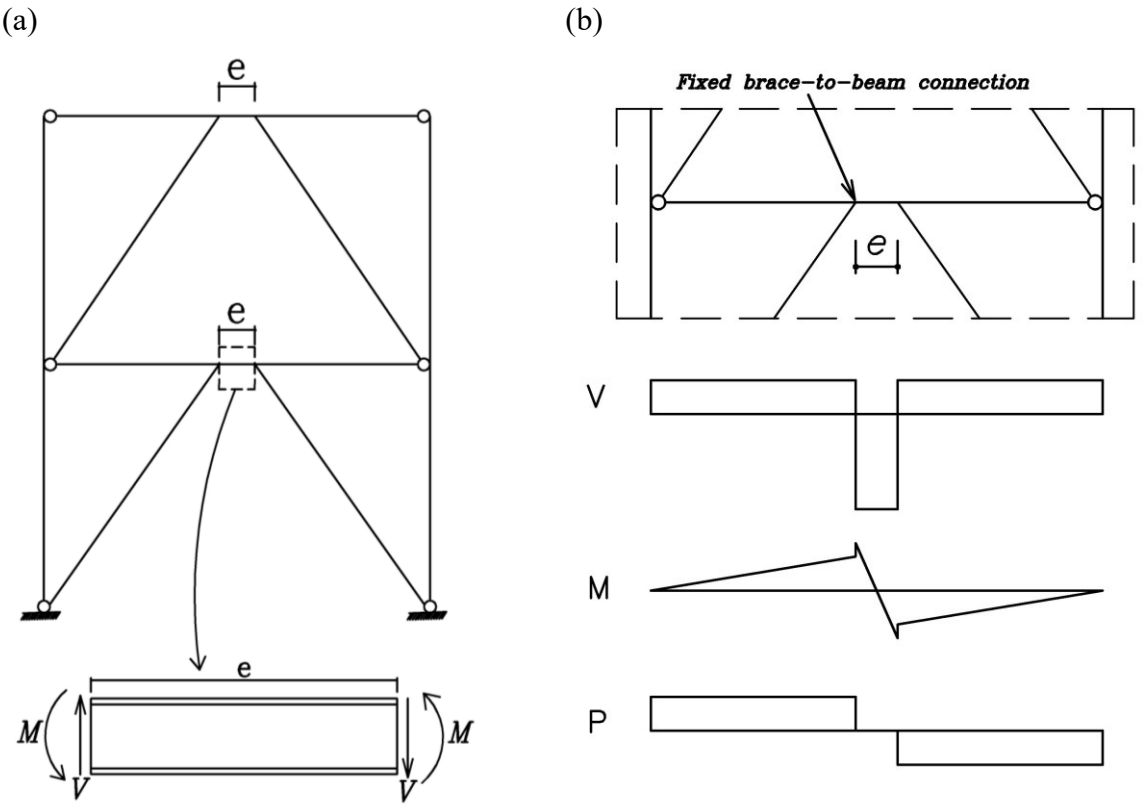

Figure 2-8. (a) Free-body diagram of the link in eccentrically braced frames; (b) Seismic force distribution in the link and beam segment outside of the link in eccentrically braced frames.

Once the link is designed as a seismic fuse, its probable shear resistance is determined (using CSA S16) to calculate the forces in the adjacent members:

$$V_{pr}=1.3R_yV_p \quad (2\text{-}4)$$

where R_y is the ratio of expected to nominal yield stress and is equal to 1.12 for W-shape sections, and V_p is the plastic shear resistance. The strain hardening is included with the 1.3 factor applied

to the nominal shear strength. Accounting for the R_y value together with the resistance factor of 0.9, the overstrength factor of 1.3×1.12/0.9=1.62 compares well with the test results.

2.5 Multi-Tiered Braced Frames

Multi-tiered braced frames differ from multi-storey braced frames because of two key characteristics of multi-tiered braced frames: 1) no diaphragms exist between the ground and roof levels, creating a single-degree-of-freedom system and 2) lack of lateral supports for columns between the ground and roof levels raises concerns regarding the stability of columns [40].

Although there is very little research into the seismic evaluation of multi-tiered EBFs (MT-EBFs), the seismic response of MT-CBFs has been widely studied in the past decades. The results obtained from numerical simulations, including detailed finite element and fibre-based models, showed that if the columns are not designed to resist the combined effects of the axial force and biaxial bending, brace tensile yielding is not uniformly distributed among tiers, causing relative lateral displacement between tiers and large in-plane bending moments in the columns [41]. Such combined demands can lead to column plastic hinging and instability, as shown in Figure 2-9. Imanpour et al. [42] showed the inadequacy of the 2010 AISC Seismic Provisions [4] for the design of steel MT-CBFs. This study found that the column flexural yielding may cause column instability. Stoakes and Fahnestock [43] examined the effectiveness of the torsional restraint at the tier levels of MT-CBF columns and found that such restraint can have a positive impact on the column stability response.

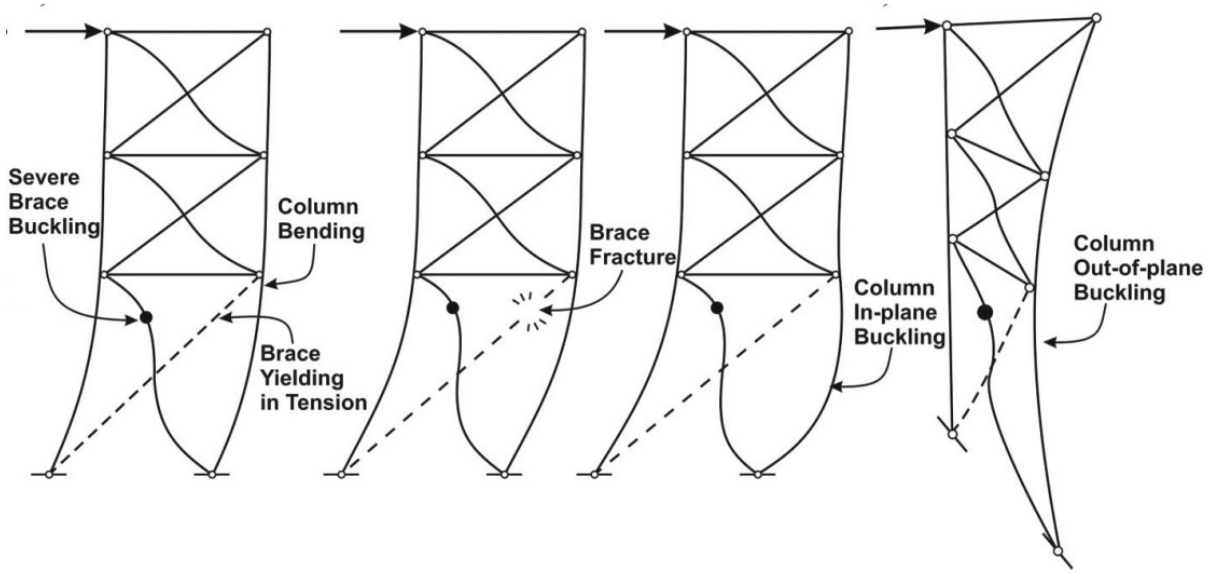

Figure 2-9. Non-uniform distribution of seismic demands in a multi-tiered concentrically braced frame inducing in-plane flexural demands on the column and triggering in-plane and out-of-plane buckling [44].

Imanpour et al. [19] examined the behaviour of MT-CBFs designed according to the 2010 AISC Seismic Provisions through a numerical parametric study. The number of tiers, the height ratios between tiers, and the column base fixity conditions were varied. They reported high in-plane flexural moments in columns resulting from high drift concentration. They observed weak-axis buckling that transitioned into torsional-flexural buckling in several cases. This study showed that higher design seismic forces did not influence the column internal forces. However, using a fixed condition at the base can improve the stability of the column. Imanpour et al. [45], in another study, proposed a design method for the design of MT-CBFs. They suggested a tier drift limit, which can be provided by the column in-plane flexural stiffness to prevent brace fracture resulting from the large deformations in tiers. The proposed method included a procedure to calculate the in-plane bending moment in the column, which was adopted in the 2016 AISC Seismic Provisions [4].

Cano and Imanpour [40] compared the seismic response of a two-tiered braced frame designed in accordance with 2010 and 2016 AISC Seismic Provisions. They showed that the 2016 AISC regulations for the design of MT-CBFs enhanced the performance of the frame, and the frame had

a more uniform lateral displacement with lower column in-plane bending moments. No instability was observed in the column; however, the column in-plane and out-of-plane bending moment in 2016 AISC was over-estimated and under-estimated, respectively.

Houreh and Imanpour [46] studied the seismic performance of MT-CBFs in low-to-moderate seismic regions where limited ductility MT-EBFs are preferred. They proposed a design method for such frames in the framework of CSA S19. In another study [47], they investigated the seismic response of MT-CBFs of the conventional construction category (Type CC) in moderate seismic regions of eastern Canada. The results of the nonlinear response history analyses (NLRHA) were then used to propose a design method.

2.6 Seismic Response of Wide-Flange Columns

There is limited research on the seismic response of wide-flange columns in multi-tiered braced frames. Stoakes and Fahnestock [48, 49] examined the seismic behaviour of isolated columns under compressive loads in combination with varying weak-axis rotations using three-dimensional finite element analysis. They found that the weak-axis yielding can significantly degrade the strong-axis buckling strength under large weak-axis rotation, particularly when there is a lack of torsional restraint at the tier levels.

In 2011, Lamarche and Tremblay [17] conducted four full-scale tests to investigate the buckling response of wide-flange columns in multi-storey braced frames. The column was a W310×129 class 1 section made of ASTM A992 steel. The monotonic and cyclic axial loading was applied to the specimens with and without eccentricity. To simulate the loading conditions in braced frames, 60% of the column nominal compressive strength was first applied, followed by cyclic axial displacement. Test results showed that in all specimens, weak-axis inelastic buckling was the main failure mode with the plastic hinge at the middle of the column. The findings also indicated that

load-carrying capacity was not compromised when columns with class 1 sections experienced limited yielding.

Newell and Uang [50] tested nine full-scale wide-flange columns under an axial force demand of 35%, 55%, and 75% of nominal axial strength in combination with up to 10% storey drift. The columns represented the bottom level of multi-storey braced frames. The specimens demonstrated a significant inter-storey drift capacity of 0.07–0.09 rad, which may be attributed to the stabilizing effect provided by the web of the stocky column, resulting in a delay in flange local buckling. Notably, global buckling did not occur in any of the test specimens.

The cyclic response of the first storey column in MRFs was investigated extensively by Elkady and Lignos [51] in a full-scale testing program. They studied the effects of various parameters on the hysteretic behaviour of columns, including boundary conditions, loading sequence, local web, and member slenderness ratios. In fixed base columns with realistically flexible top ends, the primary mode of failure was local buckling followed by out-of-plane deformations near the plastic hinge at the base of the column.

2.7 Numerical Modelling of EBFs

A numerical model to simulate the combined isotropic and kinematic shear hardening and flexural kinematic hardening was proposed by Ricles and Popov [52]. Their model was two-dimensional and consisted of a linear elastic beam with nonlinear hinges at two ends. Each zero-length hinge was divided into three sub-hinges (Figure 2-10). The series of sub-hinges were assigned a rigid-plastic force–deformation and moment–rotation relationship, producing a multilinear response for each hinge. The model was verified with experimental testing and was able to predict the link response accurately; however, it was too complex to be properly used. Ricles and Popov's model was then improved by Ramadan and Ghobarah [53]. The hinges at each end of the elastic element

in the Ricles and Popov method were replaced with two hinges associated with the in-plane flexure and shear degree-of-freedoms. The sub-hinges in the original model were substituted with translational and rotational zero-length springs, as illustrated in Figure 2-10. Each spring was assigned a bilinear action-deformation response. To achieve a multilinear behaviour, at least three springs for the shear and three for the moment were assigned at each link end. Ramadan and Ghobarah validated their model with limited experimental testing. Richards and Uang [54] performed an extensive experimental verification for the model developed by Ramadan and Ghobarah. Koboevic et al. [55] replaced the series of springs with a single spring. The Giuffré-Menegotto-Pinto material model—Steel02 material on *OpenSees*—was assigned to the spring. The verification showed a better fit between experimental and analytical results over the entire shear-rotation results compared with the previous models.

(a) (b)

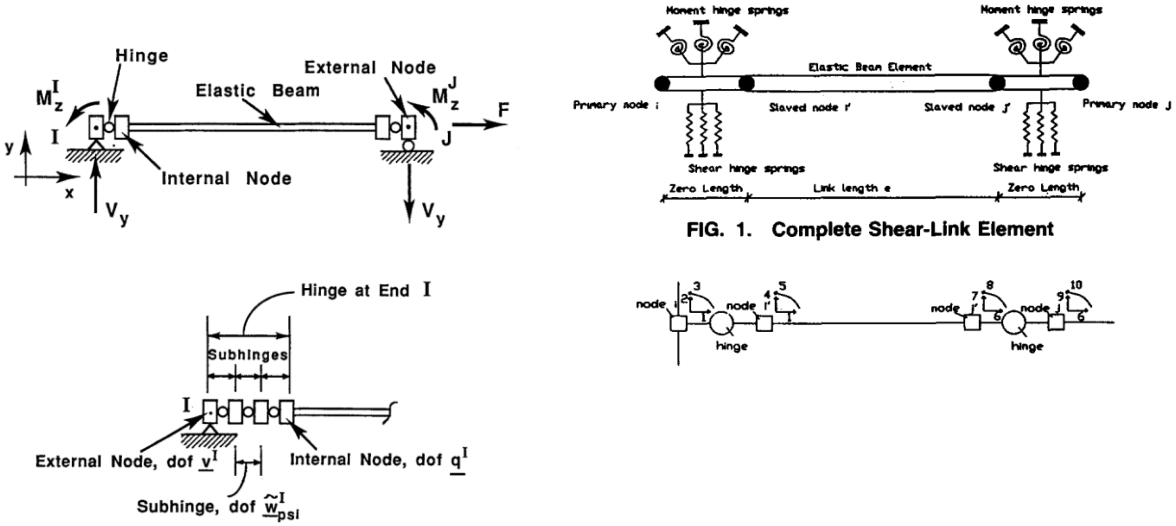

Figure 2-10. Shear link model by: (a) Ricles and Popov [52]; (b) Ramadan and Ghobarah [53].

2.8 Summary

EBFs have been the focus of many research studies in the past. In majority of these studies, lateral bracing was assumed to be provided to the link and columns through roof or floor diaphragms. In multi-tiered configuration, however, the lack of lateral bracing system in intermediate levels can negatively affect the seismic performance of the frame. Motivated by the recent studies on steel MT-CBFs, the EBF system can potentially be used as a lateral load-resisting system of steel buildings with multi-tiered configuration, in particular for high seismic areas, because EBFs can offer high lateral stiffness and energy dissipation capacity. Nonetheless, there is a research gap on the local and global behaviour of MT-EBFs under seismic loading.

Chapter 3. Seismic Response of Steel Multi-Tiered Eccentrically Braced Frames

3.1 Introduction

Tall single-storey steel buildings are extensively used in North America to house chemical plants, industrial facilities, shopping centres, airplane hangars or sports facilities. The most common type of lateral load-resisting systems in these buildings is steel braced frames. These braced frames typically consist of multiple braced panels (or tiers) that are stacked along the height of the frame, as the application of a single-panel bracing system often becomes impractical or even impossible because of the tall storey height. Intermediate horizontal struts are typically placed between braced panels to avoid unsatisfactory K-braced frame response that may cause large in-plane bending in the braced frame columns due to the unbalanced force at the intersection of the braces and columns. This bracing configuration is referred to as a multi-tiered braced frame. Various braced frame systems, including concentrically braced frames (CBFs), buckling-restraint braced frames (BRBF), and eccentrically braced frames (EBFs), can be used within a multi-tiered configuration. The majority of multi-tiered braced frame structures in North America, however, consist of concentrically braced frames because of ease of design and fabrication. However, EBFs and BRBFs are also used, in particular in regions of high seismic hazard. EBFs are used in seismic design to allow large openings and walkways through bay frames while resisting lateral load through a combination of frame action and truss action, where the bracing system provides large lateral stiffness, and the link beam forms a stable and reliable yielding mechanism. Figure 3-1 shows the main components of a steel multi-tiered eccentrically braced frame (MT-EBF) with two braced tiers.

The multi-tiered configuration offers several benefits over single-panel braced frames, which favours the extensive application of such frames in tall single-storey buildings or tall storeys of multi-storey buildings in North America. The benefits include smaller brace sizes and lengths as well as lighter column sections, as intermediate beams can laterally brace the columns in the plane of the frame. For seismic applications, smaller links are needed in the multi-tiered configuration, which can potentially reduce capacity-induced forces on braces, beams, columns, connections and footings.

The columns of MT-EBFs are designed to resist the gravity plus seismic loads in the plane of the frame, and the gravity plus wind loads in the out-of-plane direction. As shown in Figure 3-1, columns are assumed to be laterally braced in the plane of the frame at every tier level, whereas they are considered unbraced between the ground and roof levels in the out-of-plane direction. Thus, steel wide-flange sections are often used, and the column section is oriented such that out-of-plane wind loads produce strong-axis moments.

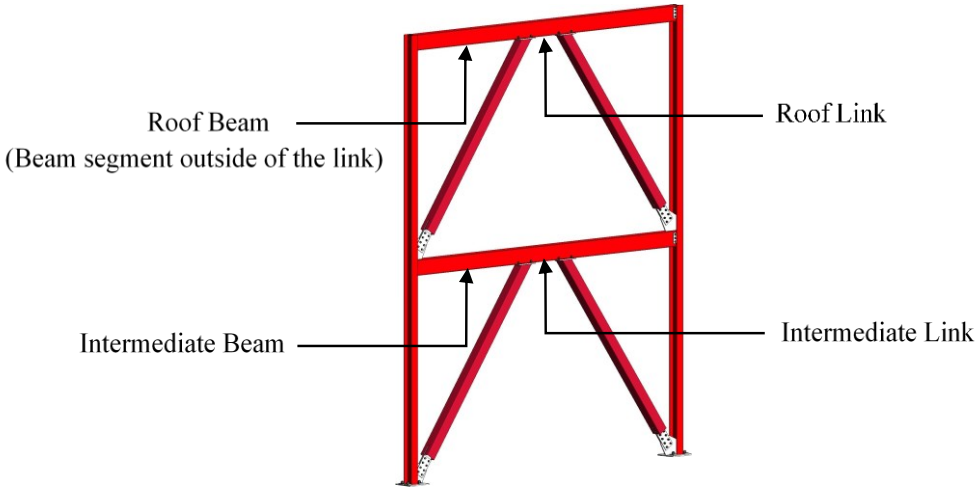

Figure 3-1. Two-tiered eccentrically braced frame.

There has been very limited research into the seismic response of steel MT-EBFs in the past. Ashrafi and Imanpour [56, 57] studied the seismic behaviour of two-tiered EBFs. The frames were designed in accordance with the Canadian steel design standard, CSA S16 [58], neglecting the additional moment demand required for multi-storey EBF columns. The link at the roof level

was considered laterally braced; however, the lateral bracing condition was altered for the link at the tier level to evaluate the need for lateral out-of-plane bracing. The results showed that if the link beams are laterally braced, the frame lateral deformations are relatively uniformly distributed between tiers as the link beams yield in shear and undergo inelastic deformations. Neither link nor column instability was observed for this detail. However, when the intermediate link beam is laterally unbraced, the frame's lateral inelastic deformations are unevenly distributed between tiers. Out-of-plane instability of the intermediate link beam was observed due to the lack of lateral out-of-plane support and large inelastic shear deformations developed in the intermediate link.

Whilst there is limited research on the seismic response of MT-EBFs, multi-tiered concentrically braced frames (MT-CBFs) were the subject of a major research program over the past decade. The seismic response of such braced frames was examined with a focus on the stability of their columns [19, 44, 45, 59]. The results of the NLRHA, together with full-scale hybrid testing, confirmed that large in-plane flexural bending is induced in the columns of MT-CBFs due to the uneven distribution of inelastic deformations developed after brace tension yielding in any one of the braced tiers while other braced tiers remain elastic. This response caused the concentration of inelastic deformations in the tier where brace tension yielding takes place first. Column moments, if excluded in design, can lead to column plastic hinging and instability. Additionally, it was shown that large inelastic deformations induced in one of the tiers could induce large deformation demands on the braces, which may cause premature fracture of braces due to low-cycle fatigue [19].

There is a lack of understanding of how steel MT-EBFs would perform under seismic loads, which necessitates the investigation of their seismic response and the identification of the influential parameters affecting their response. This chapter aims to examine the seismic response of steel MT-EBFs. A set of MT-EBFs ranging from two- to five-tiered was selected and designed

in accordance with the 2019 edition of CSA S16 [3]. Various parameters, including the frame height, tier height ratio, number of tiers, link bracing conditions, and brace-to-link connection were varied. Numerical NLRHA was then performed on the selected frames. The results obtained from the analyses were used to evaluate the seismic behaviour of MT-EBFs, in particular, the stability response of their links and columns. Finally, three alternative design strategies to improve the stability response of MT-EBFs are examined, and their seismic performance is presented. For the studied cases, the parameters that shall be considered in the design of links and columns were discussed.

3.2 Seismic Design of Multi-Tiered EBFs

3.2.1 Design Provisions

There are no special design provisions in CSA S16 for MT-EBFs, though the use of such systems is not prohibited. S16 allows MT-EBFs only when it is justified by an analysis that accounts for the effects of uneven tier drifts over the frame height at the seismic design storey drift, and lateral bracing is provided to both top and bottom flanges at the ends of the links. In contrast, S16 provides comprehensive seismic design provisions for MT-CBFs. These provisions are intended to address the concerns raised regarding the stability of MT-CBF columns. MT-CBF columns shall be designed to resist the combined effects of the axial force, in-plane and out-of-plane moments under gravity and seismic loads. S16 also requires that the tier drift be limited to 2% to control the deformation demands induced in individual braced tiers, thus reducing the likelihood of brace low-cycle fatigue fracture. Similar (not identical) provisions are specified by the AISC Seismic Provisions for Structural Steel Buildings (AISC 341) [4] for the seismic design of MT-CBFs in the U.S. The AISC Seismic Provisions do not permit the use of an EBF system with a multi-tiered configuration, which is a different perspective as compared to Canada's corresponding S16.

3.2.2 Prototype Frames

A single-storey industrial building located in Vancouver, British Columbia, Canada was selected in this study. The building dimensions vary between the frames selected here to achieve a realistic seismic base shear per frame. In the short direction, roof trusses span over the width of the building; however, open web steel joists are used between the trusses in the long direction of the building. The columns are spaced at L = 7m along the building perimeter. The seismic load-resisting system of the building consists of Ductile (Type D) EBFs located on the exterior wall in the long direction of the building. The number of braced frames per wall in the long and short directions is selected so that the seismic base shear per frame is relatively identical for different configurations.

Nine MT-EBFs ranging from two to five tiers were chosen to examine the effects of the number of tiers, frame height, tier height ratio (i.e., the height of Tier 1 h_1 relative to that of Tier 2, h_2), and brace-to-beam connection (i.e., fixed or pinned). The frames have an identical span length of 7m with heights varying from h = 9.0 – 20.5m. The geometric properties of the selected frames are given in Table 3-1. Figure 3-2 shows the geometry of the frames.

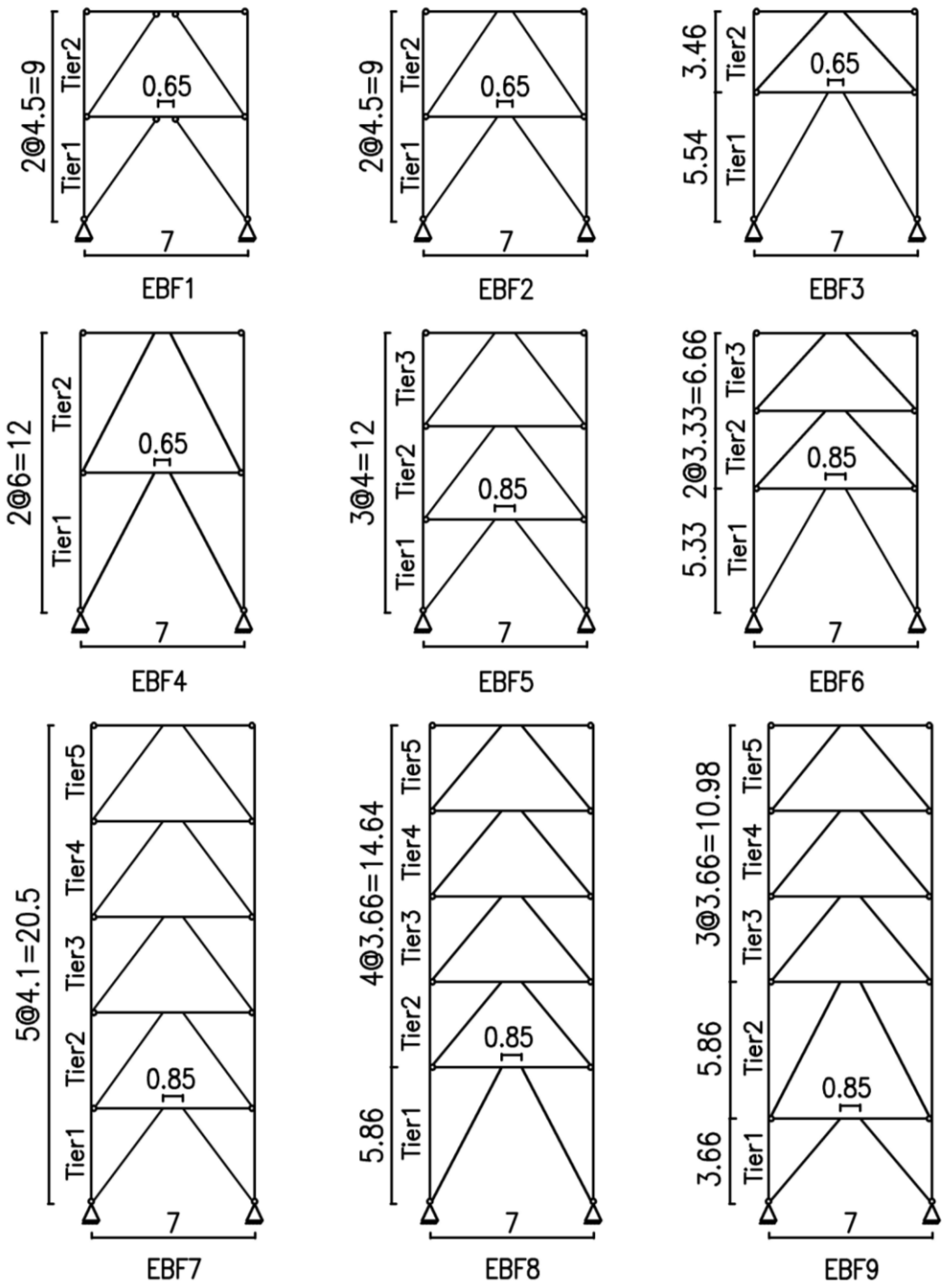

Figure 3-2. Elevation of the prototype MT-EBFs (dimensions in m).

Table 3-1. Geometry, seismic data and member sizes of the prototype MT-EBFs.

Frame	Total Height h (m)	Height Ratio h_1/h_2	No. of Tiers n	Link Length e (m)	Seismic Weight /Frame W (kN)	Design Period T_a (s)	Design Spectral Acc. g	Base Shear /Frame V (kN)	Beam Section W	Brace Section HSS	Column Section W	Brace-to-beam Connection
EBF1	9.0	1.0	2	0.65	3069.5	0.45	0.767	477	250×49	152×12.7	250×45	Pinned
EBF2	9.0	1.0	2	0.65	3069.5	0.45	0.767	477	250×49	152×12.7	250×45	Fixed
EBF3	9.0	1.6	2	0.65	3069.5	0.45	0.767	477	250×49	152×12.7	310×52	Fixed
EBF4	12.0	1.0	2	0.65	3127.3	0.60	0.686	447	310×60	203×9.5	250×58	Fixed
EBF5	12.0	1.0	3	0.85	3959.8	0.60	0.686	565	250×58	178×12.7	250×67	Fixed
EBF6	12.0	1.6	3	0.85	3959.8	0.60	0.686	565	250×58	178×12.7	250×67	Fixed
EBF7	20.5	1.0	5	0.85	5696.3	1.03	0.420	525	250×58	203×12.7	310×179	Fixed
EBF8	20.5	1.6	5	0.85	5696.3	1.03	0.420	525	250×58	203×12.7	310×179	Fixed
EBF9	20.5	0.625	5	0.85	5696.3	1.03	0.420	525	250×58	203×12.7	310×179	Fixed

3.2.3 Gravity and Seismic Loading

Gravity and seismic loading was performed in accordance with the 2015 National Building Code of Canada, NBCC [25]. The design roof dead load D is equal to 1.0 kPa. The unit weight of the exterior walls was assumed to be 0.5 kPa. The snow load computed for Vancouver is 1.64 kPa. Under the load combination D+E+0.5L+0.25S, the roof beam is subjected to a transverse distributed load of $q_{fg\text{-}b}$ = 1.41 kN/m due to gravity. A limited compressive force ($C_{fg\text{-}br} \approx 4$ kN) is induced in the braces as a result of column shortening under gravity loads.

For the selected EBFs, the ductility-related and overstrength related modification factors are R_d = 4.0 and R_o = 1.5, respectively. The building studied is located on site class C. The importance factor of the building is I_E = 1.0. The factor accounting for the increase in base shear because of higher mode effects is M_v = 1.0. The seismic weight tributary of each frame under D+0.25S is given in Table *3-1*. The design period of the structure T_a, which is equal to two times the empirical period as permitted by NBCC, and the corresponding design spectral acceleration are given in Table 3-1. The seismic-induced forces were calculated using the equivalent static force procedure. Table 3-1 provides the resulting seismic base shear per frame, including the effects of accidental torsion, P-Delta and notional loads.

3.2.4 Frame Design

The design of the structural components was performed in accordance with the 2019 edition of CSA S16. The links that consist of a segment of the beams were the first members to be designed. The links were selected to dissipate seismic-input energy through shear yielding. To ensure that the yielding mechanism is shear in the links, the link length e was chosen such that it does not exceed $1.6M_p/V_p$, where M_p and V_p are the nominal plastic moment resistance and shear resistance of the link beam, respectively while maintaining link deformations below $4\theta L/e$ where θ is the elastic design storey drift. Additionally, the link factored shear force induced under the seismic load shall not exceed the factored shear resistance of the link with zero axial load, V_r. As required by S16 for a link yielding in shear, the width-to-thickness ratio shall comply with the Class 2 limit for flanges and Class 1 limit for the web. For all frames with uniform and non-uniform tier heights, an identical continuous wide-flange cross-section was chosen for the links at the roof and tier levels based on the most critical loading scenario between links. Lower shear strength compared to the required one in some cases was deemed acceptable due to various sources of overstrength considered in design (e.g., expected yield strength and resistance factors). This was adopted to keep an identical link section for frames of the same total height but different tier heights. The selected cross-sections conform to ASTM A992 Gr. 50 steel with F_y = 345 MPa. The summary of the link design is given in Table 3-2. In the table, $\varphi = 0.9$ is the resistance factor, w is the thickness of the link web, d is the depth of the cross-section, A_w is the shear area of the cross-section, and Z is the plastic section modulus about the strong axis.

Table 3-2. Summary of link design.

Frame	Link Section W	e mm	$V_f = Vh/L$ kN	$V_r = \varphi V_p = 0.55\varphi w d F_y$ kN	A_w mm^2	Z 10^3 mm^3	$M_p = ZF_y$ kN-m	$3.6Z/A_w$ mm	$1.6M_p/V_p$ mm
EBF1	250×49	650	307	311	1820	636	219	1258	1016
EBF2	250×49	650	307	311	1820	636	219	1258	1016
EBF3	250×49	650	370	311	1820	636	219	1258	1016
EBF4	310×60	650	383	386	2262	934	322	1486	1201
EBF5	250×58	850	323	344	2016	767	265	1370	1107
EBF6	250×58	850	420	344	2016	767	265	1370	1107
EBF7	250×58	850	308	344	2016	767	265	1370	1107
EBF8	250×58	850	429	344	2016	767	265	1370	1107
EBF9	250×58	850	429	344	2016	767	265	1370	1107

S16 requires that the EBF members outside the link be designed to resist, in the elastic range, the capacity of the link so that the link can safely dissipate seismic-input energy. Once the links were sized, the adjacent members, including outer beams, braces and columns, were designed to sustain the probable shear resistance of the link, equal to $1.3R_y/\varphi$ times the factored shear resistance of the link V_r, where R_y is the ratio between the expected R_yF_y = 385 MPa and nominal yield strength. Beams are continuous members and made of the same wide-flange section selected for the link. As permitted by S16, the factored resistance of the outer beam can be amplified by φR_y when verifying the resistance of the beam under capacity-induced forces. The outer beam was designed as a beam-column to resist the combined effects of axial compression or tension force and strong-axis bending due to the gravity load plus the moment induced by the probable shear resistance of the link. It was assumed that braces are moment-connected to the beams in all EBFs, as typically done in practice, except EBF1 (Figure 3-2), where the braces are pinned to the beam; thus, the seismic-induced moment transferred to the outer beam was obtained by subtracting the moment carried by the brace from $0.65R_yV_re/\varphi$. The cross-sections selected for the links were then verified under outer beam demands. According to S16, the beam section shall comply with the width-to-thickness ratio limit specified for Class 2 sections. Table 3-3 summarizes the design of outer beams under the governing beam-column limit state. In this table, $C_{f\text{-}b}$ and $M_{f\text{-}b}$ are the axial compression force and bending

moment in the outer beam, respectively. $C_{r\text{-}b}$ is the axial compressive resistance, $M_{r\text{-}b}$ is the moment resistance of the outer beam, and U_1 is the amplification factor that accounts for the second-order (P-δ) effects. Large P-Δ effects were neglected in design as permitted by 2015 NBCC because the P-Δ amplification factor U_2 is smaller than 1.1 for the frames studied here.

Table 3-3. Summary of beam design.

Frame	Beam Section W	$C_{f\text{-}b}$ kN	$M_{f\text{-}b} = M_{fg\text{-}b} + M_{fE\text{-}b}$ kN-m	$C_{r\text{-}b}$ kN	$M_{r\text{-}b}$ N-m	$C_{f\text{-}b} / C_{r\text{-}b} + 0.85U_1M_{f\text{-}b} / M_{r\text{-}b}$
EBF1	250×49	389	162	1589	246	0.82
EBF2	250×49	384	138	1589	246	0.73
EBF3	250×49	498	135	1630	246	0.79
EBF4	310×60	358	173	1916	361	0.60
EBF5	250×58	473	188	1966	296	0.80
EBF6	250×58	567	185	2029	296	0.83
EBF7	250×58	458	170	1966	296	0.73
EBF8	250×58	512	167	1966	296	0.75
EBF9	250×58	512	167	1966	296	0.75

Braces were made of hollow structural sections (HSSs) conforming to ASTM A1085, Gr. C steel and F_y = 345 MPa. They were designed such that they resist the axial compression force $C_{f\text{-}br}$ plus a percentage (15–30%) of the link end moment $M_{f\text{-}br}$. The axial force was obtained from the vertical force equilibrium at the brace-to-beam connection when the probable link resistances were achieved. The moment transferred from the link was shared between the brace and the outer beam with respect to their flexural rigidity. The selected HSS sections shall comply with the S16 width-to-thickness ratio limit for Class 2 sections. Table 3-4 provides the summary of the brace design. In the table, $C_{r\text{-}br}$ is the factored axial compressive resistance, and $M_{r\text{-}br}$ is the factored moment resistance of the brace. The oversized brace sections in some cases are due to two reasons: 1) the brace exterior wall dimension remained smaller than the beam flange width to avoid having relatively wide connection plates; and 2) a larger brace may be selected to reduce the frame lateral displacement demand and satisfy the link rotation limit.

Table 3-4. Summary of brace design.

Frame	Brace Section HSS	$C_{f\text{-}br}$ kN	$M_{f\text{-}br}$ kN-m	$C_{r\text{-}br}$ kN	$M_{r\text{-}br} = \varphi M_{p\text{-}br}$ kN-m	$C_{f\text{-}br} / C_{r\text{-}br} + U_1 M_{f\text{-}br} / M_{r\text{-}br}$
EBF1	152×12.7	685	0.0	1043	106	0.66
EBF2	152×12.7	676	23.8	1043	106	0.84
EBF3	152×12.7	632	20.9	861	106	0.94
EBF4	203×9.5	776	28.2	1287	159	0.74
EBF5	178×12.7	788	46.9	1625	151	0.69
EBF6	178×12.7	717	39.8	1331	151	0.74
EBF7	203×12.7	773	64.7	2089	202	0.56
EBF8	203×12.7	696	53.4	1675	202	0.59
EBF9	203×12.7	696	53.4	1675	202	0.59

The columns were selected as a continuous member over the full-frame height from available wide-flange shapes conforming to ASTM A992 Gr. 50 steel. The columns were oriented such that their web is perpendicular to the plane of the frame and sized to resist the maximum axial compression force $C_{f\text{-}c}$ induced in Tier 1 due to the gravity load plus the forces developed by the probable link resistance $1.3R_yV_r/\varphi$. An effective length factor smaller than unity was used for both in-plane and out-of-plane buckling modes to account for the effect of the distributed axial loads applied along the column height [60]. An elastic Eigen buckling analysis was performed on an isolated column under the respective axial loads applied at the column top and intermediate levels using SAP2000 [61] to obtain the effective buckling lengths of the column in-plane and out-of-plane. For instance, the buckling lengths of the column in EBF2 were set equal to $0.87h_1$, $0.8h$ and h_1 for the in-plane, out-of-plane and torsional buckling modes, respectively. The additional in-plane moment $0.2M_{p\text{-}c}$, where $M_{p\text{-}c}$ is the plastic moment capacity of the column section in the plane of the frame, prescribed by S16 for columns in multi-storey EBFs was neglected in design to isolate the influence of the moment induced in the columns due to progressive yielding of the links along the frame height or link instability. Table 3-5 summarizes the key design parameters for the columns of MT-EBFs studied. In the table, $C_{r\text{-}c}$ is the factored axial compressive resistance of the column. The selected sections satisfy the width-to-thickness ratio limits for Class 2 sections.

Table 3-5. Summary of column design.

Frame	Column Section W	$C_{f\text{-}c}$ kN	$C_{r\text{-}c}$ kN	$C_{f\text{-}c} / C_{r\text{-}c}$
EBF1	250×45	658	641	1.04
EBF2	250×45	666	641	1.04
EBF3	310×52	665	718	0.93
EBF4	250×58	777	953	0.82
EBF5	250×67	1294	1399	0.93
EBF6	250×67	1291	1358	0.95
EBF7	310×179	2413	2595	0.93
EBF8	310×179	2410	2546	0.95
EBF9	310×179	2409	2595	0.93

3.3 Analytical Model

The numerical model of the MT-EBF was developed in the *OpenSees* program [26]. The model is shown in Figure 3-3a for a two-tiered EBF with identical tiers. Several techniques have been proposed in the past to numerically simulate the nonlinear shear response of EBF link beams [53, 55, 62, 63]. Motivated by the findings of these studies, the Giuffre-Menegotto-Pinto material model was used in the current study to reproduce the Bauschinger effect as well as the kinematic and cyclic hardening of steel [64]. The input parameters of the material were calibrated, as described in Ashrafi and Imanpour [56], against the data from the cyclic coupon tests performed on CSA G40.21-350WT steel coupons loaded under an incrementally increasing strain demand in room temperature by Dehghani et al. Figure 3-3b shows an example of stress – strain response of the calibrated material model against the test data). The selected parameters of the Giuffre-Menegotto-Pinto (Steel02) material assigned to the nonlinear elements (braces, columns and outer beams) in the numerical of Figure 3-3a include $b = 0.0067$, $R_0 = 23.43$, $CR_1 = 0.891$, $CR_2 = 0.07$, $a_1 = a_3 = 0.34$; and $a_2 = a_4 = 12.1$, where b is the strain-hardening ratio, R_0, CR_1, and CR_2 are parameters to control the transition from elastic to plastic branches, and a_1-a_4 are the isotropic hardening parameters. The columns and braces were simulated using a force-based nonlinear element with fibre discretization of the cross-section. For wide-flange sections, the flange and web were discretized into 20 and 10 fibres, respectively, with five fibres through the thickness. The

webs and flanges of HSS sections were divided into 10 fibres with four fibres through the thickness [65, 66]. Past studies confirmed that this element could appropriately predict the inelastic flexural buckling response of wide-flange steel columns [67] and HSS braces under cyclic loading [68]. The capability of the selected element to predict flexural buckling of wide-flange columns in steel braced frames was verified using full-scale hybrid testing [69] and a three-dimensional finite element analysis [19]. Similar elements were used for outer beams. Residual stresses were assigned to beams and columns using the pattern proposed by Galambos and Ketter [70]. Young's modulus E = 200 GPa and yield stress F_y = 345 MPa were assumed for braces, columns, and outer beams. An elastic element combined with an inelastic spring were implemented to define the link's linear and nonlinear cyclic behaviour. The elastic element was assigned E = 200 GPa, the cross-sectional area and moment of inertia of the link section; however, the nonlinear shear force – shear deformation response of the link was simulated using the Giuffre-Menegotto-Pinto material model calibrated against data from cyclic experimental tests by Okazaki et al. [10]. The input parameters used in the *OpenSees* material to best match the cyclic inelastic response of test results are b = 0.004, R_0 = 22, CR_1 = 0.925, CR_2 = 0.15, $a_1 = a_3$ = 0.12, and $a_2 = a_4$ =9. An example of the calibration for a W250×49 link is shown in Figure 3-3c. The expected yield strength R_yF_y = 385 MPa was assigned to the link except that a reduced yield strength $0.9R_yF_y$ = 347 MPa was assigned to the first tier in the two-tiered EBF, and the first two tiers in the three- and five-tiered EBFs. The latter is expected to create tiers with the lowest storey shear resistance and trigger shear yielding in such weak tiers first. The 10% reduction in the yield strength of the link accounts for plausible material or geometric variabilities and was introduced at the bottom tiers because of their potential impact on first-tier column stability, as this column carries the largest axial compression load.

The columns were assumed to be pin-supported at their base. The frame was laterally braced at the column top ends. Lateral bracing was assigned to both ends of the roof link. The intermediate links were unbraced except for case studies presented in Section 3.6, which were selected to examine the influence of link lateral bracing. The connection between the brace and the link was assumed to be rigid in the plane of the frame (except in EBF1) and pinned in out-of-plane, whereas a pinned connection was used between the brace and column in both planes. To model the rigidity of connections, elastic elements with stiffness representing the properties of the connection and adjacent members were employed. A nonlinear rotational spring representing the stiffness and strength of the beam-to-column connection was simulated at beam ends. A corotational formulation that accounts for P-Δ effects and large deformations was selected to simulate geometric nonlinearities. To account for P-Δ effects, a leaning column was created (Figure 3-3a) using an elastic element with relatively large axial and flexural stiffness. The horizontal displacement of the leaning column at its top was constrained to that of the EBF at the roof level.

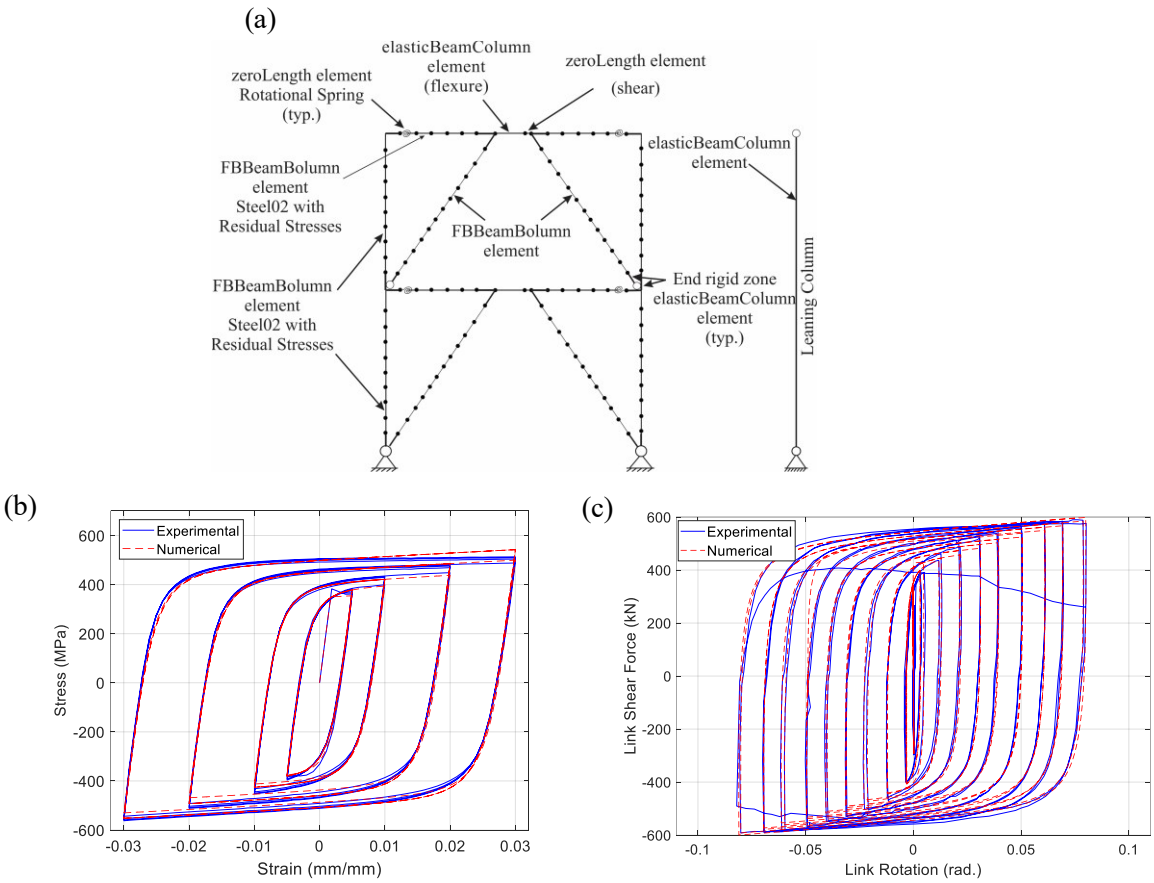

Figure 3-3. (a) MT-EBF numerical model; (b) Calibration of Giuffre-Menegotto-Pinto material model (experimental data by Dehghani et al. [71]); (c) Link hysteretic response: numerical vs. experimental (experimental data by Okazaki et al. [10]).

To reproduce the global buckling of braces, columns, and outer beams, each member was divided into ten elements [65, 66]. Initial geometric out-of-straightness was assigned to the braces, columns and outer beams. A half-sine wave with a maximum amplitude of 0.001 times the length between brace ends was considered for the braces. For the columns, bi-directional initial sinusoidal out-of-straightness corresponding to the column in-plane and out-of-plane buckling modes was assigned with a maximum amplitude of 0.001 times the length between the nodal points. The beams were assigned initial sinusoidal imperfections in-plane and out-of-plane. For in-plane buckling, a half sinewave was assigned to the length between the beam-to-column and link-to-brace connections with a maximum amplitude equal to 0.001 times the respective length; however, a half sinewave

with a maximum amplitude of 0.001 times the total length of the beam was specified in out-of-plane. Out-of-plumbness of the members were not explicitly simulated in the numerical model developed here.

Lumped masses accounting for the seismic weight of the structure were simulated at the top of the EBF columns. Mass proportional damping corresponding to 2% of critical in the structure lateral vibration mode was specified. The gravity analysis was first performed by applying the gravity loads tributary of the EBF to the top end of the braced frame columns and the remaining tributary gravity loads to the leaning column. The NLRHA was followed using the horizontal ground acceleration applied at the base of the frame.

3.4 Ground Motion Accelerations

Ground motion time histories were selected and scaled in accordance with the method prescribed by the 2015 NBCC User's Guide for Part 4 – Commentary J, Structural Commentaries [72]. The period range over which the scaling is performed ranges from 0.1s to 3.0s to cover the fundamental period of the selected frames, as shown in Table 3-1. Three scenarios were considered representing main seismic sources in Southwest British Columbia, including shallow intraplate crustal earthquakes, deep in-slab earthquakes, and subduction interplate (Cascadia) earthquakes. Using NBCC seismic hazard deaggregation for a 2% probability of exceedance in 50 years, the mean value of the magnitude and hypocentral distance (M-R) were calculated for each scenario, and a suite of 235 ground motion records was initially selected. The combination of the mean and the standard deviation values were used to filter these initial records. The records were then ranked using their respective standard deviation of $S_T(T)/S_g(T)$ over the corresponding period range where $S_T(T)$ is the target response spectrum as specified in NBCC, and $S_g(T)$ is the 5% damped pseudo-acceleration spectra of the individual ground motion component. The records with a mean value

of $S_T(T)/S_g(T)$ between 0.5 and 3.0 for crustal and Cascadia, and 0.5 and 4.6 for in-slab events were chosen from the ranked records to perform NLRHA. In total, 33 records were ultimately selected and scaled to match the modified target response spectrum. No more than three records were selected from the same event to keep the results event-independent. The scaling factor for each ground motion record is set equal to the mean value of $S_T(T)/S_g(T)$ over the corresponding period range. A second scaling factor for each suite of ground motion records was obtained, such that the mean response spectrum of each scenario suite of time histories does not fall more than 10% below $S_T(T)$ over the corresponding period range. Figure 3-4 shows for each suite the response spectrum of the scaled ground motions together with the mean spectra of the scaled records and target spectra as obtained from NBCC. Referring to Figure 3-4a, the mean spectrum of crustal records in the short period area (0.1 – 0.62 s) remain appreciably above the target spectrum despite applying selected scaling factors, because the scaling goal was set to achieve a better match at the long period area (0.62 – 1.3 s) of the crustal period range. It is deemed that this discrepancy will not affect the seismic demands induced in MT-EBFs — which act as a single-degree-of-freedom system — as the elastic fundamental period of vibration of braced frames studied here always exceed 0.62 s.

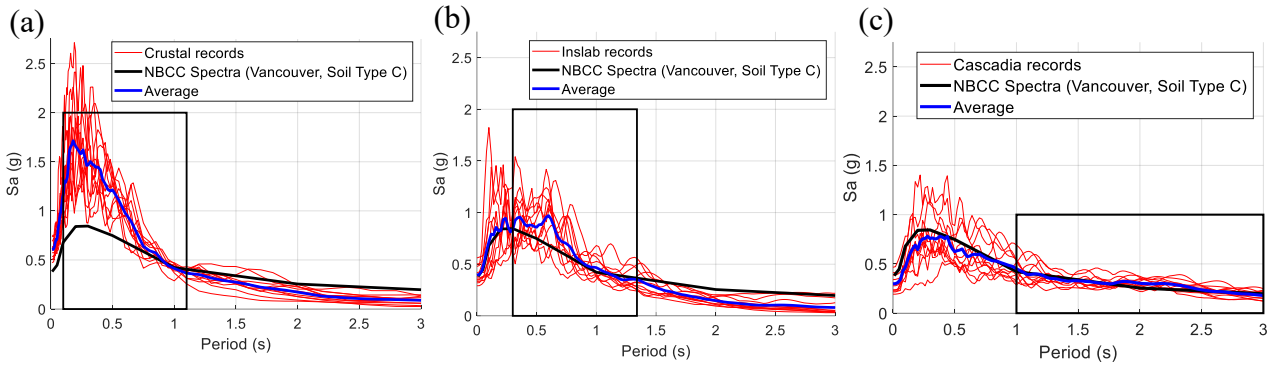

Figure 3-4. Response spectra of the scaled ground motion records:(a) Crustal; (b) In-slab; (c) Cascadia.

3.5 MT-EBF Seismic Response

NLRHA were performed to evaluate the response of the prototype frames of Figure 3-2 with an emphasis on the stability of their links and columns. The observed response for the baseline two-tiered frame (EBF1) under one of the ground motion records where link instability was observed is described first. The response of the remaining frames is then presented.

3.5.1 Single-record Case Study of Two-Tiered EBF Seismic Response

The results obtained from the NLRHA of EBF1 under 1989 Loma Prieta – Anderson Dam are illustrated here. The history of the storey and tier drifts are shown in Figure 3-5a and 3-5b, respectively. The peak storey drift is measured 1.56%h at t = 10.6 s, which is approximately 1.7 times the design storey drift. Tier drift histories show that the maximum drift takes place in Tier 1, reaching approximately 2.8%h_1 at t = 10.6 s, or nearly 1.8 times the peak storey drift, while the drift in the second tier remains below 1.0%h_2, indicating that the majority of frame nonlinear lateral deformations develop in Tier 1. Under this record, the link in the first tier yields first and delays the yielding of the link in Tier 2, which creates large inelastic shear deformations in Tier 1. This large inelastic deformation, combined with the lack of lateral bracing, led to out-of-plane buckling of the link at t = 4.9 s. The hysteretic response (i.e., shear force – shear rotation) of the links in Tiers 1 and

2 are shown in Figure 3-5c. As shown, large shear deformations develop in Tier 1 link before link buckling.

Figure 3-5d shows the history of the out-of-plane displacement of the first-tier link measured at both ends of the link. As shown, the link in Tier 1 experienced limited out-of-plane displacements at both ends until the link buckled at t = 4.9 s; the out-of-plane displacement then increased instantaneously at both ends. The link out-of-plane displacement is driven by the out-of-plane component of the brace forces acting on Tier 1 link, which itself had already moved out-of-plane because of the out-of-plane deformation of the column in compression.

Column in-plane and out-of-plane moments measured at the tier level are presented in Figure 3-5e and 3-5f, respectively, for the right-hand-side (RHS) column, which experienced the largest moment. The in-plane moment approached the plastic moment capacity of the section in weak-axis M_{py}, as a result of the non-uniform distribution of the frame lateral deformation plus link instability, which itself exacerbated the non-uniform distribution of the lateral displacement along the frame height. The out-of-plane moment induced in the strong-axis reached $0.2M_{px}$ at t = 11.1 s. This moment was caused by second-order effects in the axial compression force plus the link out-of-plane deformation, which increased significantly after link instability. At t = 7.5 s, a flexural plastic hinge formed in the RHS column at the tier level because of large in-plane and out-of-plane flexural bending in the presence of a large compression force, which finally led to out-of-plane buckling of the column. The frame deformed shape at the onset of column buckling is illustrated in Figure 3-5e. Although the column experienced in-plane moment demands, the final buckling mode involved flexural buckling in the out-of-plane direction because of the considerable out-of-plane moment induced and the fact that the column was not braced out-of-plane.

For this frame, the drift concentration in Tier 1 also imposed inelastic deformation demands on the link of this tier. Past inelastic cyclic tests on steel wide-flange links showed that such links generally fail due to web fracture under large shear deformations in the link. Such failure typically takes place at plastic link rotations varying between 0.061 to 0.12 rad [10]. Link fracture was not simulated in this study; however, in view of the large tier drift demand, it is likely that the brace connection in Tier 1 would have failed under this ground motion (Figure 3-5b), as shown in the past experimental studies [10]. Had link or connection failure been modelled, the fracture would have resulted in even higher shear force and bending on the columns and, thereby, earlier column buckling.

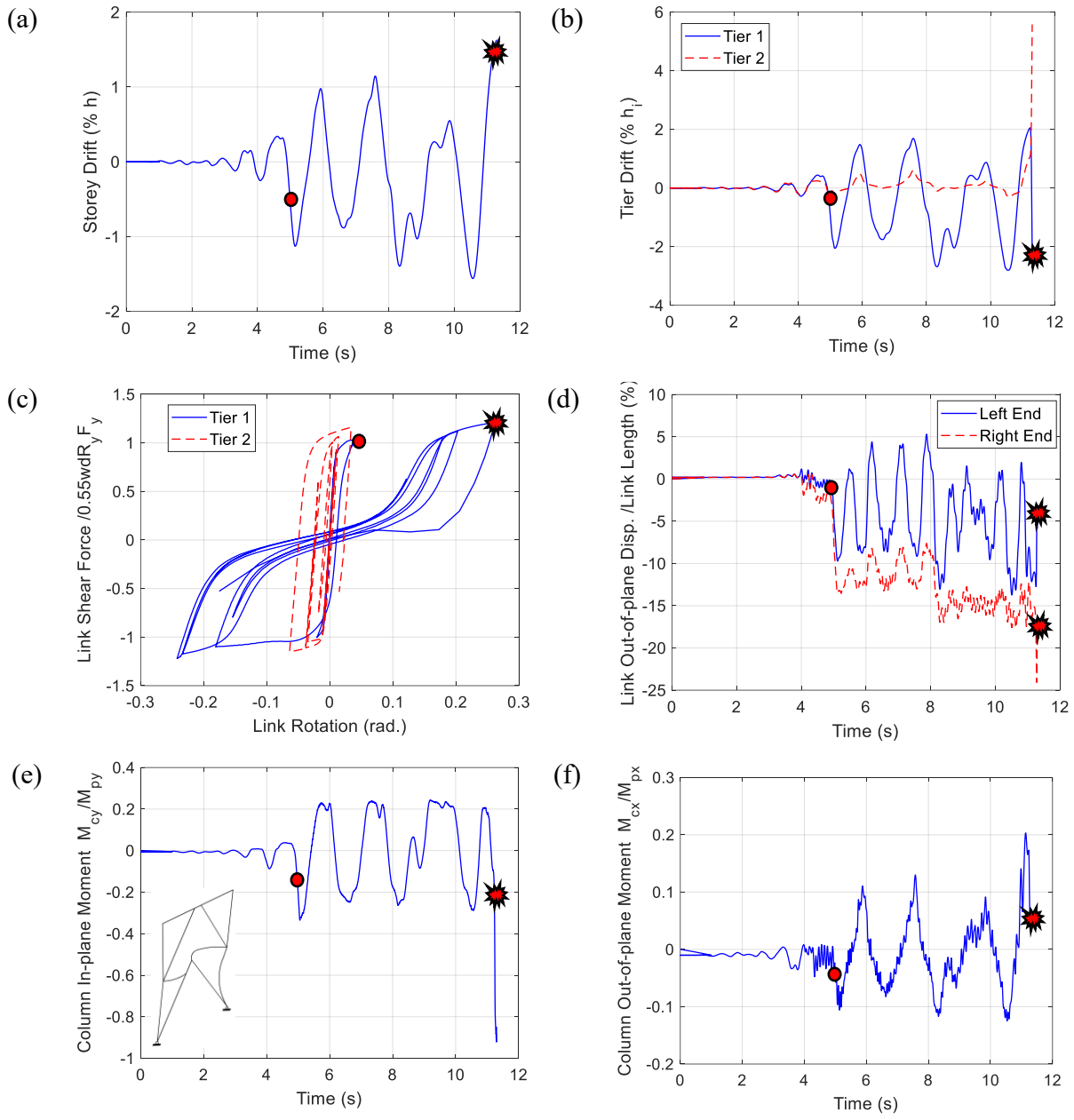

Figure 3-5. Response of two-tiered EBF under the 1989 Loma Prieta – Anderson Dam record: (a) Storey drift; (b) Tier drifts; (c) Link shear force-shear deformation in Tiers 1 and 2; (d) Link out-of-plane displacement; (e) Column in-plane moment; (f) Column out-of-plane moment and frame deformed-shape at column buckling (t = 11.3 s).

● Buckling of Tier 1 Link ✸ Column buckling

3.5.2 Parametric Study

Drift Response

The statistics of key deformation response parameters, including storey drift, tier drifts, and link deformations are given in Table 3-6. Table *3-7* summarizes the key force response parameters, link shear forces, column axial forces and moments, along with the number of cases where instability or yielding was observed in the links and columns. The statistics were computed in accordance with Commentary J of the NBCC [72] by taking the maximum of means over each earthquake ensemble for the peak response parameter. The analyses where frame collapse occurred were excluded when computing the statistics.

As shown in Table 3-6, the peak storey drift demand generally reduces when increasing the structure total height. The value reported for EBF1 is significantly larger than the other frames because of large deformations caused due to yielding and initiation of column buckling in this frame. The peak storey drift compares well to the respective design storey drift Δ for two- and three-tiered EBFs, whereas the design storey drift overestimates the frame drift in taller six-tiered EBFs.

The peak lateral displacement observed in the most critical tier where the largest inelastic deformation occurs – referred to as the critical – was divided by the respective tier height. (Figure 3-6a shows the drift profile for the frames studied. Although a higher drift was observed in the critical tier, the other tiers contributed to the lateral frame displacement as their link yielded subsequently. It is inferred that link yielding in one tier does not prevent the yielding of the other links in the frame, except when link instability occurs, which instantaneously limits the deformation in other links while exacerbating the lateral out-of-plane deformation of the buckled link. Additionally, the outer beam yielding in some cases (see Table 3-7) caused significant stiffness loss, intensifying the non-uniform distribution of lateral deformations. As shown in Figure 3-6a, for frames with the same height and different tier height ratios (EBF2 vs. EBF3,

EBF5 vs. EBF 6, and EBF7 vs. EBF 8), critical Tier 1 experiences a larger drift when the tier height ratio is increased, which can be attributed to the fact that shear yielding is delayed in the upper tiers of EBFs with a taller Tier 1; thus, Tier 1 undergoes higher nonlinear deformations. For the 12m-tall EBFs with uniform tier heights (EBFs 4&5), peak drifts in the critical tier increase when the number of tiers is increased (Figure 3-6a). Because inelastic deformations in the critical tier link are more pronounced, tier drifts resulting from a given storey drift are higher when the critical tier height is smaller.

A Drift Concentration Factor (DCF) is defined to investigate the distribution of lateral displacements over the frame height. DCF is computed by dividing the peak tier drift in the tier that experienced the largest drift by the peak storey drift. A DCF value higher than 1.0 indicates a non-uniform distribution of the lateral displacement. As shown in Table 3-6, the EBFs with non-uniform tier heights (EBFs 3, 6, 8, and 9) experienced large DCFs, which indicates a larger kink and higher in-plane bending in their columns, as will be discussed later. The DCF tends to increase in such frames as the frame height and the number of tiers increase. In contrast, smaller DCFs were observed in uniform EBFs (EBFs 2, 4, 5, and 7), which can be explained similarly to the critical tier drift.

Table 3-6. Statistics of peak deformation response parameters for MT-EBFs.

Response Parameter	EBF1	EBF2	EBF3	EBF4	EBF5	EBF6	EBF7	EBF8	EBF9
Storey drift %h	1.84 [0.99-2.49]*	0.98 [0.60-1.70]	1.03 [0.71-1.64]	0.81 [0.49-1.62]	0.93 [0.55-1.50]	1.02 [0.59-1.55]	0.94 [0.39-1.20]	0.94 [0.41-1.14]	0.91 [0.40-1.10]
Storey drift/$R_dR_o\delta_e$	1.99	1.15	1.07	0.95	0.91	0.96	0.83	0.80	0.77
DCF	1.86	1.16	1.51	1.14	1.13	1.95	1.10	2.42	2.04
$\delta_{LOut\text{-}NLRHA}/e$ %	22.92 [10.68-33.0]	4.43 [3.28-6.45]	6.32 [4.85-9.88]	2.28 [2.07-3.86]	2.09 [1.94-3.24]	4.78 [2.55-6.25]	3.00 [2.75-3.24]	3.59 [1.43-4.35]	3.27 [1.53-3.82]
γ_1 rad	0.28 [0.14-0.34]	0.11 [0.07-0.20]	0.15 [0.1-0.15]	0.09 [0.05-0.18]	0.07 [0.04-0.13]	0.15 [0.08-0.23]	0.08 [0.04-0.10]	0.18 [0.07-0.22]	0.06 [0.01-0.10]
γ_2 rad	0.08 [0.03-0.18]	0.07 [0.04-0.13]	0.01 [0.01-0.01]	0.06 [0.02-0.13]	0.07 [0.04-0.12]	0.01 [0.01-0.04]	0.07 [0.03-0.10]	0.05 [0.01-0.07]	0.14 [0.06-0.17]
γ_3 rad	-	-	-	-	0.05 [0.02-0.09]	0.01 [0.01-0.01]	0.06 [0.01-0.08]	0.01 [0.01-0.02]	0.04 [0.01-0.05]
γ_4 rad	-	-	-	-	-	-	0.06 [0.01-0.08]	0.01 [0.01-0.02]	0.01 [0.01-0.02]
γ_5 rad	-	-	-	-	-	-	0.05 [0.01-0.07]	0.01 [0.01-0.02]	0.01 [0.01-0.02]

*Values in the brackets are the minimum and maximum response parameters, respectively.

Link and Outer Beam Response

Large inelastic shear deformations in the intermediate links, combined with the lack of lateral bracing, led to the out-of-plane deformation of such links. The normalized link out-of-plane displacement, δ_{LOut}, (see Table 3-6), together with the shear force – shear deformation response, were used to identify out-of-plane buckling cases for intermediate links and link failure cases, which represents the cases where the link rotation exceeded 0.12 rad, which is set to be the limit beyond which link or connection fracture is likely based on the past experimental test programs [10]. The link instability and failure cases are reported in Table 3-7. Link instability or failure was observed in the critical tier in the majority of cases. Link out-of-plane buckling was observed due to the excessive link out-of-plane deformation and loss of link shear strength. A large out-of-plane deformation $0.23e$ was recorded for the intermediate link of EBF1 where link buckling was observed under 24 records. The comparison between link buckling cases for EBF1 and EBF2 indicates that the in-plane rigidity offered by the brace-to-beam connection in EBF2 results in lower moment demands imposed on outer beams while increasing the in-plane stiffness of the

frame, thus reducing the number of link instability cases. As shown in Table 3-6, in addition to EBF1, EBFs with non-uniform tier heights, where large critical tier drifts were observed, experienced a larger link out-of-plane displacement when compared to their uniform counterparts, which suggests that their links are more prone to instability. Links in the EBFs with identical tier heights (EBFs 2, 5, and 7), however, experienced a lower out-of-plane displacement compared to their non-uniform counterparts because a more uniform distribution of frame lateral displacement in such frames helped more uniformly distribute nonlinear deformations between links.

As shown in Figure 3-6b, the peak shear force observed for the links in EBFs with uniform tier heights approached the respective link shear resistance, which confirms that on average, link yielding occurred in all tiers and the links exhibited nearly identical strain hardening except in tall five-tiered EBF 7 where the upper tiers experienced lower strain hardening. In contrast, the links in EBFs with unequal tier heights did not experience identical strain hardening; while the link overstrength in the critical tier exceeded the anticipated value because of large link rotation developed in the link (see Table 3-6), the shear force in the non-critical tier links remained below their respective probable resistance.

The link rotation was measured and plotted in Figure 3-6c for the EBFs studied. Although link fracture was not modelled in the numerical simulations, the large rotations observed in the critical tier link of non-uniform EBFs are sufficient to cause link or connection fracture, as was observed in the past test programs [10]. The cases where an excessive link rotation (i.e., larger than 0.12 rad) was observed are reported in Table 3-7 as link failure.

Table 3-7 also presents the number of cases where flexural yielding was recorded in the outer beams that are subjected to the out-of-plane moment due to column out-of-plane displacements

combined with the tensile force and in-plane bending. It should be noted that such moments were not considered in design.

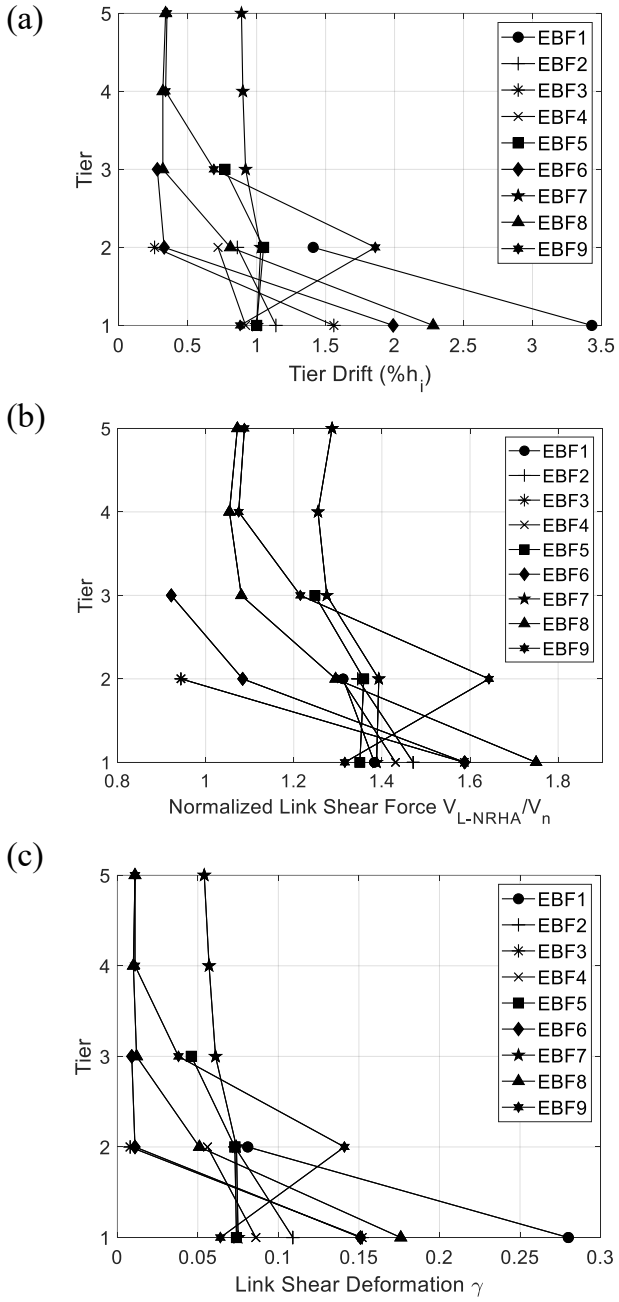

Figure 3-6. (a) Tier drifts; (b) Link shear forces; (c) Link shear deformations (links with shear deformations exceeding 0.12 rad considered fractured).

Column Response

Peak axial forces in the first-tier column segment relative to the nominal axial compressive resistance of column C_n are presented in Table 3-7. As shown, the peak demand is approximately identical in two-tiered EBFs with uniform tier heights; lower axial force ratios were observed in the EBFs with non-uniform tier heights, which is associated with non-uniform yielding of their links and the fact that lower strain hardening developed in the links of non-critical tiers.

Table 3-7. Statistics of peak force response parameters, instability and failure cases for MT-EBFs.

Response Parameter	EBF1	EBF2	EBF3	EBF4	EBF5	EBF6	EBF7	EBF8	EBF9
Link Instability / Failure	33	9	21	2	2	23	0	24	12
$(V_{L\text{-}NLRHA}/V_n)_1$	1.38 [1.25-1.42]	1.47 [1.32-1.71]	1.59 [1.44-1.88]	1.43 [1.30-1.73]	1.35 [1.25-1.53]	1.59 [1.33-1.77]	1.39 [1.19-1.46]	1.75 [1.25-1.89]	1.32 [0.97-1.41]
$(V_{L\text{-}NLRHA}/V_n)_2$	1.31 [1.19-1.35]	1.35 [1.21-1.58]	0.94 [0.85-1.13]	1.31 [1.19-1.58]	1.36 [1.25-1.54]	1.08 [0.88-1.20]	1.39 [1.18-1.46]	1.30 [0.94-1.40]	1.64 [1.26-1.74]
$(V_{L\text{-}NLRHA}/V_n)_3$	-	-	-	-	1.25 [1.15-1.42]	0.92 [0.77-1.04]	1.28 [1.11-1.34]	1.08 [0.73-1.15]	1.22 [0.92-1.29]
$(V_{L\text{-}NLRHA}/V_n)_4$	-	-	-	-	-	-	1.26 [1.07-1.32]	1.05 [0.76-1.14]	1.08 [0.78-1.15]
$(V_{L\text{-}NLRHA}/V_n)_5$	-	-	-	-	-	-	1.29 [1.10-1.35]	1.07 [0.76-1.15]	1.09 [0.82-1.16]
Beam Tension Yielding**	33	33	33	6	22	33	6	27	23
Column Instability**	8	0	0	0	0	0	0	0	0
$C_{c\text{-}NLRH}/C_n$	0.83 [0.77-0.84]	0.88 [0.82-0.98]	0.60 [0.56-0.65]	0.84 [0.79-0.97]	0.72 [0.67-0.80]	0.59 [0.52-0.64]	0.73 [0.64-0.76]	0.65 [0.47-0.69]	0.71 [0.55-0.75]
$M_{cy\text{-}NLRHA}/M_{py}$	0.88 [0.70-0.91]	0.28 [0.22-0.43]	0.62 [0.43-0.83]	0.18 [0.15-0.24]	0.22 [0.18-0.28]	0.56 [0.43-0.64]	0.10 [0.08-0.12]	0.31 [0.19-0.37]	0.36 [0.24-0.39]
$M_{cx\text{-}NLRHA}/M_{px}$	0.18 [0.08-0.25]	0.05 [0.04-0.05]	0.03 [0.02-0.05]	0.09 [0.09-0.09]	0.12 [0.11-0.12]	0.06 [0.06-0.07]	0.11 [0.08-0.13]	0.07 [0.05-0.08]	0.09 [0.05-0.09]

*Values in the brackets are the minimum and maximum response parameters, respectively.

**The number of cases is out of 33.

Statistics of the peak weak-axis in-plane moment $M_{cy\text{-}NLRHA}$ as normalized by the respective plastic moment M_{py} are given in Table 3-7, and the peak values are graphically shown in Figure 3-7a. The moment was measured at the top end of the compression-acting column segment in each tier, and the maximum value between tiers was reported for each frame. The location of the peak in-plane moment agrees with the tier where the largest lateral displacement is developed,

which creates a kink in the adjacent column segments. For instance, when comparing the in-plane bending of EBF2 vs. EBF3 and EBF5 vs. EBF6, it is found that a higher moment is induced in the columns of EBFs with unequal tier heights, due to the more pronounced non-uniform frame deformations in the frames with non-uniform tier heights. The comparison between the column in-plane moment in EBF2 and EBF4 (see Table 3-7) indicates that as the tier height increases, a smaller moment is expected in the column because a similar lateral displacement would create a smaller kink in a taller column segment (EBF 4). In general, lower in-plane bending was induced in the columns of taller frames as compared to shorter ones. As shown in Figure 3-7a, EBF1 experienced the largest in-plane bending because of large cases of link buckling, which produces a more severe non-uniform distribution of lateral deformations along the frame height.

The peak strong-axis out-of-plane moment $M_{cx\text{-}NLRHA}$, as normalized by the respective plastic moment M_{px}, was measured at the tier level for the compression-acting column. The statistics of the peak values between tiers are reported in Table 3-7, and the peak moments are graphically shown in Figure 3-7b. As shown in Table 3-6, there is a strong correlation between the number of link instability cases and the amplitude of the column out-of-plane moment. The largest out-of-plane moment was observed in EBF1 as a result of a higher number of link instabilities. Moreover, as shown in Figure 3-7b, the out-of-plane moment is more pronounced in the EBFs where the location of maximum out-of-plane imperfection was adjacent to the tier with the largest drift (EBF2 vs. EBF3, EBF5 vs. EBF6, EBF7 vs. EBF8, and EBF7 vs. EBF9) [48].

In EBF1, the combination of a high axial force with in-plane and out-of-plane moments resulted in column plastic hinging, which then led to column instability under eight records (see Table 3-7). Column yielding occurred in the tier segment where the largest link out-of-plane deformation was

observed, which triggered column instability with appreciable out-of-plane deformations due to a longer unbraced length in the out-of-plane direction and forces imposed by intermediate links. The results of the parametric studies showed that the peak in-plane and out-of-plane moments of the columns vary with the frame geometry, tier drifts, link stability response, and column flexural stiffness. Furthermore, it was found that there is a strong correlation between the occurrences of link and column buckling with link shear deformation demands and restraints provided by the brace-to-beam connection. The instabilities induced in the link and column, together with large flexural demands in the column, indicate that the instability of intermediate beams together with column moments shall be taken into consideration in the design of MT-EBFs.

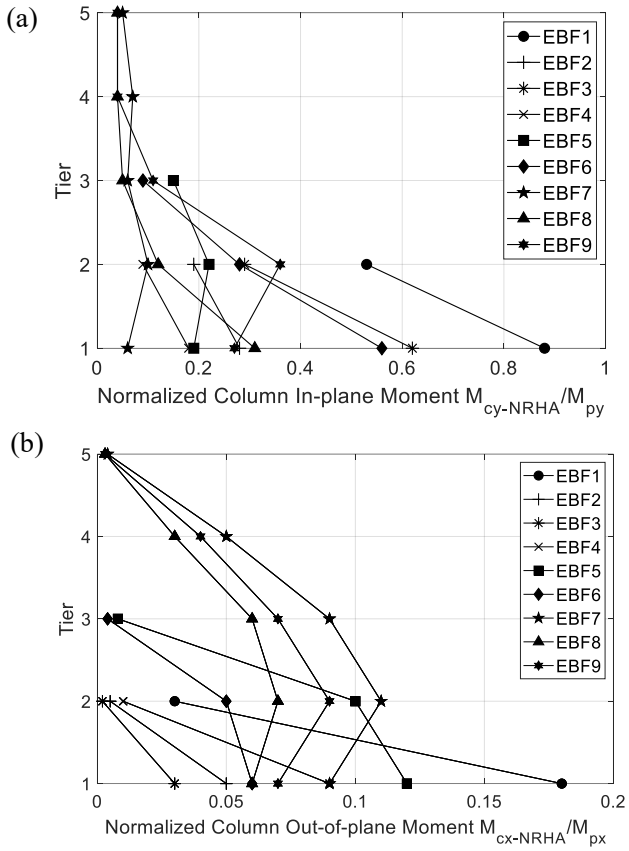

Figure 3-7. Column demands: (a) In-plane moment; (b) Out-of-plane moment.

3.6 Alternative Intermediate Link Designs

3.6.1 Intermediate Links with Lateral Out-of-plane Bracing

The effect of link lateral out-of-plane bracing on the seismic response of MT-EBFs is examined by providing nodal lateral out-of-plane braces at two ends of the intermediate link of the baseline two-tiered frame (EBF1). The NLRHA was then performed on the laterally-braced EBF1 under the same set of records used in the parametric study. The statistics of the results obtained from NLRHA were compared to those obtained from its counterpart without lateral braces, as shown in Table 3-8. The results showed that although column buckling still occurs when lateral supports are provided, the frame response has improved. No link instability occurred in braced EBF1, but the intermediate link rotation exceeded the rotation set as a failure rotation under five records. A relatively smaller critical tier drift developed in the laterally-braced frame as compared to

unbraced EBF1. Similarly, a lower DCF was found for the laterally-braced frame, which confirms a lower concentration of the frame lateral deformation. The examination of the link shear response showed that the link force exceeds the respective nominal shear resistance in all tiers of laterally-braced EBF1 without a strength loss or stiffness deterioration, as a result of concurrent link yielding, which led to a nearly uniform lateral deformation response. Several yielding cases were observed in the outer beam under the combination of flexure and tension.

Table 3-8. Statistics of peak seismic response parameters for case study frames.

Response Parameter	EBF1	EBF1-Braced	EBF1-Constrained to Columns	EBF1-Stiffer Column
Storey drift (% h)	1.84 [0.99-2.49]*	0.91 [0.48-1.28]	1.75 [0.86-2.31]	1.53 [0.62-2.09]
Storey drift/$R_dR_o\delta_e$	1.99	0.98	1.90	1.68
Critical tier drift (%h_{cr})	3.43 [1.59-4.15]	1.06 [0.54-1.94]	3.15 [1.64-4.21]	3.02 [1.05-4.12]
DCF	1.86	1.16	1.8	1.97
Beam Tension Yielding Case**	33	10	33	33
Link Instability/Failure Case**	33	5	33	32
$(V_{L\text{-}NLRHA}/V_n)_1$	1.24 [1.13-1.28]	1.64 [1.33-1.55]	1.38 [1.24-1.44]	1.36 [1.21-1.43]
$(V_{L\text{-}NLRHA}/V_n)_2$	1.31 [1.19-1.35]	1.35 [1.21-1.41]	1.31 [1.17-1.38]	1.30 [1.14-1.38]
$\delta_{Lout\text{-}NLRHA}$/e %	22.92 [10.68-33.0]	-	17.65 [10.06-23.44]	18.17 [10.33-28.04]
Column Instability Case**	9	2	11	0
$C_{c\text{-}NLRHA}/C_n$	0.83 [0.77-0.84]	0.87 [0.81-0.96]	0.82 [0.77-0.85]	0.65 [0.56-0.88]
$M_{cy\text{-}NLRHA}/M_{py}$	0.88[0.70-0.91]	0.30 [0.16-1.01]	0.86 [0.74-0.92]	0.78 [0.61-0.99]
$M_{cx\text{-}NLRHA}/M_{px}$	0.18[0.08-0.24]	0.20 [0.05-0.49]	0.79 [0.57-0.85]	0.14 [0.04-0.44]

*Values in the brackets are the minimum and maximum response parameters, respectively.
**The number of cases is out of 33.

The comparison between column moments in braced and unbraced EBF1 (Table 3-8) shows similar out-of-plane moments, because in both frames the out-of-plane component of the beam axial force (at two ends of the link), which is the main source of out-of-plane response on columns, was found to push or pull the column out-of-plane and create out-of-plane moments in the presence of initial geometric imperfections. Nonetheless, the column in-plane moment in the laterally-braced EBF1 decreased due to the more uniform tier drifts. This observation confirms that proper out-of-plane bracing shall be provided for the intermediate links of MT-EBFs and that column moments shall be considered in design even if sufficient lateral bracing is provided for intermediate links.

3.6.2 Intermediate links Designed to Resist Lateral Support Forces

The instability of the intermediate link was observed in several MT-EBF cases studied here. This confirms the need for lateral restraint against out-of-plane displacement at the ends of the intermediate link to ensure stable inelastic behaviour of the frame [7]. In multi-storey buildings, this can be achieved using a composite deck, which can provide adequate lateral bracing for the top flange of the link, along with transverse beams or direct bracing attached to the floor deck, which can brace the bottom flange of the link. Past studies, however, confirmed that short wide-flange links located between the brace end and beam-to-column connection could exhibit stable nonlinear response without lateral out-of-plane bracing as they possess adequate lateral and torsional resistance [36]. Similarly, the results of full-scale testing of EBFs showed that links with a built-up box cross-section exhibit stable seismic response with no lateral or torsional buckling [38]. The stable seismic response of box links is attributed to their large out-of-plane and torsional stiffness (i.e., larger lateral-torsional buckling resistance).

The intermediate beam of EBF1 was redesigned using the CSA S16 [3] requirement to possess sufficient lateral support strength equal to $0.06btR_yF_y$ applied as a couple at two ends of the link in order to create a torque, where b and t are the width and thickness of the link flange, respectively. This torsional moment combined with the bending moment and axial force demands developed under seismic and gravity loads were used to verify the strength of the outer beam using the method proposed by [73]. However, this approach failed to find an appropriate section due to significantly large normal stress under the warping component of the applied torque plus the axial force. An alternative approach to reduce the normal stress due to warping would employ a beam-to-column connection that can prevent warping at the beam ends. Another approach could use modular links in MT-EBFs to achieve a smaller section for the link so that

reduced demands would be applied on the outer beam due to link lateral bracing demands, easily satisfying the strength and stiffness requirements for this design approach.

3.6.3 Columns Acting as Lateral Support for Intermediate Links

The stability of intermediate beams, including links in MT-EBFs, can also be influenced by the lateral stiffness of the adjacent columns as they provide relative lateral out-of-plane stiffness to intermediate beams. To evaluate the column's strong-axis flexural stiffness on the stability response of the intermediate links, two cases were examined for EBF1: 1) lateral out-of-plane movement of the ends of the intermediate link were tied to that of the column along the intermediate beam, and 2) column strong-axis flexural stiffness was increased without lateral out-of-plane support at the intermediate link ends. The first case was selected to simulate an EBF with external intermediate beams connected to the columns, providing relative lateral bracing to the intermediate link. The second case, however, represents a typical MT-EBF with no lateral bracing at the intermediate link level but utilizing stiffer columns in the out-of-plane direction to help improve the lateral stability of the link. To achieve the second case, the columns were redesigned using the resistance specified by S16 for lateral bracing of the link as defined in Section 3.6.2. The required resistance of lateral bracing applied jointly at the top and bottom flanges was translated into a torsional moment at two ends of the link, which was then imposed on each column as strong-axis bending in out-of-plane along the intermediate beam.

Two cases were analyzed under the same set of records used in the parametric study. The statistics of NLRHA are presented in Table *3-8* for both cases. The results obtained for the first case (see EBF1-Constrained to Column) revealed that the link out-of-plane displacement was reduced when the link out-of-plane displacement was tied to that of the column, although these additional constraints imposed larger out-of-plane moments on the columns, which then led to

column instability as shown in Table 3-8. In general, no significant improvements were observed when the lateral out-of-plane movement of the link was tied to the column. The results obtained from the analysis of the case with the columns having higher flexural stiffness in the strong-axis showed that the link out-of-plane displacement is slightly reduced compared to the original EBF1. Additionally, although no column instability was observed, nearly the same number of link and outer beam failures were found compared to the original EBF1, which indicates that columns with higher strong-axis stiffness do not necessarily result in an enhanced seismic response.

3.7 Discussion and Limitations

The large deformation demands observed in the links of the prototype frames can produce high in-plane flexural moments in the link, which may result in flexural plastic hinging of the link at its ends in addition to shear yielding of the link web. To evaluate the influence of flexural yielding on the seismic response of MT-EBFs, EBF6, as one of the prototype frames, which has the largest $e/(1.6M_p/V_p) = 0.77$ – representing the frame with a link that is likely to yield in combined shear and flexure – was selected. The numerical model of Figure 3-3 was then updated to simulate the nonlinear flexural response of the intermediate and roof links in addition to the nonlinear shear behaviour originally simulated. The nonlinear flexural response of the link was reproduced using a rotational spring at each end of the link with an elastic-perfectly plastic material. The frame was then analyzed under the suite of ground motions described in Section 3.4. The statistics of the key response parameters were calculated and compared to those obtained from the model of Figure 3-3 in Table 3-9. The results obtained from the NLRHA using the refined model confirmed that including flexural plastic hinges do not have a significant impact on the frame seismic response, in particular, link and column demands. As shown in Table 3-9, the peak moment of the link in all

tiers as obtained from the NLRHA, $M_{\text{L-NLRHA}}$, normalized by the plastic moment capacity of the link M_{p} remain below one, which indicates that flexural plastic hinge did not form in the links. The reason is that flexural yielding begins first in the outer beam, which is simulated using nonlinear elements with distributed plasticity, within its fibres adjacent to the link. The propagation of yielding in the fibres of the outer beam finally led to plastic hinging under combined flexure bending and axial force at large link rotations as given in Table 3-7. The comparison between the two modelling techniques suggests that the simulation of the flexural plastic hinge in the link would provide very similar results.

Table 3-9. Statistics of peak seismic response parameters for EBF6 simulated using two modelling techniques.

	Link Modelling Technique	
Response Parameter	Nonlinear Shear Spring	Nonlinear Shear & Flexural Springs
Storey drift (% h)	1.02 [0.59-1.55]*	1.02 [0.58-1.55]
Critical tier drift (%h_{cr})	1.99 [1.05-2.96]	1.99 [1.05-2.96]
$(V_{\text{L-NLRHA}}/V_n)_1$	1.59 [1.33-1.77]	1.59 [1.33-1.77]
$(V_{\text{L-NLRHA}}/V_n)_2$	1.08 [0.88-1.20]	1.08 [0.80-1.08]
$(V_{\text{L-NLRHA}}/V_n)_3$	0.92 [0.77-1.04]	0.92 [0.77-1.04]
$\delta_{\text{LOut-NLRHA}}/e$ %	4.78 [2.55-6.25]	4.78 [2.55-5.95]
$(M_{\text{L-NLRHA}}/M_p)_1$	-	0.92 [0.81-1.00]
$(M_{\text{L-NLRHA}}/M_p)_2$	-	0.66 [0.51-0.79]
$(M_{\text{L-NLRHA}}/M_p)_3$	-	0.57 [0.48-0.64]
$C_{\text{c-NLRHA}}/C_n$	0.59 [0.52-0.64]	0.59 [0.52-0.62]
$M_{\text{cy-NLRHA}}/M_{\text{py}}$	0.56 [0.43-0.64]	0.56 [0.43-0.64]
$M_{\text{cx-NLRHA}}/M_{\text{px}}$	0.06 [0.06-0.07]	0.06 [0.06-0.08]

*Values in the brackets are the minimum and maximum response parameters, respectively.

This study focused on the evaluation of the seismic stability of links and columns in steel MT-EBFs taking into account material and geometric nonlinearities. Fractures in the link and link connections were disregarded in the numerical model developed here. Given the large shear deformations observed in the critical tier of MT-EBFs studied, the connection or link web fracture can be a limit state, which may exacerbate drift concentration and column demands. Furthermore, the instability mode associated with the link and outer beam captured using the numerical model is out-of-plane flexural buckling. Finally, the numerical model developed in this study cannot track

the complete post-buckling response of the link because of the complex stability condition of unbraced links in MT-EBFs and the interaction between the stability of the links and columns unbraced in out-of-plane. These limitations should be explored in future-related studies using a continuum finite element model.

3.8 Conclusions

This article investigates the seismic performance of steel multi-tiered eccentrically braced frames designed in accordance with the 2019 Canadian steel design standard. A nonlinear fibre-based numerical model of the frame was developed in the *OpenSees* program. The seismic response of a two-tiered EBF as a baseline frame was first presented. The seismic response of nine EBFs having different heights, number of tiers, tier relative heights, and brace-to-beam connections were then studied using NLRHA. Alternative intermediate link designs with the intention of improving the frame stability response were also examined for the baseline frame. The study focused on the stability of intermediate links and columns as well as in-plane tier drift demand and column moment demands. The key findings of this study are summarised below:

- Inelastic shear deformations of the link were concentrated in the critical tier exhibiting the lowest storey shear resistance. This behaviour was caused by uneven shear yielding that is initiated first in the critical tier. The concentration of the frame lateral deformation was more pronounced in frames with non-uniform tier heights. Additionally, drift concertation is less pronounced when the frame height increases.
- Intermediate links were prone to out-of-plane buckling as a result of significant shear yielding and lack of out-of-plane bracing in the tier level.
- Link out-of-plane buckling led to the development of large out-of-plane moment demands on the columns in the presence of column out-of-plane imperfections.

- Uneven shear yielding of the links induced relatively large in-plane bending on the columns. Such demands, in combination with an axial compression force and out-of-plane bending, led to column instability in several cases.
- Column in-plane moments were higher in frames with non-uniform tier heights. The in-plane moment reduces as the frame height increase in the frames with the same number of tiers and tier height ratio (h_1/h_2).
- Appreciable out-of-plane bending was observed in the columns of the EBFs with a more pronounced link out-of-plane deformations or a large number of instability cases and when the location of the maximum out-of-plane imperfection was adjacent to the critical tier.
- These observations indicated that frames with no lateral bracing at the intermediate beams between the tiers might experience unsatisfactory seismic response, including link instability or failure, or column buckling.
- Brace-to-beam connections changed the seismic demands on the outer beam and could significantly influence the stability of the intermediate beam. However, the effect of the connection type on the seismic performance of MT-EBFs needs to be further investigated in future studies using a more detailed finite element model.
- For the alternative intermediate link designs, the results obtained from analyses showed that link and column instability is significantly affected by providing rigid lateral support at two ends of intermediate links.
- It is inferred from the analysis of the parametric study as well as alternative intermediate link designs presented here that proper out-of-plane lateral support shall be provided for the intermediate links and that column in-plane and out-of-plane moments shall be considered in design (e.g., plastic analysis method proposed by Montuori et al. [74]). Furthermore,

intermediate links with a cross-section that has large out-of-plane flexural and torsional stiffness (e.g., HSS or built-up box sections) or intermediate links made of modular links can help improve the seismic stability of MT-EBFs.

- Enhanced seismic design provisions are required for steel MT-EBFs to properly address the observed unsatisfactory limit states while improving their seismic stability.

Future studies should investigate the seismic performance of MT-EBFs using full-scale experimental testing and continuum finite element models that explicitly account for the torsional response of the link and the rigidity of brace-to-link connections. Design recommendations should be developed for such frames, in particular, methods to laterally brace the intermediate link beams.

Chapter 4. Analysis and Design Methods for Improved Stability of Two-Tiered Steel Eccentrically Braced Frames with Continuous Wide Flange Links

4.1 Introduction

In tall single-storey buildings such as airplane hangars, chemical plants, convention centers, sports facilities, and industrial buildings, it is common to use multiple bracing panels stacked between the base and roof levels, creating a multi-tier bracing configuration. These configurations, known as steel Multi-Tiered Braced Frames (MT-BFs) are utilized when it becomes impractical or uneconomical to use only a single braced panel along the frame height. This configuration allows for smaller brace sizes, shorter braces, and practical connections while reducing the column in-plane unbraced length provided that horizontal intermediate struts are placed between tiers. MT-BFs in single-storey buildings are often placed on the exterior walls of the building and carry lateral wind and earthquake loads. They are also used in multi-storey braced frame structures with relatively tall stories compared to typical storey height (e.g., > 4 m) to accommodate large furniture or equipment or to satisfy architectural needs and to create braced bays around staircase.

While concentrically braced frames are often used in the multi-tier configuration, Multi-Tiered Eccentrically Braced Frames (MT-EBFs) present an attractive alternative, particularly in high seismic regions. MT-EBFs offers high ductility, lateral stiffness, stable and reliable yielding mechanism, e.g., shear yielding of their link beams, and architectural versatility for large openings and walkways compared to concentrically braced frames. However, providing lateral out-of-plane support to intermediate links made of I-shaped sections is not practical in the multi-tier configuration (Figure 4-1a). The absence of such bracing can lead to lateral torsional buckling (LTB) instability of the link beams located between points of out-of-plane support, e.g., base and

roof levels. This unsatisfactory response has the potential to resist the application of EBFs with the multi-tier configuration in tall single-storey buildings or tall stories of multi-storey buildings. There is a wealth of publications on the research studies conducted to evaluate the seismic performance of MT-CBFs [20, 44–46, 59, 75]. These studies primarily aimed to understand the seismic response of such frames and develop seismic design provisions within the framework of the Canadian steel design standard, CSA S16 [3] and the AISC Seismic Provisions for Structural Steel Buildings, AISC 341 [4]. These studies confirmed that inelastic lateral deformation of MT-CBFs not designed to carry additional in-plane bending is not uniformly distributed over the frame height, which can lead to significant bending on columns in the plane of the frame. If not considered in the design, the column moment demands may result in the formation of plastic hinges forming in the columns in the presence of a large axial compression force. This can ultimately lead to column instability or compromise the integrity of the frame. Additionally, large lateral deformation concentrated in the tier that yields first, i.e., the tier with the lowest storey shear resistance, can cause excessive brace deformation, which may lead to premature brace fracture [21–24].

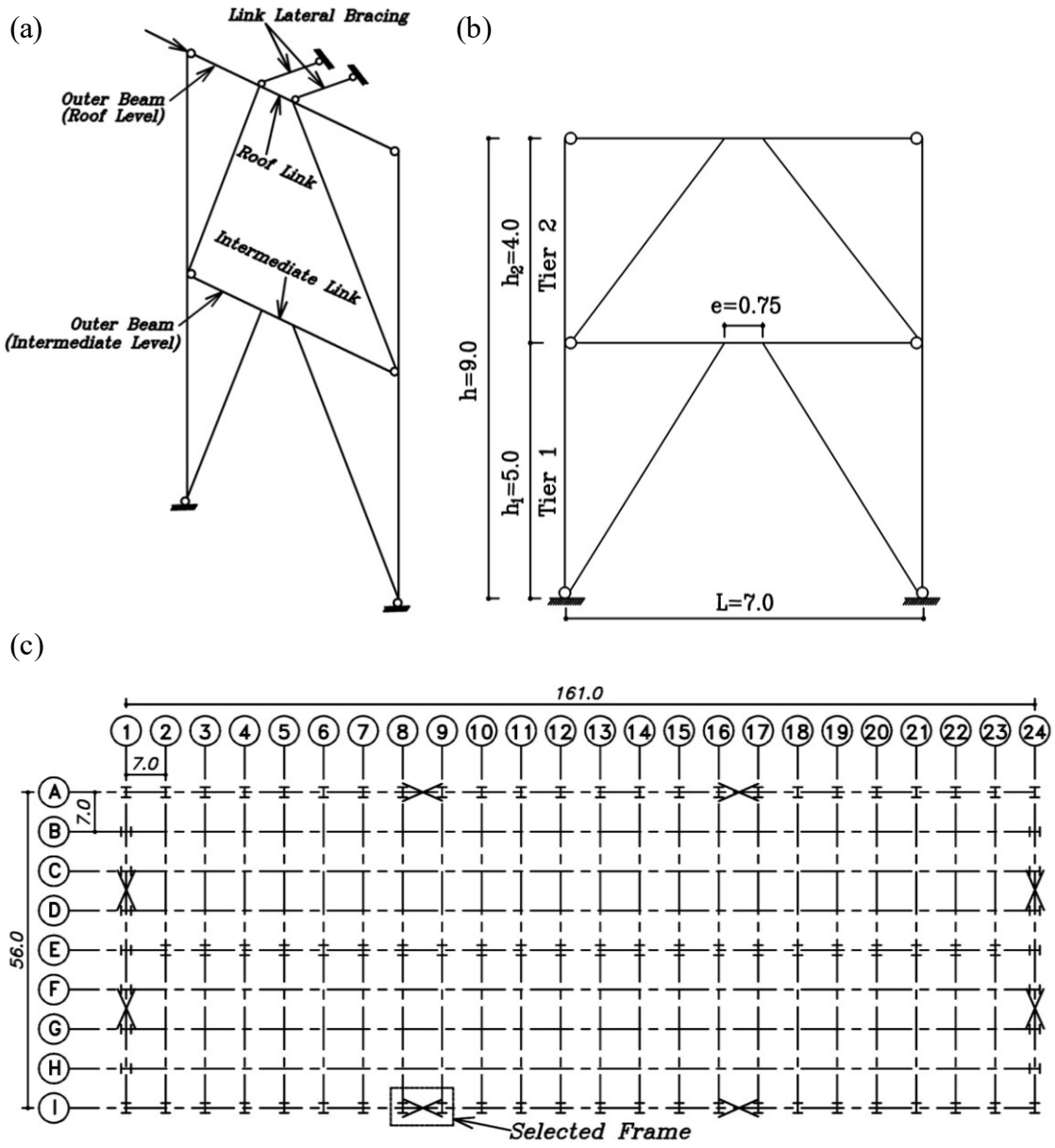

Figure 4-1. (a) Two-tiered eccentrically braced frame; (b) Frame geometry; (c) Building plan view (dimensions in m).

Although MT-CBFs have received significant research attention in the past, there is very limited information on the seismic performance and design of steel MT-EBFs. Ashrafi and Imanpour [76] studied the seismic behaviour of MT-EBFs with continuous wide-flange link beams using a fibre-based numerical model. Nonlinear response history analyses were conducted on nine frames with varying total heights (h = 9.0 – 20.5 m), number of tiers (n = 2 – 5), first-tier to second-tier height

ratio (h_1/h_2 = 1.0 – 1.6), and beam-to-column connection flexibility (fixed vs. pinned). The results confirmed that the absence of lateral bracing for intermediate links could lead to the lateral-torsional buckling (LTB) of intermediate beams, particularly when the beams are pinned at their ends. When buckling occurs in any of the intermediate beams, the response of the frame is dominated by this unsatisfactory limit state promoting uneven distribution of inelastic frame lateral deformations along the frame height and reducing rapidly the storey shear resistance provided by the link beams, which imposes relatively large in-plane shear in the columns.

Furthermore, due to the tendency of intermediate link beams to buckle out-of-plane, significant out-of-plane bending is imposed on the columns upon link buckling. Several cases of column instability were observed due to combined bi-axial bending and a large axial compression force forming flexural plastic hinging in the columns, which triggered LTB. The stability of intermediate beams is significantly improved when a rotational restraint is provided at intermediate beam ends [7].

Despite the advancement of the understanding of the seismic stability response of steel MT-EBFs using fibre-based simulations, no analysis method and design strategy is yet available to address the identified shortcomings and to ensure a stable seismic response, which itself could be the primary reason that this bracing system is prohibited in AISC 341 and is considered as a nonductile EBF in CSA S16. This chapter presents analysis and design procedures for two-tiered steel eccentrically braced frames with continuous I-shaped link beams to address unsatisfactory behaviour observed in the past studies, including link out-of-plane instability and column buckling. The methods are developed and illustrated for a prototype Ductile (Type D) MT-EBF within the framework of CSA S16. A prototype two-tiered eccentrically braced frame part of an industrial building in a high seismic area is first selected. The frame is then designed in accordance with the current CSA S16 provisions. The seismic performance of the frame is examined using nonlinear static and dynamic analyses with

an emphasis on the stability of link beams and columns. Analysis and design procedures are proposed to ensure link beams and columns remain stable under in-plane and out-of-plane demands. In addition, the proposed methods intend to prevent the concentration of inelastic demand in MT-EBF tiers. The selected prototype frame is finally redesigned based on the proposed guidelines and analyzed to verify the stability response of its intermediate link beams and columns and to assess the seismic demands induced in link beams, columns and braces.

4.2 Prototype Two-Tiered EBF

4.2.1 Configuration and Loading

A two-tiered eccentrically braced frame shown in Figure 4-1b was selected in this study. The frame acts as the lateral load-resisting system of a single-storey industrial building with dimensions plan of 161 m × 56 m (Figure 4-1c). The frame span and total height are L = 7 and h = 9 m, respectively. The total height of the frame is divided between Tiers 1 and 2 as h_1 = 5 m and h_2 = 4 m, respectively (Figure 4-1b). Unequal tier heights were intended to create a more pronounced MT-BF response. The selected building is located in Vancouver, British Columbia, Canada, on a site Class C and has four Ductile (Type D) steel EBFs in each principal direction (i.e., two braced frames per each perimeter wall) with ductility-related and overstrength-related modification factors of R_d = 4 and R_0 = 1.5, respectively.

Seismic and gravity loading was performed in accordance with the 2015 National Building Code (NBC) of Canada [25]. The roof dead load, snow load, and exterior wall weight are 1.0, 1.64, and 0.5 kPa, respectively. The total seismic weight of the building is W = 13665 kN, distributed among four braced frames in each direction. The importance factor is I_E = 1.0, and the factor accounting for the higher mode effect is M_v = 1.0. The fundamental period of the structure obtained using the NBC empirical equation is T_a = 0.23 s. The design seismic base shear calculated using the

equivalent static force procedure and a fundamental period equal to $2T_a$ as permitted by NBC is 540 kN per frame.

4.2.2 Seismic Design

The members of the prototype frame were designed in accordance with the CSA S16-19. Key design parameters are described herein; additional information regarding the seismic design of steel EBFs can be found in [77]. Identical wide-flange steel sections conforming to ASTM A992 Gr. 50 steel with F_y = 345 MPa, where F_y is the material yield strength, were selected for the links to resist the design base shear in shear assuming a shear yielding mechanism. The selected cross-sections comply with the width-to-thickness ratios corresponding to Class 2 flanges and Class 1 webs as required by CSA S16 for link beams yielding in shear. Details of selected links are presented in Table 4-1. In the table, V_f and V_r are the link factored shear force and shear resistance, respectively, w is the web thickness, d is the overall depth of the section, φ = 0.9 is the resistance factor, A_v is the shear area of the section, Z is the plastic modulus of the section about its strong-axis, and M_p is the plastic moment capacity of the section.

Table 4-1. Summary of link beam design.

Tier	Section	e mm	V_f kN	$V_r = \varphi V_p$ $=\varphi 0.55wdF_y$ kN	A_v mm^2	Z mm^3	$M_p=ZF_y$ kN-m	$3.6Z/A_v$ mm	$1.6M_p/V_p$ mm
2	W310×60	750	309	386	2262	934000	322	1486	1201
1	W310×60	750	386	386	2262	934000	322	1486	1201

Diagonal braces were chosen from square Hollow Structural Sections (HSS) conforming to ASTM A1085 Gr. C steel with F_y = 345 MPa. Braces were designed to carry in tension and compression the probable link resistance in each tier plus a portion of bending moment developed at the end of the link when it reaches its probable shear capacity. This moment was calculated based on the flexural stiffness of braces relative to that of the beam outside the link, the outer beam hereafter. Therefore, a combined axial compression force $C_{f\text{-}br}$ and an in-plane moment $M_{br\text{-}in}$ was used to

size the braces. The braces satisfied the CSA S16 width-to-thickness ratio limit for Class 2 HSSs. Table 4-2 gives a summary of the brace design. In the table, $C_{r\text{-}br}$ is the factored axial compressive resistance and $M_{r\text{-}br}$ is the factored moment resistance of the brace.

Table 4-2. Summary of brace design.

Tier	Brace section ($d \times t$)	$C_{f\text{-}br}$ kN	$M_{br\text{-}in}$ kN-m	$C_{r\text{-}br}$ kN	$M_{r\text{-}br}=\varphi M_{p\text{-}br}$ kN-m	$C_{f\text{-}br}/C_{r\text{-}br}+0.85U_1M_{f\text{-}br}/M_{r\text{-}br}$
2	HSS203×7.9	883	38	1402	136	0.74
1	HSS203×7.9	821	34	1254	136	0.76

Columns were continuous over the height of the frame and selected from wide-flange sections conforming to ASTM A992 Gr. 50 steel. Column cross-sections were oriented so that their flanges are parallel to the plane of the frame. Columns were assumed to be pinned at the base and roof levels, though torsional restraint was provided at those two locations. The effective lengths of the columns in-plane and out-of-plane were computed using eigen buckling analyses accounting for the continuity of the column and distributed axial loads along the member height, which resulted in $0.83h_1$ and $0.77h$for the in-plane and out-of-plane buckling, respectively. The columns were designed to resist an axial load produced by gravity plus the shear yielding of link beams, equal to $C_f = 693$ kN. A W200×42 column with a factored compressive resistance of $C_r = 699$ kN was selected to carry this load. The connections of the frame were designed per AISC Seismic Design Manual [78].

4.3 Finite Element Model

A three-dimensional finite element model (FEM) of the prototype frame was constructed in the ABAQUS software package [27], taking into account material and geometric nonlinearities. The model is expected to reproduce potential instability modes in the links and columns, including lateral-torsional and flexural buckling. Figure 4-2 shows the FEM of the two-tiered EBF of Figure 4-1b. Four-node reduced integration shell elements (S4R) were used for beams, braces, and columns

to achieve a reasonable trade-off between accuracy and computational efficiency. The elastic properties of steel were defined using Young's modulus E = 200 GPa and Poisson's ratio ν = 0.3. The Voce-Chaboche constitutive model, combining nonlinear isotropic hardening proposed by Voce [79] to model cyclic hardening with nonlinear kinematic hardening proposed by Chaboche et al. [80] to reproduce the Bauschinger effect, was used to define the cyclic inelastic response of steel.

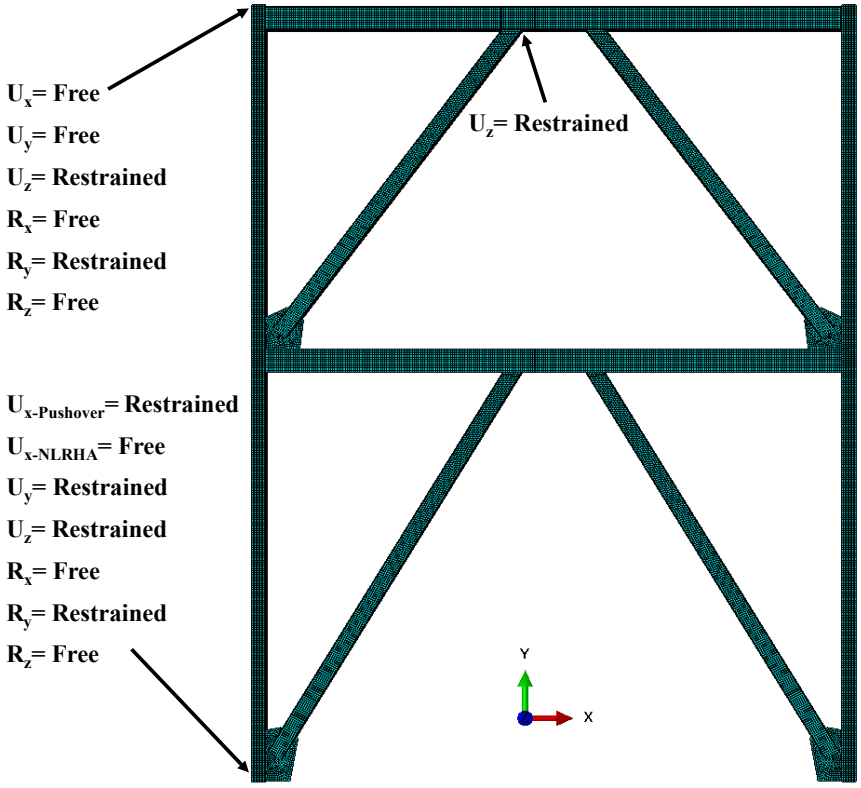

Figure 4-2. Finite element model of the two-tiered EBF (leaning column not shown; boundary conditions are symmetric for the other half of the frame).

The steel material used for wide-flange columns involved kinematic hardening parameters with two backstresses, yield stress at zero strain equal to 0.345 GPa, kinematic hardening modulus C_1 = 1.5 GPa and C_2 = 0.07 GPa, and the rate at which C decreases γ_1 = 15 and γ_2 = 20, plus cyclic hardening parameters, the maximum change in the yield surface Q_∞ = 0.14 GPa and the rate at which the yield surface changes b = 1.5. These parameters were obtained by calibrating the steel material using the

experimental test data of steel wide-flange columns [81]. Figure 4-3a shows the comparison between the normalized weak-axis moment – drift ratio from the experiment against that predicted by the numerical model developed in this study.

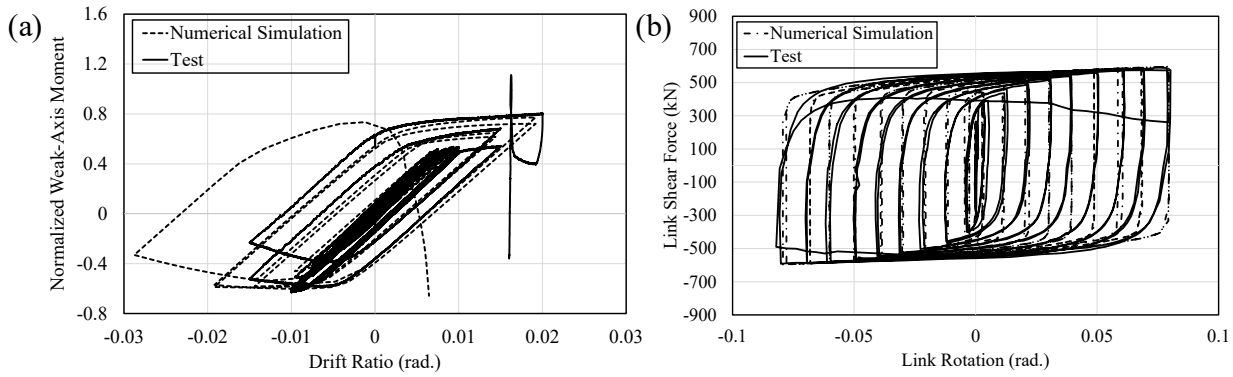

Figure 4-3. (a) Moment – drift ratio response of W250×101 column (experimental data provided by Minouei [81]); (b) Shear force – shear deformation of W250×49 link (experimental data by Okazaki et al. [10]).

Although EBF braces were designed to remain essentially elastic under design earthquake, localized plastic behaviour may occur under large deformations or when instability takes place in the frame. Hence, a constitutive model similar to that assigned to columns was used for braces with the hardening parameters proposed by Fell [82], including C_1=9.997 GPa, γ_1 =70, Q_∞=0.128 GPa, and b=6.0. The link beams were assigned the steel material with the expected yield stress $R_y F_y$= 0.385 GPa, where R_y is the ratio between the expected yield stress to nominal yield stress, and inelastic cyclic response simulated using the Voce-Chaboche constitutive model for which the cyclic and kinematic hardening parameters were calibrated using the experimental data conducted by Okazaki et. al [10], which consisted of short shear links made of wide-flange sections as those selected for the prototype frame. The parameters used to define the material model were C_1=1.1 GPa, γ_1=20, Q_∞=0.07 GPa, and b=12.0. Figure 4-3b shows the comparison of shear force – shear strain response from the W250×49 link specimen versus numerical prediction. Tie constraints were

used to connect frame members. At column bases, the column cross-section and the gusset plate were coupled to a reference point, which was fixed for translation and twist (Figure 4-2). The horizontal translation of the column bases was released only in the nonlinear response history analysis (NLRHA). The top end of the columns was restrained against out-of-plane translation and twist. The out-of-plane translation of the ends of the roof link was restrained as shown in Figure 4-2.

The beams were assigned an initial out-of-straightness in the plane of the frame following a half-sinewave pattern between beam-to-column and brace-to-beam connections with a maximum amplitude of 0.001 times the respective unbraced length. For out-of-plane buckling, initial sinusoidal out-of-straightness with an amplitude of 1/1000 of the unsupported member length was specified where the unbraced length for the intermediate strut was the length between two ends while the distance between the beam-to-column and the brace-to-beam connections was taken as the unsupported length of the roof beam. Initial imperfections pertaining to the first buckling mode of diagonals were assigned to them in-plane and out-of-plane with a maximum amplitude of 0.001 times the brace length between end connections. For the columns, initial sinusoidal out-of-straightness corresponding to their in-plane and out-of-plane buckling modes was created with a maximum amplitude of 0.001 times the tier height and total frame height, respectively. Out-of-plumbness of the members were not explicitly simulated in the numerical model developed here. The residual stress pattern proposed by Galambos and Ketter [70] was specified for wide-flange sections. A leaning column simulated using an elastic deformable wire element with a pin base was included in the model to reproduce P-Δ effects associated with the gravity system tributary to the selected two-tiered EBF. The in-plane translational degree-of-freedom of the leaning column at its top end was coupled to that of the braced frame at the roof level. The gravity loads tributary toof the

braced frame columns and the leaning column were applied at their top ends. The gravity analysis proceeded with either a nonlinear static (pushover) or dynamic response history analysis. In the pushover analysis, a monotonically increasing lateral in-plane displacement was applied to the top end of the braced frame columns until a target displacement of 297 mm, i.e., 3.3%h, was attained. The dynamic analysis was performed by applying an earthquake acceleration time history at the base of the frame in the horizontal direction. The selected ground motion record, the 2001 Geiyo – HRSH07 Japan earthquake record, produced the largest storey drift demand based on NLRHA performed under a suite of 33 ground motion records using a computationally-efficient fibre-based numerical model created in the *OpenSees* program [26]. Table 4-3 shows the statistics of the key response parameters from the NLRHA performed in *OpenSees*. Refer to Ashrafi and Imanpour [76] for the assumptions of the fibre-based model and details of the ground motion records. In the dynamic analysis, the inertia forces were reproduced by specifying two concentrated masses, each corresponding to half of the frame seismic weight at the top end of the EBF columns. The Rayleigh damping technique with mass and stiffness proportional damping ratios corresponding to 2% of critical in the structural lateral vibration mode was used to create a classical damping matrix. Nonlinear geometry formulation was activated in the analyses.

Table 4-3. Statistics of peak responses from fibre-based model of the two-tiered EBFs.

Response Parameter	Standard Two-Tiered EBF	Improved Two-Tiered EBF with W310×74 columns	Improved Two-Tiered EBF with W360×162 columns
Storey drift / $R_d R_o \Delta_e$	0.98 [0.66-1.41]	0.79 [0.44-1.12]	0.82 [0.42-1.01]
Tier 2 Drift (%)	0.59 [0.32-1.01]	0.65 [0.27-0.99]	0.73 [0.33-1.07]
Tier 1 Drift (%)	1.66 [1.15-2.28]	1.17 [0.72-1.74]	1.05 [0.62-1.47]
Tier 1 Link Inelastic Rotation	0.13 [0.09-0.18]	0.09 [0.05-0.15]	0.08 [0.04-0.12]
$\gamma_{1\text{-exp}}$ /Tier 1 Link Inelastic Rotation	-	-	0.94 [0.65-2.04]
$M_{fy\text{-}c}/M_{y\text{-NLRHA}}$	-	3.03 [2.49-3.73]	-
$M_{fx\text{-}c}/M_{x\text{-NLRHA}}$	-	1.08 [0.93-1.18]	1.03 [0.92-1.11]

*Values in the brackets are the minimum and maximum response parameters.

4.4 Seismic Response of Standard Two-Tiered EBF

4.4.1 Nonlinear Static Analysis

The lateral response and failure mechanism of the prototype frame, Standard Two-Tiered EBF, was first examined using the pushover analysis. The pushover analysis is expected to provide an insight into the lateral response and collapse mechanism of steel MT-EBFs as they behave as a single-degree-of-freedom system where the frame response is dictated by the roof displacement.

Figure 4-4a illustrates the normalized storey shear versus storey drift. Frame lateral response remained in the elastic range until the first-tier link yielded at 0.33% storey drift as shown in the link shear response in Figure 4-4b. The roof link in the second tier yielded later at a storey drift of 0.66% (Figure 4-4b) beyond which appreciable overstrength developed in the link beams (link overstrength of 1.5 and 1.4 in the first- and second-tier link beams), which contributed to increasing the frame lateral resistance. Overall, a system-level overstrength of almost 2.0 was observed at 3.0% storey drift. Referring to Figure 4-4b, the first-tier link attracted higher shear than the second-tier link due to the frame geometry. As the first-tier link underwent higher shear, it started to yield before the roof link. This response was responsible for larger inelastic deformations in the first tier compared to the

second tier because shear yielding in the second-tier link was delayed (0.33% vs. 0.66% storey drift). This delay resulted in unequal tier drifts as shown in Figure 4-4c, which presents tier drifts against storey drift. This non-uniform distribution of tier drifts created a kink in the columns, resulting in in-plane flexural bending. Figure 4-4e shows the variation of weak-axis bending in the right column normalized by the respective plastic capacity of the cross-section, M_{py}. Referring to Figure 4-4c and 4-4e, a good correlation was found between tier drifts and column moment. The moment reached its maximum value (before column buckling) when the second-tier link began to yield at 0.66% storey drift, beyond which the column demands reduced as the columns began to straighten. Although column moment demands reduced as the lateral frame displacement increased, the first-tier link experienced out-of-plane displacements as shown in Figure 4-4d, due to the lack of out-of-plane support at its ends. The link out-of-plane displacement imposed strong-axis bending in the columns, which themselves lacked out-of-plane support at the intermediate beam level where this demand is imposed. The out-of-plane displacement of the first-tier link reached $0.12e$, where e is the length of the link, at 3.1% storey drift, which formed flexural plastic hinges in the column under combined strong-axis bending and axial force as shown in Figure 4-4g. A slight increase in the frame lateral displacement led to column instability at 3.2% storey drift, which was initiated out-of-plane and then changed to LTB response due to limited in-plane bending acting in conjunction with the axial force and out-of-plane bending.

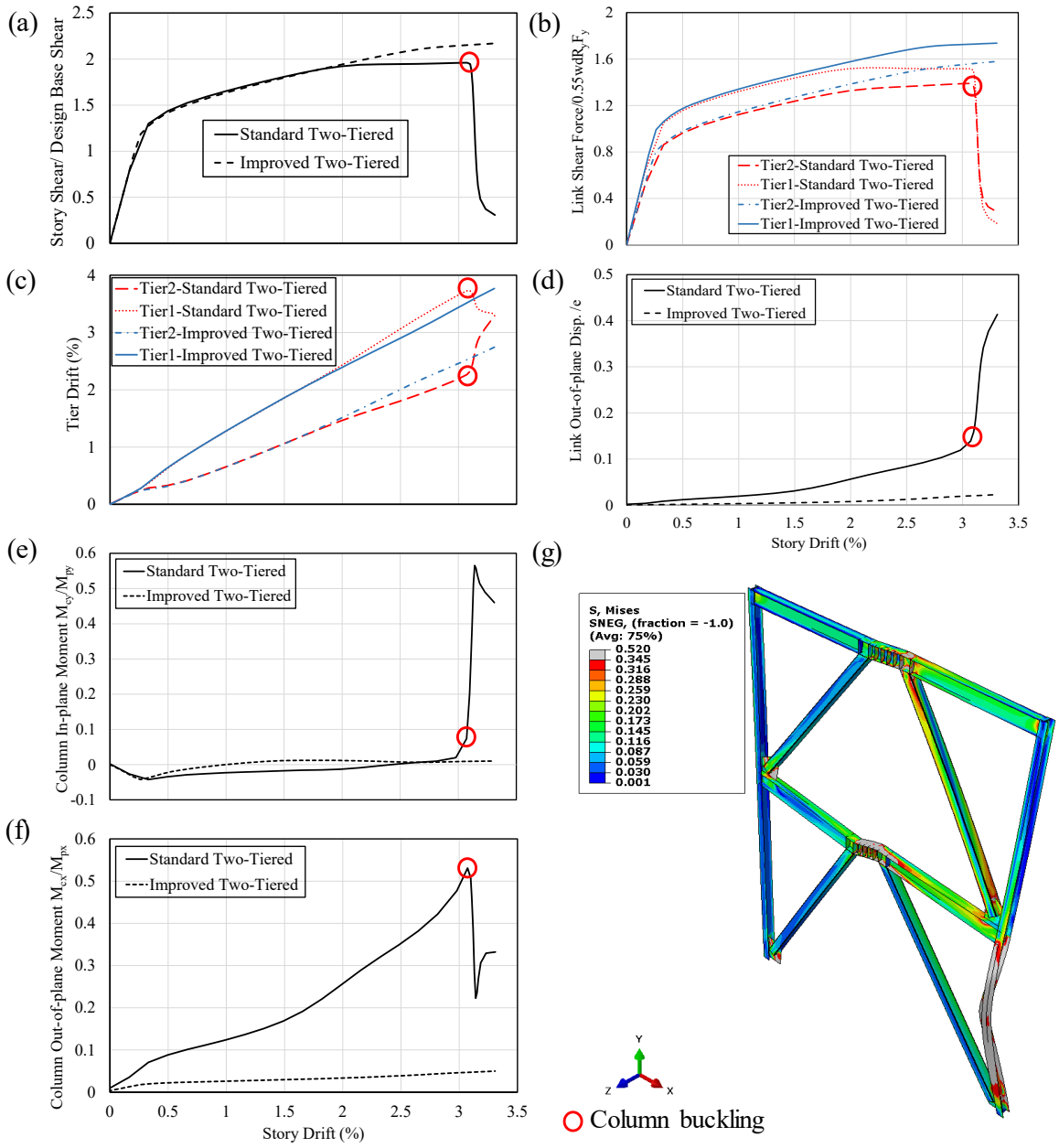

Figure 4-4. Response of two-tiered EBF from the nonlinear static analysis: (a) Storey shear vs. storey drift; (b) Link shear force vs. storey drift; (c) Tier drifts vs. storey drift; (d) Link out-of-plane displacement vs. storey drift; (e-f) Right-column in-plane and out-of-plane moment vs. storey drift; g) Frame deformed-shape and von-Mises stress (in kN/mm^2) at column buckling (3.2% storey drift).

Another important observation from the pushover analysis pertained to the rotation produced in the beam-to-column and brace-to-column connections due to shear deformation developed in the link, which resulted in in-plane bending in brace and beam ends where they meet the column at

the tier level. Such moments are ultimately transferred to the columns and should be considered in design.

4.4.2 Nonlinear Response History Analysis

The seismic response of the Standard two-tiered EBF was evaluated using the NLRHA under the 2001 Geiyo - HRSH07 Japan earthquake record using the detailed FEM developed here. Tier drifts versus the storey drift from the NLRHA are presented in Figure 4-5a. Similar to pushover analysis results, the link in the first tier yielded first and capped storey shear while the second-tier link remained elastic. The link in the roof level yielded as the frame lateral deformation increased due to strain hardening of the yielded first-tier link, which increased storey shear such that the link in the roof level started to yield. This response, i.e., delay in shear yielding of the links, produced a greater rotation in the link that yielded first (Figure 4-5b), thus resulting in uneven distribution of lateral frame deformation along the frame height when storey drift exceeded 0.5% (Figure 4-5a). Figure 4-5c shows the out-of-plane displacement of the left-end of the first-tier link versus respective tier drift. As shown, the link tends to move out-of-plane due to the lack of lateral support at its ends. This out-of-plane displacement was exacerbated as this tier underwent inelastic deformations because inelastic response, on the one hand, reduced shear, flexural and axial stiffness of the link and, on the other hand, promoted higher out-of-plane forces due to brace forces acting on this link in the presence of initial out-of-plane imperfection.

The histories of normalized in-plane and out-of-plane bending in the right column are presented in Figure 4-5d and 4-5e, respectively. Column experienced a maximum in-plane moment of $0.24M_{py}$ at t = 14.5 s, mainly due to uneven distribution of the lateral frame deformation (Figure 4-5a). Column out-of-plane bending produced by out-of-plane forces imposed by deformed first-tier outer beam acting on an imperfect column reached a peak value of $0.6M_{px}$ at t = 14.5 s (Figure 4-5e). The

combination of in-plane and out-of-plane bending formed flexural plastic hinges in the first-tier segment of the left column in the presence of a large axial force produced due to link capacities and gravity loads. Plastic hinging proceeded with column LTB at $t = 21$ s as shown in Figure 4-5f.

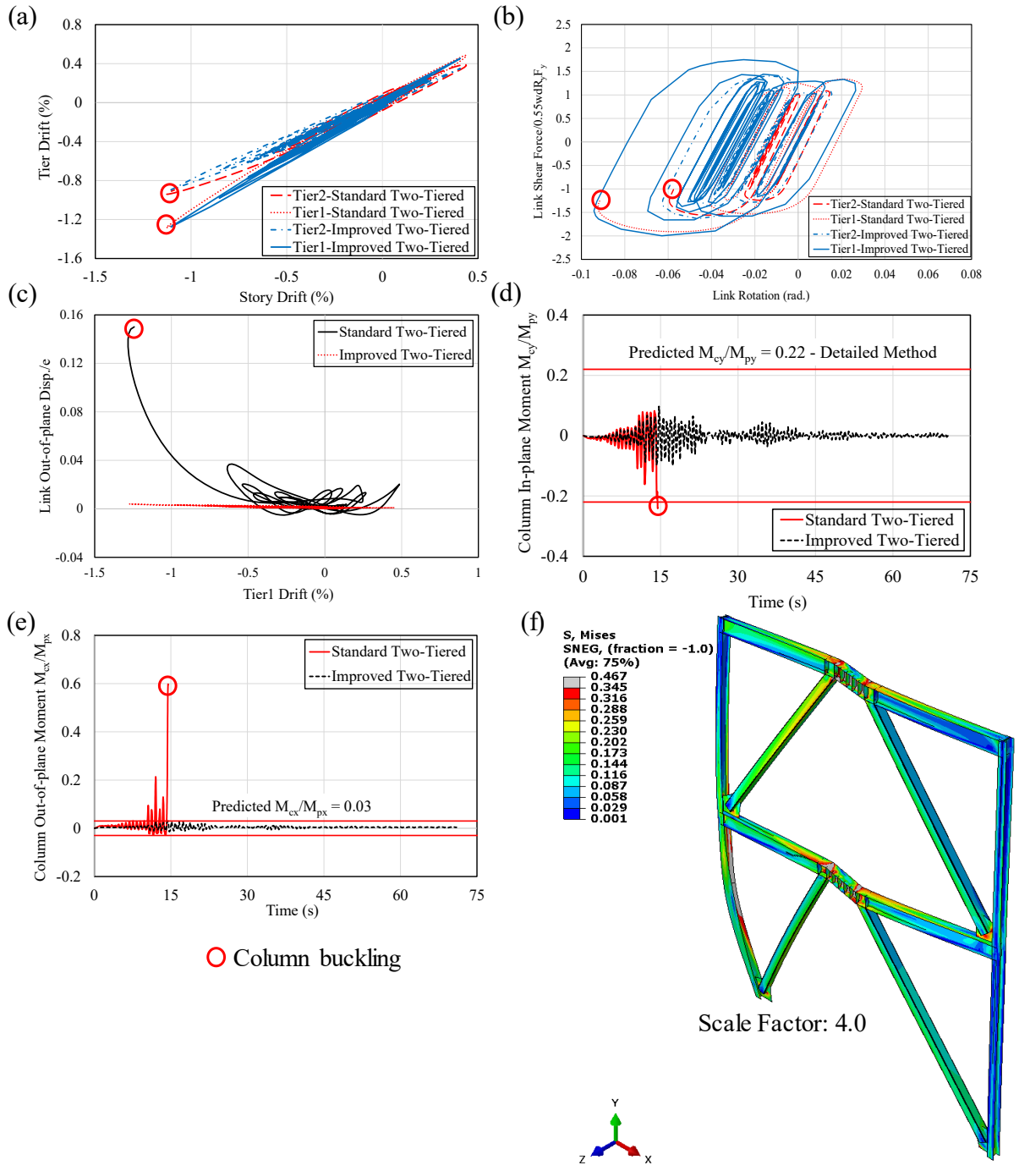

Figure 4-5. Response of two-tiered EBF from dynamic analysis under the 2001 Geiyo - HRSH07 Japan earthquake: (a) Tier drifts vs. storey drift; (b) Link shear force vs. link rotation; (c) Link out-of-plane displacement vs. Tier 1 drift; (d-e) Column in-plane and out-of-plane bending history; (f) Deformed shape and Von-Mises stress (in kN/mm^2) distribution at t = 14.5 s.

4.5 Proposed Analysis and Design Method

The results obtained from the response evaluation of a set of prototype two-tiered EBFs reported in Ashrafi and Imanpour [76] and that presented in this study confirm that delay in link shear yielding plus the lack of out-of-plane lateral support at the intermediate link level produce moments in the columns that must be accounted for in their design. Uneven distribution of lateral deformation may also lead to excessive link rotation in the link that yields first exceeding the link rotation limit. e.g., 0.08 rad for shear links. A special analysis and design method are required to address link out-of-plane buckling and column instability in two-tiered EBFs. The proposed method involves analysis and design requirements for intermediate beams, columns and link rotation, which are presented in five steps: 1) intermediate beam out-of-plane moment; 2) brace out-of-plane moment; 3) column out-of-plane moment; 4) column in-plane moment; and 5) link rotation.

Step 1: Intermediate Beam Out-of-plane Moment

Intermediate beams are designed to provide out-of-plane lateral support to diagonal braces where they meet the respective intermediate beam. The intermediate beam in each tier acts as the bracing system for the diagonal braces of of that tier and should therefore possess sufficient stiffness and strength:

$$P_b = \beta(\Delta_0 + \Delta_b)C_f / L_b \quad (4\text{-}1)$$

where P_b is the nodal lateral bracing force, Δ_0 is the initial geometric imperfection of the member being braced, Δ_b is the displacement of the bracing system under P_b, C_f is the axial load in the braced member, and L_b is the length between the lateral braces. Strength and stiffness of the intermediate beam should be adjusted under P_b as a point load in the out-of-plane direction at the end of the link, as shown in Figure 4-6, representing the force required to brace the compression-acting diagonal brace. This force creates out-of-plane bending on the outer beam and the link beam with a peak

moment of $M_{fy\text{-}b}=[P_bL_{ob}(L\text{-}L_{ob})]/L$, where L_{ob} is the length of the outer beam (Figure 4-6). Once the out-of-plane bending moment in the outer beam is determined, the link beam is verified under bi-axial bending moments using the interaction equation $(M_{fx\text{-}l}/M_{rx\text{-}l}) + (M_{fy\text{-}b}/M_{ry\text{-}l}) \leq 1.0$ where $M_{fx\text{-}l}$ and $M_{fy\text{-}b}$ are design in-plane and out-of-plane bending moments, respectively. $M_{rx\text{-}l}$ and $M_{ry\text{-}l}$ are factored strong-axis and weak-axis moment resistances, respectively. The same out-of-plane moment $M_{fy\text{-}b}$ acting on the outer beam about its weak-axis is used to verify its strength and stability in conjunction with in-plane bending and an axial compression force, as described earlier. In design, an effective length equal to the full length of the intermediate beam can be used conservatively to verify out-of-plane and LTB modes, taking into account partial yielding in the outer beam adjacent to the link when the link undergoes significant shear deformation [55]. For in-plane and torsional buckling checks, the length between the column and brace-to-beam connection should be used.

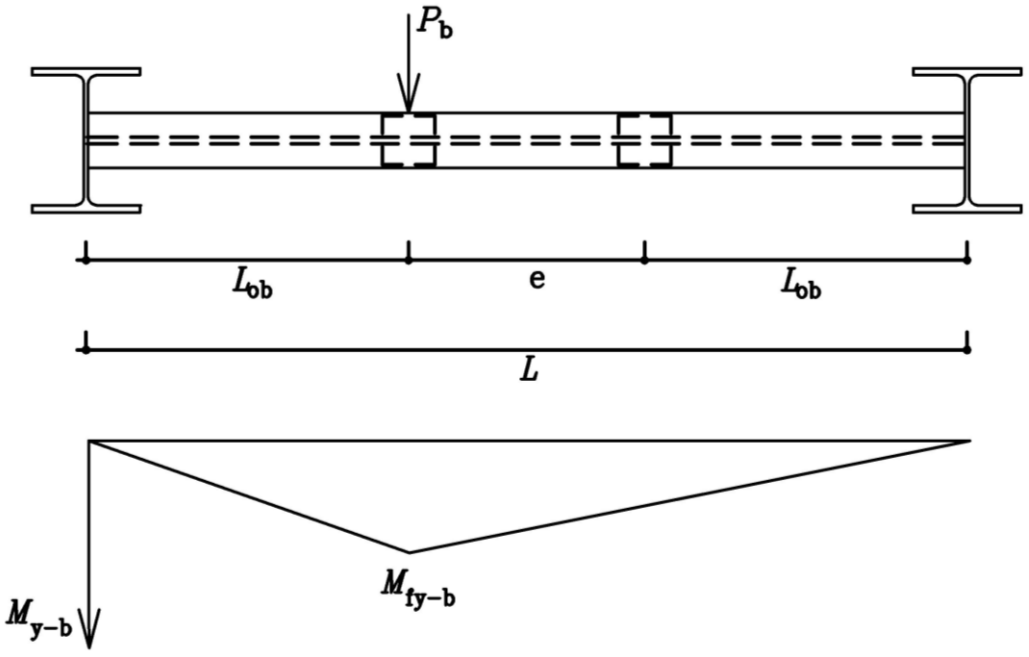

Figure 4-6. Out-of-plane moment of the intermediate beam.

Step 2: Brace Out-of-plane Moment

The diagonal braces connecting to the intermediate beam in each tier are used to brace the ends of their links torsionally. This can be achieved by moment-connecting the braces to the bottom flange of intermediate beams to torsionally brace the beam. This moment connection induces out-of-plane bending in the braces and outer beams equal to the torque T required to provide torsional bracing at each end of the link, which can be computed as a torsional moment produced by a fraction of the yielding capacity of link beam flanges:

$$T = 0.06 b_f t_f R_y F_y h_0 \quad (4\text{-}2)$$

where b_f and t_f are flange width and thickness, respectively, and h_0 is the distance between the flange centroids. The contribution of outer beams in carrying the applied torque is ignored here, and it is assumed that the torque is resisted by the braces connected to the ends of the intermediate link. Diagonal braces should therefore be designed using the P-M-M interaction equation under this out-of-plane moment in combination with in-plane bending and an axial compression force induced in the brace under link expected resistances as described earlier. It is significant to note that web stiffeners are required at the brace to intermediate beam location, along the brace flanges, to ensure both flanges of the intermediate beam are engaged under the applied torque.

Step 3: Column Out-of-plane Moment

Although multi-tiered EBF columns are not braced out-of-plane at the intermediate beam levels, they should possess sufficient strength and stiffness to provide lateral out-of-plane support to intermediate beams and diagonal braces connected to these beams (Figure 4-7a). The larger of the nodal bracing forces computed using Eq. (4-1) to brace the intermediate beam and Tier 1 braces at the intermediate beam level is applied as a concentrated out-of-plane load on the column (Figure 4-7b) creating strong-axis bending, which reaches its maximum value at the intermediate beam level and is estimated as $M_{fx\text{-}c} = P_b h_1 h_2 / h$ (Figure 4-7c). The reason that the larger of beam and

brace bracing forces is considered in design is that either the Tier 1 outer beam adjacent to the column under consideration or one of Tier 1 braces is in compression and imposes out-of-plane demands on the column.

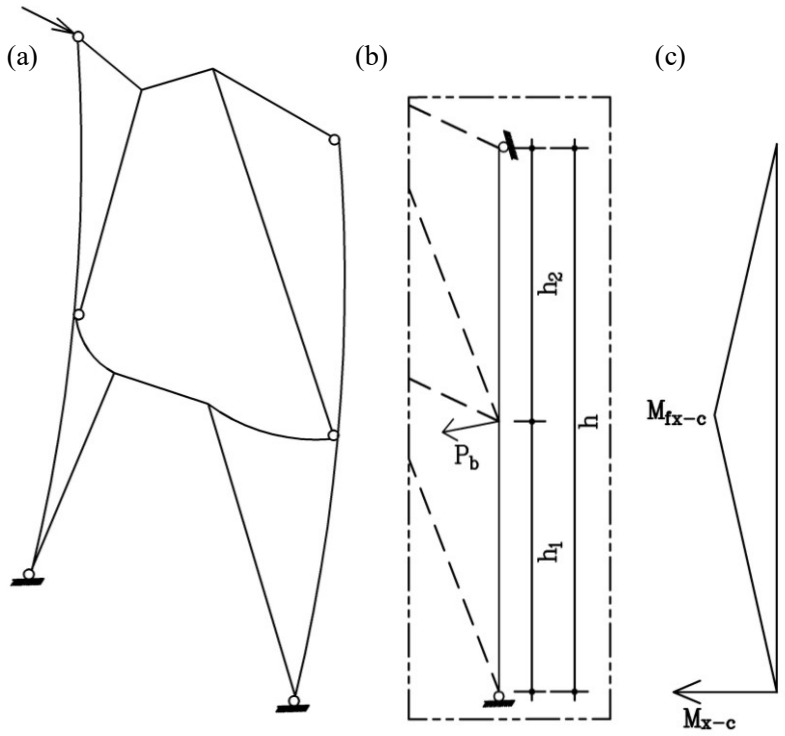

Figure 4-7. Column out-of-plane demand: (a) Frame deformed shape with excessive out-of-plane deformation of the intermediate beam; (b) Out-of-plane demand generated on the column due to link and brace out-of-plane response; (c) Column out-of-plane moment.

Step 4: Column In-plane Moment

In-plane bending is imposed in the columns of two-tiered EBFs due to the sequential yielding of links starting from the tier with the highest design shear to shear resistance ratio or critical tier hereafter (e.g., Tier 1 link in the prototype frame here). The moment is expected to peak when link shear yielding is triggered in the tier that yields after significant plastic deformation is developed in the critical tier. Furthermore, the detailed finite element analysis performed here showed that column in-plane moment demands highly depend on the rigidity of beam-to-column and brace-to-column connections. Two approaches, including (a) *detailed method* and (b) *simplified method*, are proposed

here to predict column in-plane bending demands in view of the observations from the analysis of Standard Two-Tired EBF. In the first method, the flexural stiffness of beam-to-column and brace-to-column connections are explicitly accounted for in determining column moment, whereas the second approach neglects the beneficial effects of these connections on column demands resulting in a conservative, yet simplified moment prediction compared to the first method. This in-plane moment in combination with the out-of-plane moment calculated above and the axial force described in Section 4.2.2 is used to size two-tiered EBF columns. The two methods are described below.

Detailed Method

Peak column in-plane bending is reached when the link in the roof level just yields while the link in the first tier has already yielded and gained additional shear strength. This loading condition as shown in Figure 4-8a features a shear force equal to $1.35R_yV_p$ in the first-tier link and a shear force of R_yV_p in the roof link, where V_p is the plastic shear capacity of the link $V_p = 0.55A_vF_y$ and $A_v = wd$ is the shear area of the link The link overstrength of 1.35 was taken from the experimental observation by Okazaki et al. [10] for wide-flange links yielding in shear. Once the shear strength of the links is set, the shear rotation developed at each link at the respective strength can be obtained using the relationship between the link shear force and shear deformation as schematically shown in Figure 4-8a. Referring to this figure, the rotation in the first tier link γ_1 when its force reaches $1.35R_yV_p$, is computed using Eq. (4-3) and that of the second link γ_2 when this link just yielded is calculated using Eq. (4-4):

$$\gamma_1 = \frac{53}{3}\frac{R_yV_p}{GA_v} \tag{4-3}$$

$$\gamma_2 = \frac{R_yV_p}{GA_v} \tag{4-4}$$

Knowing the shear rotation of the links and frame geometry, the drift ratio of each tier θ_i (i = 1 and 2) can be approximated as $\theta_i = \gamma_i e/L$ as shown in Figure 4-8b. Tier drift ratios θ_i computed for a two-tiered EBF would always be unequal even if tier heights are the same because of the delay in yielding of the links [76].

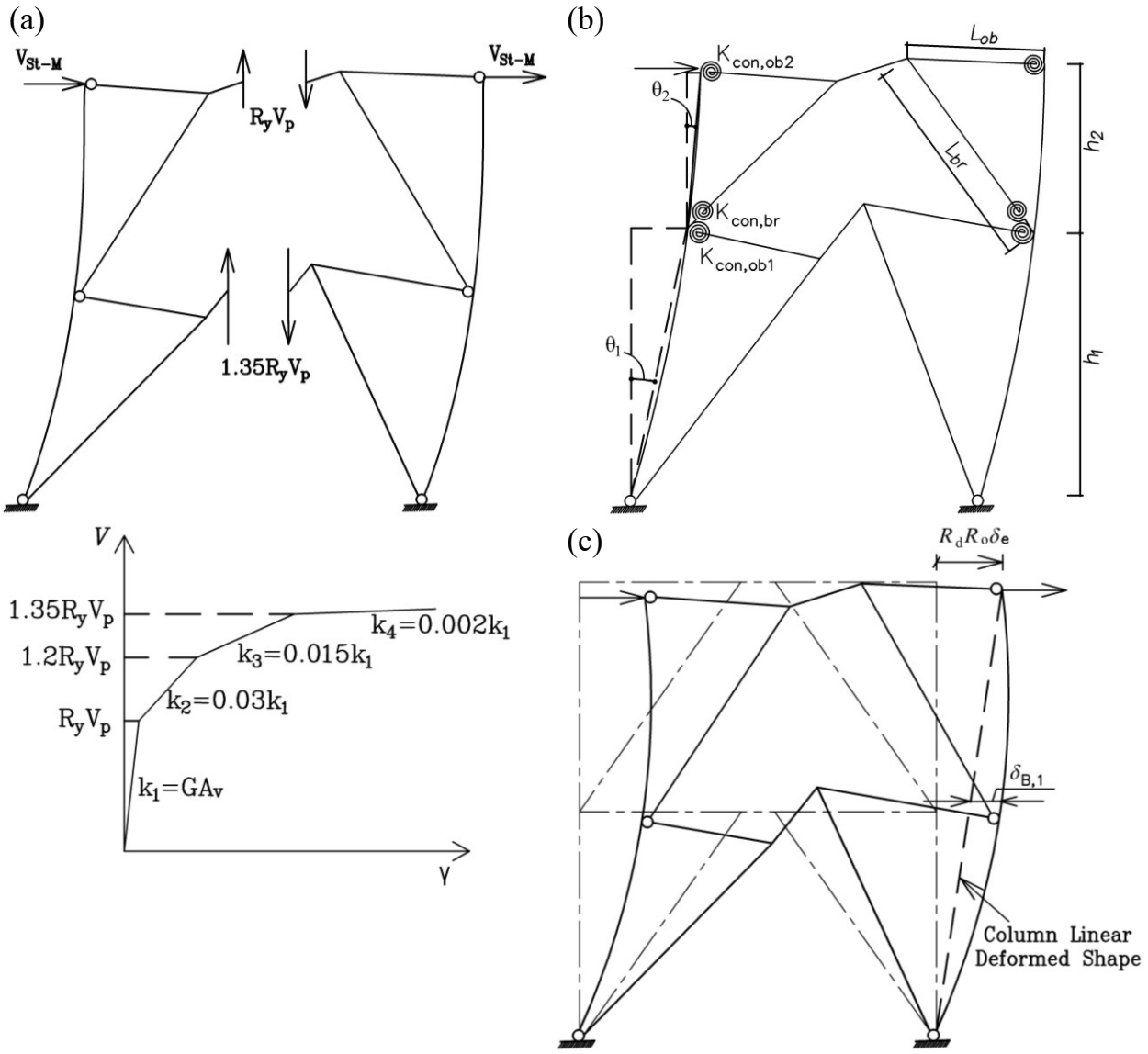

Figure 4-8. (a) Free-body diagram of the frame at the maximum column moment and link shear force – shear deformation response (adopted from Koboevic et al. [55]); (b) Two-tiered EBF deformed shape at peak column in-plane bending; (c) Lateral deformation profile at design storey drift.

Differential tier drifts create bending in the outer beams, braces, and columns. The moments in the outer beam and braces are quantified using the rotational stiffness of the respective elements (i.e., the intermediate outer beam, brace, and adjacent column) meeting in the joint where the peak column moment occurs taking into account the flexural stiffness provided by their end connections (Figure 4-8b). Flexural stiffness of the outer beam in Tier 1 $K_{con,ob1}$ and the brace $K_{con,br}$ are obtained from the experimental test program by Stoakes and Fahnestock [83] as follows:

$$K_{con,ob1}=10.6\,(EI_{x\text{-}ob}/L_{ob}) \tag{4-5}$$

$$K_{con,br}=10.6\,(EI_{x\text{-}br}/L_{br}) \tag{4-6}$$

where L_{br} is the length of the diagonal brace in Tier 1, $I_{x\text{-}ob}$ and $I_{x\text{-}br}$ are the strong-axis moment of inertia of the beam and the brace, respectively. Flexural stiffness of the outer beam in the roof level $K_{con,ob2}$ is adopted from the experimental test data reported by Liu and Astaneh [84]:

$$K_{con,ob2}=1.3\,(EI_{x\text{-}ob}/L_{ob}) \tag{4-7}$$

where L_{ob} is the outer beam length. Using flexural stiffness of springs, modified stiffness of the outer beam K_{ob}, brace K_{br}, top column segment K_{tc}, and bottom column segment K_{bc} are found as follows:

$$K_{ob}=\frac{K_{con,ob1}(3EI_{x\text{-}ob}/L_{ob})}{K_{con,ob1}+(3EI_{x\text{-}ob}/L_{ob})}=2.34\,(EI_{x\text{-}ob}/L_{ob}) \tag{4-8}$$

$$K_{br}=\frac{K_{con,br}(4EI_{x\text{-}br}/L_{br})}{K_{con,br}+(4EI_{x\text{-}br}/L_{br})}=2.9\,(EI_{x\text{-}br}/L_{br}) \tag{4-9}$$

$$K_{bc}=3EI_{y\text{-}c}/h_1 \tag{4-10}$$

$$K_{tc}=3EI_{y\text{-}c}/h_2 \tag{4-11}$$

in which $I_{y\text{-}c}$ is the weak-axis moment of inertia of the column. Once the stiffness values are computed, in-plane moments of the outer beam and brace are determined, assuming that these elements remain elastic before the frame reaches its expected storey drift:

$$M_{ob} = K_{ob}(\theta_1 - \theta_2) \quad (4\text{-}12)$$

$$M_{br} = K_{br}(\theta_1 - \theta_2) \quad (4\text{-}13)$$

The in-plane moments imposed on top and bottom segments of the column are therefore obtained by taking the difference between the moment induced in the outer beam and that imposed in the brace, $M_c = M_{ob} - M_{br}$, and distributing between the top and bottom column segments based on their respective flexural stiffness:

$$M_{fy\text{-}bc} = (K_{bc}/(K_{bc}+K_{tc}))M_c \quad (4\text{-}14)$$

$$M_{fy\text{-}tc} = (K_{tc}/(K_{bc}+K_{tc}))M_c \quad (4\text{-}15)$$

The in-plane moment induced in each column segment in combination with the out-of-plane moment resulting from brace or beam bracing as described in Step 3 and an axial compression force due to gravity loads plus link capacities are used to redesign two-tiered EBF columns using the P-M-M interaction equation. It should be noted that the bending and axial force demands represent the peak values experienced by columns before the design storey drift is reached and do not occur concomitantly, but this approach yields a conservative estimate of column demands in design.

Simplified Method

An alternative simplified approach to obtain the column peak in-plane moment is presented here. This approach neglects the beneficial effects of beam-to-column and brace-to-column connections, assuming those connections are pinned. This assumption allows computing column moments only using link probable resistances as shown in Figure 4-8a. Similar to the detailed method, the peak column in-plane moment is determined when the link resistance in Tier 1 reached $1.35R_yV_p$, and the second-tier link just attained its yielding capacity R_yV_p. From moment equilibrium at the base of the left column, storey shear resistance when the peak column in-plane moment is attained $V_{St\text{-}M}$ is obtained:

$$V_{\text{St-M}} = (1.35R_{\text{y}}V_{\text{p}}+R_{\text{y}}V_{\text{p}})(L/2h) \quad (4\text{-}16)$$

Setting up force equilibrium at the brace-to-beam connection gives the axial force in the outer beam at the roof level, $P_{\text{ob,2}}$:

$$P_{\text{ob,2}} = R_{\text{y}}V_{\text{p}}((0.5\rho e+L_{\text{ob}})/h_2) \quad \text{where } \rho = \frac{EI_{\text{x-ob}}/L_{\text{ob}}}{EI_{\text{x-ob}}/L_{\text{ob}}+EI_{\text{x-br}}/L_{\text{br}}} \quad (4\text{-}17)$$

in which ρ is the ratio between the flexural stiffness of the outer beam and the sum of flexural stiffness of the outer beam and that of the brace.

Introducing Eqs. (4-16) and (4-17) in the relationship that describes column shear in the second-tier segment $V_{\text{c,2}} = P_{\text{ob,2}} - V_{\text{St-M}}$ and multiplying column shear by the height of Tier 2 gives the peak in-plane moment of the column as:

$$M_{\text{fy-c}}=R_{\text{y}}V_{\text{p}}(0.5\rho e+L_{\text{ob}}\text{-}1.175(L/h)h_2) \quad (4\text{-}18)$$

Step 5: Compute Link Rotation

The link rotation in the critical tier should be controlled to ensure that the link is not subjected to excessive inelastic deformation that may cause premature fracture in the link or its connections when a roof displacement corresponding to design storey drift $R_dR_o\delta_e$ is attained. Using the profile of the lateral deformation shown in Figure 4-8c, which involves lateral deformation due to the roof displacement and deformation due to column bending, $\delta_{B,1}$, the link rotation in Tier 1, $\gamma_{\text{1-exp}}$, is computed as:

$$\gamma_{\text{1-exp}}=\frac{L}{(R_{\text{d}}R_{\text{o}}/4)e}\left[\frac{R_{\text{d}}R_{\text{o}}\delta_{\text{e}}}{h}+\frac{V'_{\text{c,1}}h_1\ h_2}{3EI_{\text{y-c}}}\right] \quad (4\text{-}19)$$

where $V'_{\text{c,1}}$ is the shear force in the first-tier column segment when the frame reaches $R_{\text{d}}R_{\text{o}}\delta_{\text{e}}$ and is computed as $V'_{\text{c,1}} = M'_{\text{y-c}}/h_1$ where $M'_{\text{y-c}}$ is the column in-plane moment at the intermediate beam level computed following the steps described in the simplified method assuming a link shear of $1.35R_{\text{y}}V_{\text{p}}$ in the critical tier and $0.85\times1.35R_{\text{y}}V_{\text{p}} = 1.15R_{\text{y}}V_{\text{p}}$ in the other tier. The link shear capacities

at expected storey drift proposed here are the average values obtained from NLRHA of two-tiered EBFs with I-shaped link beams.

4.6 Design Example

The prototype two-tiered EBF is redesigned in this section to demonstrate the proposed analysis and design requirements. This frame is referred to as Improved Two-Tiered EBF. The links are first designed under the design seismic base shear plus an out-of-plane bending moment due to out-of-plane lateral bracing forces at the brace-to-beam connections. Nevertheless, it is unlikely that the additional out-of-plane moment would change the link selection when shear yielding dominates the link response. It is recommended that the intermediate and roof beams are specified from the same heat to reduce the effect of material variability on link overstrength, thus promoting sequential yielding of the links. Once the links are sized, the remaining elements of the frame, including braces, intermediate beams, and columns, are designed or verified following the proposed requirements. Finally, the link rotation in the critical tier (Tier 1 in this example) is checked.

Step 1 (**Intermediate Beam Out-of-plane Moment):** the nodal lateral bracing force applied to the intermediate beam is determined from Eq. (4-1), assuming $\Delta_b = \Delta_0 = L/1000 = 7$ mm. Since diagonal braces carry bending in addition to an axial force, the axial compression in Eq. (4-1) is amplified to account for the influence of bending $M_{fx\text{-}b}$ on member stability by adding $M_{fx\text{-}b}/(d\text{-}t_f)$ to the existing axial force, where d is the overall depth of the section and t_f is the flange thickness. Using brace axial force and bending moment induced by the link resistance in Tier 1, an equivalent axial force of 995 kN is obtained, which is used in Eq. (4-1) to compute lateral bracing force $P_b = 4.7$ kN assuming $\beta = 2$ and Tier 1 brace length $L_{br,1} = 5896$ mm. This force is then applied out-of-plane to the intermediate beam at the brace-to-beam connection (Figure 4-6) to verify the strength and stiffness of the intermediate beam. A larger W250×73 intermediate beam with higher stiffness and strength

is finally selected to carry the applied loads. Given that the link is part of the intermediate beam, the change in the outer beam section means a new link beam in Tier 1, which will affect the seismic-induced demands on the Tier 1 braces, Tier 1 outer beam and columns. The W250×73 link will therefore be used below to verify these members. The same cross-section is used for the roof beam. Using the new link section in Tier 1 that changes the brace axial force and bending moment, the equivalent axial force is obtained as 986 kN, which gives an updated lateral bracing force of P_b = 3.3 kN using Eq. (4-1). The updated out-of-plane moment in the intermediate beam is equal to 6 kN-m. Bi-axial bending is verified in the link using the CSA S16 interaction equation with $M_{rx\text{-}l}$ = 307 kN-m and $M_{ry\text{-}l}$ = 144 kN-m. The interaction equation ratio for this check is found as 0.5.

Once the link in Tier 1 is designed, its outer beam is verified under the demands induced by the link, plus the additional out-of-plane moment calculated in this step. The summary of the intermediate beam design is given in Table 4-4.

Table 4-4. Summary of outer beam design parameters in the Improved Two-Tiered EBF.

Tier	Beam section	$C_{f\text{-}b}$ kN	$M_{fx\text{-}b}$ kN-m	$M_{fy\text{-}b}$ kN-m	$C_{r\text{-}b}$ kN	$M_{rx\text{-}b}$ kN-m	$M_{ry\text{-}b}$ kN-m	Interaction Equation*
2	W250×73	523	202	0	2877	383	144	0.63
1	W250×73	424	207	6	1261	357	144	0.86

* CSA S16 P-M-M interaction equation: $\frac{C_{f\text{-}b}}{C_{r\text{-}b}}+\frac{0.85U_{1x}M_{fx\text{-}b}}{M_{r\text{-}b}}+\frac{\beta U_{1y}M_{fy\text{-}b}}{M_{r\text{-}b}}$

Step 2 (Brace Out-of-plane Moment): the torque required to torsionally brace the two ends of the W250×73 link, designed under design base shear as described earlier, is obtained from Eq. (4-1):

T=0.06$b_f t_f R_y F_y h_0$ = 0.06×254×14.2×1.12×345×(254-14.2) =20.1 kN-m from Eq. (4-2)

The required brace out-of-plane moment is then calculated as:

$$M_{br\text{-}out}=\frac{T}{\sin\theta_1}=\frac{20.1}{\sin 58}=24 \text{ kN-m}$$

where θ_1 is the angle between first-tier braces and the horizontal plane. The selected HSS203×203×7.9 for the first-tier braces can resist the combination of $M_{\text{br-out}}$ = 24 kN-m and the demands arising from the link reaching its shear capacity, including the in-plane moment $M_{\text{br-in}}$ = 37 kN-m and axial compression force $C_{\text{f-br}}$. The summary of brace design for both tiers is provided in Table 4-5.

Table 4-5. Summary of the brace design in the Improved Two-Tiered EBF.

Tier	Brace section (d×t)	$C_{\text{f-br}}$ kN	$M_{\text{br-in}}$ kN-m	$M_{\text{br-out}}$ kN-m	$C_{\text{r-br}}$ kN	$M_{\text{r-br}}=\varphi M_{\text{p-br}}$ kN-m	$\frac{C_{\text{f-br}}}{C_{\text{r-br}}}+\frac{0.85U_1M_{\text{br-in}}}{M_{\text{r-br}}}+\frac{0.5U_1M_{\text{br-out}}}{M_{\text{r-br}}}$
2	HSS203×203×7.9	851	41	0	1393	136	0.81
1	HSS203×203×7.9	796	37	24	1254	136	0.90

* CSA S16 P-M-M interaction equation: $\frac{C_{\text{f-br}}}{C_{\text{r-br}}}+\frac{0.85U_1M_{\text{br-in}}}{M_{\text{r-br}}}+\frac{0.5U_1M_{\text{br-out}}}{M_{\text{r-br}}}$

Step 3 (Column Out-of-plane Moment): the column out-of-plane is obtained under the larger of the nodal lateral bracing forces P_b required to brace out-of-plane the compression-acting diagonal brace (P_b = 7.5 kN) and outer beam (P_b = 6.6 kN) obtained from Eq. (4-1). The resulting maximum out-of-plane bending moment on the column under P_b = 7.5 kN is 16.6 kN-m. However, when applying this force to the column, it is found that weak-axis flexural stiffness of the initial column design (W200×42) is not sufficient, and a stiffer section should be used. A larger W310×74 column is finally selected to meet the stiffness requirement for lateral bracing under P_b = 4.7 kN associated with diagonal braces while satisfying the strength and stability requirements under the out-of-plane bending moment equal to $M_{\text{fx-c}}$ = 11 kN-m plus the in-plane moment determined in Step 4 and the axial compression force induced under gravity loads plus link resistances.

Step 4 (Column In-plane Moment – Detailed Method): the link rotations when the column in-plane moment reaches its maximum, i.e., the link in the critical tier has gained significant overstrength but the link in the non-critical tier just yielded, is first calculated using Eqs. (4-3) and (4-4):

$$\gamma_1 = \frac{53}{3}\frac{R_y V_p}{GA_v} = \frac{53\times1.12\times416.4}{3\times77\times254\times8.64} = 0.048$$ from Eq. (4-3)

$$\gamma_2 = \frac{R_y V_p}{GA_v} = \frac{1.12\times416.4}{77\times254\times8.64} = 0.003$$ from Eq. (4-4)

The corresponding drift ratio for each tier is then obtained as follows:

$\theta_1 = \gamma_1 e/L = 0.048\times750/7000 = 0.0051$

$\theta_2 = \gamma_2 e/L = 0.003\times750/7000 = 0.00032$

Flexural stiffness of the outer beam, brace, and column segments are computed as:

$K_{ob} = 2.34\,EI_{x\text{-}ob}/L_{ob} = 2.34\times200\times113\times10^6/3125 = 16923$ kN-m from Eq. (4-8)

$K_{br} = 2.9\,EI_{x\text{-}br}/L_{br} = 2.9\times200\times37877060/5108 = 4308$ kN-m from Eq. (4-9)

$K_{bc} = 3\,EI_{y\text{-}c}/h_1 = 3\times200\times903\times10^4/5000 = 1084$ kN-m from Eq. (4-10)

$K_{bc} = 3\,EI_{y\text{-}c}/h_2 = 3\times200\times903\times10^4/4000 = 1355$ kN-m from Eq. (4-11)

In-plane bending moments induced in the outer beam and Tier 2 braces are:

$M_{ob} = K_{ob}(\theta_1\text{-}\theta_2) = 16923 \times (0.0051 - 0.00032) = 81$ kN-m from Eq. (4-12)

$M_{br} = K_{br}(\theta_1\text{-}\theta_2) = 4308 \times (0.0051 - 0.00032) = 21$ kN-m from Eq. (4-13)

The difference between the brace and beam bending moments is transferred to the column:

$M_c = M_{ob}\text{-}M_{br} = 81 - 21 = 60$ kN-m

The unbalanced moment is then distributed between the top and bottom column segments:

$M_{fy\text{-}bc} = (K_{bc}/(K_{bc}+K_{tc}))60 = 27$ kN-m from Eq. (4-14)

$M_{fy\text{-}tc} = (K_{tc}/(K_{bc}+K_{tc}))\times60 = 33$ kN-m from Eq. (4-15)

The columns are sized to carry the combined effect of an axial compression force, $C_{f\text{-}c}$ = 671 kN, out-of-plane moment, $M_{fx\text{-}c}$ = 11 kN-m, and in-plane moment $M_{fy\text{-}c}$ = 27 kN-m, while providing sufficient out-of-plane flexural stiffness as described in Step 3. A W310×74 column with the factored axial compression resistance of $C_{r\text{-}c}$ = 1247 kN, strong-axis moment resistance of $M_{rx\text{-}c}$ = 366 kN-m,

weak-axis moment resistance of $M_{ry\text{-}c}$ = 108 kN-m, and strong-axis moment of inertia of $I_{x\text{-}c}$ = 163×10^6 mm^4 is finally selected to meet stiffness, strength, and stability requirements. The final interaction ratio is found as 0.66, suggesting that the stiffness requirement governs the column design.

A similar approach should be used to determine column in-plane moment demand when the second tier is critical. For two-tiered EBFs with uniform tier properties or approximately equal storey shear resistances in adjacent tiers, both critical tier scenarios should be evaluated in design to account for unavoidable variations in material strength [11, 12], link cross-sectional properties [10], increase in material strength due to strain rate effects [13–18], and link connections. To account for these uncertainties, potential critical tier scenarios can be identified by varying the link resistances by a given margin, e.g., 10%.

Step 4 (Column In-plane Moment – Simplified Method): the storey shear resistance when the peak column in-plane moment develops is calculated using Eq. (4-16):

$$V_{\text{St-M}} = \frac{(1.35R_yV_p+R_yV_p)L}{2h} = \frac{(1.35\times1.12\times416.4 + 1.12\times416.4)\times7000}{2\times9000} = 426 \text{ kN} \quad \text{from Eq. (4-16)}$$

The axial force in the roof outer beam in then calculated as (using ρ = 0.85):

$P_{ob,2}$ =

$R_yV_p((0.5\rho e+L_{ob})/h_2)$ =$1.12\times416.4\times(0.5\times0.85\times750+3125)/4000 = 402$ kN from Eq. (4-17)

The shear force in the column as the difference between the storey shear resistance and the outer beam axial force $V_{c,2}$ = 402 – 426 = -24 kN is used to determine column bending moment as:

$M_{fy\text{-}c}= V_{c,2}h_2 = 24\times4 = 97$ kN-m from Eq. (4-18)

The selected column section (W310×74) using the detailed method found insufficient should the simplified method be used in the design. A W310×79 column section with an interaction ratio of 0.96 is therefore selected.

Step 5 (Link Rotation):

The inelastic link rotation in the critical tier (Tier 1) is computed as the sum of the rotation produced by the overall frame drift and that created by distortion due to column bending, which itself is caused by non-uniform distribution of inelastic lateral deformation. To determine the rotation due to column bending, the shear force in the first-tier column is first computed assuming the proposed link shear forces ($1.35R_yV_p$ in Tier 1 and $0.85\times1.35R_yV_p$ in Tier 2) using $\rho = 0.85$:

$V_{c,1}{}' = R_yV_p(0.57\rho e + 1.15L_{ob} - 1.25(Lh_2)/h)/h_1 = 6$ kN

Link rotation in Tier 1 using δ_e=17.3 mm and the weak-axis moment of inertia of the W310×74 column, $I_{y\text{-}c} = 23.4\times10^6$ mm^4, is:

$$\gamma_{1\text{-exp}} = \frac{L}{(R_dR_o/4)e}\left[\frac{R_dR_o\delta_e}{h} + \frac{V_{c,1}'h_1\ h_2}{3EI_{y\text{-}c}}\right] = 0.12 \text{ rad} \qquad \text{from Eq. (4-19)}$$

Inelastic link rotation in Tier 1 exceeds the allowable link rotation for shear links (i.e., 0.08 rad). Flexural stiffness of the columns in the plane of the frame (the second term in Eq. (4-19)) can be increased to meet the link rotation requirements. Alternatively, the designer can select larger braces to reduce the frame overall drift, which would reduce the first term in Eq. (4-19). In this example, a larger W360×162 column with a weak-axis moment of inertia of $I_{y\text{-}c}= 186\times10^6$ mm^4 is selected to provide sufficient in-plane stiffness reducing inelastic link rotation in Tier 1 to γ_1= 0.076 rad while meeting strength and stability requirements under applied gravity and seismic loads. Inelastic link rotation in Tier 2 should be verified using the same approach if the second tier becomes critical.

4.7 Seismic Response of Improved Two-Tiered EBF

4.7.1 Nonlinear Static Analysis

Nonlinear static analysis of Improved Two-tiered EBF is performed here to validate the proposed analysis and design requirements. The column section selected at the end of *Step* 4 – Detailed

Method (W310×74) was used to perform the analysis. The results of the pushover analysis of the improved frame are compared in Figure 4-4 against those obtained from the pushover analysis of Standard Two-tiered EBF. Referring to the normalized storey shear in Figure 4-4a, no strength degradation or instability was observed in the improved frame until the target storey drift of 3.3% as opposed to the standard design in which the right column buckled at 3.2% storey drift. A similar observation can be made when comparing the link shear forces in Figure 4-5b where appreciable strain hardening was recorded for both links in the improved design.

Tier drifts shown in Figure 4-4c indicate that the tiers experienced a lower drift overall, mainly because of the higher flexural stiffness of the columns of the improved frame. The limited concentration of the frame lateral deformation in the improved induced in-plane bending moment in the columns with a maximum amplitude of approximately $0.05M_{py}$ as shown in Figure 4-4e. Figure 4-4d shows the intermediate link out-of-plane displacement, which is considered as the main contributor to column out-of-plane bending. In the improved design, this displacement is limited to $0.05e$, imposing minor out-of-plane bending demands in the columns with a peak value of $0.05M_{px}$ as shown in Figure 4-4f. Overall, the lateral response of the prototype frame has improved when applying the proposed requirements.

4.7.2 Nonlinear Response History Analysis

Nonlinear time history analysis was performed on Improved Two-tiered EBF under the same ground motion record used to evaluate the seismic performance of Standard Two-tiered EBF 2001 Geiyo – HRSH07 Japan earthquake record, to first evaluate the seismic stability of the enhanced frame and validate the moment predictions by the proposed method in this study. Similar to the pushover analysis, the improved design with the column selected in *Step* 4, excluding the link rotation check (*Step* 5), was evaluated. Improved frame columns did not experience instability under this ground

motion. Figure 4-5a shows tier drifts versus storey drift. As shown, lateral frame deformation was distributed almost evenly between tiers as opposed to the standard frame, where appreciable drift developed in Tier 1. This observation is also confirmed using the stable link response referring to the link shear force – shear deformation response in Figure 4-5b. Referring to Figure 4-5a, significantly lower storey drift was observed in the improved frame compared to the original EBF, which could be attributed to stiffer columns selected for the improved frame despite excluding the link rotation check in the column design for the purpose NLRHA.

The out-of-plane displacement of the intermediate link at its left end is shown in Figure 4-5c. Thepeak displacement observed for the improved frame is approximately 0.4% of the link length, which is significantly lower than that recorded for the standard frame, promoting a more stable link shear response in the new design. The limited out-of-plane movement of the intermediate link in the improved EBF also reduced the out-of-plane flexural demand on the columns as shown in Figure 4-5e for the left column. The comparison between the design predictions for column in-plane and out-of-plane moments and peak NLRHA moments for Improved Two-tiered EBF in Figure 4-5d and 4-5e confirm that the proposed analysis and design method can properly predict in-plane ($0.2M_{py}$ from design vs. $0.1M_{py}$ from NLRHA) and out-of-plane ($0.03M_{px}$ from design vs. $0.03M_{px}$ from NLRHA) moments in the columns. Note that the prediction by the detailed method is used to compare in-plane moments. For the frame example, the in-plane moment estimated by the simplified method is equal to $0.8M_{py}$, almost eight times the peak moment from NLRHA, suggesting conservatism implicit in this method.

The computationally-efficient fibre-based numerical model of the MT-EBF described earlier was used o perform NLRHA on (*i*) Standard Two-tiered EBF, (*ii*) Improved Two-tiered EBF with W310×74 columns selected ignoring the link rotation check, and (*iii*) Improved Two-tiered EBF

with W360×162 columns selected taking into account the link rotation check under 33 seismic records scaled to match the design response spectra of the selected site [76]. Statistics of key design response parameters, including storey drift normalized by design storey drift, tier drifts, inelastic link rotation in Tier 1, design prediction normalized by the inelastic link rotation in Tier 1, design predictions (detailed method was used to estimate the in-plane moment) normalized by respective column in-plane and out-of-plane moments, are given in Table *4-3*. The peak storey drift reached the design storey drift for the standard EBF whereas in the other two frames with bigger size columns the storey drift stayed below the design storey drift. Comparing the tier drift values showed that selecting a stiffer column enforced a more uniform distribution of inelastic lateral deformation. This can be confirmed by the lower values of Tier 1 drifts and higher values for Tier 2 drifts as the column size increased. Additionally, selection of a stiffer column was effective in reducing the Tier 1 inelastic link rotation and satisfying the 0.08 rad limit adopted in design.

Referring to Table 4-3, the prediction of inelastic link rotation is acceptable for the frame with W360×162 column. Statistics of column in-plane moments confirmed that the proposed method conservatively predicts the column in-plane moments. This conservatism is largely associated with the assumptions made to determine link rotations when the peak moment in the column develops. This conservatism can be avoided if the designer access to NLRHA data for the frame under consideration. Column out-of-plane moments given in Table 4-3 indicate that the moments from the proposed method match well the NLRHA recorded in the columns.

4.8 Conclusions

This chapter proposed analysis and design requirements to improve seismic stability of two-tiered steel eccentrically braced frames with continuous wide-flange link beams. A two-tiered EBF was first designed in accordance with the CSA S16-19. The seismic response of the frame was examined

through nonlinear static and dynamic analyses. New analysis and design requirements were proposed for two-tiered EBFs in five steps. The proposed requirements were used to redesign the two-tiered EBF while demonstrating design steps. Nonlinear static and response history analyses were performed to evaluate the seismic performance of the enhanced frame and validate the proposed requirements. The key findings of this study can be summarized as follows:

- The EBF designed in accordance with CSA S16 exhibited non-uniform tier drifts, with Tier 1 attracting more drift than Tier 2, which imposed in-plane flexural bending on the columns while creating large inelastic rotation in the first-tier link. Additionally, the intermediate link beam experienced excessive out-of-plane deformation due to the lack of out-of-plane lateral bracing.
- Out-of-plane deformation of the intermediate link beam imposed out-of-plane demands on the columns and braces. Out-of-plane bending in the column combined with in-plane flexural bending and axial force demands led to column buckling.
- New analysis and design provisions, including strength, stability and stiffness requirements for the braces, intermediate beam and columns, were proposed. These requirements aim to make use of intermediate beams to limit out-of-plane deformation of diagonal braces, torsionally brace the link beam in the intermediate level using diagonal braces, make use of columns to brace the intermediate beam out-of-plane, estimate and account for in-plane bending demand of the columns due to delay in shear yielding of the links and limit inelastic link rotation.
- Two methods were proposed to predict column in-plane flexural demand. The first (detailed) method explicitly considers the influence of flexural stiffness of intermediate beam-to-column and brace-to-column connections in moment demand induced in the columns, while the second (simplified) method neglects the beneficial effect of these connections. It was confirmed that the simplified method yields a more conservative moment demand.

- Flexural stiffness of the columns in the plane of the frame was used to reduce inelastic link rotation in the tier that yields first (critical tier).
- Seismic response of the improved two-tiered EBF designed using the proposed requirements was significantly improved by limiting intermediate beam and column out-of-plane deformation, and link rotation. Furthermore, the results of NLRHA showed that column bending demands and link rotations are properly predicted using the proposed method.
- The proposed requirements indicate that out-of-plane flexural stiffness and strength of both column and intermediate beam are beneficial in improving frame response. In practice, intermediate beams with large weak-axis flexural stiffness and columns with large strong-axis flexural stiffness should be favoured.

The seismic response and design of two-tiered EBFs with continuous wide-flange links were studied here. Future studies should evaluate and propose seismic design requirements for multi-tiered EBFs with more than two tiers and multi-tiered EBFs with tubular link beams that are expected to be more beneficial for seismic stability of such frames. Experimental testing should be conducted to validate the proposed design requirements. Although the analysis and design requirements proposed in this study were presented in the context of the Canadian steel design standard, they can be adopted in the U.S. seismic design provisions for steel structures.

Chapter 5. Seismic Analysis and Design of Three- and Four-Tiered Steel Eccentrically Braced Frames with Continuous Built-up Tubular Links

5.1 Introduction

Steel multi-tiered braced frames (MT-BFs) are commonly used as the lateral load-resisting system of building structures when the storey height is large, preventing the application of diagonal braces that extend within the storey. The multi-tiered configuration divides the height of the storey into multiple braced panels stacked between the base and the roof. These frames are found in tall single-storey buildings such as industrial buildings, shopping centers and airplane hangars, or between the floor diaphragms in multi-storey buildings with tall stories (e.g., > 5m) to accommodate large equipment, pools, convention centers and hotel lobbies. Figure 5-1a shows an example of a four-tiered eccentrically braced frame in a single-storey building. The multi-tiered configuration can also be used to frame the staircase structure in multi-storey buildings and steel truss bridge piers. In building structures, the application of MT-BFs results in shorter and smaller braces and columns sizes when the intermediate beams or struts are utilized to support columns in-plane. Eccentrically braced frames (EBFs) with the multi-tiered configuration are often chosen in high seismic regions due to their high ductility capacity, stable and reliable yielding mechanism, large lateral stiffness, and architectural versatility.

Research studies in the past decade [44–47, 59, 85] have focused on multi-tiered concentrically braced frames (MT-CBFs). These studies have confirmed that bracing members in the tier with the least storey shear resistance, known as the critical tier, tend to yield and reach their post-buckling capacity before other tiers. This promotes a non-uniform distribution of frame inelastic deformation along the frame height. As a result, there are unbalanced horizontal shear forces between tiers, caused by uneven storey shear resistances contributed by braces of adjacent tiers, which impose significant

in-plane bending on the columns. The combination of in-plane moment demands and a large axial compression force in the column can lead to column instability under major seismic events. Additionally, the concentration of frame inelastic lateral deformation in the critical tier may result in excessive deformations in the braces of the critical tier, potentially leading to brace low cycle fatigue fracture. To improve the seismic stability of steel MT-CBFs, seismic analysis and design methods have been proposed for steel MT-CBFs with two [45] and more tiers [85]. These guidelines have been incorporated into the American (AISC 341 2022) [4] and Canadian (CSA S16 2019) [3] steel design standards. However, specific design requirements are yet available for steel multi-tiered eccentrically braced frames (MT-EBFs), in particular those with continuous tubular link beams, are not yet available despite their practical application.

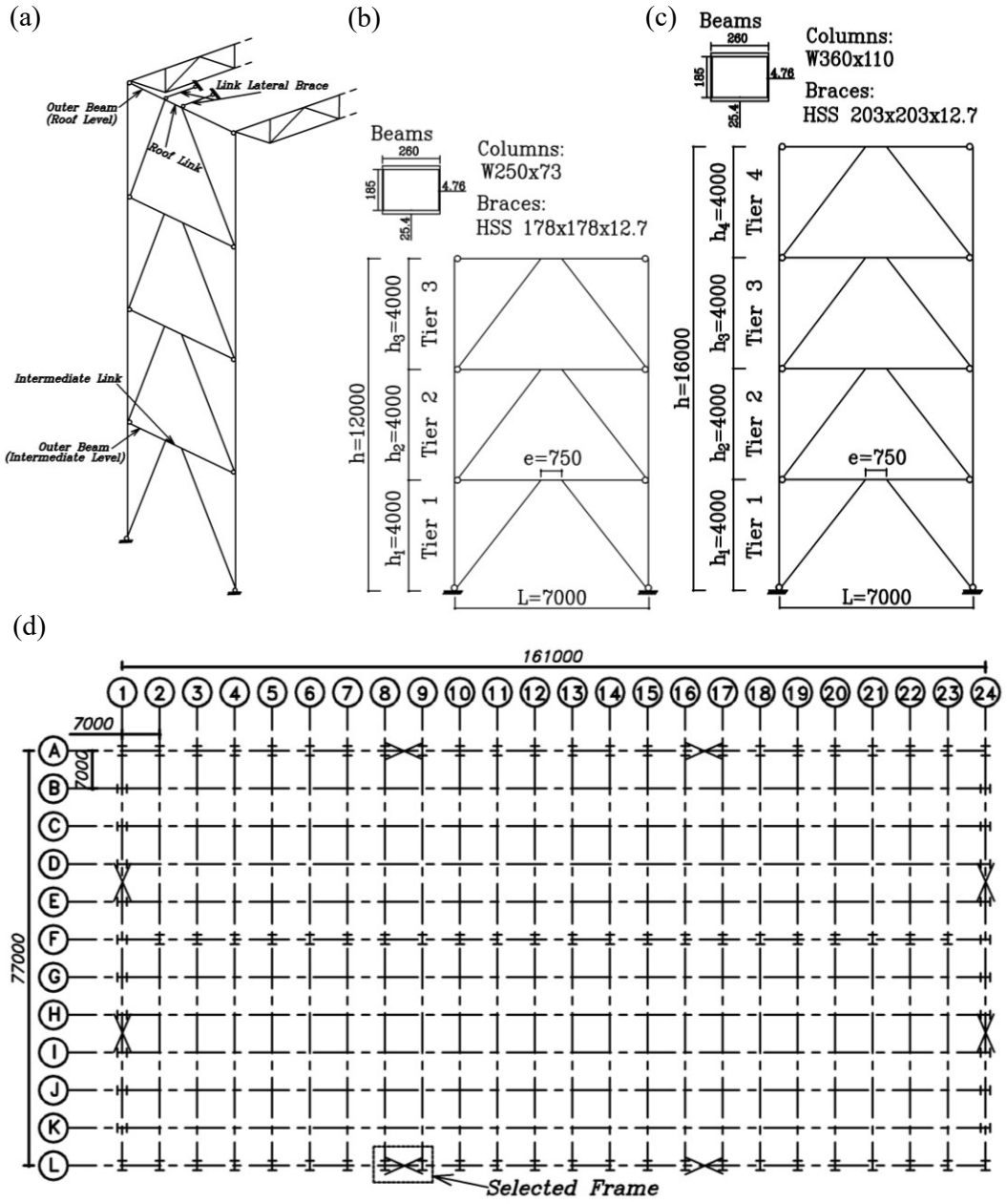

Figure 5-1. (a) Four-tiered eccentrically braced frame part of a single-storey building; (b) Prototype three-tiered eccentrically braced frame; (c) Prototype four-tiered eccentrically braced frame; (d) Building plan view (dimensions in mm).

The lateral stability of steel wide-flange link beams in EBF structures has been extensively studied in the past [5–8], resulting in stability design recommendations for the links in the multi-storey EBFs. Hjelmstad and Lee [7] examined the effect of lateral bracing on the propped cantilever beams under cyclic loads. Their findings demonstrated that beams without lateral bracing exhibited smaller

energy dissipation capacity compared to beams with lateral bracing, which necessitated the presence of lateral bracing with sufficient strength and stiffness at the link ends. Additionally, Engelhardt and Popov [8] tested long link beam specimens and observed lateral-torsional buckling due to insufficient lateral bracing. Similarly, in a study on the lateral behaviour of a three-storey EBF, Manheim [6] observed lateral torsional buckling of the beams without lateral bracing.

In MT-EBFs, providing lateral bracing for intermediate links (Figure 5-1a) is not feasible due to the absence of floor diaphragms at intermediate beam levels. This limitation negatively affects the stability of intermediate links and columns. Ashrafi and Imanpour [76] investigated the seismic response of MT-EBFs with continuous I-shaped link beams designed to yield in shear. The results confirmed that intermediate links without lateral out-of-plane support are prone to out-of-plane buckling, which can compromise the stability of columns due to relatively large induced out-of-plane bending and axial compression forces. Moreover, out-of-plane buckling of intermediate beams typically occurs in the beam with the least shear resistance, as it accumulates higher plastic strains and possesses lower out-of-plane stiffness. This response promotes an uneven distribution of frame lateral deformation along the frame height, leading to excessive rotation demands in the link beam that yields first. These large plastic rotations can cause premature fracture of the link or its connections. Furthermore, the unequal storey shear resistances contributed by MT-EBF links, due to delays in yielding, or progressive yielding of links, result in in-plane shear and moderated bending in the columns. A design method has been proposed for two-tiered eccentrically braced frames with continuous I-shaped link beams in the previous chapter. The method includes analysis and design recommendations for intermediate beams, braces, and columns of two-tiered EBFs, which have been validated using detailed finite element simulations. Past studies have confirmed that the seismic response of MT-EBFs consisting of I-shaped beams is predominately influenced by the out-of-plane

stability of their links. This has motivated design engineers to use box sections, such as welded tubular or hollow structural sections, as intermediate links. This solution effectively addresses large out-of-plane deformation and out-of-plane instability of intermediate beams in EBFs with the multi-tiered configuration. The reason behind this choice is the large torsional and out-of-plane flexural stiffness exhibited by box sections, which significantly reduces the tendency of intermediate links to develop out-of-plane instability. Berman and Bruneau [38] conducted experimental studies to examine the cyclic response of tubular links used in bridge piers, where providing lateral bracing can be challenging [30, 35]. The results of their study demonstrated the ductile and stable hysteretic response of tubular links. However, the seismic response of MT-EBFs with unbraced intermediate links made of tubular sections has not yet been examined, and there are currently no design recommendations available for such MT-EBFs.

The objective of this chapter is to investigate the seismic response of three- and four-tiered EBFs with welded tubular links and propose seismic design recommendations to enhance their stability. A prototype three-tiered EBF is initially selected and designed in accordance with the 2019 CSA S16 [3] seismic provisions for standard multi-storey EBFs. Nonlinear static and dynamic analyses are then used to evaluate the seismic response of this frame and estimate the in-plane and out-of-plane bending moments in their columns. A set of design guidelines is proposed to select intermediate beams, considering the stability response of unbraced intermediate links and the progressive yielding of links, predict the seismic demands on columns and choose appropriate column sections, and control link rotation due to the progressive yielding of the links. To demonstrate and verify the proposed method, it is finally applied to three-tiered and four-tiered prototype EBFs.

5.2 Seismic Response of Three-Tiered EBF

5.2.1 Selected Braced Frame

The seismic response of the three-tiered EBF shown in Figure 5-1b, referred to as standard three-tiered EBF hereafter, is studied using nonlinear static and dynamic analyses. In this study, the selected frame acts as the lateral load-resisting system for an industrial building with a plan dimension of 77 m × 161 m (Figure 5-1d) and a height of 12 m. There are two EBFs on each exterior wall, resulting in a total of four braced frames in each principal direction of the building. The exterior columns are spaced 7 m apart. The selected braced frame is designed in accordance with CSA S16. The structure is assumed to be located in Vancouver, British Columbia, Canada on site Class C. A ductile EBF system with a ductility-related modifications factor $R_d = 4.0$ and an overstrength-related modification factor $R_0 = 1.5$ are chosen. The selected building falls into the category of a normal building with an important factor of I_E=1.0. The factor accounting for higher mode effects is M_v=1.0. The roof dead load (D) and snow load (S) are assumed as 1.0 kPa and 1.64 kPa, respectively. The exterior wall load is equal to 0.5 kPa. The fundamental period of the structure, calculated using the empirical equation specified in the National Building Code (NBC) of Canada is T_a= 0.3 s. The seismic weight of the building is computed as $W_E = 18875$ kN. Utilizing the equivalent static force procedure with an increased period equal to $2T_a$, a seismic coefficient and base shear were calculated to be 0.114 g and 679 kN, respectively.

The link beam is made of welded tubular sections made of ASTM A572 Gr. 50 steel with a specified yield strength of $F_y = 345$ MPa. This link beam is designed to act as a seismic fuse experiencing shear yielding under lateral seismic loads. The length of the link, denoted as e is 750 mm and is chosen to meet the shear link requirement of $e < 1.6M_p/V_p$ where $M_p = ZF_y = 508$ kN-m represents the link's plastic moment resistance and $V_p = 0.55(2wd)F_y = 426$ kN is the link's plastic shear

resistance. In these equations, w is the thickness of the web, and d denotes the overall depth of the section. According to CSA S16, the link cross-section shall meet the flange width-to-thickness ratio of $285/(F_y)^{0.5}$ and the web depth-to-thickness ratio of $750/(F_y)^{0.5}$. A tubular cross-section with a flange width of $b_f = 260$ mm, flange thickness of $t_f = 25.4$ mm, $d = 235.8$ mm, and $w = 4.76$ mm is finally selected for the links. This section provides a factored shear resistance of $V_r = \varphi V_p = 384$ kN, where φ is the resistance factor equal to 0.9. The factored shear resistance of the selected link is almost equal to the factored shear force induced in the links $V_f = 388$ kN under the design base shear. The outer beams, braces, and columns are sized to resist the demands arising from the probable (or expected) shear capacity of the link, which is computed by amplifying the factored shear resistance of the link by $1.45R_y/\varphi$, where R_y is the ratio between the expected yield strength, R_yF_y=385 MPa, and the specified yield strength of the material. It is assumed that braces are moment-connected to the beams; thus, the seismic-induced in-plane moment is distributed between the brace and outer beam based on their in-plane flexural stiffness. The selected cross-section for the link is used for the outer beams, as the roof and intermediate beams are continuous. The resistance of the outer beams, which have a factored axial compressive resistance of $C_{r\text{-}ob} = 2869$ kN and a factored moment resistance $M_{r\text{-}ob} = 568$ kN-m is verified under the combined effect of an axial force $C_{f\text{-}ob} = 606$ kN and in-plane bending $M_{f\text{-}ob} = 227$ kN-m. The axial force–bending moment interaction ratio is obtained as 0.63.

Braces are designed under a factored axial compression force of $C_{f\text{-}br} = 976$ kN and a factored bending moment of $M_{f\text{-}br} = 32$ kN-m. An HSS 178×178×12.7 conforming to ASTM A1085, Gr. C steel with $F_y = 345$ MPa is selected for the braces. Brace factored axial compressive resistance and factored moment resistance are $C_{r\text{-}br} = 1616$ kN and $M_{r\text{-}br}$=151 kN-m, respectively. The

resulting axial force–bending moment interaction ratio is 0.76. It is important to note that slightly oversized braces are chosen to meet the stringent link rotation limit of 0.08 rad.

For the columns, a W250×73 section conforming to ASTM A992 Gr. 50 steel is selected for the columns to resist in compression a factored axial force of $C_{f\text{-}c}$ = 1501 kN, resulting from both gravity and seismic loads. The columns are oriented in a way that out-of-plane wind loads create strong-axis bending. The columns' base and top end are assumed to be pinned. The torsional and out-of-plane buckling loads are computed considering the full height of the column, while the intermediate beams brace the column in-plane. The effective lengths of columns for in-plane and out-of-plane buckling are computed, taking into account the distribution of axial loads along the height of the column [60]. The factored axial compressive resistance of the selected column is $C_{r\text{-}c}$ = 1560 kN.

The anticipated roof displacement of the frame is equal to $R_d R_0 \delta_e$=127 mm, which corresponds to a storey drift of 1.06%, meeting the 2.5% drift limit according to the NBC. The link rotations in the first, second and third tiers are 0.051 rad, 0.069 rad, and 0.078 rad, respectively, which are lower than the 0.08 rad Limit prescribed by CSA S16.

The wind load results in a distributed lateral load of 3.5 kN/m on EBF columns, creating a factored strong-axis moment of 88 kN-m. This moment combined with an axial force of 51 kN under the wind load combination gives an axial force–bending moment interaction ratio of 0.4.

5.2.2 Numerical Model

A detailed finite element model (FEM) of the prototype three-tiered braced frame is developed using the ABAQUS program [27]. The FEM shown in Figure 5-2a utilizes four node-reduced integration shell elements (S4R) to construct columns, beams, stiffeners, and braces. A mesh size of 25 mm was found to be sufficient based on mesh sensitivity analysis to achieve computational efficiency without compromising accuracy. Geometric and material nonlinearities were considered in the FEM. The

elastic behaviour of the steel was defined using Young's modulus E = 200 GPa and Poisson's ratio ν = 0.3. The Voce-Chaboche metal plasticity model [79] with kinematic and isotropic hardening parameters was chosen to reproduce the inelastic cyclic behaviour of steel.

Individual component-based calibrations were performed to ensure that the FEM developed here can accurately replicate the seismic stability response of MT-EBFs. The buckling response of the wide-flange column was validated against the experimental test data reported by Balazadeh-Minouei [81]. The parameters proposed by Fell et al. [82] to simulate the cyclic response of steel HSS were adopted. The hardening parameters of tubular beam elements (kinematic hardening modulus C_1=900 MPa, the rate at which C_1 decreases $\gamma_1 = 25$, the maximum change in the yield surface $Q_\infty = 30$ MPa, and the rate at which the yield surface changes $b = 2$) were obtained from the calibration performed against the experimental test data reported by Berman and Bruneau [38], which consisted of a similar short link designed to yield in shear. Figure 5-3a shows the comparison between link shear force–rotation response from the numerical simulation and the test. As shown, a very good correlation was achieved, indicating that the FEM accurately reproduces link stiffness, strength, and overstrength.

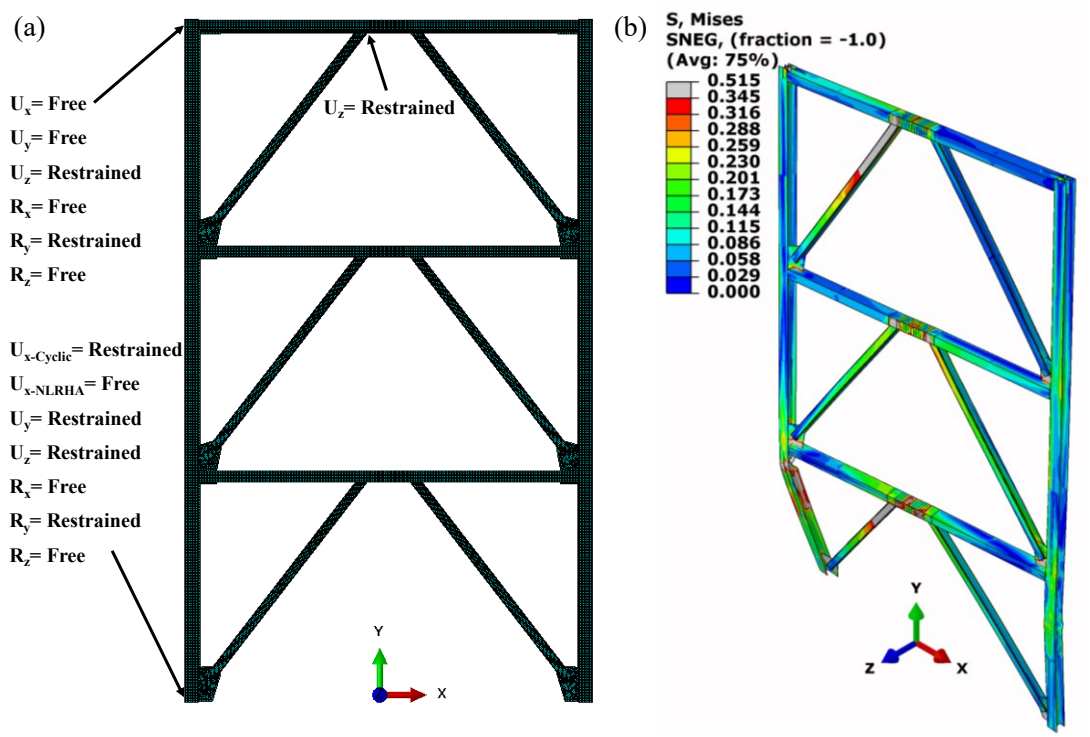

Figure 5-2. Three-tiered EBF: (a) Finite element model (Boundary conditions are shown for the left half of the frame, and the leaning column is not shown for simplicity); (b) Deformed shape and von Mises stress (in kN/mm^2) distribution at the end of cyclic pushover analysis.

The assigned boundary conditions for the FEM are shown in Figure 5-2a. The base of the columns and the edges of the brace corner gusset plates in Tier 1 are coupled to a reference point where the vertical and lateral out-of-plane translational degrees-of-freedom (DOFs) U_y and U_z and torsion θ_y are restrained. In the static analysis, the translation along the horizontal axis U_x is fixed, while a free condition is assigned in the dynamic analysis. The top ends of the columns are restrained against out-of-plane translation and twist, U_z and θ_y. The out-of-plane displacement at the ends of the roof level was restrained to simulate lateral support provided by the roof system.

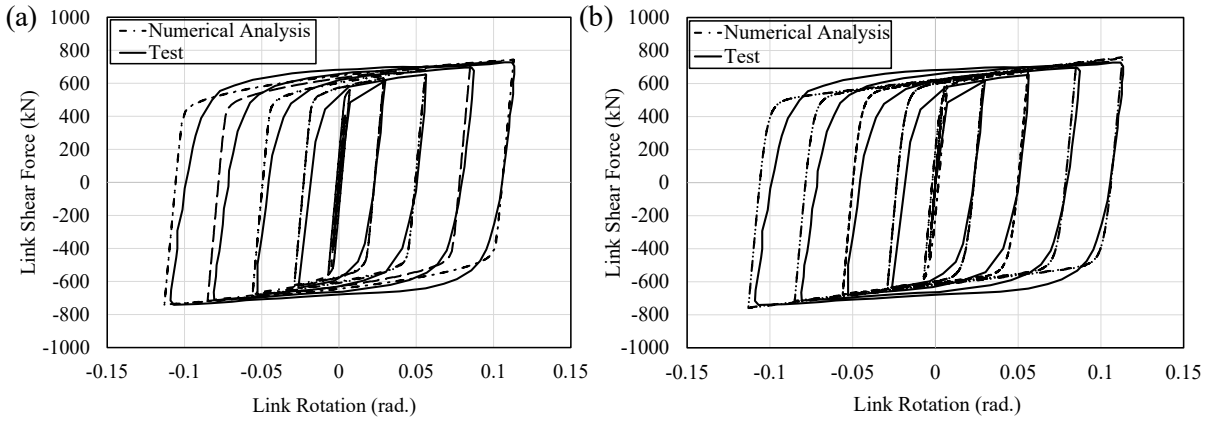

Figure 5-3. Tubular link shear force – rotation: (a) Prediction by the ABAQUS FEM vs. test data; (b) Prediction by the OpenSees fibre-based model vs. test data (data from Berman and Bruneau [38]).

To trigger global buckling in the frame members, the initial geometric out-of-straightness is assigned to beams, columns, and braces as a half-sinewave pattern between the unsupported member length with a maximum amplitude of 1/1000 times the respective length. Out-of-plumbness of the members was not explicitly simulated in the numerical model developed here. The wide-flange sections were assigned residual stresses based on the pattern proposed by Glambos and Ketter [70]. Additionally, an elastic wire element is incorporated into the model as a leaning column, reproducing P-Δ effects due to the gravity loads tributary to the braced frame. The base of the leaning column has the same boundary conditions as the EBF columns. In the horizontal direction, the translational DOF of the top end of the leaning column was coupled to that of the top of braced frame columns. The expected yield strength R_yF_y was assigned to the link beam, while the specified yield strength F_y was used for the other elements. To account for variability in material properties, e.g., yield strength, cross-sectional area, initial imperfections, and boundary conditions of the link, the expected yield strength was reduced by 10% in Tier 1 and increased by the same ratio in Tier 3. This assumption is expected to create a weaker Tier 1 compared to other tiers and a weaker Tier 2 compared to Tier 3, promoting progressive yielding from the bottom to the top.

The gravity loads tributary of the braced frame and leaning columns were applied through a static analysis at their top ends. This step is followed by either a cyclic nonlinear static (cyclic pushover) analysis or a nonlinear response history analysis (NLRHA). In the cyclic pushover analysis, a gradually changing cyclic displacement history was applied horizontally to the top ends of the braced frame columns. The displacement history follows the AISC 341 [4] loading protocol for prequalifying link-to-column connections, which is translated to the roof displacement assuming a $\delta_{roof} = \gamma he/L$, where γ represents the link rotation, h is the total height of the frame, and L is the frame span. The maximum amplitude of the roof displacement is 193 mm, corresponding to a storey drift of 1.61% which is 1.2 times the maximum storey drift observed in the NLRHA.

For the NLRHA, the transient analysis method was used by applying a ground motion time history to the base of the frame in the horizontal direction. Two lumped masses, each equal to half of the frame's seismic weight divided by gravitational acceleration, were assigned to the top end of each EBF column. The Rayleigh damping method with mass and stiffness proportional damping, corresponding to a critical damping ratio of 2% in the first and second translational vibration modes, was used to construct the classical damping matrix. A suite of 33 earthquake ground motion records, comprising of three earthquake scenarios likely to occur in Vancouver, BC, including crustal, deep in-slab and interface subduction (11 records per each scenario) was selected and scaled to match, on average, the NBC design response spectrum of the selected site. To identify the ground motion record that produces the largest lateral displacement demand on the frame, a computationally-efficient fiber-based numerical model, originally developed by the authors [76] in *OpenSees* [26], was used to perform 33 NLRHA. The fiber-based numerical model was created by replacing wide-flange beams in the original model with tubular ones. The nonlinear cyclic response of the link was reproduced using a nonlinear spring element in *OpenSees*. The same experimental test data [38] used to calibrate

the link response in the detailed FEM was also used to determine the Giuffre-Menegotto-Pinto material model parameters in *OpenSees* as $b = 0.0065$, $R_0 = 19.94$, $CR_1 = 0.83$, $CR_2 = 0.068$, $a_1 = a_3 = 0.02$, and $a_2 = a_4 = 11$. The hysteresis response predicted by the proposed model in *OpenSees* is compared in Figure 5-3b to that obtained from the test. The statistical parameters of the peak displacement response, including the storey drift, are summarized in Table 5-1 for the standard three-tiered EBF. Based on the results obtained from the NLRHA performed using the fiber-based model, the ground motion from the 2010 Maule – LACHb Chile earthquake record led to a storey drift (i.e., 1.27%h) that exceeded the design storey drift, i.e., 1.06%.

Table 5-1. Statistics of peak response parameters for three- and four-tiered EBFs.

Parameter	Standard Three-tiered EBF	Improved Three-tiered EBF-1	Improved Three-tiered EBF-2	Standard Four-tiered EBF	Improved Four-tiered EBF-1	Improved Four-tiered EBF-2
Storey drift %	0.88 [0.5–1.36]*	0.85 [0.5–1.26]	0.81 [0.49-1.28]	0.75 [0.40–1.08]	0.72 [0.41–1.12]	0.72 [0.4-1.15]
Storey drift/$R_dR_o\Delta_e$	0.83 [0.47-1.29]	0.85 [0.5-1.26]	0.86 [0.52-1.36]	0.70 [0.37-1.0]	0.72 [0.41-1.13]	0.74 [0.41-1.18]
$\gamma_{4\text{-NLRHA}}$ rad	–	–	–	0.03 [0.01-0.06]	0.03 [0.01-0.07]	0.03 [0.01-0.07]
$\gamma_{3\text{-NLRHA}}$ rad	0.04 [0.01–0.08]	0.04 [0.01–0.07]	0.04 [0.01-0.08]	0.03 [0.01-0.06]	0.03 [0.01-0.07]	0.03 [0.01-0.07]
$\gamma_{2\text{-NLRHA}}$ rad	0.06 [0.03–0.11]	0.06 [0.03–0.1]	0.06 [0.03-0.1]	0.06 [0.02-0.09]	0.06 [0.03-0.09]	0.06 [0.03-0.01]
$\gamma_{1\text{-NLRHA}}$ rad	0.09 [0.06–0.14]	0.09 [0.06-0.13]	0.08 [0.06-0.13]	0.09 [0.05-0.12]	0.09 [0.05-0.12]	0.08 [0.05-0.12]
$\gamma_{1\text{-exp}}$ / $\gamma_{1\text{-NLRHA}}$	–	0.98 [0.69-1.58]	0.83 [0.56-1.26]	–	1.19 [0.86-1.92]	0.93 [0.65-1.47]
$M_{fy\text{-}c,3\text{-NLRHA}}/M_{py}$	–	–	–	0.09 [0.06-0.09]	0.07 [0.06-0.07]	0.05 [0.04-0.05]
$M_{fy\text{-}c,2\text{-NLRHA}}/M_{py}$	0.12 [0.11–0.13]	0.1 [0.09-0.11]	0.08 [0.07-0.09]	0.11 [0.08-0.11]	0.09 [0.07-0.1]	0.09 [0.08-0.1]
$M_{fy\text{-}c,1\text{-NLRHA}}/M_{py}$	0.08 [0.07-0.09]	0.07 [0.06–0.07]	0.06 [0.06-0.07]	0.07 [0.06-0.08]	0.06 [0.05-0.06]	0.07 [0.06-0.07]
$M_{fx\text{-}c,3\text{-NLRHA}}/M_{px}$	–	–	–	0.04 [0.04-0.05]	0.02 [0.018-0.021]	0.02 [0.02-0.024]
$M_{fx\text{-}c,2\text{-NLRHA}}/M_{px}$	0.1 [0.08-0.13]	0.03 [0.02-0.03]	0.014 [0.013-0.015]	0.07 [0.06-0.08]	0.03 [0.026-0.032]	0.03 [0.03-0.04]
$M_{fx\text{-}c,1\text{-NLRHA}}/M_{px}$	0.12 [0.1–0.16]	0.03 [0.02–0.03]	0.013 [0.012-0.015]	0.06 [0.05–0.06]	0.02 [0.02-0.024]	0.03 [0.02-0.03]
$M_{fy\text{-}c,3}/M_{fy\text{-}c,3\text{-NLRHA}}$	–	–	–	–	3.1 [3.1-3.7]	2.6 [2.6-3.3]
$M_{fy\text{-}c,2}/M_{fy\text{-}c,2\text{-NLRHA}}$	–	3.7 [3.4-4.1]	1.9 [1.6-2.1]	–	2.4 [2.2-3.14]	1.5 [1.3-1.6]
$M_{fy\text{-}c,1}/M_{fy\text{-}c,1\text{-NLRHA}}$	–	5.3 [5.3-6.2]	2.5 [2.1-2.5]	–	3.7 [3.7-4.4]	1.9 [1.9-2.2]
$M_{fx\text{-}c,3}/M_{fx\text{-}c,3\text{-NLRHA}}$	–	–	–	–	2.6 [2.5-2.9]	2.7 [2.3-2.7]
$M_{fx\text{-}c,2}/M_{fx\text{-}c,2\text{-NLRHA}}$	–	1.3 [1.3-2.0]	1.5 [1.4-1.6]	–	1.7 [1.6-2.0]	1.8 [1.5-1.8]
$M_{fx\text{-}c,1}/M_{fx\text{-}c,1\text{-NLRHA}}$	–	1.3 [1.3-2.0]	1.6 [1.4-1.8]	–	2.6 [2.2-2.6]	1.8 [1.8-2.7]

*Values in brackets are the minimum and maximum response parameters, respectively.

5.2.3 Cyclic Pushover Analysis

The cyclic pushover analysis was performed to examine the stability response of the standard frame, considering the cyclic hardening of the links. At a 0.24% storey drift cycle, Tier 1 link started to yield before the other two links due to its lower shear yielding capacity. Shear yielding then

developed in the second-tier link at a 0.26% storey drift cycle followed by the third-tier link at a 0.29% storey drift cycle. Figure 5-4a shows the link shear forces normalized by their respective yielding capacity compared to their respective rotation. As shown, more pronounced rotation and strain hardening were observed in Tier 1 compared to other tiers, and in Tier 2 compared to the third tier. This response stems from the delays in shear yielding between the links, which created a higher lateral displacement in Tier 1 compared to the other tiers, and similarly, a higher lateral displacement in the second tier compared to Tier 3, as shown in Figure 5-4c. The hysteresis plots in Figure 5-4a also confirm a stable nonlinear cyclic response, before column yielding and instability, for the tubular link part of MT-EBFs, which aligns with previous studies on tubular links without out-of-plane lateral bracing [30, 35, 38]. This observation is further supported by the link out-of-plane displacements measured at their left end, as shown in Figure 5-4e. Intermediate links showed no out-of-plane displacements ($< 0.06e$ in Tiers 1 and 2) until plastic hinge forming in the right column at the 1.6% drift cycle. However, the delays in link yielding resulted in an uneven distribution of shear forces in the links, leading to uneven axial forces and moments in the diagonal braces between the tiers. To compensate for the differences between the storey shear resistances produced by the braces at each tier, shear and in-plane bending was induced in the columns. The in-plane moments in Tier 1 and Tier 2 segments of the left column, recorded just below the beam, were normalized by the plastic moment capacity of the column section about its weak axis, M_{py}, as shown in Figure 5-4g. During each inelastic cycle, the moments at Tier 1 and Tier 2 levels reached their maximum values when yielding was initiated in the adjacent stronger tier. Notably, the first-tier column segment exhibited the maximum in-plane moment of $0.12M_{py}$ at a storey drift of -0.14% before instability occurred in the right column.

In addition to the in-plane response, the columns also experienced significant strong-axis bending due to the out-of-plane components of beam axial forces acting on imperfect columns at Tiers 1 and 2 beam levels. The compressive axial force in the column further exacerbated the out-of-plane response. This out-of-plane component of the beam axial force is generated by braces connected to imperfect unbraced intermediate beams. Normalized strong-axis moments, measured at the top end of the first- and second-tier segments of the left column, are shown in Figure 5-4i. The maximum strong-axis moment that occurred at the Tier 1 beam level before the right column yielded, reaching 43% of the strong-axis moment capacity of the section, M_{px} at a storey drift of -1.28%. The combination of in-plane and out-of-plane bending, along with the presence of a large axial force due to gravity and seismic loads, resulted in a partial plastic hinge forming in the first-tier segment of the right column at the 1.6% drift cycle. However, there was no instability observed in the column [86]. In the subsequent cycles, when the storey drift reached -0.27%, the combination of in-plane and out-of-plane bending, plus the large axial force, eventually triggered buckling of the left column. This instability was caused by the formation of a flexural plastic hinge in the first-tier segment of the left column. Figure 5-2b shows the deformed shape of the frame and von-Mises stress distribution at column buckling. The final buckled shape showed an out-of-plane flexural response, with Tier 1 experiencing significant deformation. After column buckling, the link out-of-plane displacement and column demands significantly increased due to excessive displacements in both the in-plane and out-of-plane directions.

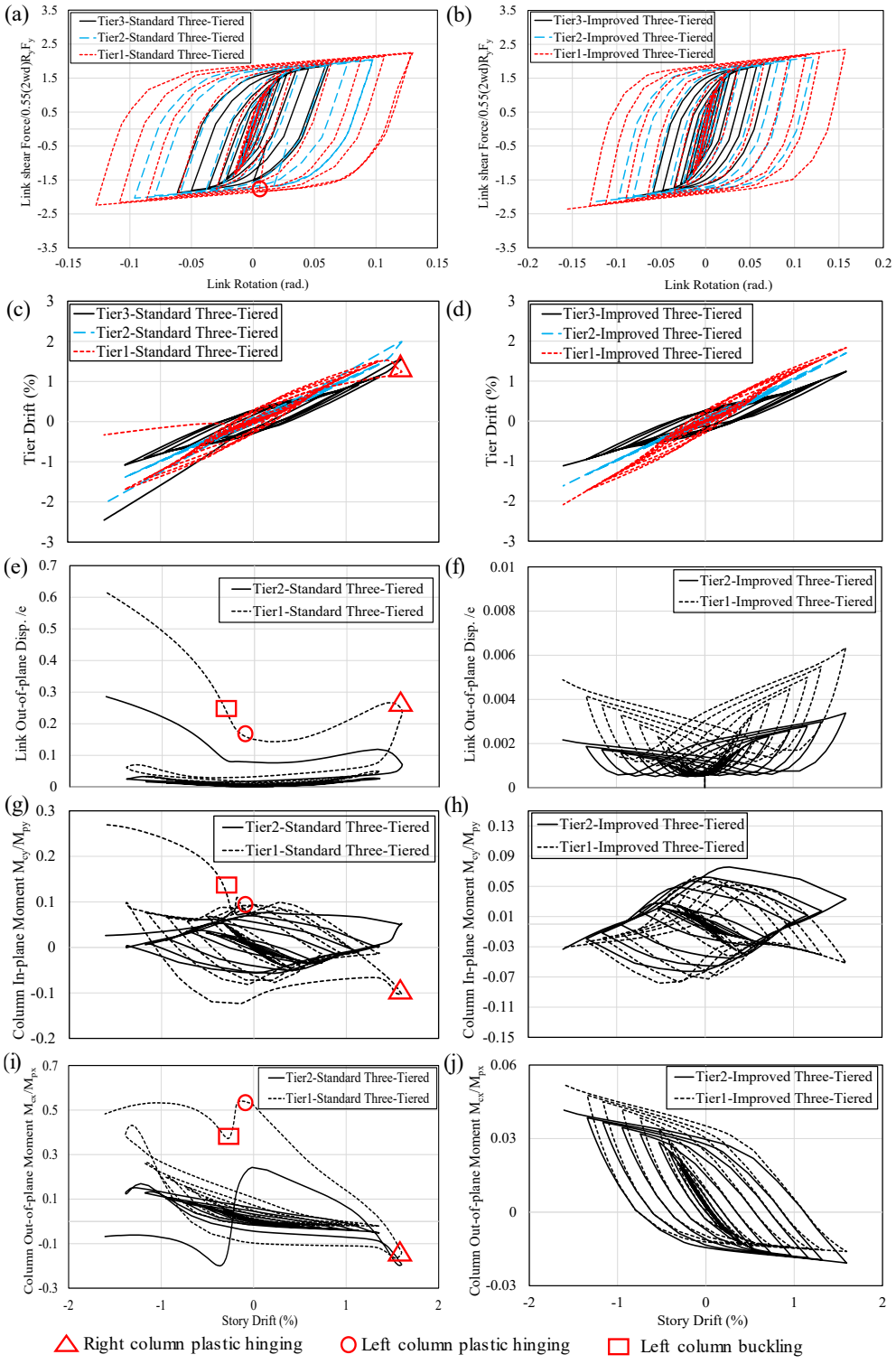

Figure 5-4. Cyclic pushover analysis of three-tiered EBF: (a-b) Link shear force vs. link rotation; (c-d) Tier drifts vs. storey drift; (e-f) Link out-of-plane displacement vs. storey drift; (g-h) Left-column in-plane moments vs. storey drift; (i-j) Left-column out-of-plane moments vs. storey drift.

5.2.4 Nonlinear Response History Analysis

Nonlinear response history analysis was conducted to evaluate the displacement and force demands on the prototype two-tiered EBF under the 2010 Maule – LACHb Chile earthquake record. Figure 5-5a illustrates the tier drifts versus storey drift, showing a uniform lateral deformation until the first tier yielded at a 0.32% storey drift due to its lower shear capacity. As the link in the first tier underwent strain hardening, the second-tier link began to yield, followed by the third-tier link at 0.34% and 0.35% storey drifts, respectively. The difference in the shear overstrength and shear deformation among the links can be observed in Figure 5-5c. Compared to the third-tier link, which achieved an overstrength of 1.8 and a maximum rotation of 0.05 rad, the first-tier link reached an overstrength of 2.2 and a maximum rotation of 0.06 rad. Due to the uneven distribution of frame lateral deformation between tiers, flexural bending deformation is induced in the columns, creating a kink in the plane of the frame at each intermediate beam level. The column in-plane moments were recorded in the first- and second-tier segments of the right-hand side column, as shown in Figure 5-5e.

Link out-of-plane displacements shown in Figure 5-5g remained below 0.1e, which had an insignificant influence on the hysteresis response of the links. However, this deformation produced an out-of-plane component of the beam axial force, leading to significant out-of-plane bending in both columns, with more pronounced demands below Tier 1 intermediate beam (Figure 5-5i). In-plane and out-of-plane bending induced in the first-tier segment of the right column at t = 59.7 s reached $0.04M_{py}$ and $0.87M_{px}$, respectively. This created a flexural plastic hinge in the column, resulting in out-of-plane buckling similar to the cyclic pushover analysis.

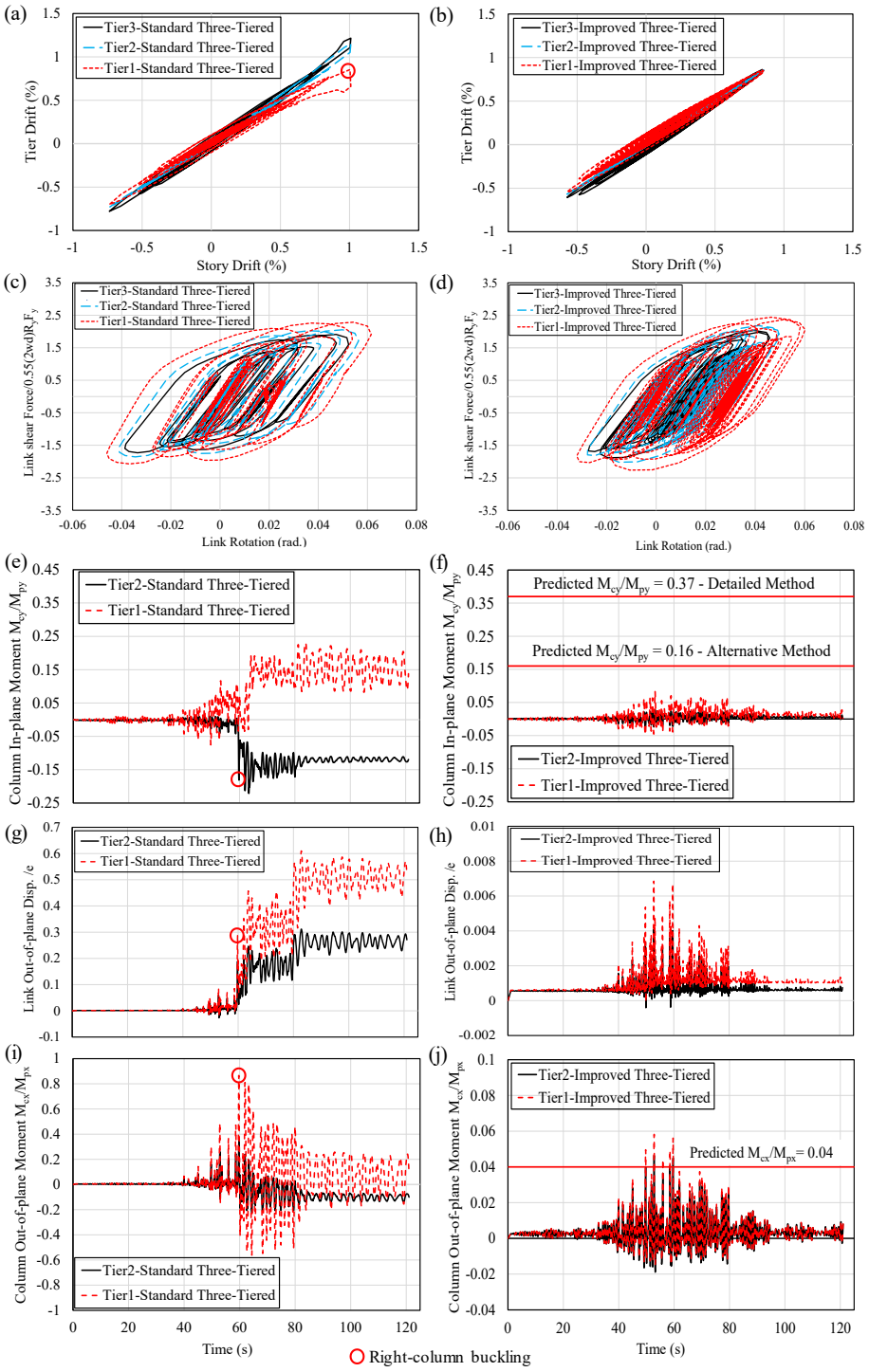

Figure 5-5. Response history analysis of three-tiered EBF under the 2010 Maule – LACHb Chile earthquake: (a-b) Tier drifts vs. storey drifts; (c-d) Link shear force vs. link rotation; (e-f) Right-column in-plane bending history; (g-h) Link out-of-plane displacements history; (i-j) Right-column out-of-plane bending history.

5.3 Proposed Analysis and Design Method for MT-EBFs with Tubular Links

The seismic response of MT-EBFs presented earlier and in the previous study conducted by the authors [76] emphasizes the need for special analysis and design procedures to estimate and address out-of-plane bending induced in intermediate beams, in-plane and out-of-plane bending on the columns, and link rotation demands due to delays in link yielding. The section proposes new analysis and design requirements that consist of procedures to analyze and quantify seismic demands arising from the multi-tier response, size intermediate beams and columns, and verify link inelastic rotation. To illustrate the effectiveness of the proposed procedures, they are demonstrated for the prototype three-tiered EBF. The three-tiered EBF redesigned using the proposed requirements is referred to as the improved three-tiered EBF.

5.3.1 Beam Design

The intermediate beams in MT-EBFs should possess sufficient stiffness and strength to provide out-of-plane lateral support for the braces. The beams should therefore be designed to resist an additional nodal bracing force, P_b, which acts as a point load on the intermediate beam at the intersection of link, as shown in Figure 5-6a, following Clause 9 of CSA S16:

$$P_b=\beta(\Delta_0+\Delta_b)C_f/L_b \quad (5\text{-}1)$$

where Δ_0 and Δ_b represent the initial misalignment and displacement of the bracing system (i.e., the intermediate beam), C_f refers to the axial compression force in the braced member (i.e., diagonal braces), and L_b is the unbraced length between lateral supports. Assuming a pinned condition at the ends of the intermediate beam in flexure out-of-plane, P_b induces out-of-plane bending in the link and outer beams of Tier 1 (Figure 5-6a) with a maximum amplitude of $M_{fy\text{-}b}=[P_bL_{ob}(L\text{-}L_{ob})]/L$, where L_{ob} denotes the length of each outer beam. Since Δ_b varies with the nodal bracing force, a few iterations are required to determine P_b. For the prototype frame, this force was determined as

$P_b = 3.8$ kN using $L = 7$ m and $L_{ob} = 3.125$ m, resulting in an out-of-plane moment of $M_{fy\text{-}b} = 6.6$ kN-m. This moment was then used to redesign the intermediate beam in combination with a design in-plane moment of $M_{fx\text{-}b} = 227$ kN-m and an axial force of $C_{f\text{-}b} = 606$ kN due to the probable shear resistance of the first-tier link. The effective length of the intermediate beam was set to the full length of the beam for out-of-plane buckling. For in-plane buckling, the length between the column and brace-to-beam connection was used as the unbraced length. The axial compressive, strong-axis, and weak-axis bending resistances of the outer beam originally selected outer beam are $C_{rb} = 2869$ kN, $M_{rx\text{-}b} = 568$ kN-m and $M_{ry\text{-}b} = 419$ kN-m, respectively. Under the applied axial force and bi-axial bending demands, the axial force-moment interaction ratio of the outer beam was 0.63. In this braced frame example, the original cross-section of the intermediate beam was found to possess sufficient stiffness and strength to provide lateral bracing for the braces. Similar checks were also performed for the intermediate beam of Tier 2. However, if a stronger cross-section is required for the outer beam due to the additional out-of-plane bending demand introduced here, it may be necessary to revisit the design of the links.

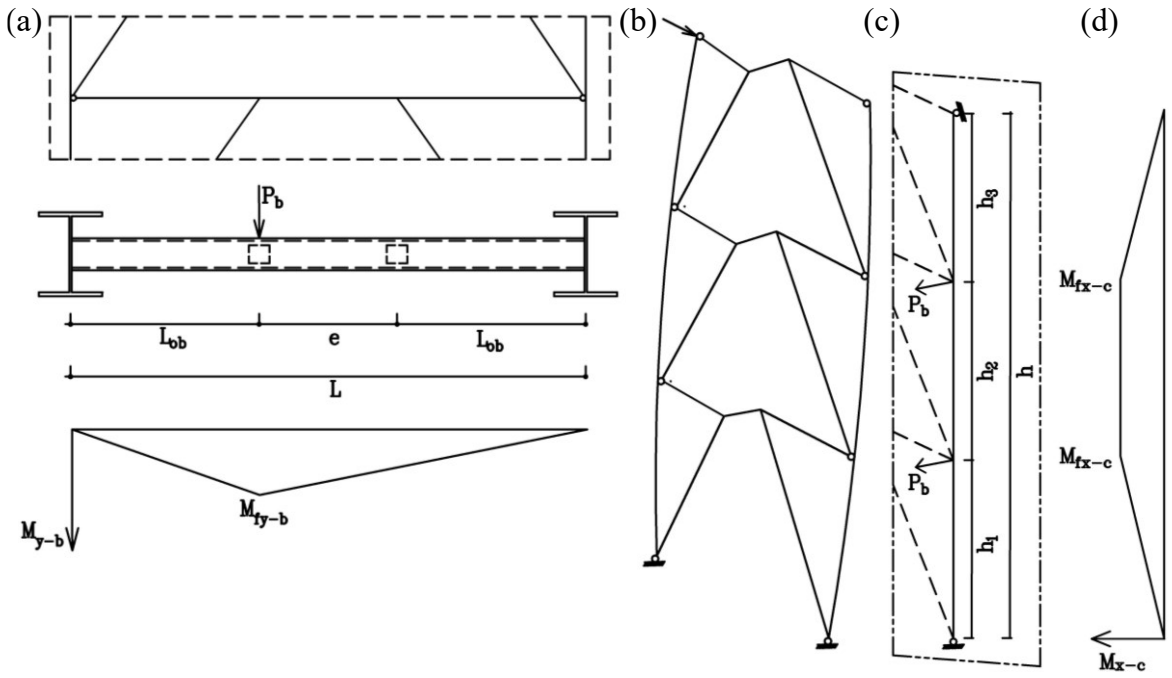

Figure 5-6. (a) Bracing force and out-of-plane bending moment of intermediate beams; (b) Frame deformed shape under lateral load with exaggerated out-of-plane deformation; (c) Bracing forces acting on the column out-of-plane; (c) Column out-of-plane bending moment.

5.3.2 Column Design

Out-of-plane Bending Moment

Column out-of-plane bending moment is determined by assuming that the columns laterally brace the intermediate beams and the braces at every intermediate beam level (Figure 5-6b). The nodal bracing force, computed using Eq. (5-1) at every intermediate beam level, is then applied as a point load on the column in the out-of-plane direction (Figure 5-6c), resulting in strong-axis bending, as shown in Figure 5-6d. For the prototype frame with equal tier heights and equal bracing forces, P_b, the maximum bending moment, $M_{fx\text{-}c}$, can be obtained as $M_{fx\text{-}c}=P_b h_1$ in which P_b should be taken as the larger of the nodal bracing forces required to laterally brace the diagonal brace and the intermediate beam at a given intermediate beam level. In the case of the three-tiered frame example, the bracing forces required to brace diagonal braces and the intermediate beam at every intermediate beam level are 7.2 kN and 7.7 kN, respectively. The larger of these two forces, applied at each

intermediate beam level on the column, creates a column strong-axis moment of 31 kN-m, which will be used to design the columns, in combination with in-plane bending and an axial compression force.

In-plane Bending Moment

As observed in the three-tiered EBF studied here, columns undergo in-plane bending due to the delays in yielding of the links along the frame height, e.g., progressive yielding of the links. The yielding of the links initiates in the tier with the largest design shear to shear resistance ratio, i.e., the first tier in the prototype frame, and then propagates to the tier with the second largest design shear to shear resistance ratio. This process continues until the link in the tier with the least design shear to shear resistance ratio yields. The tier with the largest design shear to shear resistance ratio is referred to as the critical tier. Progressive link yielding leads to an uneven distribution of inelastic frame deformation between the tiers as the tier that yielded first tends to deform more in the inelastic range than the tier that yielded last as the lateral roof displacement increases. Due to the significant rotation demands induced in outer beams once the link yields and experiences an appreciable inelastic rotation (e.g., 0.08 rad) within the tier, the braces and the outer beam engage in bending developed in the column due to the non-uniform distribution of inelastic deformation. The moment induced in either the brace or outer beam meeting a beam-to-column joint is a function of the flexural stiffness of the member and its connection to the column, e.g., beam-to-column or brace-to-column connection. This study proposes a detailed method and an alternative simplified method to predict column in-plane bending. In the detailed method, the flexural stiffness of beam-to-column and brace-to-column connections is explicitly accounted for when calculating the moment. In contrast, the other approach assumes these connections are pinned in flexure.

(a) Detailed Method

Column in-plane bending moment reaches its peak at every intermediate beam level when yielding is just initiated in the link of the adjacent tier. In the three-tiered EBF example, the peak in-plane moment in Tier 1 is achieved when yielding is just initiated in Tier 2 link (Analysis Step I); at this point, the first tier link has already experienced several inelastic cycles and strain-hardened such that the resistance of this link can be set equal to its probable resistance, while the third tier link is in the elastic range or approaches yielding. Thus, the resistance of this link and the one that just yielded can be conservatively set equal to their probable resistances, excluding the effect of strain-hardening. When the third-tier link just started to yield, the in-plane moment in Tier 2 reaches its peak value (Analysis Step II). At this point, the links in Tiers 1 and 2 have reached their probable resistances. Thus, the resistance of Tier 3 link can be replaced by its probable resistance, ignoring the strain-hardening effect. The resistance of the other two links can also be set equal to their probable resistances. The number of analysis steps is equal to the number of tiers minus one, assuming that a full plastic mechanism takes place before the design storey drift is attained, which is deemed realistic for MT-EBFs with three or more tiers [76]. Figure 5-7a illustrates Analysis Step I for the three-tiered EBF example. Figure 5-7b shows the schematic of the link shear force versus shear deformation, which assumes that the link yields at $0.55(2wd)R_yF_y$ and reaches its probable (or expected) strength at $0.55(2wd)R_{sh}R_yF_y$ where R_{sh} denotes the strain hardening coefficient and is equal to 1.45 for the links with tubular cross-sections according to CSA S16. As shown in Figure 5-7a, at Analysis Step I, the first tier link reached $0.55(2wd)R_{sh}R_yF_y$ while the resistance of the links in Tiers 2 and 3 is equal to $0.55(2wd)R_yF_y$. Using Figure 5-7b, the respective link rotation for each tier can be computed, which gave the rotation in Tier 1 as $\gamma_1=15.92R_yF_y/G$, where G is the shear modulus of steel (equal to 77 GPa), and the rotations in Tiers 2 and 3 as $\gamma_2=\gamma_3=0.55R_yF_y/G$. The assumed link

shear force–rotation response (backbone curve) in Figure 5-7b is based on limited experimental data, while conforming to CSA S16 overstrength capacity for continuous tubular links. A more refined backbone curve should be developed in the future to compute in-plane flexural demands of MT-EBF columns as more test data becomes available. Once the link rotations are known, the tier drift ratios θ_i (where i = 1, 2, 3) can be approximated assuming $\theta_i = \gamma_i e/L$, where γ_i is the link rotation in the respective tier. In the frame example, the link rotations and tier drifts in Tiers 1 – 3 are $\gamma_1 = 0.08$ rad, $\gamma_3 = \gamma_2 = 0.0028$ rad, and $\theta_1 = 0.86\%$, $\theta_2 = \theta_3 = 0.03\%$, respectively.

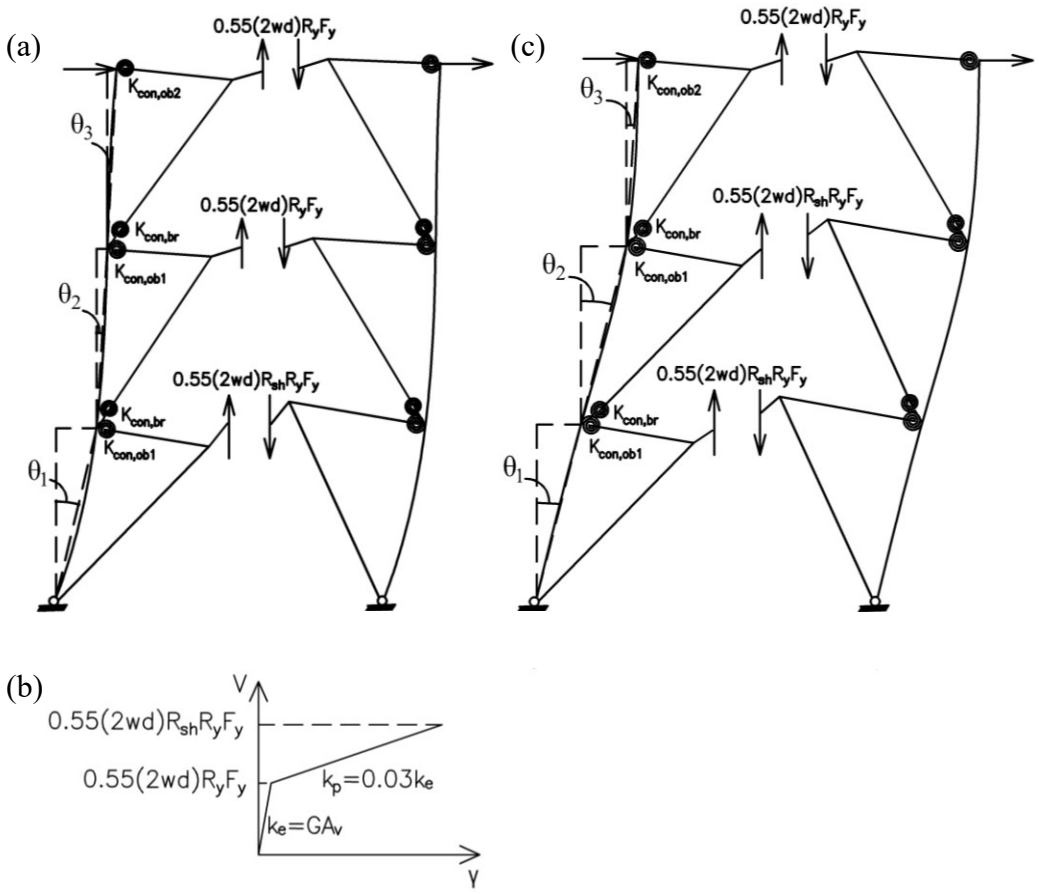

Figure 5-7. Detailed analysis method for three-tiered EBF (Tier 1 is critical): (a) Frame deformation and link forces at Analysis Step I; (b) Link shear force versus shear deformation; (c) Three-tiered EBF deformation and link forces at Analysis Step II.

The in-plane moment demands in the outer beam, brace, and column at every intermediate beam level can be back-calculated using relative tier drifts. For example, the difference between Tier 1 and Tier 2 drifts ($\theta_1 - \theta_2 = 0.83\%$) creates in-plane bending in the first-tier intermediate beam, the second-tier brace meeting the first-tier intermediate beam, and the column segment extending within the first and second tiers. The moments in the beam and brace are proportional to their rotational stiffness. The flexural stiffness of the beam and brace involves the stiffness of the member and that provided by the connection. The flexural stiffness of the intermediate beam-to-column connection, $K_{con,ob1}$, and that of the brace-to-column connection, $K_{con,br}$, were adopted from the experimental tests conducted by Stoakes and Fahnestock [83] as $K_{con,ob1}=10.6\ EI_{x\text{-}ob}/L_{ob}$ and $K_{con,br}=10.6\ EI_{x\text{-}br}/L_{br}$, respectively, where $I_{x\text{-}ob}$ and $I_{x\text{-}br}$ are the in-plane (strong-axis) moment of inertia of the outer beam and the brace, respectively. The stiffness of the beam-to-column connection (the roof beam in an MT-EBF) $K_{con,ob2}$ was obtained from the experimental tests performed by Liu and Astaneh [84] as $K_{con,ob2} = 1.3EI_{x\text{-}ob}/L_{ob}$. Knowing these stiffness parameters, the stiffness of the outer beam, K_{ob}, and brace, K_{br}, can be determined as follows:

$$K_{ob}= \frac{2.34EI_{x\text{-}ob}}{L_{ob}} \tag{5-2}$$

$$K_{br}= \frac{2.9EI_{x\text{-}br}}{L_{br}} \tag{5-3}$$

The bending moments in the outer beam, M_{ob}, and brace, M_{br}, can now be calculated using the stiffness of each segment as $M_{ob} = K_{ob}(\theta_1 - \theta_2)$ and $M_{br} = K_{br}(\theta_1 - \theta_2)$. The difference between these two moments is distributed between the first-tier and second-tier column segments, $M_{yc,i}$ in proportion to their flexural stiffness. This results in the column in-plane moment of $M_{fy\text{-}c,i} = K_{c,i}/(K_{c,i} + K_{c,i+1})$. The in-plane moments developed in the intermediate beam level of Tier 2 are calculated using the same approach. Since the difference between tier drifts in Tiers 2 and 3

is equal to zero in Analysis Step I, no moment is induced due to the relative deformation of Tier 2 with respect to Tier 3. However, bending will be induced in the third-tier column segment due to the continuity of the column.

In the prototype frame, the flexural stiffness of the outer beam and brace at the intermediate beam level of Tier 1 are K_{ob}= 22750 kN-m and K_{br}= 4028 kN-m, respectively. This generates in-plane moments in Tier 1 outer beam M_{ob}=189 kN-m and the Tier 2 brace M_{br}=33 kN-m. The difference between these moments is distributed evenly between the first- and second-tier column segments as $M_{fy\text{-}c,1} = M_{fy\text{-}c,2}$ = 78 kN-m assuming both column segments have identical flexural stiffness at the first intermediate beam joint. This in-plane moment, combined with the out-of-plane moment calculated previously $M_{fx\text{-}c}$ = 31 kN-m, and an axial compression force due to the gravity plus the probable resistances of the links $C_{f\text{-}c}$ = 1501 kN are used to select a stronger W360×101 column for the prototype frame by satisfying the CSA S16 axial force – bending moment interaction equation (= 0.92). For this column, the factored axial compressive resistance, moment resistance about the strong axis and moment resistance about the weak axis are $C_{r\text{-}c}$ = 2331 kN, $M_{rx\text{-}c}$ = 425 kN-m and $M_{ry\text{-}c}$ = 188 kN-m, respectively. It should be noted that these demands do not necessarily coexist as the proposed approach here aims to obtain the largest effect, resulting in conservative design demands.

The in-plane bending moments of the column when the frame reaches Analysis Step II are computed, assuming that Tier 3 link just has yielded while Tiers 1 and 2 links have reached their probable resistances. As such, the resistances of the links in Tiers 1 and 2 are equal to $0.55(2wd)R_{sh}R_yF_y$ while the resistance of Tier 3 link is set equal to $0.55(2wd)R_yF_y$. The deformed shape of the frame and the link shear forces at Analysis Step II are shown in Figure 5-7c. Using the approach described for Analysis Step I, the in-plane moments can be calculated for the prototype frame. Based on the link

resistances, the link rotations in Tiers 1 and 2 are obtained as $\gamma_1 = \gamma_2 = 15.92 R_y F_y / G$ and the rotation in Tier 3 is equal to $\gamma_3 = 0.55 R_y F_y / G$, which can then be converted to tier drift ratios similar to Analysis Step I. The difference between Tier 2 and Tier 3 drifts induces in-plane moments in the second-tier intermediate beam and third-tier braces. Therefore, the moment in the intermediate beam and the brace is calculated based on their respective stiffness (Eqs. (5-2) and (5-3)). The difference between the moment in the intermediate beam and the brace is transferred to the column. This moment is distributed between the column segments in the second and third tiers based on their respective stiffness.

For the prototype frame, the link rotations and tier drifts under link forces corresponding to Analysis Step II are $\gamma_1 = \gamma_2 = 0.08$ rad, $\gamma_3 = 0.0028$ rad, and $\theta_1 = \theta_2 = 0.86\%$, $\theta_3 = 0.03\%$ in Tiers 1 to 3, respectively. The bending moment in the second-tier intermediate beam and the third-tier brace are then obtained as 189 kN-m and 33 kN-m, respectively. The difference between these moments is distributed evenly between the second- and third-tier column segments resulting in $M_{fy\text{-}c,2} = M_{fy\text{-}c,3} =$ 78 kN-m. The column section selected in Analysis Step I (W360×101) is verified under the axial force, in-plane and out-of-plane moments induced in each tier. The selected section is found to be sufficient.

The sequence of link yielding can be influenced by factors such as the frame geometry, e.g., tier heights, unavoidable variations in material strength and link cross-sectional properties, fabrication tolerances, variations in connection details, and the increase in material strength due to strain rate effects [10–18]. In design, it is necessary to examine all plausible critical tier scenarios to determine the most critical in-plane moment in the columns. To account for these uncertainties in design, potential critical tier scenarios can be identified by varying the link resistances by a certain margin, for example 10%. As an example, let us consider the scenario where Tier 2 link yields first, followed

by link yielding in Tier 3 and then Tier 1 for the three-tiered prototype frame. For this link-yielding scenario, Analysis Step I involves a loading condition where the link resistance in Tiers 1 and 3 reaches $0.55(2wd)R_yF_y$ while the resistance of Tier 2 link is set to $0.55(2wd)R_{sh}R_yF_y$ (Figure 5-8a). The respective link rotations can then be obtained using Figure 5-7b. Following similar steps as described earlier for the first link-yielding scenario, the moments in the brace, outer beam, and column can be calculated based on the relative rotations between adjacent tiers. The in-plane flexural demands in the first- and second-tier column segments are found to be $M_{fy\text{-}c,1} = M_{fy\text{-}c,2} = 78$ kN-m. As the lateral roof displacement increases, link yielding occurs in Tier 3, leading to Analysis Step II in which the shear resistance of the links in Tiers 2 and 3 is set equal to $0.55(2wd)R_{sh}R_yF_y$ while the resistance of Tier 1 link is taken as $0.55(2wd)R_yF_y$ (Figure 5-8b). This step creates column in-plane flexural moments of $M_{fy\text{-}c,1} = M_{fy\text{-}c,2} = 78$ kN-m. The columns should then be verified under the combination of in-plane bending from this link-yielding scenario, out-of-plane bending, and an axial compression force. For the prototype frame, this link-yielding scenario did not affect the column design. Given the nature of the proposed method that functions based on the relative link rotation between adjacent tiers, the number of potential link yielding scenarios can be adjusted in design if the geometry of the tiers and member sizes are identical. For instance, one yielding scenario would be sufficient to obtain column in-plane bending demands for the prototype three-tiered frame. However, the scenario where Tier 2 link yields first was shown here for the prototype frame to demonstrate potential link yielding scenario.

In design, it is recommended that the engineer prescribes tubular links of the MT-EBF to be fabricated from the same heat. This will effectively reduce the variability in the shear strength of the links between tiers.

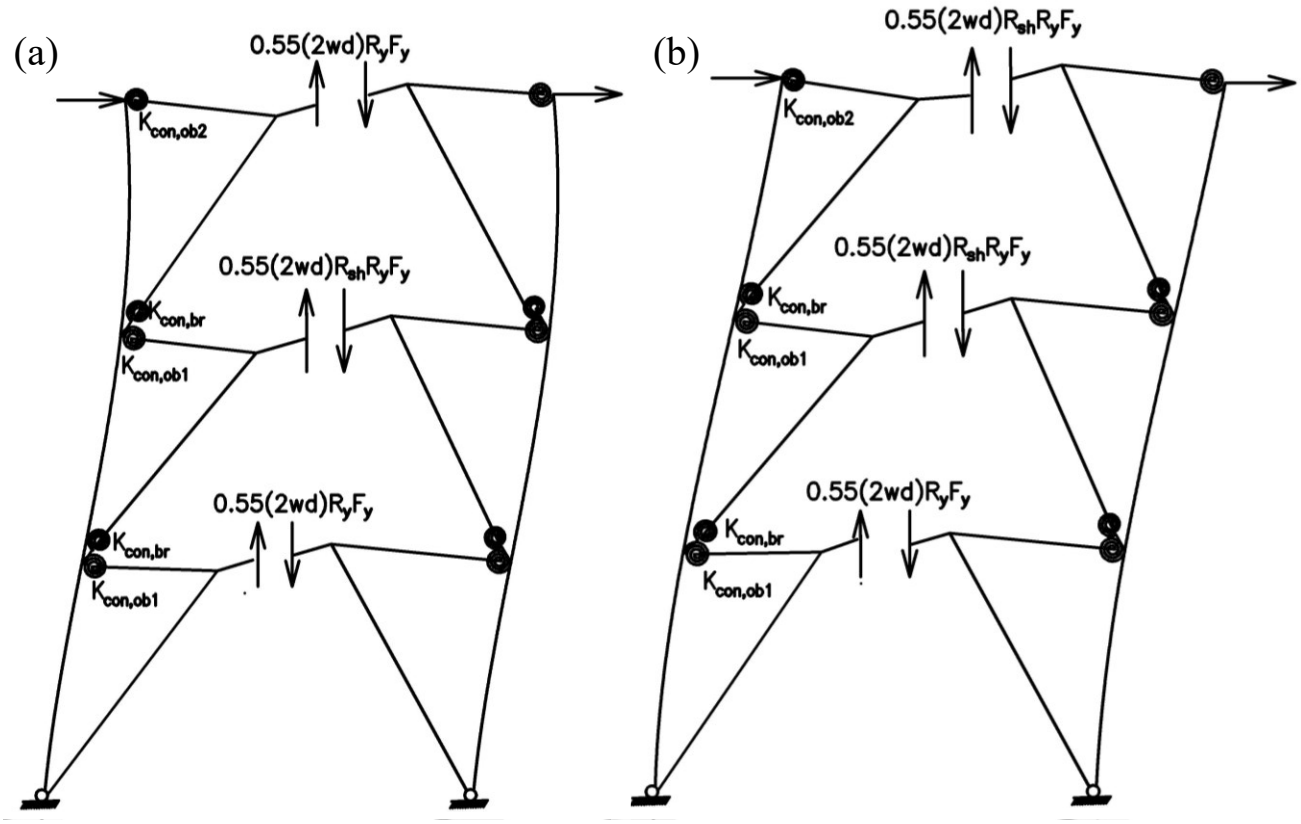

Figure 5-8. Detailed analysis method for three-tiered EBF (Tier 2 is critical): (a) Frame deformation and link forces at Analysis Step I; (b) Three-tiered EBF deformation and link forces at Analysis Step II.

(b) Alternative Method

An alternative analysis method is proposed in this section to determine the in-plane demands of MT-EBF columns. This simplified analysis method neglects the influence of the flexural stiffness of brace-to-column and beam-to-column connections on the frame in-plane response. In order to determine column moment demands, one of the columns is isolated from the MT-EBF with in-plane lateral support at each tier level, representing the lateral stiffness provided by diagonal braces. The isolated column is then subjected to a lateral settlement at any intermediate beam level, corresponding to the plastic deformation induced in each tier, as the elastic frame deformation is not expected to create flexure in the columns. The amplitudes of lateral settlements are obtained assuming progressive yielding of the links, similar to the detailed method. For the three-tiered frame

example, Analysis Step I involves a link shear resistance of $0.55(2wd)R_{sh}R_yF_y$ in the first tier and $0.55(2wd)R_yF_y$ assigned to the second and third tiers, as shown in Figure 5-9a (δ_i in this figure represents the relative tier lateral displacement). Using Figure 5-7b, the inelastic link rotation in each tier (i.e., the difference between the link rotations corresponding to shear $0.55(2wd)R_{sh}R_yF_y$ and $0.55(2wd)R_yF_y$ in Figure 5-7b) can be obtained and translated to the lateral plastic displacement of each tier using $\delta_{p,i} = \gamma_{p,i}eh_i/L$ as shown in Figure 5-9b for the three-tiered EBF at Analysis Step I, where $\gamma_{p,i}$ is the inelastic link rotation in each tier and is equal to $15.37R_yF_y/G$. Knowing the inelastic link rotation in Tier 1, the lateral plastic displacement of the first tier can be computed as follows:

$$\delta_{p,1}=\frac{15.37R_yF_yeh_1}{LG} \tag{5-4}$$

Using the classical three-moment equation with the anticipated frame deformation pattern (or applied settlements), the isolated column moments at Tiers 1 and 2 intermediate beam levels can be obtained as $M_{fy\text{-}c,1}= 1.6EI_{y\text{-}c}\delta_{p,1}/h_1^2$ and $M_{fy\text{-}c,2}= -0.4EI_{y\text{-}c}\delta_{p,1}/h_1^2$, respectively, as shown in Figure 5-9c. For the frame example, the lateral plastic displacement under link shear forces associated with Analysis Step I is identical in all the tiers and is equal to δ_p=33 mm. The column in-plane bending moments using the three-moment equation are therefore obtained as $M_{fy\text{-}c,1}$= 37 kN-m and $M_{fy\text{-}c,2}= -9$ kN-m for the W250×101 column.

Link shear forces at Analysis Step II correspond to $0.55(2wd)R_{sh}R_yF_y$ in Tiers 1 and 2, and $0.55(2wd)R_yF_y$ in Tier 3 (Figure 5-9d) as described in the detailed method. For this step, the respective lateral plastic displacements of the selected isolated column are shown in Figure 5-9e. Using the three-moment equation, the column in-plane bending moments in Tiers 1 and 2 are

therefore $M_{fy\text{-}c,1}$= -0.4$EI_{y\text{-}c}\delta_{p,1}/h_1^2$ and $M_{fy\text{-}c,2}$= 1.6$EI_{y\text{-}c}\delta_{p,1}/h_1^2$, respectively, as shown in Figure 5-9f. These moments are obtained as $M_{fy\text{-}c,1}$= − 9 kN-m and $M_{fy\text{-}c,2}$= 37 kN-m for the frame example. For both analysis steps, the strength and stability of the columns are verified in each segment under the in-plane moment obtained from the alternative method, plus the out-of-plane moment and an axial compression load described earlier. A W250×101 column is chosen, which is lighter than the column selected when using the detailed in-plane moment calculation. Column in-plane flexural moments obtained using the alternative method are lower than those obtained using the detailed method. This could be attributed to the fact that the alternative method imposes the lateral displacement corresponding to plastic deformation of each tier to the columns, which is deemed to better represent multi-tier response. Further evaluation of the proposed methods is needed in future studies. Similar to the detailed method, other plausible link-yielding scenarios should be examined to obtain the most critical bending moment demand on the columns.

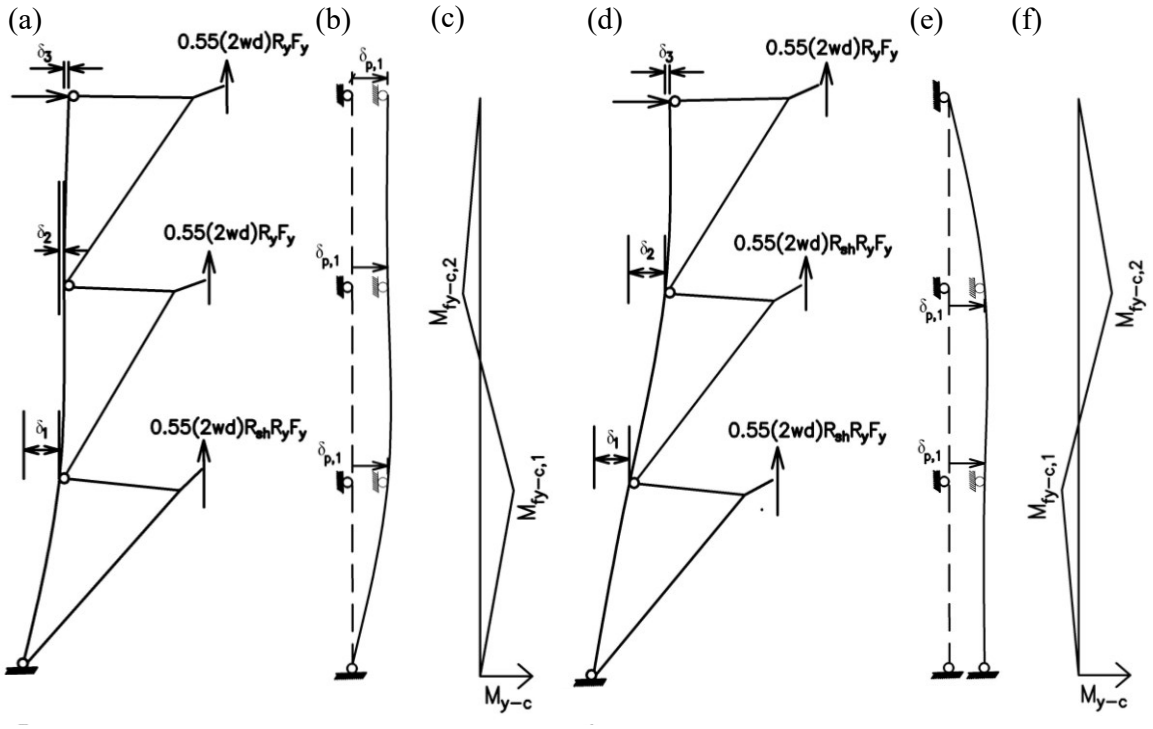

Figure 5-9. Alternative analysis method for three-tiered EBF (Analysis Step I & Analysis step II): (a&d) Frame lateral deformation and link forces; (b&e) Lateral plastic displacements; (c&f) Column in-plane bending moment.

5.3.3 Link Rotation Check

MT-EBF links undergo uneven plastic rotations due to progressive yielding, forming a full-yielding mechanism before the lateral displacement corresponding to the design storey drift is attained at the roof. This creates a large plastic rotation in the tier that yields first (the critical tier). The plastic rotation of the critical tier link γ should not exceed the limit associated with the link or connection fracture, which is typically provided by steel design standards, e.g., 0.08 rad for shear links as per CSA S16. The inelastic link rotation due to roof displacement is expressed as a function of the frame geometry and frame inelastic drift, which itself is equal to frame elastic drift $\Delta_e = \delta_e/h$ determined under the factored seismic load multiplied by an amplification factor to translate elastic deformation to plastic deformation, which is 4 for frames located in high seismic regions of Canada as per CSA S16), where δ_e is the frame elastic displacement under the factored seismic load. Thus,

the inelastic link rotation due to roof displacement at each tier is calculated as $4\Delta_e(L/e)$. The additional inelastic rotation is introduced in the critical link due to column bending δ_B because of progressive link yielding, as shown in Figure 5-10a. The deformation caused by column bending can be calculated using a simply-supported isolated column, as shown in Figure 5-10b, under the point loads applied at the intermediate beam levels, each is computed as the difference between the column shear forces above and below the intermediate beam level, e.g., $\Delta V_{c,1}$ and $\Delta V_{c,2}$ at Tier 1 and Tier 2, respectively, in the frame example shown in Figure 5-10a. To determine the column shear forces, the link shear in the critical tier is set equal to the link probable yield strength; the link probable yield strength in subsequent yielding tier is reduced by 1%, e.g., 0.99 times the link probable strength in Tier 2 and 0.98 times the link probable strength in Tier 3 in the frame example. The bending deformation of the isolated column, represented by $\delta_{B,1}$ and $\delta_{B,2}$ in Figure 5-10a, is then calculated using mechanics principles or a structural analysis program. The total link inelastic rotation in the critical tier, e.g., Tier 1 in the frame example, can finally be computed as follows:

$$\gamma_{1\text{-exp}}=4\left[\frac{\delta_e}{h}+\frac{\delta_{B,1}}{R_d R_0 h_1}\right]\left(\frac{L}{e}\right) \tag{5-5}$$

For the three-tiered EBF shown in Figure 5-1b, the link shear forces required to determine the lateral deformation due to column bending when the first tier is critical are as follows: $1.45R_y0.55(2wd)F_y$= 692 kN, $1.44R_y0.55(2wd)F_y$= 687 kN, and $1.43R_y0.55(2wd)F_y$= 683 kN in Tiers 1-3, respectively. The resulting unbalanced forces at the first and second tier levels are found as $\Delta V_{c,1}$ = 4.4 kN and $\Delta V_{c,2}$ = 3.5 kN, respectively. Solving the isolated column of Figure 5-10b with the original section designed for strength using the detailed method W360×101 under these point loads results in deflections $\delta_{B,1}$ = 21.1 mm and $\delta_{B,2}$ = 20.7 mm, at Tier 1 and Tier 2, respectively. Introducing δ_e = 20 mm from the elastic analysis of the frame under the factored seismic load and $\delta_{B,1}$ into Eq. (5-5),

gives $\gamma_1 = 0.09$ rad. This rotation exceeds the limit of 0.08 rad. The design engineer may examine the possibility of increasing brace sections to reduce the overall lateral displacement of the frame or using a larger column to minimize lateral tier displacement caused by column bending. For this design example, a larger W360×162 is chosen to reduce the inelastic link rotation in Tier 1 to 0.07 rad. If the engineer opts for a stiffer column to meet the inelastic link rotation limit, alternatively, more effective column cross-sections, such as tubular sections or built-up cruciform sections made of welded wide-flanges can be used. Other scenarios of link yielding should be verified using the proposed simply-supported column model. In the frame example, the inelastic link rotation in Tier 2, when this tier is critical, is equal to 0.07 rad, which is smaller than the limit of 0.08 rad.

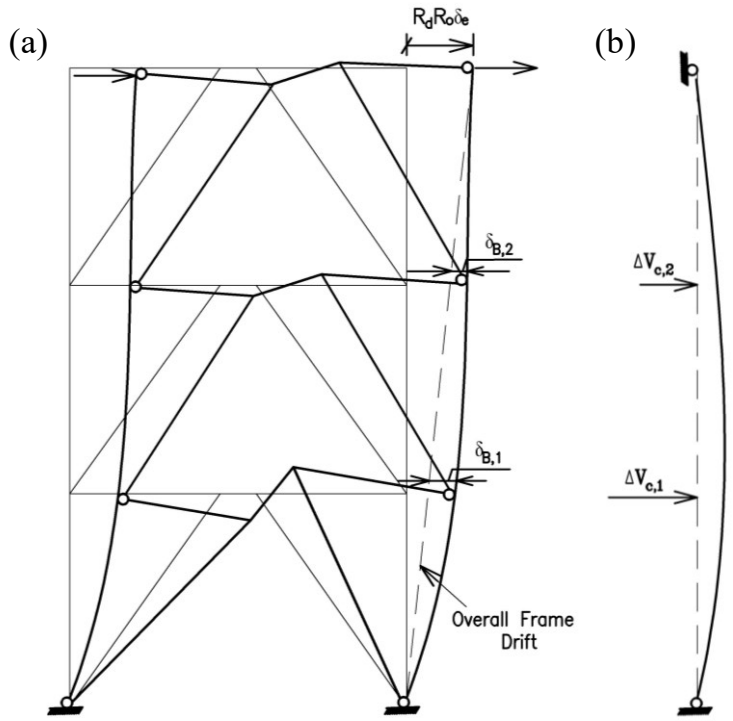

Figure 5-10. Inelastic link rotation check at full-yielding mechanism: (a) Frame lateral deformation; (b) Simply-supported column model.

5.4 Seismic Response of Improved Multi-Tiered EBFs

The cyclic pushover and nonlinear response history analyses on the enhanced three-tiered EBF and four-tiered EBF designed using the proposed method are performed to validate the proposed analysis and design requirements. The results of the cyclic pushover analysis and NLRHA (under an individual record) are first presented for the enhanced three-tiered EBF with W360×101 columns designed using the detailed method excluding the link rotation check. Then, the statistics of NLRHA of the three-tiered and four-tiered EBFs under the 33 ground motion records described earlier are then discussed.

Under cyclic pushover analysis, no link or column buckling was observed. The link shear force–rotation response shown in Figure 5-4b indicates that all three links exhibit stable cyclic response without strength degradation. Progressive link yielding resulted in a non-uniform distribution of the frame lateral deformation between the tiers, as shown in Figure 5-4d, where Tier 1 experienced

the largest deformation and Tier 3 underwent the smallest tier drift at any given roof displacement cycle. The out-of-plane displacement of the first- and second-tier links shown in Figure 5-4f confirms a considerably smaller out-of-plane response in the improved frame compared to the standard frame. This response also contributes to reducing column out-of-plane bending as shown in Figure 5-4j for the Tier 1 segment of the left column. Compared to the standard three-tiered frame, relatively lower in-plane bending was observed in the columns (Figure 5-4h) with a maximum value of $0.08M_{py}$.

The results obtained from NLRHA of the enhanced three-tiered EBF under the 2010 Maule – LACHb Chile earthquake record are presented in Figure 5-5. The normalized link shear force – rotation shown in Figure 5-5d confirms that the link in Tier 1 yields first. Shear yielding is then propagated to the second tier and finally to the third tier. Owning to the increased flexural stiffness of the column in the enhanced frame compared to the standard design, the links progressively yielded without significant delays, creating approximately uniform tier drift distributions as shown in Figure 5-5b. Relatively small in-plane bending was observed in the columns due to the almost uniform lateral frame distribution among tiers. The history of the in-plane bending moment in the left column is shown in Figure 5-6f. The largest moment recorded on the column at the first intermediate beam level is equal to $0.08M_{py}$ at $t = 53.1$ s. The moments predicted by the proposed detailed and alternative methods are $0.37M_{py}$ and $0.16M_{py}$, respectively, suggesting the inherent conservatism in the analysis method due to the assumptions associated with the link resistances. Figure 5-6h shows the link out-of-plane displacement history that stayed below $0.01e$ at the first- and second-tier levels, indicating the effectiveness of increased out-of-plane stiffness provided to the intermediate beams and the columns. Column out-of-plane moments at the intermediate beam levels are shown for the left column in Figure 5-7j. The peak out-of-plane moments in the first-

and second-tier levels are $0.06M_{px}$ and $0.05M_{px}$, respectively. The predicted out-of-plane moment using the proposed method here is $0.04M_{px}$, indicating that the method can effectively estimate the column moments.

In addition to the three-tiered frame example described earlier, a four-tired EBF with an identical base shear was selected and designed first, excluding the proposed requirements in this study (Standard Four-tiered EBF), and then redesigned following the proposed requirements (Improved Four-tiered EBF). The geometry of the frame and selected members using the CSA S16 method are shown in Figure 5-1c. The four-tiered EBF was redesigned as per the proposed recommendations of Section 5.3. The original sections selected for beams and braces remained unchanged but W410×149 columns were required to carry additional moment demands and stability requirements introduced here, excluding the link inelastic rotation check (Improved Four-tiered EBF-1). The detailed analysis method was used to obtain column in-plane bending demands. The columns were also verified to meet the link inelastic rotation limit, as proposed in Section 5.3.3, which required larger W360×162 columns (Improved Four-tiered EBF-2). Similar sets of designs were also generated for the three-tiered EBF example (Improved Three-tiered EBF-1 and Improved Three-tiered EBF-2). The statistics of NLRHA of standard and improved three- and four-tiered EBFs — including the storey drift, inelastic link rotations and column moments — under 33 ground motion records are given in Table 5-1. $M_{fy\text{-}c,1}$, $M_{fy\text{-}c,2}$ and $M_{fy\text{-}c,3}$ are the predicted column in-plane moments at Tiers 1–3 using the detailed method. $M_{fx\text{-}c,1}$, $M_{fx\text{-}c,2}$ and $M_{fx\text{-}c,3}$ are the predicted column out-of-plane moments from the proposed method. $M_{fy\text{-}NLRHA}$ and $M_{fx\text{-}NLRHA}$ are the maximum in-plane and out-of-plane moments in the column from NLRHA. The statistics for each response parameter are reported as the maximum of means over each earthquake ensemble. Referring to Table 5-1, the storey drift values for the standard and improved EBFs are always

lower than the design storey drift. The ratio of storey drift obtained from NLRHA to the respective design storey drift ($R_dR_0\Delta_e$) is always lower than unity, suggesting that the code-specified design storey drift may over-predict the lateral deformation of multi-tiered EBFs. Appreciable inelastic rotation developed in the first-tier link of standard frames (EBF) and improved frames designed excluding the link rotation check (labelled as EBF-1), mainly due to progressive link yielding, which began in Tier 1. The recorded rotations in Tier 1 of these frames exceed the code-prescribed link rotation limit. The results of the link rotation for the improved frames designed taking into account the link rotation check (EBF-2) confirmed the benefit of using a stiffer column to limit inelastic link rotation in the tier that yields first and develops significant shear deformation as the full plastic mechanism is achieved. The predicted inelastic link rotation in Tier 1 $\gamma_{1\text{-exp}}$ normalized by the observed inelastic link rotation $\gamma_{\text{i-NLRHA}}$ confirmed the capability of the proposed link rotation check in this study.

The peak column in-plane flexural demands, $M_{\text{fy-c,i-NLRHA}}$ (i = 1–3), normalized by the respective weak-axis plastic moment, M_{py}, are summarized in the table. The moments were recorded at the top end of the column in each tier. Overall, observed column in-plane flexural moments do not vary significantly between tiers (in the order of $0.08M_{\text{py}}$). The parameter $M_{\text{fy-c,i}}/M_{\text{fy-c,i-NLRHA}}$ (i = 1–3) in Table 5-1 is the ratio of the design in-plane flexural moment to the peak value of the moment from the analysis given at each tier at the top end of the tier column segment. The values obtained from this ratio confirmed that the detailed method proposed to estimate column in-plane flexural demands offers a conservative prediction of column demands (on average 2.9 times the observed value). This conservatism is mainly attributed to the assumed link rotations associated with the initiation of link yielding and when the link is fully strain-hardened. However, this conservatism is accepted in light of the simplicity of the method.

The peak column out-of-plane flexural demands, $M_{fx\text{-}c,i\text{-}NLRHA}$ (i = 1–3), measured at the top end of the column at each tier normalized by the respective strong-axis plastic moment, M_{px}, are given in Table 5-1. For each frame, out-of-plane moments are almost the same at tier levels, indicating that the source out-of-plane moment is the out-of-plane response of braces and intermediate beams. Moreover, stiffer columns in improved EBFs help minimize the out-of-plane response of outer beams and diagonal braces creating lower out-of-plane flexural demands on the column (on average 64% lower moment). Referring to Table 5-1, the ratio between the predicted out-of-plane moment and the moment obtained from the analysis, $M_{fx\text{-}c,i}/\ M_{fx\text{-}c,i\text{-}NLRHA}$ (i = 1–3), indicates that the method proposed here can conservatively predict column out-of-plane flexural demands (on average, prediction is 1.9 times higher than observed values). This implicit conservatism is due to the assumption of link shear forces, i.e., $0.55(2wd)1.45R_yF_y$, when the maximum out-of-plane moment occurs.

5.5 Conclusion

This study examined the seismic performance of three- and four-tiered steel eccentrically braced frames with continuous tubular links and proposed analysis and design methods to improve their stability response under seismic loading. A prototype three-tiered EBF was designed in accordance with the 2019 Canadian steel design standard. A three-dimensional finite element model of the frame was created, and the cyclic pushover and nonlinear response history analyses were conducted to evaluate the frame seismic performance, with an emphasis on the stability response of intermediate links and columns. New analysis and design requirements were proposed with a particular focus on the stability and strength of intermediate beams, braces, and columns, and link rotation demands. The three-tiered EBF and four-tiered EBF were redesigned using the proposed method, and nonlinear analyses were performed to verify the link and column stability conditions and to evaluate

the adequacy of the proposed requirements in estimating column moments and link inelastic rotations. The key findings of this study can be summarized as follows:

- Tubular links in the intermediate tiers of multi-tiered EBFs can exhibit a stable response and develop significant strain hardening despite the absence of lateral supports at their ends.
- The three-tiered EBF designed in accordance with CSA S16 experienced progressive link yielding starting at the critical tier and propagating among tiers until the link in the strongest tier yielded. This response led to a non-uniform distribution of frame lateral deformation between tiers, inducing in-plane flexural demand on the columns. Additionally, the combination of this demand, a large axial compression force induced by gravity loads and link resistances, and out-of-plane bending moment imposed on the columns due to the out-of-plane response of intermediate beams and braces, resulted in column plastic hinging and out-of-plane instability. Furthermore, progressive link yielding generated excessive rotational demand on the link that yields first, potentially leading to premature failure in the link or its connections.
- New analysis and design requirements were proposed to enhance the stability response of three- and four-tiered EBFs when the frame responds in the inelastic range, achieving a full-yielding mechanism. The proposed method includes: 1) minimum stiffness and strength requirements for bracing out-of-plane diagonal braces connected to intermediate beams, utilizing the out-of-plane stiffness and strength of the intermediate beams, 2) minimum stiffness and strength requirements to brace out-of-plane intermediate beams by leveraging the column out-of-plane strength and stiffness, 3) required column in-plane flexural strength due to progressive link yielding, and 4) a link inelastic rotation limit to prevent premature failure in the link due to frame lateral displacement plus the deformation caused by the column bending.

- Two step-by-step procedures, detailed and alternative analysis methods, were proposed to predict column in-plane flexural demands attributable to progressive link yielding as the frame reaches the design storey drift and forms a full-yielding mechanism. The detailed method considers the influence of rotational stiffness of braces, outer beams, and their connections on column in-plane flexural demands, while the alternative method utilizes lateral plastic deformation of tiers to determine column in-plane demands.
- The in-plane flexural stiffness of MT-EBF columns can be utilized to control additional link inelastic rotation resulting from column flexural deformation due to progressive link yielding. The proposed design requirements can properly predict the column in-plane and out-of-plane moments and link inelastic rotations. Frames designed using these requirements demonstrated an improved response without column instability.

The proposed analysis and design requirements were developed and numerically validated for three- and four-tiered EBFs. Future studies should focus on a wide range of MT-EBF configurations. In addition, the backbone curve for the link shear force–rotation needs refinement through more experimental data. It is essential to compare the detailed and alternative methods for predicting column in-plane moment with more design examples. Moreover, full-scale experimental testing should be conducted to further validate and refine the proposed methods. Finally, the analysis and design methods proposed here can be adapted for two-tiered EBFs with continuous tubular links, as they have a less complicated seismic response.

Chapter 6. Conclusions

6.1 Summary

This Ph.D. thesis aimed to first evaluate the seismic response of steel multi-tiered eccentrically braced fames (MT-EBFs) with a focus on the stability of intermediate link beams and columns, and then to propose analysis and design methods within the framework of CSA S16 to improve seismic stability of such frames. MT-EBFs selected in this study are part of single-storey steel buildings located on Vancouver, British Columbia (seismic category 4). The link beams studied here are continuous I-section or continuous built-up tubular members designed to yield primarily in shear.

A set of nine MT-EBFs was first selected by varying the number of tiers, frame heights, tier height ratios, link lateral bracing conditions, and brace-to-link connections. The prototype EBFs were designed in accordance with the 2019 CSA S16. A fibre-based numerical model of MT-EBFs was developed in the *OpenSees* program. The model was used to perform nonlinear static and response history analyses. To perform the dynamic analysis, a set of 33 ground motion records representing three different seismic sources in western Canada was considered. The influential geometric parameters, including frame height, tier height ratio, number of tiers, link bracing conditions, and brace-to-link connection type, were evaluated using several response parameters, such as storey drift, tier drift, link rotation, link out-of-plane deformation, link shear force demand, and column in-plane and out-of-plane flexural bending demands. Analysis and design procedures were proposed to improve the stability condition of intermediate link beams and columns in two-tiered EBF with continuous wide-flange links. The method was validated using the continuum-based finite element model of the frame that accounts for the flexibility of the connections and lateral-torsional stability mode of the link beams. The proposed design involves torsional bracing of

intermediate link ends using diagonal braces and the estimation of in-plane and out-of-plane flexural bending demands of the columns. Analysis and design methods were also proposed for three- and four-tiered EBFs with continuous built-up tubular link beams. In MT-EBFs with built-up tubular links, out-of-plane deformation of intermediate links is expected to be limited because they have higher torsional and out-of-plane stiffness than I-sections. The proposed method for these EBFs was validated using nonlinear static and dynamic analyses performed on detailed finite element models of the braced frames. Finally, the design of an experimental test program was presented that would evaluate the seismic performance of MT-EBFs and experimentally validate the proposed design methods.

6.2 Scientific Contributions

The main scientific contributions of this Ph.D. research project are as follows:

- Corroborated fibre-based and continuum-based numerical model were developed for response evaluation of steel MT-EBFs.
- Analysis and design methods were developed in the context of the Canadian steel design standard to enhance the stability response of steel multi-tiered EBFs with continuous I-section links and those with continuous built-up tubular links.
- The proposed methods can appropriately estimate the in-plane and out-of-plane flexural bending demands of the columns and estimate inelastic link rotation in the intermediate links.

6.3 Conclusions and Design Recommendations

The main findings of this Ph.D. thesis are summarized below:

The results of nonlinear dynamic analyses performed on MT-EBFs not specifically designed for multi-tier response confirmed the following:

- Intermediate links of MT-EBFs with continuous I-section links are prone to out-of-plane buckling due to significant shear yielding and lack of out-of-plane bracing. This response can lead to large out-of-plane flexural demands on columns, ranging from $0.03M_{px}$ to $0.18M_{px}$, where M_{px} is the strong-axis plastic moment capacity of the beam. In MT-EBFs with continuous built-up tubular links, columns experience out-of-plane flexural bending that varies between 0.1 and $0.16M_{px}$, which is induced by the out-of-plane deformation of intermediate beams.
- Uneven shear yielding (or progressive shear yielding) of links, particularly in frames with non-uniform tier heights, create excessive inelastic rotation in the link that yields first. This response induces relatively large in-plane bending on the columns and, combined with the axial compression force and out-of-plane bending demands, can lead to column instability. Column in-plane flexural bending varies between $0.1–0.62M_{py}$, where M_{py} is the weak-axis plastic moment capacity of the beam, where the lower-bound represents moments induced from uneven shear yielding of links, and the upper-bound represents the moments recorded at the verge of column instability due to link out-of-plane buckling.
- MT-EBF columns experience considerable in-plane and out-of-plane moments from seismic loads combined with a large axial compression force under gravity loads and probable link resistances. Flexural moment demands are not accounted for in the design based on the current seismic design provisions.
- Due to the progressive yielding of links, the lateral deformation is not distributed uniformly along the height of the frame. This causes excessive rotational demands on the link that yields first, which may cause premature failure in the link or its connections.

- The response of MT-EBFs with continuous I-section links can be significantly improved by providing lateral support at both ends of the intermediate links or by using a rigid connection between the brace and beam. This finding, however, needs further verification using detailed finite element simulations or full-scale testing.

For MT-EBFs with continuous I-section or continuous tubular links, the following general recommendations are proposed:

- The proposed method outlines a procedure to predict seismic-induced demands from the multi-tier response in the frame members. It also sets minimum strength and stiffness requirements for the diagonal braces, intermediate beams, and columns.
- Intermediate beams should have adequate strength and out-of-plane stiffness to provide point lateral bracing to connected diagonal braces. A method is proposed to quantify the out-of-plane bending moment in the intermediate beams and set the minimum out-of-plane stiffness for the intermediate beams. Designers can benefit from the use of wide-flange sections with large weak-axis flexural stiffness as intermediate link beams.
- The strength of the columns should be sufficient to resist the combination of axial force and biaxial flexural bending. In addition, a minimum out-of-plane stiffness is required for the column to laterally brace diagonal braces and outer beams at the intermediate levels. A method is proposed to estimate in-plane and out-of-plane bending moments in the columns along with minimum out-of-plane stiffness requirements for the columns.
- Inelastic link rotation in the tier that yields first, where relatively high frame deformation develops due to the progressive yielding of link beams, should be limited

to 8% in wide-flange links designed to yield primarily in shear. A mechanics-based method is proposed to estimate inelastic link rotation.

For two-tiered EBFs with continuous I-section links, the following analysis and design recommendations are proposed:

- The proposed method takes advantage of the out-of-plane strength and stiffness of the intermediate beams to limit out-of-plane deformation of diagonal braces, leverages the out-of-plane strength of diagonal braces to provide torsional bracing to intermediate links at their ends, utilizes the column out-of-plane flexural stiffness and strength to laterally brace the diagonal braces and outer beams at intermediate levels, predicts the in-plane flexural demands in the column due to the progressive yielding, and uses the in-plane flexural stiffness of the columns to control the inelastic link rotation.
- The connection between the brace and the intermediate link should be designed to transfer the moment capacity of the brace to allow the brace to torsionally brace two ends of the intermediate link. The out-of-plane moment at each end of the link resulting from projecting the torque required to laterally brace the link ends in accordance with CSA S16 on braces should be considered in the design of the braces.
- Two methods are proposed to estimate column in-plane flexural bending caused by progressive link shear yielding until the full plastic mechanism is achieved in the frame. In the detailed method, the relative inelastic rotation of adjacent tiers is converted to the unbalanced bending moment distributed between the columns of the adjacent tiers based on the column's flexural stiffness. In the simplified method, however, column bending is directly computed using link probable resistances. It is noteworthy that in the detailed method, the effect of beam-to-column and brace-to-column connections is

included, while the simplified method neglects the beneficial contribution of those connections. Therefore, the simplified method was found to predict column in-plane moment demands conservatively.

- The proposed method was demonstrated on a prototype two-tiered EBF with continuous wide-flange link beams. The frame response was significantly improved by minimizing link and column out-of-plane deformation, and by limiting inelastic link rotation to the allowable link inelastic rotation (i.e., 0.08 rad).
- The prediction capability of the column in-plane and out-of-plane flexural moments and inelastic link rotation was evaluated using dynamic analyses performed on a two-tiered EBF. The predicted demands to the peak demands from the dynamic analyses were 3.03, 1.08, and 0.94 for column in-plane bending recorded at the first-tier segment of the column, column out-of-plane bending recorded at the first-tier segment of the column, and inelastic link rotation in Tier 1, respectively. Overall, the proposed method was found to be conservative in predicting column moment demands.

For three- and four-tiered EBFs with continuous built-up links, the following analysis and design recommendations are proposed:

- The proposed analysis and design methods use out-of-plane strength and stiffness of the intermediate tubular beams to laterally brace diagonal braces connected to the respective intermediate beam, estimate the in-plane and out-of-plane moments of the columns, and set a minimum out-of-plane stiffness for the columns to limit link inelastic rotation in the tier that yields first.
- Two analysis methods are introduced to quantify the column in-plane bending due to progressive yielding when the frame reaches the full plastic mechanism. For each

method, analysis steps corresponding to the initiation of link shear yielding were defined to obtain the maximum in-plane moment in each tier as link shear yielding propagates from one tier to another. In addition, the scenarios corresponding to the location of the critical tier (i.e., the tier with the largest design shear to shear resistance ratio) are defined to achieve the most critical bending moment condition on the columns. The detailed method includes the flexural stiffness of the brace-to-column and beam-to-column connections ignoring the continuity of the columns, whereas the alternative method excludes the effect of connections but acknowledges the continuity of the column along the height. The detailed method was found to result in conservative moment predictions compared with the alternative method, likely becasue the plastic lateral deformation of each tier is applied to the column in the alternative method which is a better representation of multi-tier response.

- The proposed method was applied to three- and four-tiered EBFs with continuous built-up tubular links. The proposed design recommendations could enhance the seismic performance of the frames and address the concerns associated with the stability of their columns.
- The proposed method was validated using the results from the dynamic analyses of the same three- and four-tiered EBFs. The predicted demands to the peak demands from dynamic analyses for column in-plane flexural moments measured at the first-tier column segment, out-of-plane flexural moments measured at the first-tier column segment, and inelastic link rotation in Tier 1 were 5.3, 1.3, and 0.83, respectively for three-tiered EBF. These ratios for the four-tiered EBF were 3.7, 2.6, and 0.93,

respectively. The overly conservative prediction for column in-plane flexural bending is associated with the assumed link shear forces in the analysis.

- The proposed method for three- and four-tiered EBFs with continuous built-up links can be used to design two-tiered EBFs with continuous built-up links.

6.4 Limitations

The author acknowledges the limitations of this Ph.D. dissertation as follows:

- The prototype frames designed in this study were part of a single-storey industrial building located on site Class C in Vancouver, British Columbia. These frames were designed in accordance with the Canadian steel design standard, CSA S16.
- The ground motions were selected for the dominant seismic events in Western Canada, including crustal, deep in-slab, and subduction interplate (Cascadia) earthquakes.
- The ground motions were scaled to a hazard level corresponding to 2% probability of exceedance in 50 years in accordance with 2015 NBC.
- The base condition of the columns in the braced frames was assumed to be pinned to achieve the most severe stability condition on the columns. Partial fixity of the column bases may improve their stability response due to increased stiffness provided by the base connection.
- The chevron EBF configuration was selected as the most common type of EBF structure in Canada because they can take advantage of simple beam-to-column connections.
- The link beams in the prototype frames were either continuous wide-flange sections or continuous built-up tubular members that yield primarily in shear.
- The number of tiers for prototype frames ranges from two to five, and their heights vary from 9.0 to 20.5 m.

6.5 Recommendations for Future Work

- A full-scale experimental test should be performed to verify the results obtained from numerical simulations and validate the proposed design methods.
- The effect of frame base fixity on the stability response of the column should be investigated using a continuum-based finite element model accounting for column connection and footing flexibility.
- Other configurations of EBF systems applicable to certain architectural design considerations should be studied in the future, and the proposed method should be refined to cover such frames.
- Investigation should be done on MT-EBFs with intermediate link beams made of continuous wide-flange sections oriented such that the in-plane bending occurs about their weak-axis, responding in the elastic region with the capability of self-centring. This system consists of the roof beam made of modular (or replaceable) wide-flange link oriented in the strong-axis and connected to the intermediate beam of the tier below using vertical ties. This configuration of MT-EBF will eliminate the need for lateral out-of-plane bracing for intermediate beams, because these beams are not expected to yield and will provide much higher out-of-plane flexural stiffness against possible out-of-plane demands expected in tier levels.
- The application of hollow structural section (HSS) links in MT-EBFs should be studied because of their high torsional and out-of-plane stiffness, which can be beneficial in MT-EBFs where no physical out-of-plane bracing is practical.
- The application of MT-EBFs in multi-storey buildings should be investigated, and the proposed method should be adjusted to include such frames.

- The link shear force – shear rotation backbone curve of built-up tubular links should be improved in future studies based on the results of experimental tests. This will allow the refinement of the column in-plane moment in the proposed method for three- and four-tiered EBFs by obtaining a better estimation of link overstrength.
- Future studies should expand the proposed analysis and design methods to other link-yielding mechanisms (flexural yielding or a combination of shear and flexural yielding).
- The ductility- and overstrength-related force modification factors (R_d and R_O) for MT-EBFs should be established by performing collapse response evaluation studies following the methodology proposed in FEMA P695 [87].

Bibliography

[1] J. Vincent, "Seismic Retrofit of the Richmond-San Rafael Bridge," in *2nd US Seminar on Seismic Design, Evaluation, and Retrofit of Steel Bridges. Report no. UCB/CEE-Steel*, 1996, pp. 215–232.

[2] "Personal Communication, Bushbohlman, Trevor Whitney, 2020."

[3] Canadian Standard Association - CSA, "CAN/CSA S16-19 : Design of steel structures," ON, 2019.

[4] American Institute of Steel Construction-AISC, "ANSI/AISC 341-22, Seismic provisions for structural steel buildings," Chicago, IL, 2022.

[5] C. W. Roeder and E. P. Popov, "Inelastic behavior of eccentrically braced steel frames under cyclic loadings," Earthquake Engineering Research Center, University of California, Berkley, CA, Report No. UCB/EERC-77/18, 1977.

[6] D. N. Manheim, "On the design of eccentrically braced frames," PhD Thesis, University of California, Berkeley, 1982.

[7] K. D. Hjelmstad and S.-G. Lee, "Lateral buckling of beams in eccentrically-braced frames," *J. Constr. Steel Res.*, vol. 14, no. 4, pp. 251–272, 1989.

[8] M. D. Engelhardt and E. P. Popov, "Experimental performance of long links in eccentrically braced frames," *J. Struct. Eng.*, vol. 118, no. 11, pp. 3067–3088, 1992.

[9] E. P. Popov and M. D. Engelhardt, "Seismic Eccentrically Braced Frames," *J. Constr. Steel Res.*, vol. 10, no. 1, pp. 321–354, 1988.

[10] T. Okazaki and M. D. Engelhardt, "Cyclic loading behavior of EBF links constructed of ASTM A992 steel," *J. Constr. Steel Res.*, vol. 63, no. 6, pp. 751–765, 2007.

[11] R. J. Dexter, M. Graeser, W. K. Saari, C. Pascoe, C. A. Gardner, and T. V. Galambos,

"Structural shape material property survey," University of Minnesota, Minneapolis, 2000.

[12] B. J. Schmidt and F. M. Bartlett, "Review of resistance factor for steel: Data collection," *Can. J. Civ. Eng.*, vol. 29, no. 1, pp. 98–108, 2002.

[13] N. R. Rao, M. Lohrmann, and L. Tall, "Effects of strain rate on the yield stress of structural steels," *J. Mater.*, vol. 1, no. 3, pp. 238–248, 1966.

[14] T. L. Anderson, *Fracture mechanics*, 2nd Ed. Boca Raton, FL.: CRC Press, 1995.

[15] R. Tremblay and A. Filiatrault, "Seismic impact loading in inelastic tension-only concentrically braced steel frames: Myth or reality?," *Earthq. Eng. Struct. Dyn.*, vol. 25, no. 12, pp. 1373–1389, 1996.

[16] M. Bruneau, C.-M. Uang, and R. Sabelli, *Ductile design of steel structures*, 2nd Ed. New York: McGraw-Hill Education, 2011.

[17] C. P. Lamarche and R. Tremblay, "Seismically induced cyclic buckling of steel columns including residual-stress and strain-rate effects," *J. Constr. Steel Res.*, vol. 67, no. 9, pp. 1401–1410, 2011.

[18] R. Moreau, C. A. Rogers, and R. Tremblay, "Inelastic performance of the 'Modified-hidden-gap' connection for square HSS brace members," in *Proc. 10th National Earthquake Engineering Conf.*, 2014, no. 1010.

[19] A. Imanpour, R. Tremblay, A. Davaran, C. Stoakes, and L. A. Fahnestock, "Seismic performance assessment of multitiered steel concentrically braced frames designed in accordance with the 2010 AISC seismic provisions," *J. Struct. Eng.*, vol. 142, no. 12, 2016.

[20] A. Imanpour, "Seismic design of columns in two-story steel concentrically braced frames with bracing members intersecting columns between floors," *Structures*, vol. 33, no. March, pp. 3885–3896, 2021.

[21] R. Tremblay, “Inelastic seismic response of steel bracing members,” *J. Constr. Steel Res.*, vol. 58, no. 5–8, pp. 665–701, 2002.

[22] R. Tremblay, M.-H. Archambault, and A. Filiatrault, “Seismic response of concentrically braced steel frames made with rectangular hollow bracing members,” *J. Struct. Eng.*, vol. 129, no. 12, pp. 1626–1636, 2003.

[23] P.-C. Hsiao, D. E. Lehman, and C. W. Roeder, “A model to simulate special concentrically braced frames beyond brace fracture,” *Earthq. Eng. Struct. Dyn.*, vol. 42, no. 2, pp. 183–200, 2013.

[24] B. V. Fell, A. M. Kanvinde, G. G. Deierlein, and A. T. Myers, “Experimental investigation of inelastic cyclic buckling and fracture of steel braces,” *J. Struct. Eng.*, vol. 135, no. 1, pp. 19–32, 2009.

[25] National Research Council -NRC (2015)., “National Building Code of Canada, NBCC 2015,” Ottawa, Ontario, Canada, 2015.

[26] S. Mazzoni, F. McKenna, M. H. Scott, and G. L. Fenves, “Open system for earthquake engineering simulation (OpenSees).” Pacific Earthquake Engineering Research Center (PEER), University of California, Berkeley, CA, 2006.

[27] “ABAQUS [Computer sofware].” Dassault Systèmes, Waltham, MA.

[28] K. D. Hjelmstad and E. P. Popov, “Seismic Behavior of Active Beam Links in Eccentrically Braced Frames,” Earthquake Engineering Research Centre, University of California, Berkeley, CA, Report No. UCB/EERC-83/15, 1983.

[29] K. Kasai and E. P. Popov, “A Study of Seismically Resistant Eccentrically Braced Steel Frame Systems,” Earthquake Engineering Resesearch Centre, University of California, Berkley, CA, Report No. UCB/EERC 86/01, 1986.

[30] J. W. Berman and M. Bruneau, “Tubular Links for Eccentrically Braced Frames. II: Experimental Verification,” *J. Struct. Eng.*, vol. 134, no. 5, pp. 702–712, 2008.

[31] K. Kasai and E. P. Popov, “General Behavior of WF Steel Shear Link Beams,” *J. Struct. Eng.*, vol. 112, no. 2, pp. 362–382, 1986.

[32] G. Yiğitsoy, C. Topkaya, and T. Okazaki, “Stability of Beams in Steel Eccentrically Braced Frames,” *J. Constr. Steel Res.*, vol. 96, pp. 14–25, 2014.

[33] P. W. Richards, “Cyclic Stability and Capacity Design of Steel Eccentrically Braced Frames,” University of California, San Diego, 2004.

[34] C. C. McDaniel, C. M. Uang, and F. Seible, “Cyclic Testing of Built-up Steel Shear Links for the New Bay Bridge,” *J. Struct. Eng.*, vol. 129, no. 6, pp. 801–809, 2003.

[35] J. W. Berman and M. Bruneau, “Tubular links for eccentrically braced frames. I: Finite element parametric study,” *J. Struct. Eng.*, vol. 134, no. 5, pp. 692–701, 2008.

[36] K. D. Hjelmstad and E. P. Popov, “Characteristics of Eccentrically Braced Frames,” *J. Struct. Eng.*, vol. 110, no. 2, pp. 340–353, 1984.

[37] J. M. Ricles and E. P. Popov, “Composite Action in Eccentrically Braced Frames,” *J. Struct. Eng.*, vol. 115, no. 8, pp. 2046–2066, 1989.

[38] J. W. Berman and M. Bruneau, “Experimental and analytical investigation of tubular links for eccentrically braced frames,” *Eng. Struct.*, vol. 29, no. 8, pp. 1929–1938, 2007.

[39] K. D. Hjelmstad and E. P. Popov, “Cyclic Behavior and Design of Link Beams,” *J. Struct. Eng.*, vol. 109, no. 10, pp. 2387–2403, 1983.

[40] P. A. Cano, “Evaluation of the Seismic Design Methods for Steel Multi-tiered Concentrically Braced Frames,” MSc thesis, University of Alberta, 2019.

[41] A. Imanpour and R. Tremblay, “Analytical Assessment of Stability of Unbraced Column in

Two-Panel Concentrically Braced Frames," in *2012 CSCE Conference*, 2012, no. June, pp. 1–10.

[42] A. Imanpour, C. Stoakes, R. Tremblay, L. Fahnestock, and A. Davaran, "Seismic Stability Response of Columns in Multi-tiered Braced Steel Frames for Industrial Applications," in *Proceedings of the 2013 Structures Congress: Bridging Your Passion with Your Profession*, 2013, pp. 2650–2661.

[43] C. D. Stoakes and L. A. Fahnestock, "Three-dimensional Finite Element Simulation of the Seismic Behavior of Multitier Concentrically Braced Frames," in *Proceedings of the 2014 Structures Congress*, 2014, pp. 2675–2686.

[44] A. Imanpour and R. Tremblay, "Seismic design and response of steel multi-tiered concentrically braced frames in Canada," *Can. J. Civ. Eng.*, vol. 43, no. 10, pp. 908–919, 2016.

[45] A. Imanpour, R. Tremblay, L. A. Fahnestock, and C. Stoakes, "Analysis and design of two-tiered steel braced frames under in-plane seismic demand," *J. Struct. Eng.*, vol. 142, no. 11, 2016.

[46] E. Derakhshan Houreh and A. Imanpour, "A simplified seismic design method for limited-ductility steel multi-tiered concentrically braced frames in moderate seismic regions," *Can. J. Civ. Eng.*, vol. 49, no. 1, pp. 121–133, 2022.

[47] E. Derakhshan Houreh and A. Imanpour, "Seismic response and design of steel multi-tiered concentrically braced frames of the conventional construction category in moderate seismic regions of Eastern Canada," *Can. J. Civ. Eng.*, vol. 49, no. 3, pp. 432–444, 2022.

[48] C. D. Stoakes and L. A. Fahnestock, "Strong-Axis Stability of Wide Flange Steel Columns in the Presence of Weak-Axis Flexure," *J. Struct. Eng.*, vol. 142, no. 5, pp. 1–13, 2016.

[49] C. D. Stoakes and L. A. Fahnestock, “Influence of weak-axis flexural yielding on strong-axis buckling strength of wide flange columns,” *Struct. Stab. Res. Counc. Annu. Stab. Conf. 2012*, pp. 414–423, 2012.

[50] J. D. Newell and C.-M. Uang, “Cyclic Behavior of Steel Wide-Flange Columns Subjected to Large Drift,” *J. Struct. Eng.*, vol. 134, no. 8, pp. 1334–1342, 2008.

[51] A. Elkady and D. G. Lignos, “Full-Scale Testing of Deep Wide-Flange Steel Columns under Multiaxis Cyclic Loading: Loading Sequence, Boundary Effects, and Lateral Stability Bracing Force Demands,” *J. Struct. Eng.*, vol. 144, no. 2, pp. 1–15, 2018.

[52] J. M. Ricles and E. P. Popov, “Inelastic Link Element for EBF Seismic Analysis,” *J. Struct. Eng.*, vol. 120, no. 2, pp. 441–463, 1994.

[53] B. T. Ramadan and A. Ghobarah, “Analytical Model for Shear-link Behavior,” *J. Struct. Eng.*, vol. 121, no. 11, pp. 1574–1580, 1995.

[54] P. Richards and C.-M. Uang, “Development of Testing Protocol for Short Links in Eccentrically Braced Frames,” Department of Structural Engineering, University of California, San Diego, Report No. SSRP-2003/08, 2003.

[55] S. Koboevic, J. Rozon, and R. Tremblay, “Seismic performance of low-to-moderate height eccentrically braced steel frames designed for north american seismic conditions,” *J. Struct. Eng.*, vol. 138, no. 12, pp. 1465–1476, 2012.

[56] A. Ashrafi and A. Imanpour, “Seismic response of steel multi-tiered eccentrically braced frames,” in *12th Canadian Conference on Earthquake Engineering*, 2019, pp. 1–8.

[57] A. Ashrafi and A. Imanpour, “Analytical Assessment of the Seismic Performance of Two-tiered Eccentrically Braced Frames,” in *12th Pacific Structural Steel Conference*, 2019.

[58] Canadian Standard Association-CSA, “CAN/CSA S15-14: Design steel structures,” ON,

2014.

[59] P. A. Cano and A. Imanpour, “Evaluation of AISC seismic design methods for steel multi-tiered special concentrically braced frames,” *AISC Eng. J.*, vol. 57, no. 3, 2020.

[60] S. T. Dalal, “Some non-conventional cases of column design,” *Eng. J. -AISC*, vol. 6, no. 1, pp. 28–39, 1969.

[61] Computers and Structures Inc. (CSI), “Structural Software for Analysis and Design-SAP 2000.” Walnut Creek, CA.

[62] M. Bosco, E. M. Marino, and P. P. Rossi, “Importance of link models in the assessment of the seismic response of multi-storey ebfs designed by ec8,” *Ing. Sismica*, vol. 33, no. 3, pp. 82–93, 2016.

[63] P. W. Richards and C.-M. Uang, “Testing Protocol for Short Links in Eccentrically Braced Frames,” *J. Struct. Eng.*, vol. 132, no. 8, pp. 1183–1191, 2006.

[64] F. C. Filippou, E. P. Popov, and V. V. Bertero, “Effects of Bond Deterioration on Hysteretic Behavior of Reinforced Concrete Joints,” Earthquake Engineering Research Center, University of California, Berkeley, CA, Report EERC 83-19, 1983.

[65] E. Karamanci and D. G. Lignos, “Computational Approach for Collapse Assessment of Concentrically Braced Frames in Seismic Regions,” *J. Struct. Eng.*, no. 2008, 2014.

[66] A. Aguero, C. Izvernari, and R. Tremblay, “Modeling of the Seismic Response of Concentrically Braced Steel Frames Using the OpenSees Analysis Environment,” *Int. J. Steel Constr.*, vol. 2, no. 3, pp. 242–274, 2006.

[67] C. P. Lamarche and R. Tremblay, “Seismically Induced Cyclic Buckling of Steel Columns including Residual-stress and Strain-rate Effects,” *J. Constr. Steel Res.*, vol. 67, no. 9, pp. 1401–1410, 2011.

[68] P. Uriz, F. C. Filippou, and S. A. Mahin, “Model for Cyclic Inelastic Buckling of Steel Braces,” *J. Struct. Eng.*, vol. 134, no. 4, pp. 619–628, 2008.

[69] A. Imanpour, M. Leclerc, R. Siguier, and R. Tremblay, “Application of Hybrid Simulation for the Evaluation of the Buckling Response of Steel Braced Frame Columns,” *Ernst Sohn, ce/papers Spec. Issue*, vol. 1, no. 2–3, pp. 2877–2886, 2017.

[70] T. V. Galambos and R. L. Ketter, “Columns under combined bending and thrust,” *J. Eng. Mech. Div.*, vol. 85, no. 2, pp. 135–152, 1959.

[71] M. Dehghani, R. Tremblay, and M. Leclerc, “Fatigue Failure of 350WT Steel Under Large-strain Seismic Loading at Room and Subfreezing Temperatures,” *Constr. Build. Mater.*, vol. 145, pp. 602–618, 2017.

[72] NRC-Commentaries, *User’s Guide – NBC 2015 Structural Commentaries (Part 4 of Division B)*. Ottawa, ON: Associate Committee on the National Building Code, 2015.

[73] P. A. Seaburg and C. J. Carter, “Steel Design Guide Series 9: Torsional Analysis of Structural Steel Members,” American Istitute of Steel Construction, Chicago, IL, 2003.

[74] R. Montuori, E. Nastri, and V. Piluso, “Theory of Plastic Mechanism Control for MRF-EBF dual systems: Closed form solution,” *Eng. Struct.*, vol. 118, pp. 287–306, 2016.

[75] A. Imanpour and R. Tremblay, “Seismic performance evaluation and design of multi-tiered steel concentrically braced frames,” in *10th U.S. National Conference on Earthquake Engineering*, 2014.

[76] A. Ashrafi and A. Imanpour, “Seismic response of steel multi-tiered eccentrically braced frames,” *J. Constr. Steel Res.*, vol. 181, 2021.

[77] A. Filiatrault, R. Tremblay, C. Christopoulos, B. Folz, and D. Pettinga, *Elements of earthquake engineering and structural dynamics*, 3rd Ed. Presses Internationales

Polytechnique, 2013.

[78] American Institute of Steel Construction-AISC, *Seismic design manual*, 3rd Ed. Chicago, IL, 2012.

[79] E. Voce, "The relationship between stress and strain for homogeneous deformation," *J. Inst. Met.*, vol. 74, pp. 537–562, 1948.

[80] J. L. Chaboche, K. D. Van, and G. Cordier, "Modelization of the strain memory effect on the cyclic hardening of 316 stainless steel," in *5th Int. Conf. on Structural Mechanics in Reactor Technology*, 1979.

[81] Y. B. Minouei, "Seismic evaluation and retrofit of existing concetrically braced steel frames in Canada," Civil, Goelogical and Mining Engineering Department, Polytechnique Montreal, 2017.

[82] B. V. Fell, "Large-scale testing and simulation of earthquake-induced ultra low cycle fatigue in bracing members subjected to cyclic inelastic buckling," Civil and Enviromental Engineering, University of California Davis, 2008.

[83] C. D. Stoakes and L. A. Fahnestock, "Cyclic flexural testing of concentrically braced frame beam-column connections," *J. Struct. Eng.*, vol. 137, no. 7, pp. 739–747, 2011.

[84] J. Liu and A. Astaneh-Asl, "Cyclic testing of simple connections including effects of slab," *J. Struct. Eng.*, vol. 126, no. 1, pp. 32–39, 2000.

[85] A. Imanpour and R. Tremblay, "Analysis methods for the design of special concentrically braced frames with three or more tiers for in-Plane seismic demand," *J. Struct. Eng.*, 2017.

[86] A. Imanpour *et al.*, "Development and application of multi-axis hybrid simulation for seismic stability of steel braced frames," *Eng. Struct.*, vol. 252, no. November 2021, p. 113646, 2021.

[87] A. T. Council, *Quantification of building seismic performance factors*. US Department of Homeland Security, FEMA, 2009.

[88] Americal Institute of Steel Construction, *Seismic Design Manual*, 3rd Edition. 2018.

[89] J. Packer, D. Sherman, and M. Lecce, *Design Guide 24: Hollow Structural Section Connections*. American Istitute of Steel Construction, 2010.

Appendix A. Experimental Specimens

A.1 Introduction

The design of eccentrically braced frame (EBF) specimens and test setup is described in this appendix. Three two-tiered EBFs representing the lateral load-resisting system of a single-storey steel building are designed to investigate the seismic response of MT-EBFs, verify the results of numerical simulation presented in Chapters 3–5, and validate the proposed design methods outlined in Chapters 4 and 5 for MT-EBFs with I-section and built-up tubular links, respectively. The experimental test setup was designed to impose gravity (in force-controlled mode) and lateral seismic loads expected under a design level hazard earthquake (in displacement-controlled mode). The details of member sizes and limit state checks for each specimen are presented here. Structural drawings are provided in Appendix B.

The test matrix consisting of three full-scale two-tiered EBF specimens is given in Figure A-1. The geometries of Specimens 1 and 2 are identical, and both consist of wide-flange link beams. Specimen 1 is designed in accordance with 2019 CSA S16 provisions assuming both links are laterally braced while the intermediate link is unbraced during the test. Specimen 2 is designed using the proposed design method presented in Chapter 4. Specimen 3, which consists of continuous built-up tubular beams, is intended to reduce the tendency of the intermediate link to lateral-torsional buckling and is therefore designed as per the requirements described in Chapter 5 adapted for two-tiered EBFs.

The frame specimens also include the column base connection and footing to examine their effects on the seismic response of EBFs. Columns are made of W-shapes and are oriented so that in-plane demands create weak-axis bending. Braces consist of square hollow structural sections (HSSs). Roof and intermediate beams of Specimens 1 and 2 are made of wide flange sections. Wide-flange

sections are made of ASTM A992 Gr. 50 steel with F_y = 345 MPa, and HSSs conform to ASTM A1085 Gr. C steel with F_y = 345 MPa. Tubular beams of Specimen 3 plus connection plates are made of ASTM A572 Gr. 50 steel with F_y = 345 MPa.

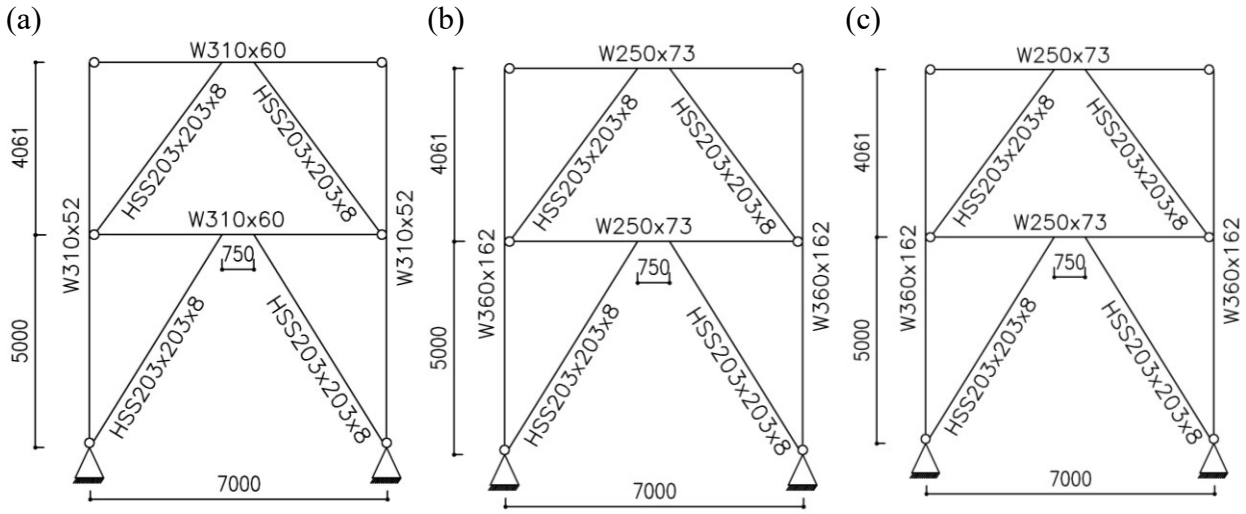

Figure A-1. (a) Specimen 1; (b) Specimen 2; (c) Specimen 3 (dimensions in mm).

The specimens span 7000 mm. The total height of the specimens is 9061 mm divided between two tiers as h_1 = 5000 mm and h_2 = 4061 mm. Unequal tier heights are chosen to intentionally initiate shear yielding in the first-tier link, followed by yielding in the second-tier link, creating progressive link yielding.

The frames are loaded vertically using two 500 kN vertical hydraulic actuators connected to the strong floor and then laterally displaced at the roof level using two 1000 kN horizontal hydraulic actuators as shown in Figure A-2. The lateral bracing systems to brace the columns and the roof link are attached to the strong wall as shown in Figure A-2.

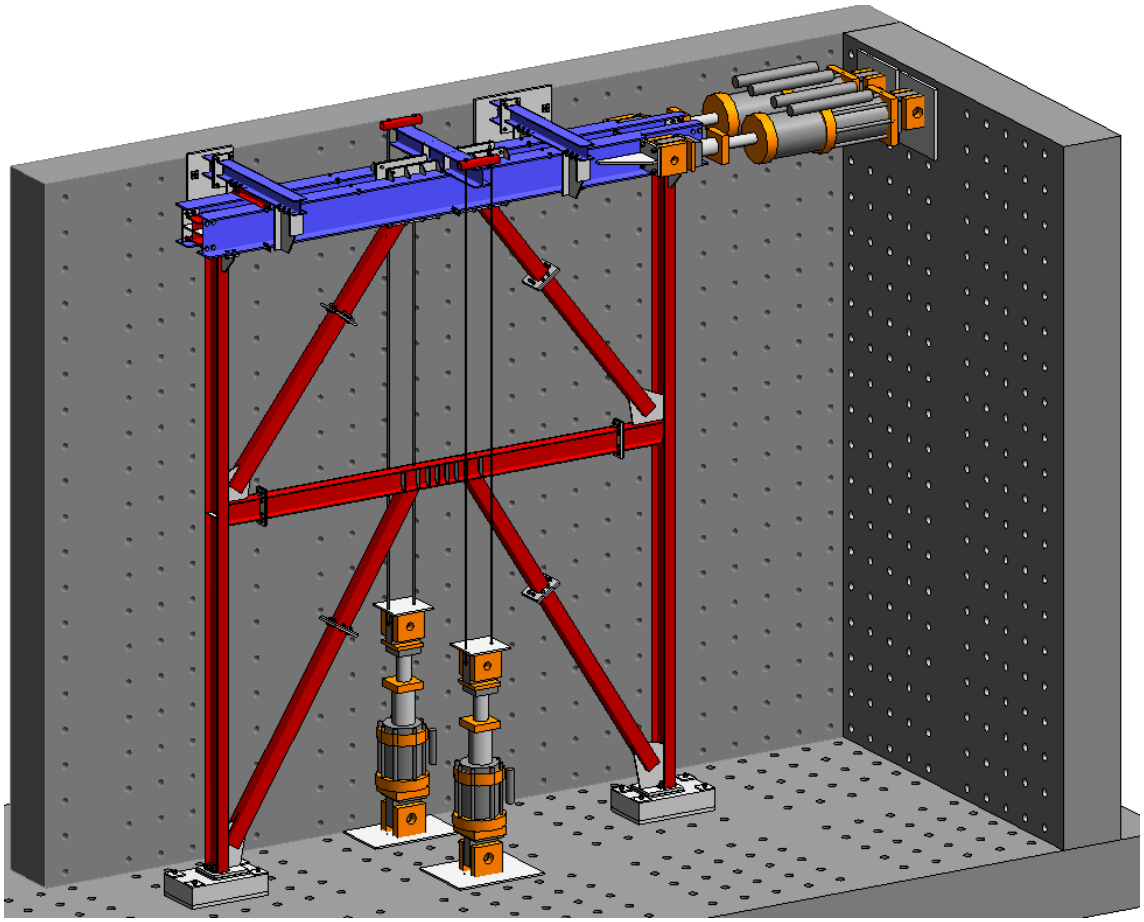

Figure A-2. Two-tiered eccentrically braced frame experimental test setup.

To facilitate transportation and assembly of specimens and remove any weld work in the laboratory, each specimen is divided into four segments, as shown in Figure A-3. The segments are connected to each other in the laboratory using end-plate bolted connections, as shown in Figure A-3. To assemble the specimens, two segments containing the columns (Segments 1 and 2) are first set on the footings, which themselves are anchored to the strong floor, while laterally secured with temporary supports. The remaining two segments (Segments 3 and 4) are then swung in and bolted to the column subassemblies.

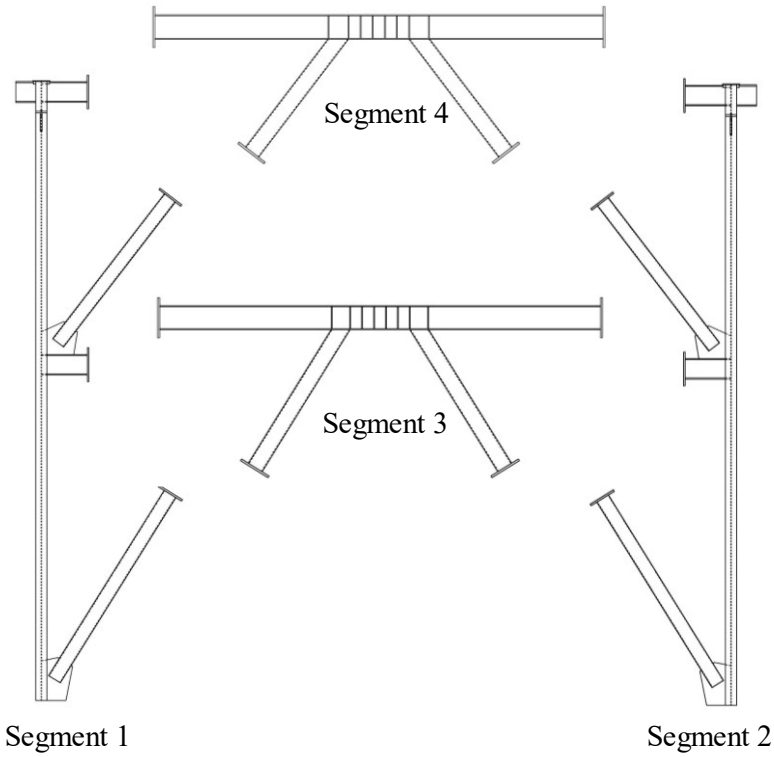

Figure A-3. Four segments of the test specimens.

A.2 Specimen Design

Specimen 1

Specimen 1 was designed under gravity and seismic loads as described for the two-tiered frame with continuous wide-flange links in Section 4.2.1. The design method described in Section 4.2.2 was followed to size the link beams, braces, and columns. A W310×60 link was selected to resist the shear and flexure from the applied lateral loads, assuming that the links yield in shear. Braces and columns were designed to resist gravity loads plus probable shear resistance of the link beam; a link strain hardening parameter of 1.4 was assumed instead of the code-specified value of 1.3 because recent experimental tests on wide-flange shear links constructed of ASTM A992 exhibited an average strain hardening factor of 1.4 [10]. Given that the link beams are continuous, outer beams were checked to resist, in the elastic range, the combined effects of axial force and strong-

axis bending induced by the probable shear resistance of the link. Frame geometry and selected members are shown in Figure A-4. Note that the W310×107 beam stubs shown at the roof level are part of the loading system, which is described in Section A.4.1.

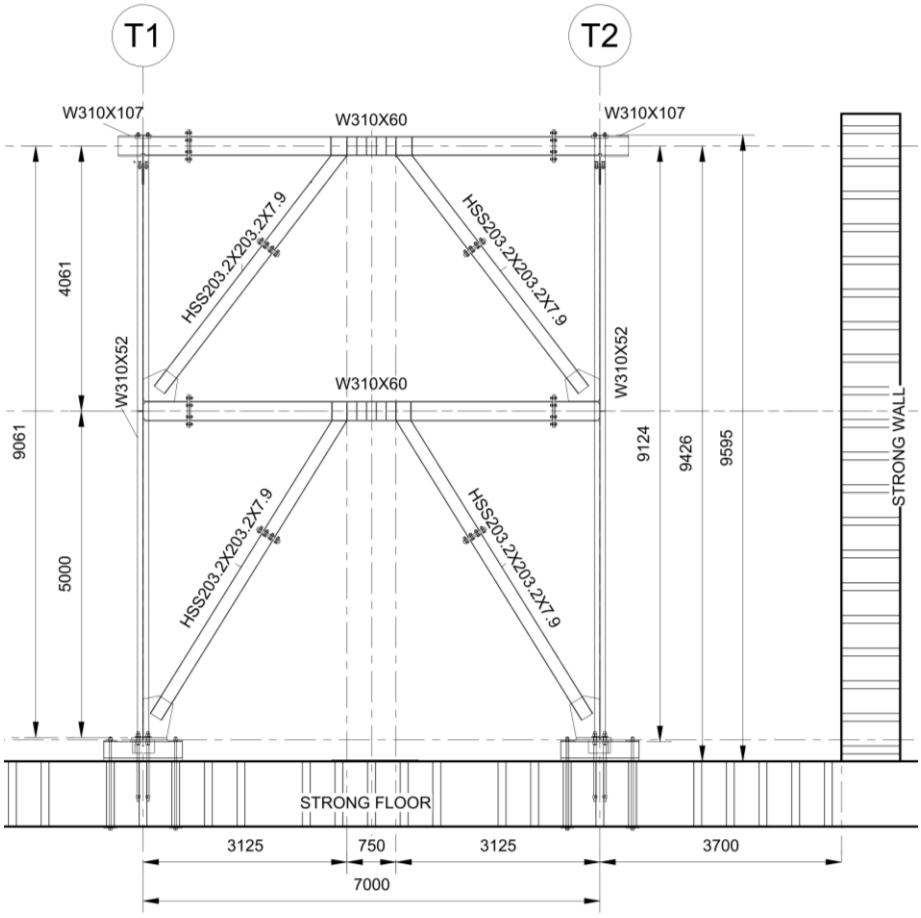

Figure A-4. Geometry and selected members for Specimen 1 (dimensions in mm).

Specimen 2

The gravity and seismic loads for Specimen 2 are the same as for Specimen 1. The design procedures in Section 4.5 were followed to redesign Specimen 1 as Specimen 2. Because of the minimum out-of-plane strength and stiffness requirements for the intermediate beam in the proposed method, the W310×60 link beam was changed to W250×73. In-plane and out-of-plane bending moments combined with an axial force induced by gravity and the seismic loads were used to design the columns. Moreover, the weak-axis flexural stiffness of the column was used to

limit inelastic link rotation in Tier 1. Figure A-5 shows the frame dimensions and the final selected members.

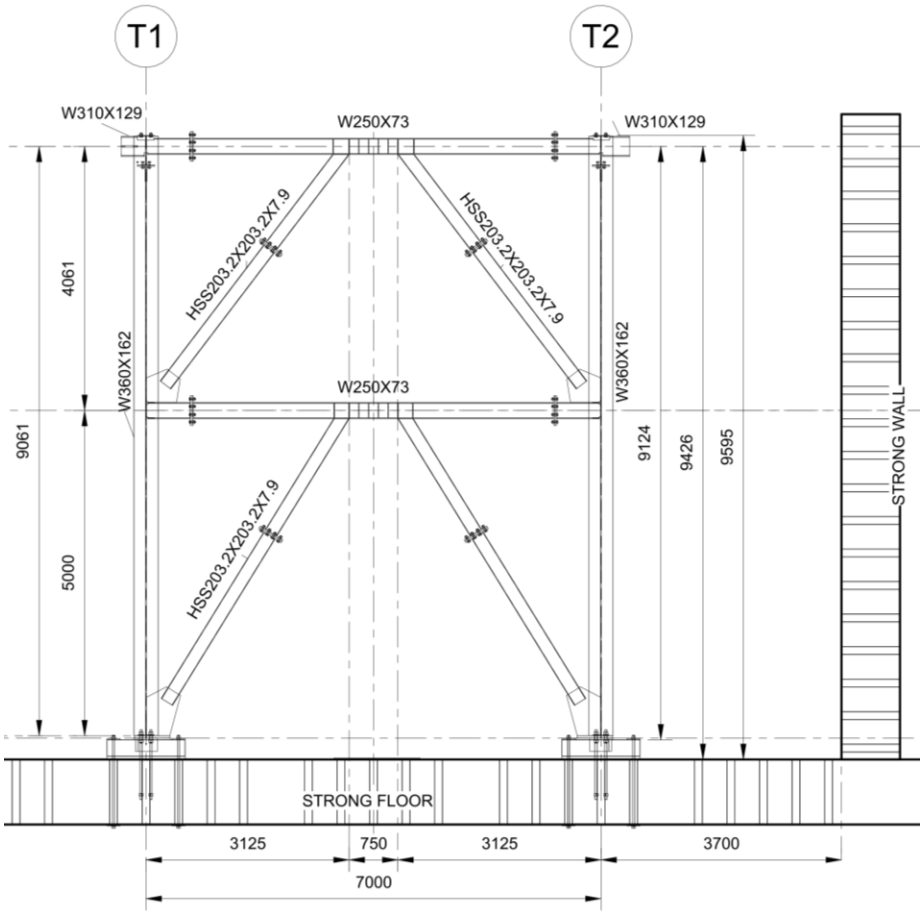

Figure A-5. Geometry and selected members for Specimen 2 (dimensions in mm).

Specimen 3

The gravity and seismic loads of Specimen 3 are identical to those described for Specimen 1. The design steps described in Section 5.2.1 were used to design the links, outer beams, braces, and columns. A built-up tubular link was used in this specimen. Braces, columns, and outer beams were then designed to resist the probable shear resistance of the links. The strain hardening parameter used for the probable shear resistance of the link was set at 1.6 instead of the code-specified value of 1.45 acknowledging the findings from recent experimental tests on built-up

tubular links [30], showing that post-yield capacity of such links may exceed the value prescribed by CSA S16. Figure A-6 shows the geometry and selected members for Specimen 3.

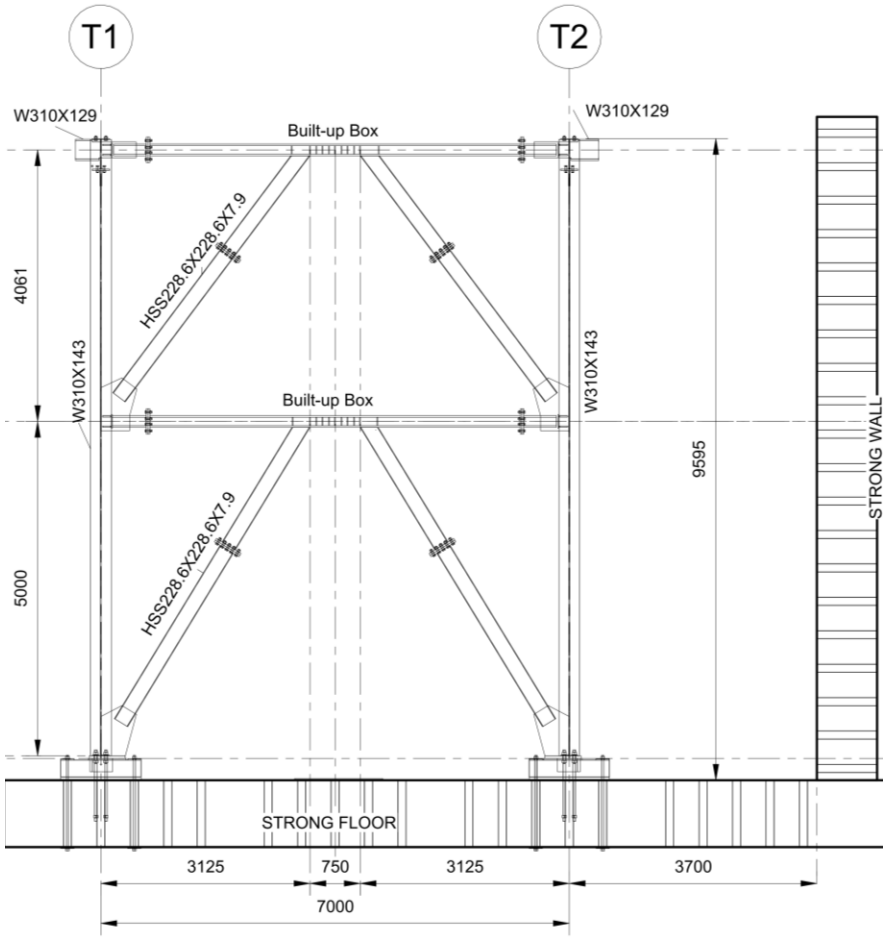

Figure A-6. Geometry and selected members for Specimen 3 (dimensions in mm).

A.3 Connection Design

Frame connections were designed to resist the demands induced by probable link resistances as per CSA S16 following design steps described in the AISC Seismic Design Manual [88]. The key design considerations and checks for the connections of all three specimens are presented here.

A.3.1 Brace Splice

The brace splice was designed as a bolted end-plate connection (Figure A-7) under an axial tension force of 916 kN and a flexural bending moment equal to 46 kN-m for Specimens 1 and 2, and 1069

kN and 103 kN-m for Specimen 3, respectively. As proposed by AISC Design Guide 24 [89], the moment is converted to an equivalent axial force and is added to the original design tensile force. The thickness of the end plate t_p is set by verifying prying action in the connection as follows:

$$t_p \geq \sqrt{4.44(P_u/n)b'/pF_{py}} \quad \text{(A-1)}$$

where P_u is the design axial force, n is the number of bolts, b' is the clear distance between the bolts and the HSS, p is the length of end-plate tributary to each bolt, and F_{py} = 345 MPa is the yield strength of the end-plate. The bolts were selected to resist the combination of tensile and shear forces in the braces: 1668 kN and 13 kN for Specimens 1 and 2, respectively, and 2536 kN and 29 kN for Specimen 3, respectively. The size and number of bolts were chosen to ensure that the shear and tensile strengths of bolts are greater than applied forces. Additionally, the bolts were proportioned to resist the interaction of shear and tensile forces.

A set of 25-mm bolts conforming to ASTM A325 are selected and placed on four sides of the connection plate as shown in Figure A-7 (8 bolts for Specimens 1 and 2, and 12 bolts for Specimen 3). HSS braces are connected to the end-plate using fillet welds designed to take the applied tensile force in shear assuming an E49XX electrode with a tensile strength of X_u = 490 MPa. Additionally, the combined tensile and shear strength of the welds was checked against the brace tension and shear forces. Table A-1 gives a summary of key design limit states verified for brace splices.

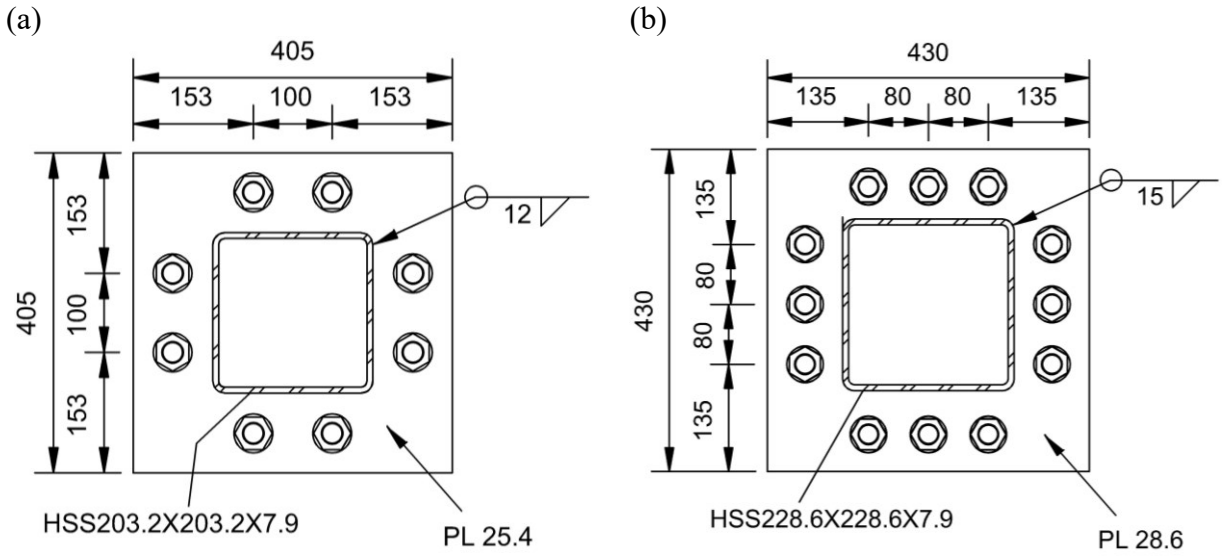

Figure A-7. Brace splice connections: (a) Specimens 1 and 2; (b) Specimen 3 (dimensions in mm).

Table A-1. Brace splice place design: limit states and demand-to-capacity ratios.

Limit State	Specimen 1	Specimen 2	Specimen 3
End-plate tensile yielding	0.88	0.89	0.94
End-plate shear yielding	0.13	0.14	0.16
End-plate shear rupture	0.26	0.27	0.36
End-plate bearing/tear-out	0.004	0.004	0.005
Bolt failure in tension	0.82	0.83	0.56
Bolt failure in shear	0.01	0.01	0.02
Fillet weld shear failure	0.78	0.80	0.84

A.3.2 Beam Splice Connections

The intermediate and roof beams of Specimens 1 and 2 are spliced with an extended end plate as shown in Figure A-8a and A-8b, respectively. The location of the splice was chosen where the bending moment demand is at a minimum on the beam to reduce the plate thickness and the number of bolts. Only one type of the beam splice connections was designed based on the most critical loading conditions in Specimens 1 and 2 to ease fabrication. The connection was designed to carry a design bending moment equal to the strong-axis bending moment in the beam 79 kN-m

plus an equivalent bending moment 84 kN-m, which is the axial force obtained by multiplying the beam axial force by the distance between the centroid of flanges.

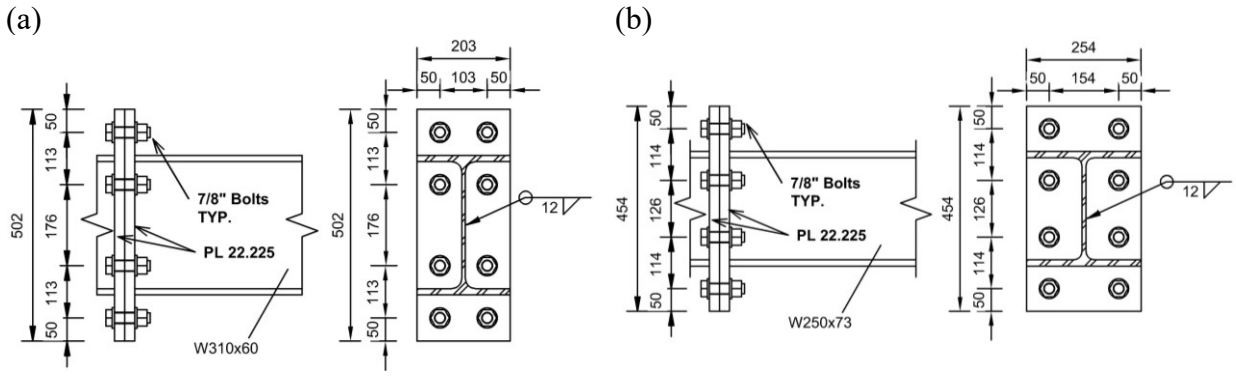

Figure A-8. Wide-flange beam splice connections: (a) Specimen 1; (b) Specimen 2 (dimensions in mm)

The following limit states were verified in design:

- Bolt failure under combined tension and shear
- Tensile yielding of the end-plate
- Shear yielding and rupture of the end-plate
- Bearing and tear-out failure of the end-plate
- Fillet weld fracture

Table A-2 summarizes the design limit states for the wide-flange beam splice connections of Specimens 1 and 2.

Table A-2. Wide-flange beam splice design: limit states and demand-to-capacity ratios.

Limit State	Specimen 1	Specimen 2
End-plate tensile yielding	0.86	0.83
End-plate shear yielding	0.30	0.26
End-plate shear rupture	0.47	0.37
End-plate bearing/tear-out	0.06	0.06
Bolt failure in tension	0.88	0.91
Bolt failure in shear	0.13	0.12
Fillet weld shear failure	0.61	0.64

Similar to Specimens 1 and 2, the intermediate and the roof beams in Specimen 3 are spliced with an end plate (Figure A-9). The splice was designed to carry a design axial tension force equal to the axial tension force in the beam 664 kN plus an equivalent axial tension force 495 kN, which is the flexural bending obtained by dividing the bending moment by the depth of the section. The design limit states for tubular beam splices are the same as those verified for HSS brace splices as described in Table A-1. Table *A-3* summarizes the design limit states for tubular beam splices of Specimen 3.

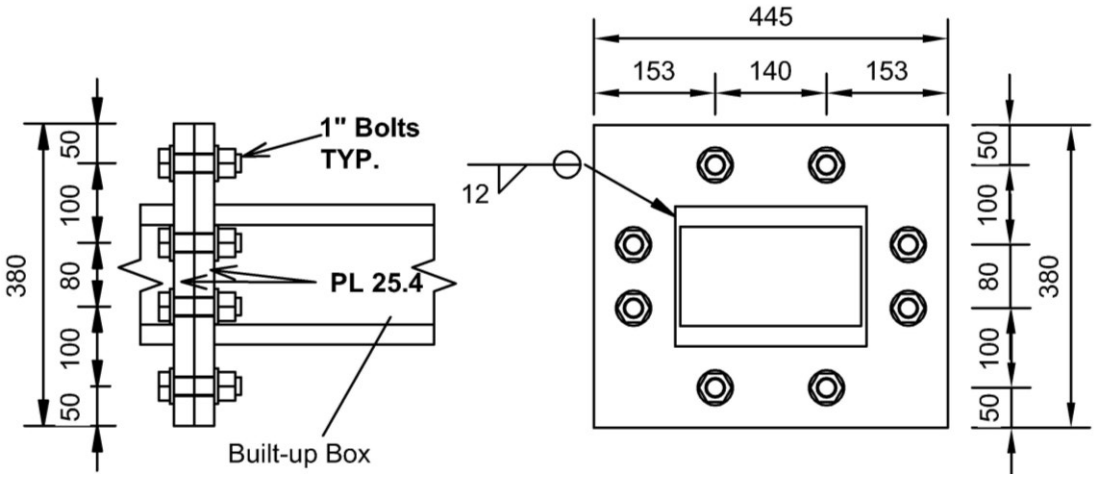

Figure A-9. Built-up tubular splice connection in Specimen 3 (dimensions in mm).

Table A-3. Built-up tubular beam splice design: limit states and demand-to-capacity ratios.

Limit State	Specimen 3
End-plate tensile yielding	0.72
End-plate shear yielding	0.01
End-plate shear rupture	0.17
End-plate bearing/tear-out	0.02
Bolt failure in tension	0.58
Bolt failure in shear	0.06
Fillet weld shear failure	0.80

A.3.3 Tier 1 Gusset Plate

The details of brace gusset plates in Tier 1 are shown in Figure A-10 for all three specimens. As shown, a slotted connection was used to connect the brace to the gusset plate to transfer the brace axial force. The gusset plate is welded to the base plate and the column web.

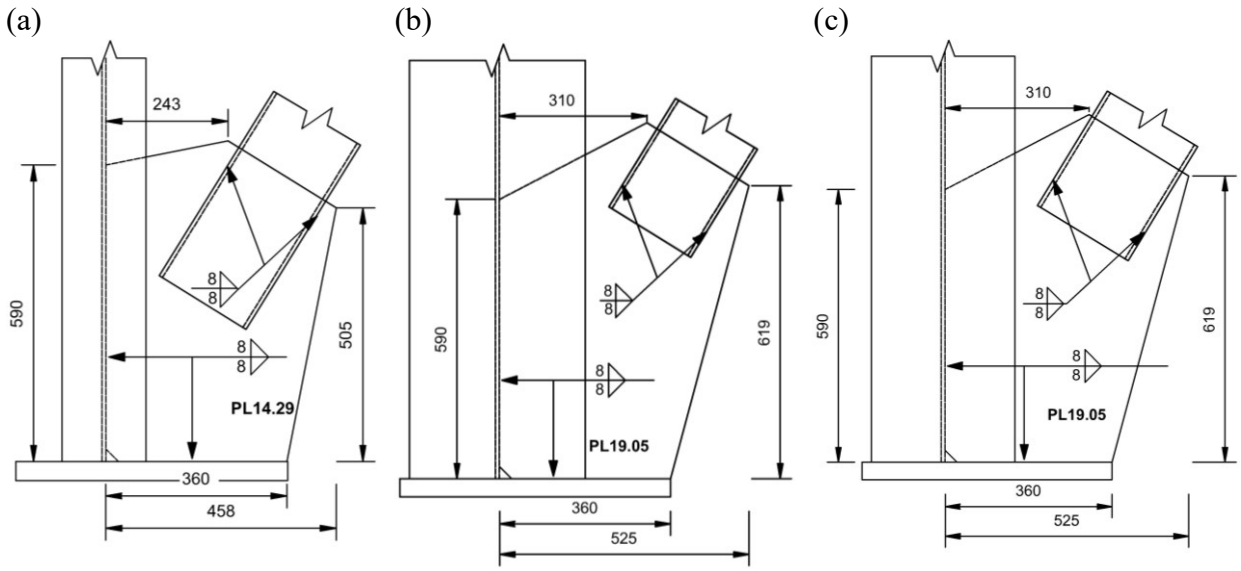

Figure A-10. Tier 1 gusset plate dimensions: (a) Specimen 1; (b) Specimen 2; (c) Specimen 3 (dimensions in mm).

The uniform force method (UFM) was used to analyze the brace-to-column gusset plate connection. The work point was located at the intersection of the column centreline and the top surface of gusset plate. Brace axial force was decomposed into a horizontal force in the gusset-to-base plate interface and a vertical load in the gusset-to-column connection. The weld between the base plate and the gusset plate was designed for this horizontal force and the weld between the column web and the gusset plate was sized for the vertical component of the brace axial force. The yielding limit state of the gusset plate in the Whitmore section was controlled under the brace axial force: 884 kN for Specimen 1, 857 kN for Specimen 2, and 999 kN for Specimen 3. Buckling of the gusset plate was checked over the unrestrained length under the same axial force. Additionally, the gusset plate thickness should be large enough to transfer the forces at the intersection of both

the base plate and the column web. Table *A-4* summarizes the design of the first-tier gusset plate connections.

Table A-4. Tier 1 brace-to-beam/column connection design: limit states and demand-to-capacity ratios.

Limit State	Specimen 1	Specimen 2	Specimen 3
Brace-to-gusset weld shear failure	0.60	0.58	0.68
Brace shear rupture	0.52	0.50	0.59
Gusset plate yielding at Whitmore section	0.35	0.26	0.28
Gusset plate buckling	0.62	0.45	0.50
Gusset plate shear rupture	0.58	0.42	0.49
Gusset-to-base plate weld shear failure	0.66	0.64	0.75
Gusset-to-base plate shear yielding	0.44	0.32	0.37
Gusset-to-column weld shear failure	0.65	0.63	0.73
Gusset-to-column shear yielding	0.44	0.32	0.37

A.3.4 Tier 2 Gusset Plate

Specimens 1 *&* 2

The brace gusset plate connection to the intermediate beam in Tier 2 consists of welded connections to the top flange of the intermediate beam and the column web as shown in Figure A-11a and A-11b. Similar to Tier 1, the slotted HSS brace was welded to the gusset plate. The UFM was used to analyze the connection and determine the forces. Brace axial force was decomposed into the shear and normal forces at the intersection of the gusset plate with both the beam flange and the column web. In addition to the limit states described in Section A.3.3, the gusset plate thickness was chosen so that the tensile yielding capacity of the gusset plate remains greater than the tensile force at the intersection of gusset plate with the beam flange and column web. The yielding and crippling limit states of the beam web were controlled under the concentrated compressive load at the intersection of the gusset plate and the beam flange. Table *A-5* presents the limit states and demand-to-capacity ratios for second-tier gusset plate connections.

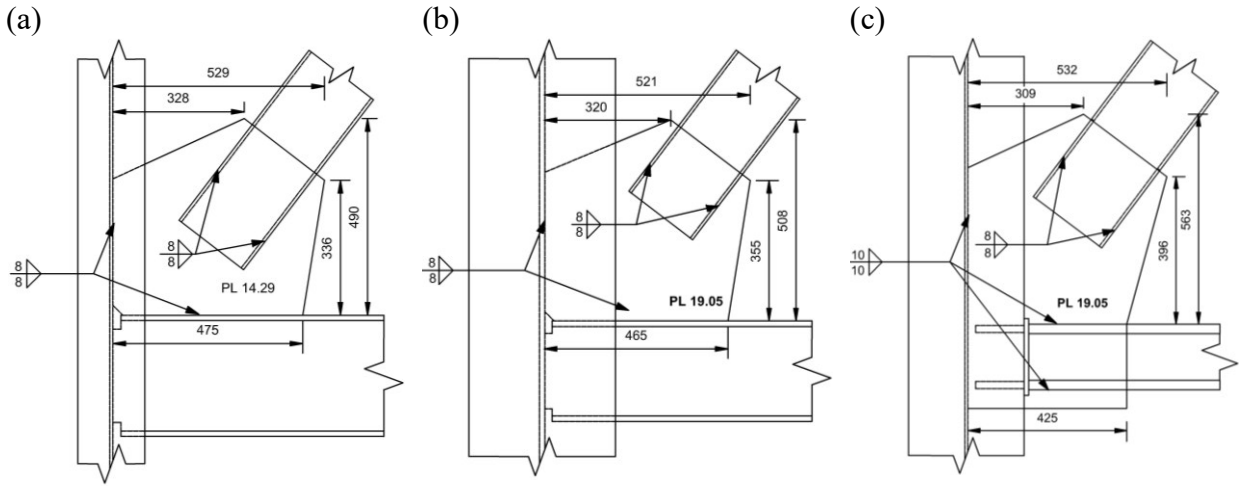

Figure A-11. Tier 2 brace gusset plate connections: (a) Specimens 1; (b) Specimen 2; (c) Specimen 3 (dimensions in mm).

Specimen 3

Brace end connections in Specimen 3 are different from those in Specimens 1 and 2, because Specimen 3 consists of built-up box beams. The brace-to-beam gusset plate was therefore inserted in the tubular beam and welded to both the top and bottom flanges of the box as shown in Figure A-11c. This connection detail allows for better distribution of vertical tensile force at the intersection of gusset plate and beam flanges while minimizing the excessive deformation in the flange of the tubular beam. Table A-5 gives a summary of the design for the brace-to-beam/column connections.

Table A-5. Tier 2 brace-to-beam/column connection design: limit states and demand-to-capacity ratios.

Limit State	Specimen 1	Specimen 2	Specimen 3
Brace-to-gusset filler weld shear failure	0.64	0.62	0.73
Brace shear rupture	0.55	0.54	0.63
Gusset plate tensile yielding at Whitmore section	0.38	0.27	0.30
Gusset plate buckling	0.48	0.34	0.41
Gusset plate shear rupture	0.62	0.45	0.52
Gusset-to-beam weld shear failure	0.75	0.71	0.68
Gusset shear yielding at the face of the beam	0.41	0.32	0.40
Gusset tensile yielding at the face of the beam	0.16	0.11	0.10
Gusset-to-column weld shear failure	0.67	0.65	0.62
Gusset shear yielding at the face of the column	0.45	0.33	0.39
Gusset tensile yielding at the face of the column	0.01	0.01	0.01
Beam web yielding/crippling	0.50	0.30	0.70

A.3.5 Brace-to-beam Connection

The connection between the brace and the beam was designed as a flexurally rigid connection following CSA S16 provisions using a complete joint penetration (CJP) groove weld. Figure A-12 shows the brace-to-beam connections.

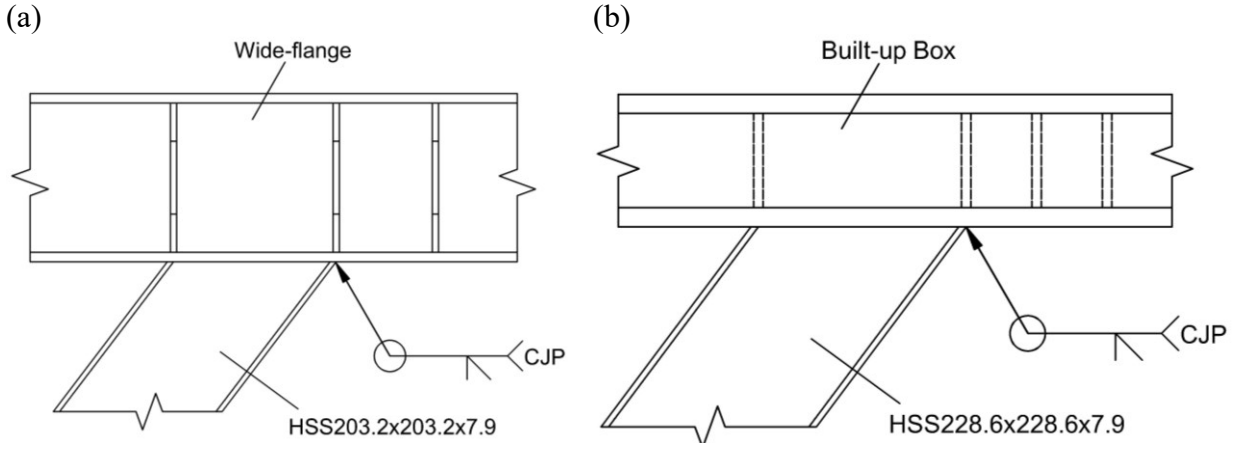

Figure A-12. Brace-to-beam connection: (a) Specimens 1and 2; (b) Specimen 3

A.3.6 Column Base Plate

Column base plates are anchored to a concrete footing, which itself is connected to the laboratory strong floor using six anchor rods, four at each corner of the rectangular footing and two at the

middle of the footing, connecting the 51-mm thick plate at the bottom of the footing to the strong floor, as shown in Figure A-13a and A-13b. The column base plate is anchored in the concrete footing using four 38-mm anchor rods, threaded in the 102-mm steel plate, as shown in Figure A-13b.

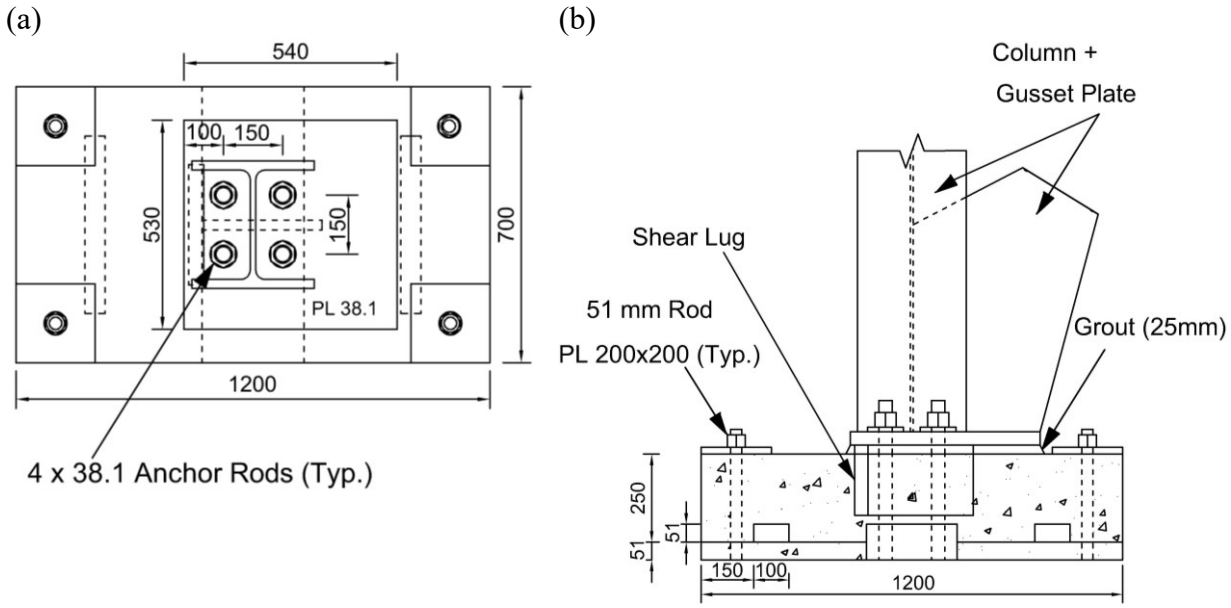

Figure A-13. Column base plate and concrete footing details (Specimen 1 shown): (a) Plan view; (b) Elevation view (dimensions in mm).

The column base plate was sized to ensure the concrete bearing resistance was not exceeded under design loads obtained from the link capacity forces plus gravity loads. The thickness of the baseplate was obtained by verifying plate yielding under compression and uplift forces of 1487 kN and 1211 kN for Specimen 1, 1447 kN and 1172 kN for Specimen 2, and 1679 kN and 1403 kN for Specimen 3, respectively. Base plate anchor rods are designed to resist the design tension force. Table A-6 summarizes the key limit states of the base plates.

Table A-6. Base plate design: limit states and demand-to-capacity ratios.

Limit State	Specimen 1	Specimen 2	Specimen 3
Concrete bearing	0.58	0.45	0.56
Base plate yielding	0.93	0.75	0.71
Anchor rod tensile failure	0.51	0.50	0.58

A.3.7 Link Stiffeners

Specimens 1 & 2

Link stiffeners consist of full-depth intermediate and end stiffeners welded to the flanges and the web of the link beam as shown in Figure A-14. The end stiffeners were provided on both sides of the web, whereas the intermediate stiffeners are placed on one side of the web spaced at 150 mm. Two additional stiffeners were installed along the HSS brace walls in the beam web to prevent web crippling and yielding due to the brace axial force. According to CSA S16, the thickness of the stiffeners shall be greater than w for intermediate stiffeners and $0.75w$ for end stiffeners, where w is the greater of the thickness of the link web and 10 mm; therefore, a thickness of 10 mm was selected.

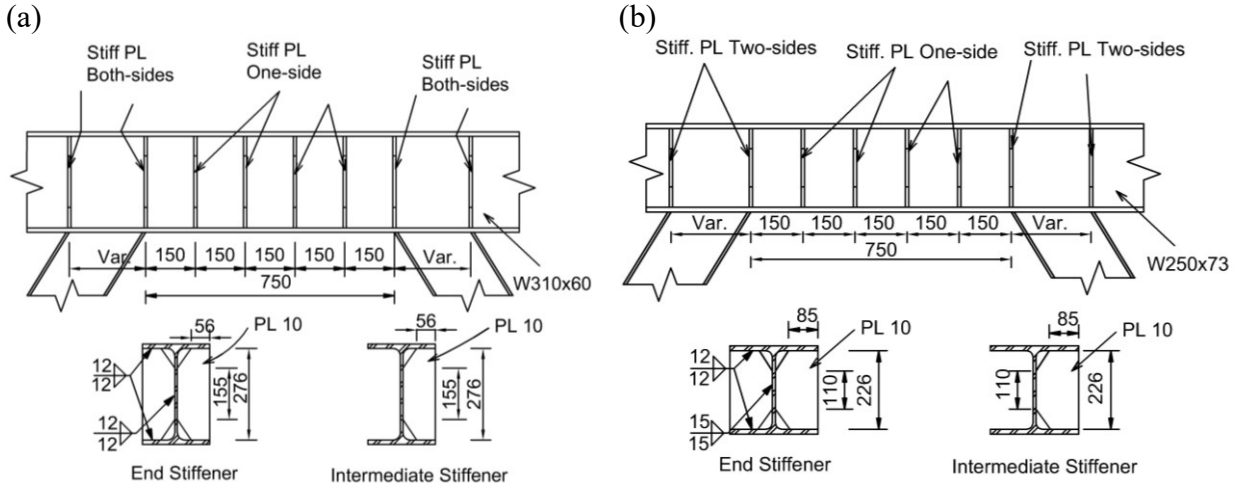

Figure A-14. Link stiffeners: (a) Specimens 1; (b) Specimen 2 (dimensions in mm).

Specimen 3

Tubular link stiffeners were placed inside the box section with spacing of 94 mm. They are welded to the bottom flange and both webs. As for Specimens 1 and 2, additional stiffeners were provided at the brace-to-beam connection inside the box to increase the resistance under the brace force (Figure A-15). The link stiffener thickness was chosen so that it was greater than $0.75w$, where w is the greater of the link web thickness and 13 mm.

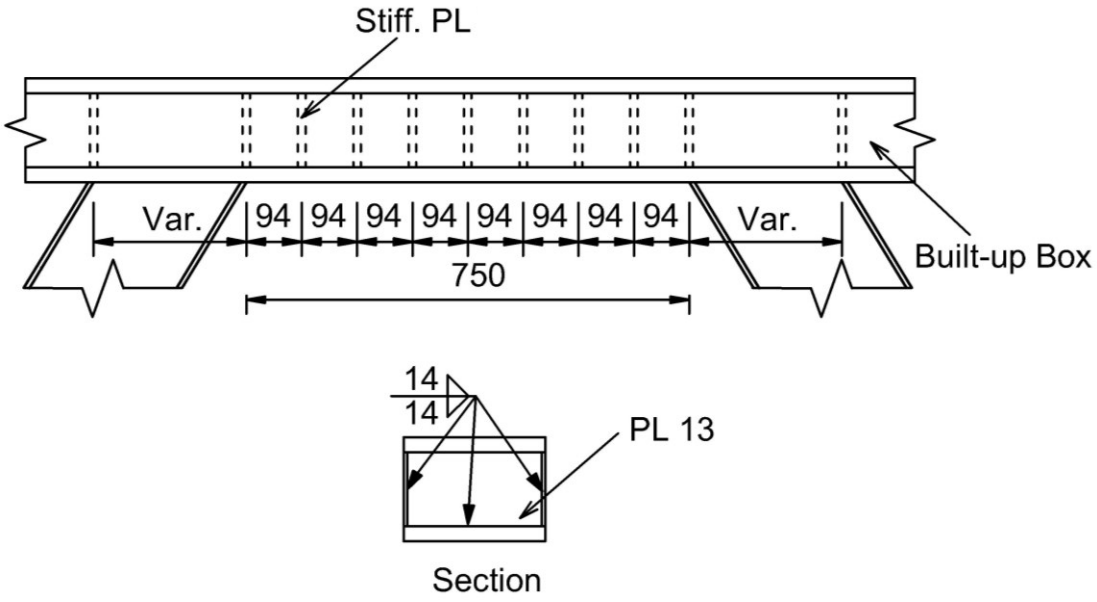

Figure A-15. Link stiffeners in Specimen 3 (dimensions in mm).

A.4 Experimental Setup

A.4.1 Loading Beam and Horizontal Load Path

Two parallel loading beams made of steel (W530×165) profiles (Figure A-2) were designed to impose the horizontal forces produced by horizontal hydraulic actuators and vertical (gravity) load produced by vertical hydraulic actuators to the top end of the columns as shown in Figure A-16a and 6-16b, respectively. Each hydraulic actuator is connected to one of the loading beams through a haunch plate as shown in Figure A-16a, which is intended to transfer the applied load to the web of the loading beam. To transfer the applied lateral load to the roof beam of the specimen, the loading beam is bolted to two extended W310×107 beams in Specimen 1 and W310×129 beams in Specimens 2 and 3 at either end of the frame as shown in Figure A-16b.

The horizontal actuators create an axial force of 378 kN in the loading beam, which is computed based on the probable shear resistance of the links with a safety factor of 1.5. This load is distributed evenly between the two loading beams. The concentrated gravity loads imposed by the vertical actuators generate a strong-axis bending moment of 362 kN-m in each loading beam.

Additionally, a weak-axis bending moment of 261 kN-m was added in design to account for the moment produced by the lateral bracing system of the roof link. The strength and stability of the loading beam were verified under cross-sectional strength, overall member strength, and lateral-torsional buckling strength limit states. The respective demand-to-capacity ratios are 0.73, 0.90, and 0.96, respectively. The axial load in the loading beam is transferred to the web of the roof beam extension outside of each column through a welded T, which is welded to the roof beam extension and bolted to the loading beams as shown in Figure A-16b. This plate is then connected with a welded connection. The following limit states were verified to design the T-plates: bolts failure in shear, bearing and tear-out failure of the plate, shear yielding of the plate, tensile yielding and rupture of the plate, and fillet weld fracture. Table A-7 summarizes the limit states and the demand-to-capacity ratios for the T-plates.

Table A-7. Loading beam to T design: limit states and demand-to-capacity ratios.

Limit State	Demand-to-Capacity Ratio
Bolts failure in shear	0.35
Bearing and tear-out failure of the plate	0.43
Shear yielding of the plate	0.65
Tensile yielding and rupture of the plate	0.24
Fillet weld fracture	0.55

Two vertical hydraulic actuators are attached to the strong floor to impose the vertical gravity load to the loading beam through pulling vertical rods connected to a W250×101 profile that is bolted to the top flange of the loading beams as shown in Figure A-17. This setup maintains the gravity load while the frame moves laterally. The loading beam finally imposes the vertical load of the actuators to the top of the columns through a stiffened seated connection as shown in Figure A-16b. The stiffened seated connection was designed for a concentrated load of 103 kN, which is equal to the vertical reaction force of the loading beam due to the gravity load. The vertical and horizontal plates of the seated connection are welded to the column flange at each end. The length and

thickness of the vertical plate should be adequate to transfer the vertical reaction force without shear and tensile yielding. Additionally, the local buckling limit (i.e., width-to-thickness ratio limit) and the crippling of the vertical plate were verified. A summary of the limit states for the stiffened seated connection is presented in Table A-8.

Table A-8. Stiffened seated connection design: limit states and demand-to-capacity ratios.

Limit States	Demand-to-Capacity Ratio
Vertical plate yielding	0.05
Vertical plate shear yielding	0.07
Vertical plate crippling	0.14
Vertical plate local buckling	0.98
Vertical plate-to-column weld shear failure	0.13

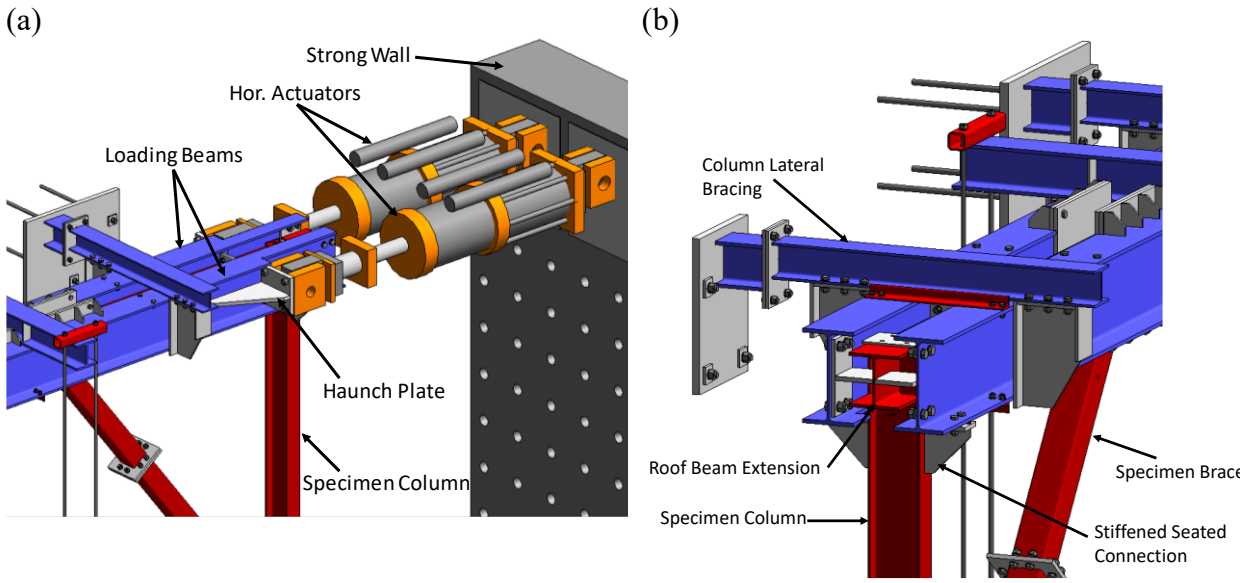

Figure A-16. Loading beam: (a) Details of horizontal actuator and loading beam connections; (b) Details of the frame column and the loading beam connections.

A.4.2 Out-of-plane Lateral Support

Out-of-plane lateral support systems were designed to laterally brace the top end of columns and the ends of the link beam at the roof level while accommodating the in-plane horizontal and vertical displacements of the frame. The loading beam is laterally braced at its two ends near the columns using two W200×59 profiles running perpendicular to the loading beam, as shown in Figure A-17.

These profiles are connected to the strong wall. Two copped W-shapes are bolted to the bottom flange of the lateral support beam to sandwich the load beams, as shown in Figure A-17c. These copped W-shapes are in contact with the loading beams and prevent out-of-plane movement of the beams. The lateral support system is designed to resist a concentrated load applied at the most critical location (i.e., bottom edge of the plate) to create the maximum demands. This concentrated load was calculated as 136 kN, which is the aggregate of the required lateral bracing force for the columns, loading beams, and roof beam. The following limit states were controlled for the design of the lateral support: plate compressive yielding, plate shear yielding, plate crippling, bolts shear failure, bolts tension failure, fillet weld rupture. Table A-9 presents a summary of frame lateral support system design.

Table A-9. Frame lateral support system design: limit states and demand-to-capacity ratios.

Limit State	Demand-to-capacity Ratio
Plate compressive yielding	0.04
Plate shear yielding	0.10
Plate crippling	0.10
Bolts shear failure	0.48
Bolts tension failure	0.56
Fillet weld rupture	0.93

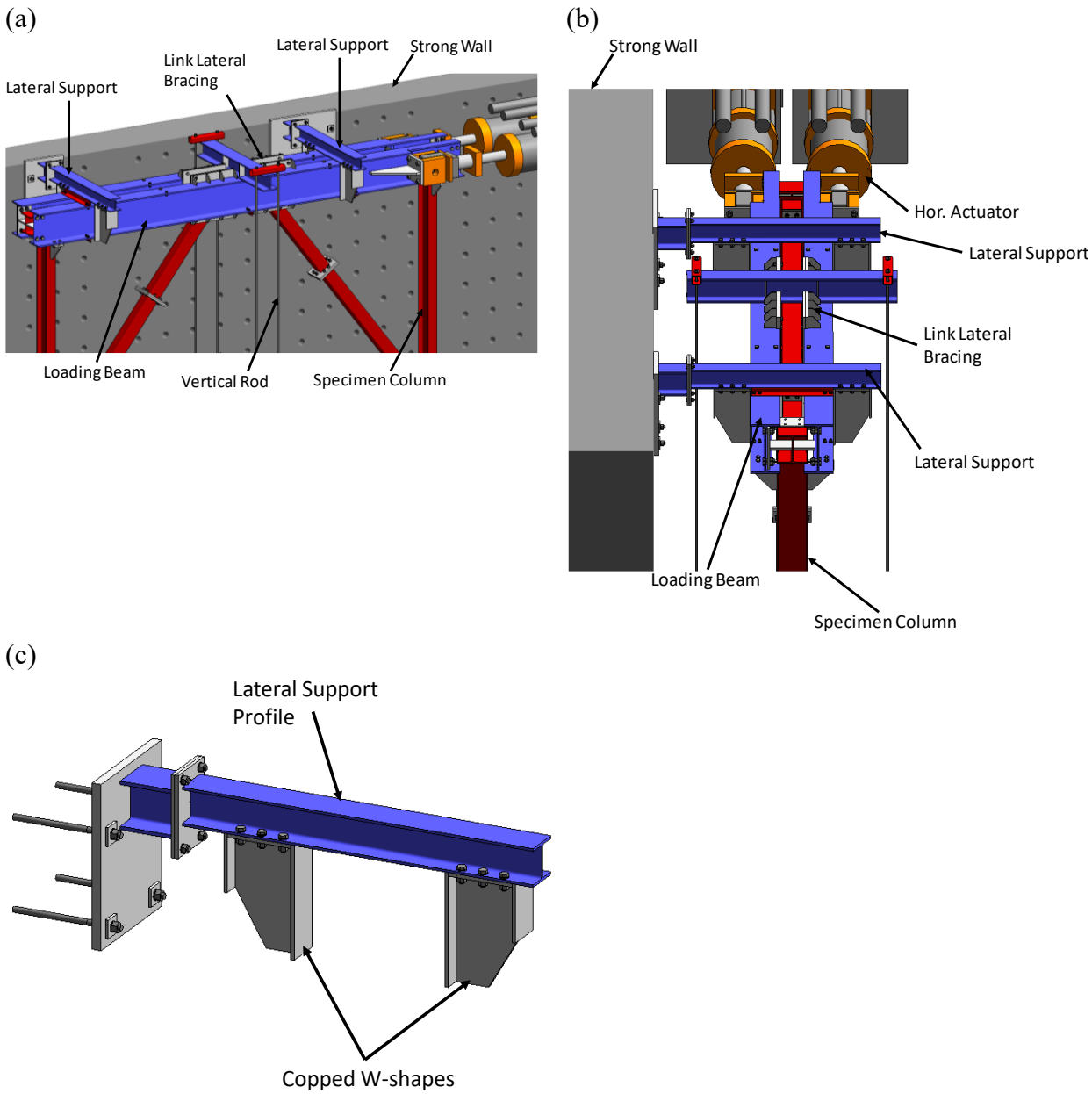

Figure A-17. Frame lateral support system: (a) Side view; (b) Top view; (c) Perspective view.

The link out-of-plane lateral support system is composed of two plates connected to the flanges of the loading beam adjacent to the specimen roof beam, as shown in Figure A-18. This system was designed to prevent out-of-plane movement of the two ends of the roof link beam by making contact between the plates and the link beam while the frame is displaced in vertical and horizontal directions. The strength of the plates was verified under the required lateral bracing force of the

link at each end, which is equal to 62 kN. The plates are extended above the loading beam to accommodate vertical displacement of the roof beam as the frame deforms. The stiffeners at the back of the plate (Figure A-18) are designed to shear and tensile yielding capacities of 376 kN and 513 kN to resist applied bracing forces.

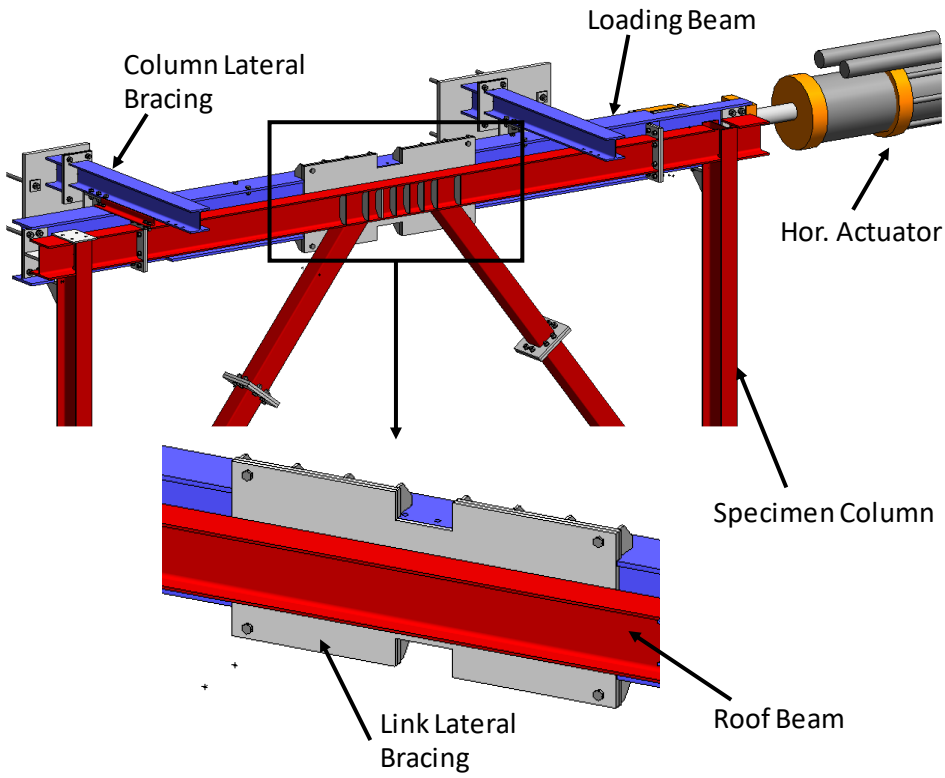

Figure A-18. Link lateral supports at the roof level (only one of the loading beams is shown for clarity).

A.5 Summary

This appendix outlined the design of a full-scale experimental test program, which aimed to examine the seismic response of steel multi-tiered EBFs, verify the numerical models developed in this project, and validate the proposed design requirements in Chapters 4 and 5. The experiments will be conducted at the University of Alberta in the future.

Appendix B. Member Design for Experimental Specimens

This appendix presents a summary of the member design for the test specimens following the loading assumptions and design steps outlined in Chapters 4 and 5.

Specimen 1

The base shear for this specimen is 540 kN. Specimen 1 is designed based on the steps outlined in Chapter 4 for Standard EBF.

Table B-1. Summary of link design for Specimen 1.

Tier	Section	e mm	V_f kN	$V_r = \varphi V_p$ $=\varphi 0.55wdF_y$ kN	A_v mm^2	Z mm^3	$M_p=ZF_y$ kN-m	$3.6Z/A_v$ mm	$1.6M_p/V_p$ mm
2	W310×60	750	313	386	2262	934000	322	1486	1201
1	W310×60	750	386	386	2262	934000	322	1486	1201

Table B-2. Summary of outer beam design for Specimen 1.

Tier	Beam Section W	$C_{f\text{-}b}$ kN	$M_{f\text{-}b}$ kN-m	$C_{r\text{-}b}$ kN	$M_{r\text{-}b}$ kN-m	$C_{f\text{-}b} / C_{r\text{-}b} + 0.85U_1M_{f\text{-}b} / M_{r\text{-}b}$
2	W310×60	580	229	1956	361	0.84
1	W310×60	471	233	1751	361	0.82

Table B-3. Summary of brace design for Specimen 1.

Tier	Brace section ($d \times t$)	$C_{f\text{-}br}$ kN	$M_{br\text{-}in}$ kN-m	$C_{r\text{-}br}$ kN	$M_{r\text{-}br}=\varphi M_{p\text{-}br}$ kN-m	$C_{f\text{-}br}/C_{r\text{-}br}+0.85U_1M_{f\text{-}br}/M_{r\text{-}br}$
2	HSS203×7.9	946	41	1393	136	0.80
1	HSS203×7.9	884	36	1254	136	0.82

Table B-4. Summary of column design for Specimen 1.

Column Section W	$C_{f\text{-}c}$ kN	$C_{r\text{-}c}$ kN	$C_{f\text{-}c} / C_{r\text{-}c}$
W310×52	736	814	0.90

Specimen 2: The design base shear is 540 kN. Specimen 2 is designed based on the steps outlined in Chapter 4 for Improved EBF and using the proposed detailed method for the in-plane response.

Table B-5. Summary of link design for Specimen 2.

Tier	Section	e mm	V_f kN	$V_r = \varphi V_p$ $=\varphi 0.55 wdF_y$ kN	A_v mm^2	Z mm^3	$M_p=ZF_y$ kN-m	$3.6Z/A_v$ mm	$1.6M_p/V_p$ mm
2	W250×73	750	313	375	2195	990000	342	1624	1312
1	W250×73	750	386	375	2195	990000	342	1624	1312

Table B-6. Summary of outer beam design for Specimen 2.

Tier	Beam Section W	$C_{f\text{-}b}$ kN	$M_{f\text{-}b}$ kN-m	$C_{r\text{-}b}$ kN	$M_{r\text{-}b}$ kN-m	$C_{f\text{-}b} / C_{r\text{-}b} + 0.85U_1M_{f\text{-}b} / M_{r\text{-}b}$
2	W250×73	563	218	2877	383	0.68
1	W250×73	457	222	1261	357	0.93

Table B-7. Summary of brace design for Specimen 2.

Tier	Brace section ($d \times t$)	$C_{f\text{-}br}$ kN	$M_{br\text{-}in}$ kN-m	$C_{r\text{-}br}$ kN	$M_{r\text{-}br}=\varphi M_{p\text{-}br}$ kN-m	$C_{f\text{-}br}/C_{r\text{-}br}+0.85U_1M_{f\text{-}br}/M_{r\text{-}br}$
2	HSS203×7.9	916	44	1393	136	0.88
1	HSS203×7.9	857	39	1254	136	0.98

Table B-8. Summary of column design for Specimen 2.

Column Section W	$C_{f\text{-}c}$ kN	$M_{fx\text{-}c}$ kN-m	$M_{fy\text{-}c}$ kN-m	$C_{r\text{-}c}$ kN	$M_{rx\text{-}c}$ kN-m	$M_{ry\text{-}c}$ kN-m	$C_{f\text{-}c}/C_{r\text{-}c}+0.85U_{1x}M_{fx\text{-}c}/M_{rx\text{-}c}$ $+0.5U_{1y}M_{fy\text{-}c}/M_{ry\text{-}c}$
W360×162	719	9	27	4527	978	472	0.21

Specimen 3: The design base shear for this specimen is 546 kN. This specimen is designed based on the design steps outlined in Chapter 5 Improved EBF and using the proposed detailed method to determine column in-plane moments. The design steps described in Chapter 5 are adjusted for two-tiered EBFs.

Table B-9. Summary of link design for Specimen 3.

Tier	Section	e mm	V_f kN	$V_r = \varphi V_p$ $=\varphi 0.55wdF_y$ kN	A_v mm^2	Z mm^3	$M_p=ZF_y$ kN-m	$3.6Z/A_v$ mm	$1.6M_p/V_p$ mm
2	Tubular	750	317	387	2233	966448	338	1558	1259
1	Tubular	750	390	387	2233	966448	338	1558	1259

Table B-10. Summary of outer beam design for Specimen 3.

Tier	Beam Section W	$C_{f\text{-}b}$ kN	$M_{f\text{-}b}$ kN-m	$C_{r\text{-}b}$ kN	$M_{r\text{-}b}$ kN-m	$C_{f\text{-}b} / C_{r\text{-}b} + 0.85U_1M_{f\text{-}b} / M_{r\text{-}b}$
2	Tubular	664	211	4544	379	0.70
1	Tubular	539	220	2385	379	0.84

Table B-11. Summary of brace design for Specimen 3.

Tier	Brace section ($d \times t$)	$C_{f\text{-}br}$ kN	$M_{br\text{-}in}$ kN-m	$C_{r\text{-}br}$ kN	$M_{r\text{-}br}=\varphi M_{p\text{-}br}$ kN-m	$C_{f\text{-}br}/C_{r\text{-}br}+0.85U_1M_{f\text{-}br}/M_{r\text{-}br}$
2	HSS229×7.9	1069	98	1698	175	0.99
1	HSS229×7.9	999	89	1560	175	0.99

Table B-12. Summary of column design for Specimen 3.

Column Section W	$C_{f\text{-}c}$ kN	$M_{fx\text{-}c}$ kN-m	$M_{fy\text{-}c}$ kN-m	$C_{r\text{-}c}$ kN	$M_{rx\text{-}c}$ kN-m	$M_{ry\text{-}c}$ kN-m	$C_{f\text{-}c}/C_{r\text{-}c}+0.85U_{1x}M_{fx\text{-}c}/M_{rx\text{-}c}$ $+0.5U_{1y}M_{fy\text{-}c}/M_{ry\text{-}c}$
W310×143	865	15.1	21.2	3829.6	748	345	0.28

Appendix C. Experimental Specimens Drawings

GENERAL NOTES:

1. ALL DIMENSIONS ARE IN MILLIMETERS UNLESS NOTED OTHERWISE (UNO)
2. FOR ANY CLARIFICATION, CONTACT ABOLFAZL ASHRAFI AT ASHRAFI@UALBERTA.CA OR (780) 566 - 8038
3. PROVIDE A COPY OF MILL TEST REPORT FOR ALL STRUCTURAL STEEL
4. ALL DRAWING TO BE PLOTTED ON A3 PAPER

SCOPE:

1. THREE EXPERIMETAL FRAMES USED TO EXAMINE MULTI-TIERED SPECIAL ECCENTRICALLY BRACED FRAMES (MT-EBFs)
2. ONE LOADING FRAME AND A SET OF CONCRETE FOOTINGS

MATERIALS:

1. COLUMNS: ASTM A992 Fy=345 MPa
2. BEAMS: ASTM A992 Fy= 345 MPa, Fymax=480 MPa
3. BRACES: ASTM A1085 Fy= 345 MPa
4. CONNECTIONS: ASTM A572 Fy=350 MPa
5. ANCHOR RODS: ASTM A193 B7
6. BOLT: ASTM A325 UNO UNLESS NOTED OTHERWISE
7. COLUMNS, BEAMS, AND BRACES SHALL BE MANUFACTURED FROM THE SAME HEAT

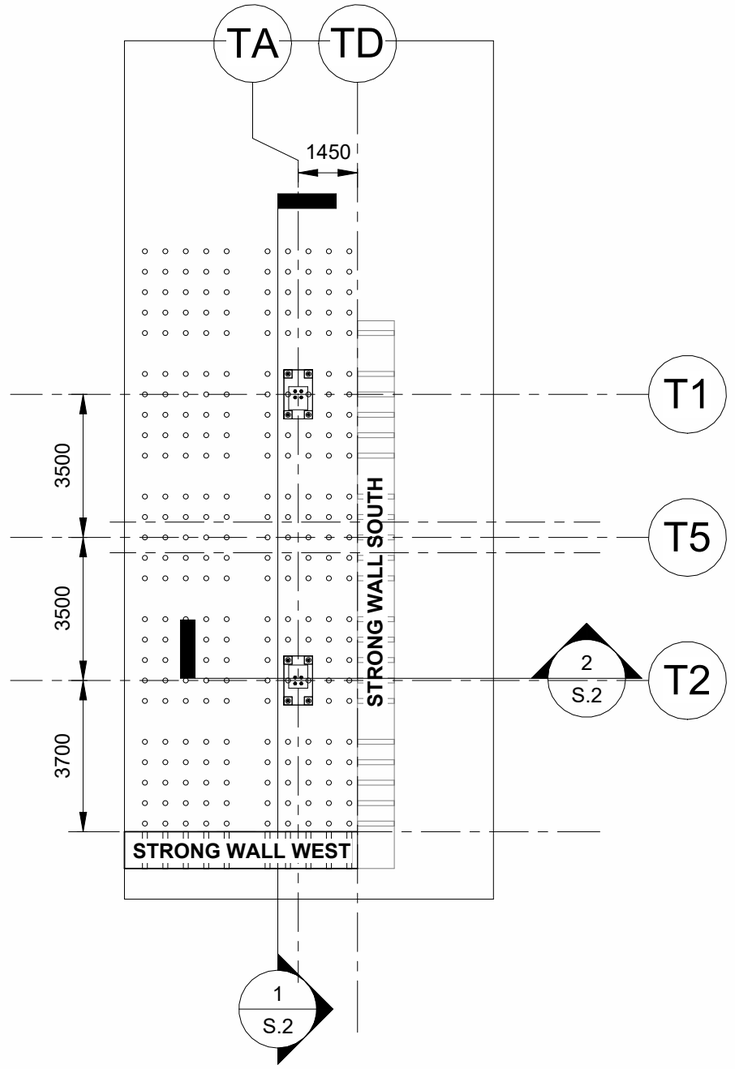

1 TOF
1 : 150

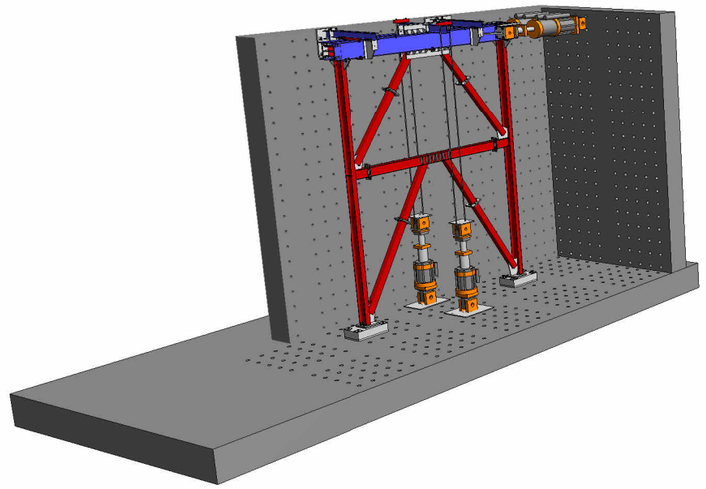

2 3D View 1

No.	Description	Date

UoA MT-EBFs

SPECIMEN 1

GENERAL

Project number	EBF
Date	Mar 29, 2022
Drawn by	A.A.
Checked by	XX
Scale	1 : 150

S.1

2023-03-19 11:18:39 PM

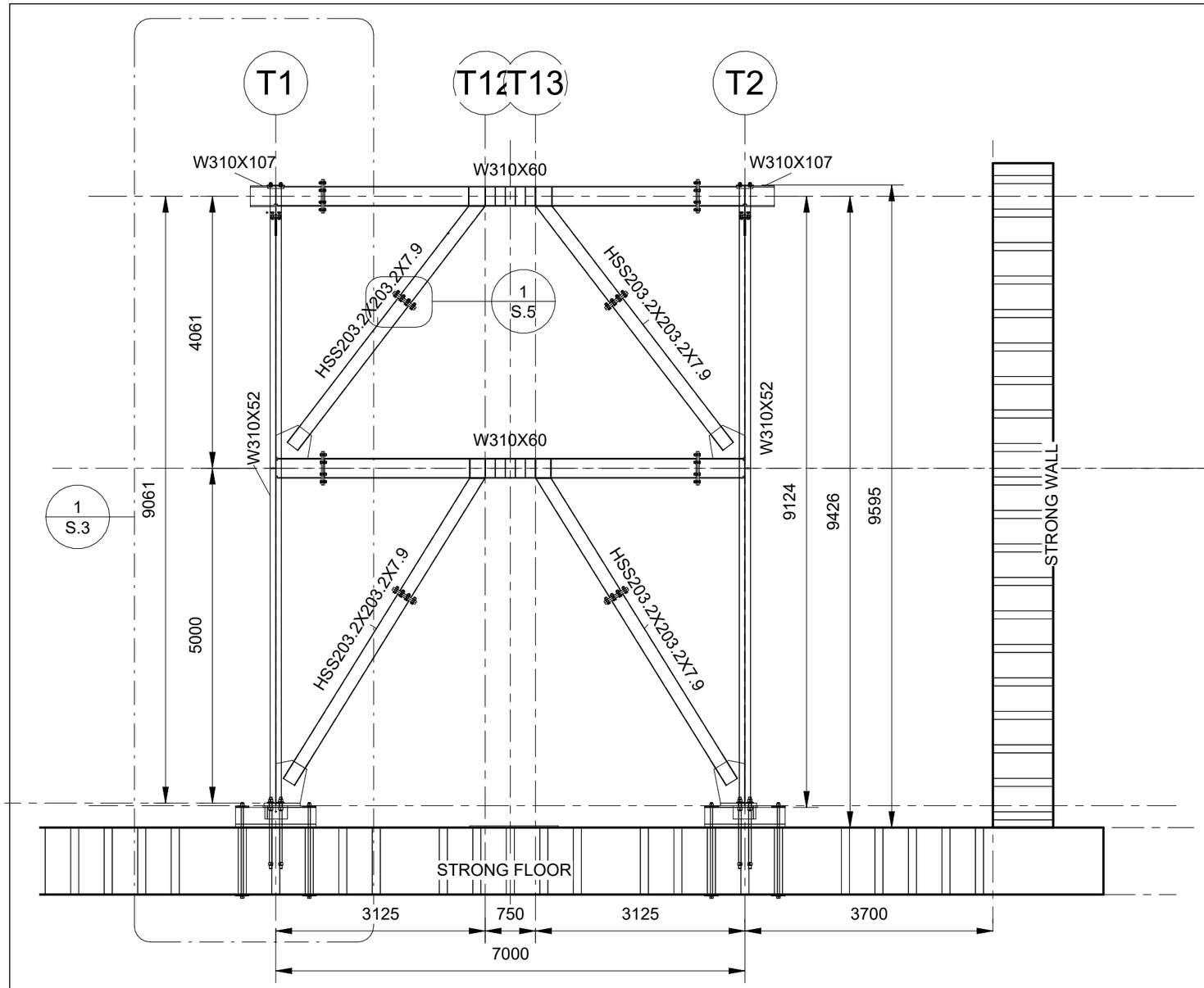

1 FRONT ELEVATION
1 : 75

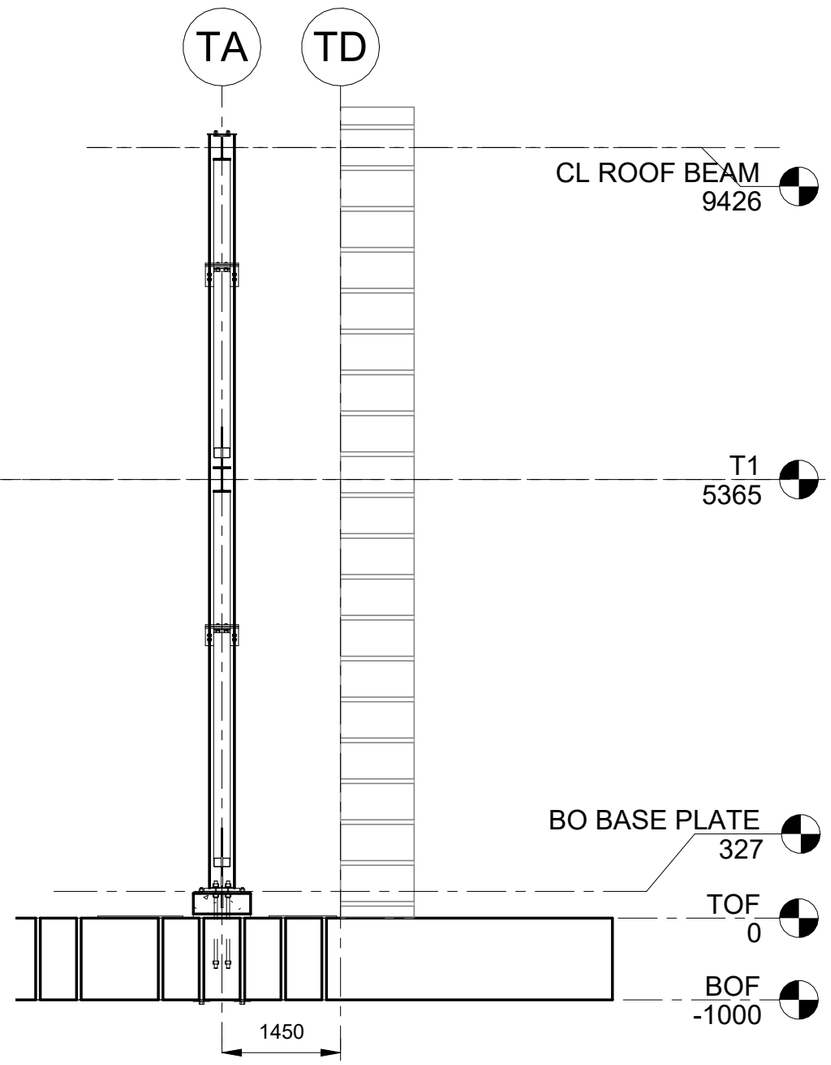

2 SIDE ELEVATION
1 : 75

No.	Description	Date

UoA MT-EBFs

SPECIMEN 1

ELEVATIONS

Project number	EBF
Date	Mar 29, 2022
Drawn by	A.A.
Checked by	Checker
Scale	1 : 75

S.2

2023-03-19 11:18:40 PM

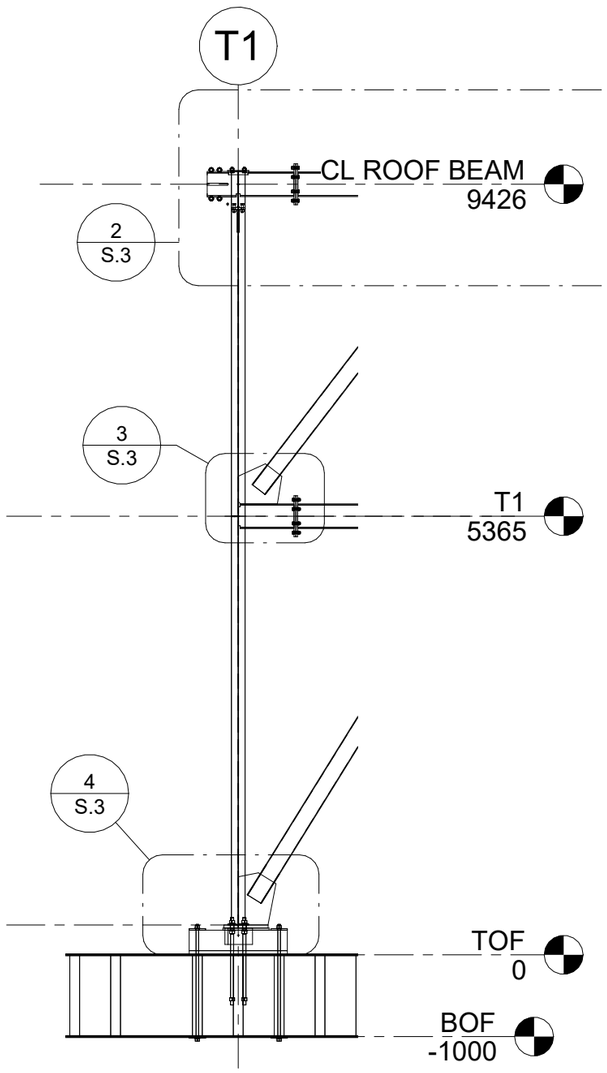

1 FRONT ELEVATION - COLUMN
1 : 75

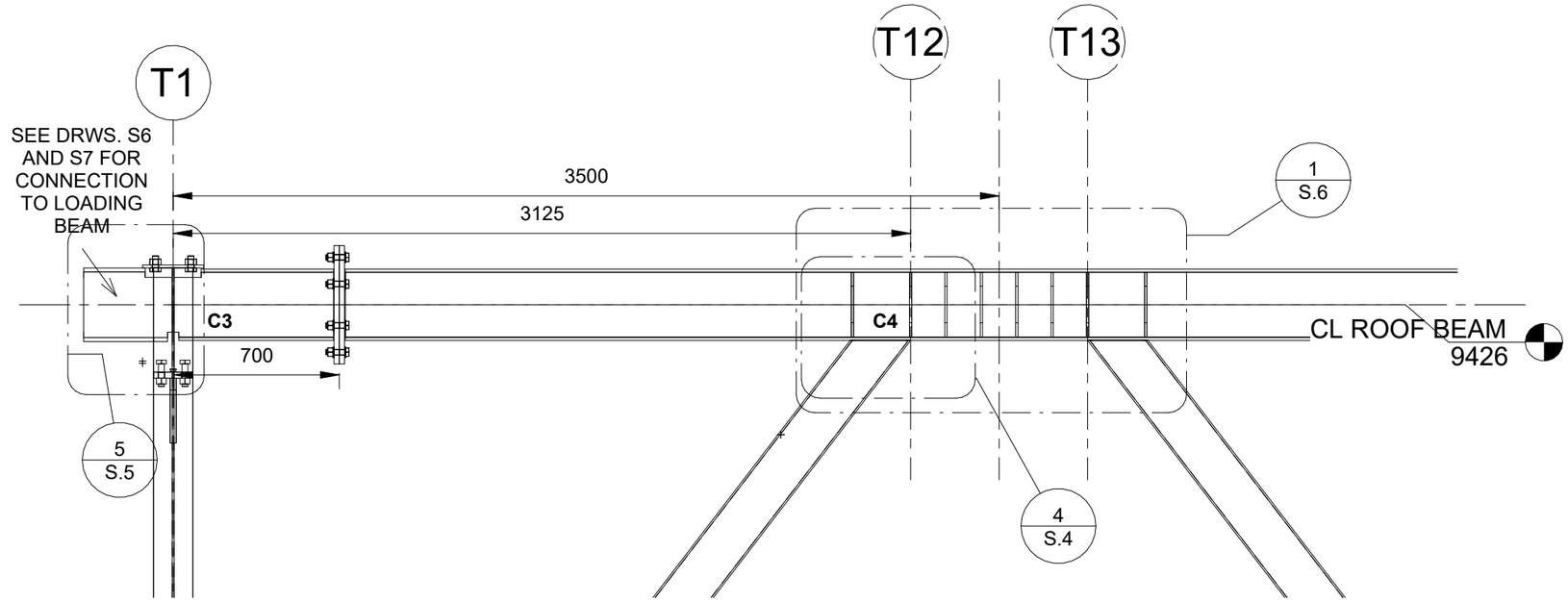

2 FRONT ELEVATION - TOP COLUMN
1 : 25

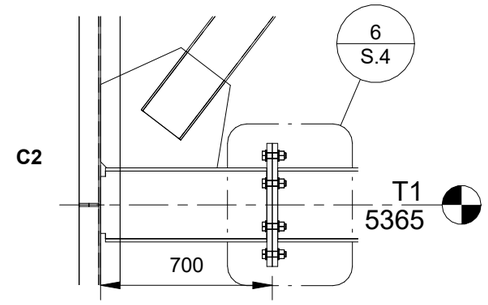

3 FRONT ELEVATION - MIDDLE COLUMN
1 : 25

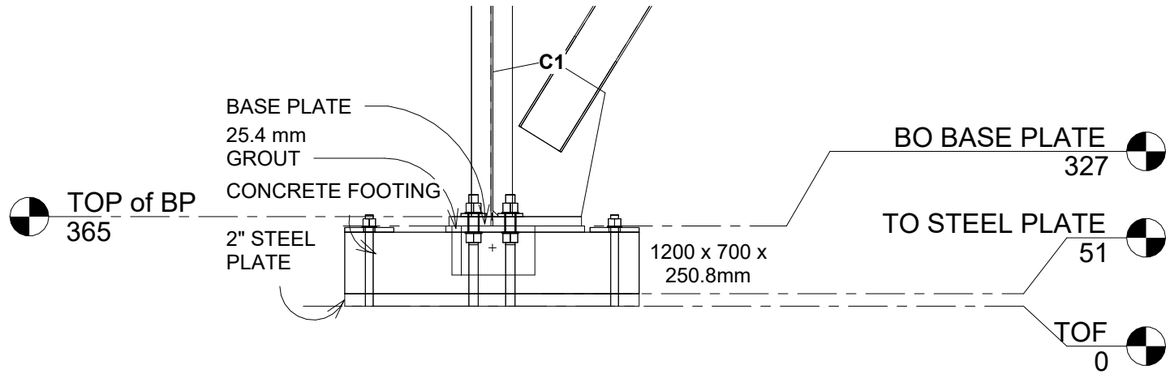

4 FRONT ELEVATION - BOTTOM COLUMN
1 : 25

No.	Description	Date

UoA MT-EBFs

SPECIMEN 1

FRONT ELEVATION DETAILS

Project number	EBF
Date	Mar 29, 2022
Drawn by	A.A.
Checked by	Checker
Scale	As indicated

S.3

2023-03-19 11:18:41 PM

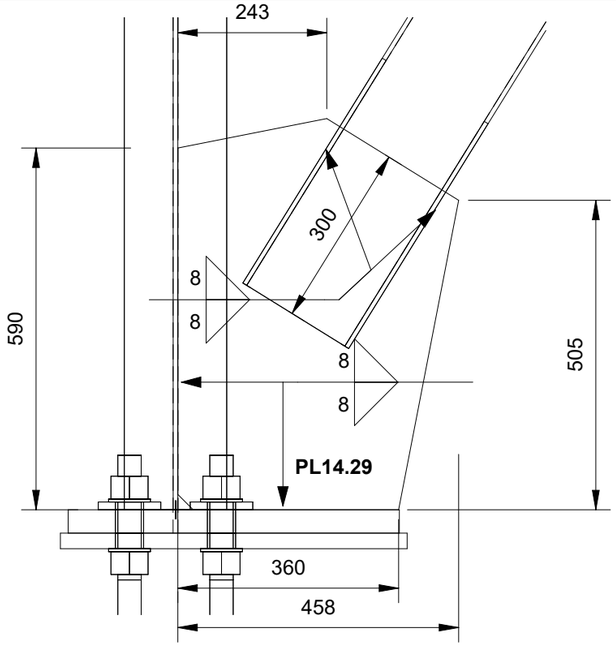

1 CONNECTION DETAIL C1
1 : 10

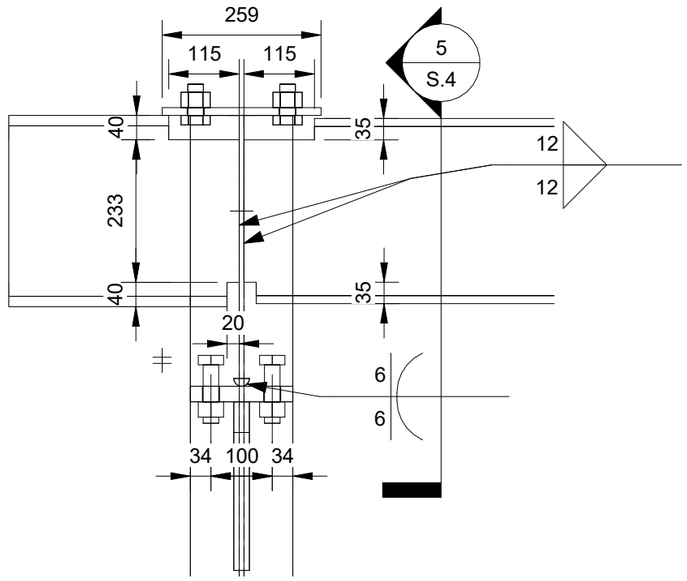

3 CONNECTION DETAIL C3
1 : 10

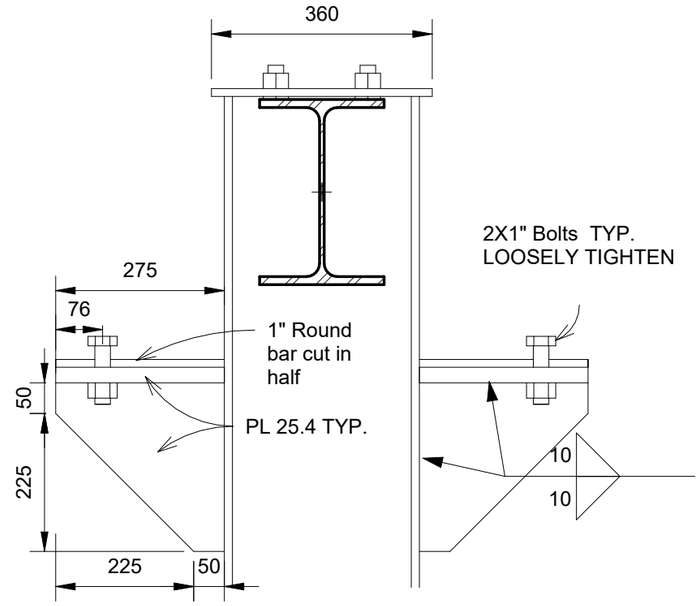

5 CONNECTION DETIAL C3-SIDE VIEW
1 : 10

2 CONNECTION DETAIL C2
1 : 10

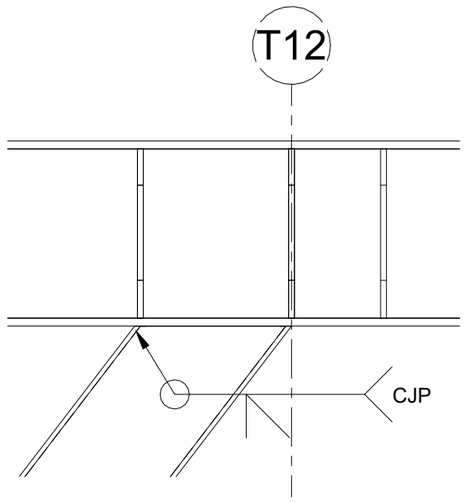

4 CONNECTION DETAIL C4
1 : 10

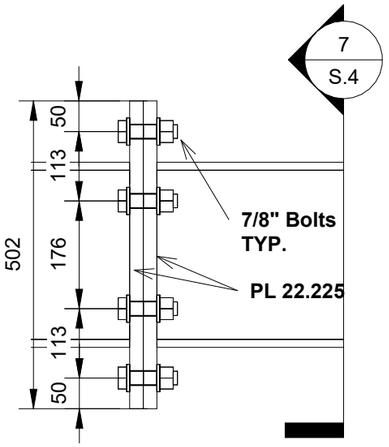

6 BEAM SPLICE TYP.
1 : 10

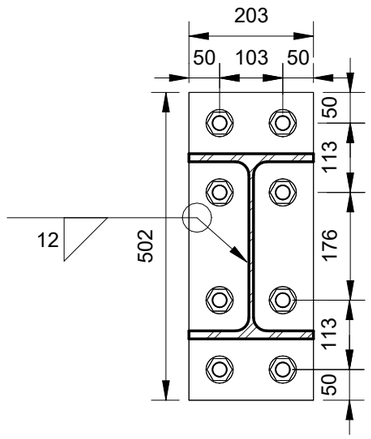

7 BEAM SPLICE TYP. SIDE VIEW
1 : 10

No.	Description	Date

UoA MT-EBFs

SPECIMEN 1

CONNECTION DETAILS

Project number	EBF
Date	Mar 29, 2022
Drawn by	A.A.
Checked by	Checker
Scale	1 : 10

S.4

2023-03-19 11:18:42 PM

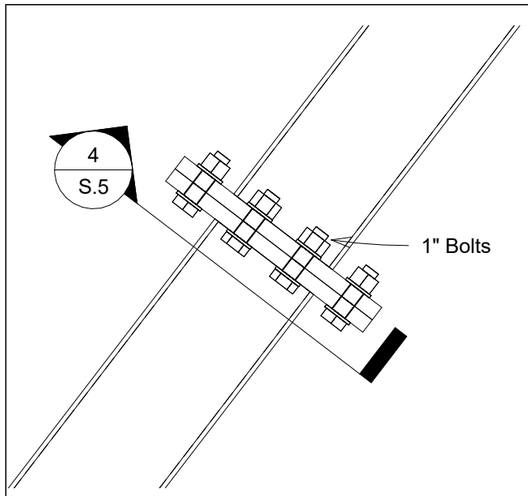

1 BRACE SPLICE-TYP.
1 : 10

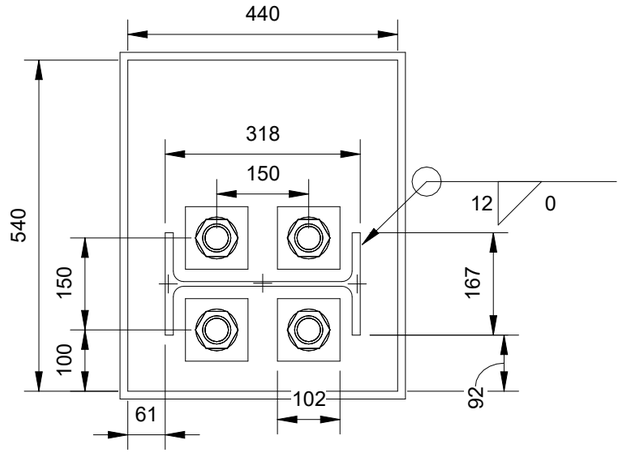

2 BASE PLATE DETAIL
1 : 10

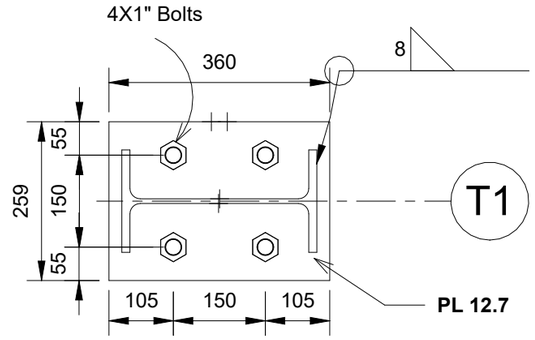

3 ENDPLATE AT COLM. TOP - PLAN VIEW
1 : 10

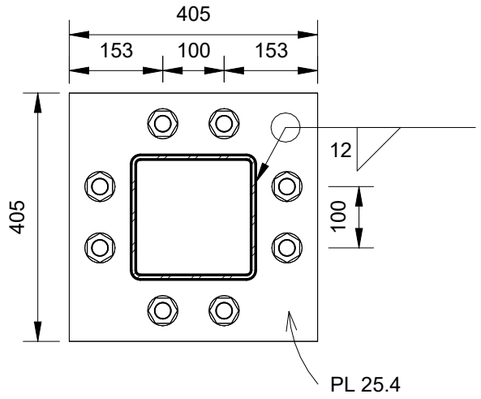

4 BRACE SPLICE TYP.-SIDE VIEW
1 : 10

BASE PLATE: 38.1mm THICK
GROUT: 25.4 mm THICK UNDERNEATH
ANCHOR WASHERS: 2.7mm THICK
ANCHORS: 1-1/2" DIAMETER
ANCHORS: 400mm LONG
BASEPLATE AND WASHER HOLE DIAMETER: MIN. 65mm
SHEAR LUG ATTACHED BENEATH BASEPLATE (SEE DRW. S13)

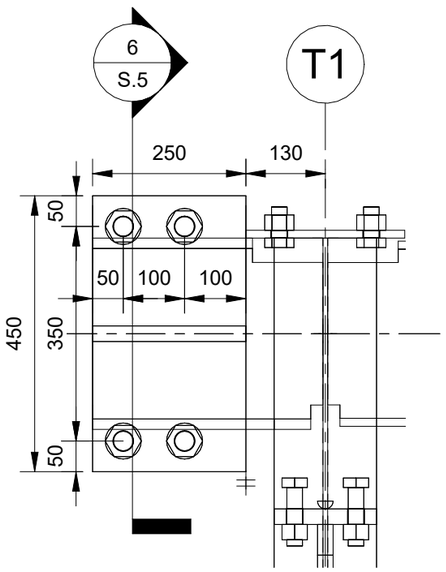

5 LOADING BEAM-TO-FRAME CONNECTION
1 : 10

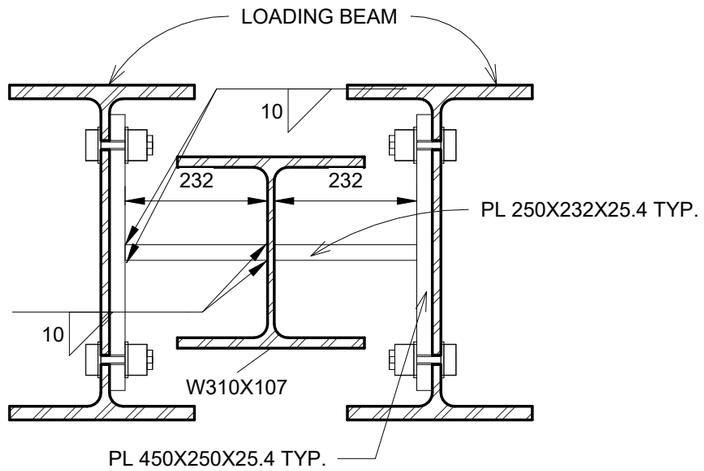

6 LOADING BEAM-TO-FRAME CONNECTION-SIDE VIEW
1 : 10

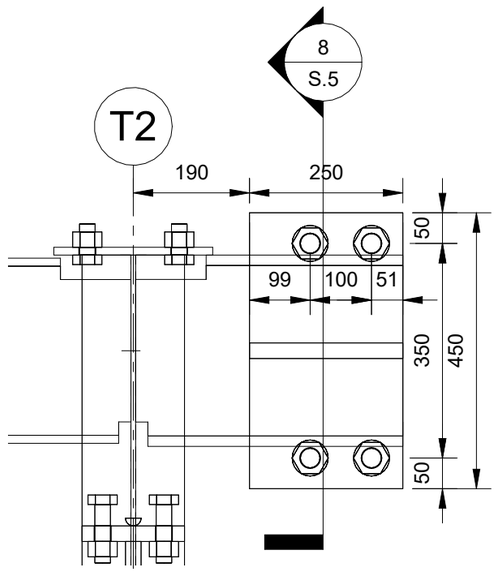

7 LOADING BEAM-TO-FRAME CONNECTION-ACTUATOR SIDE
1 : 10

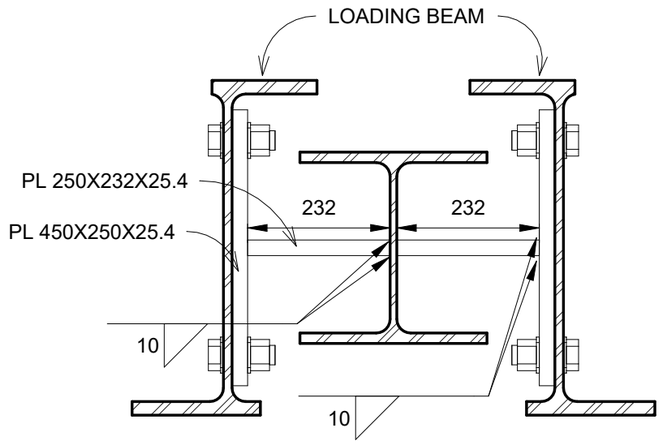

8 LAODING BEAM-TO-FRAME CONNECTION-ACTUATOR SIDE-SIDE VIEW
1 : 10

No.	Description	Date

UoA MT-EBFs

SPECIMEN 1

CONNECTION DETAILS

Project number	EBF
Date	Mar 29, 2022
Drawn by	A.A.
Checked by	Checker
Scale	1 : 10

S.5

2023-03-19 11:18:43 PM

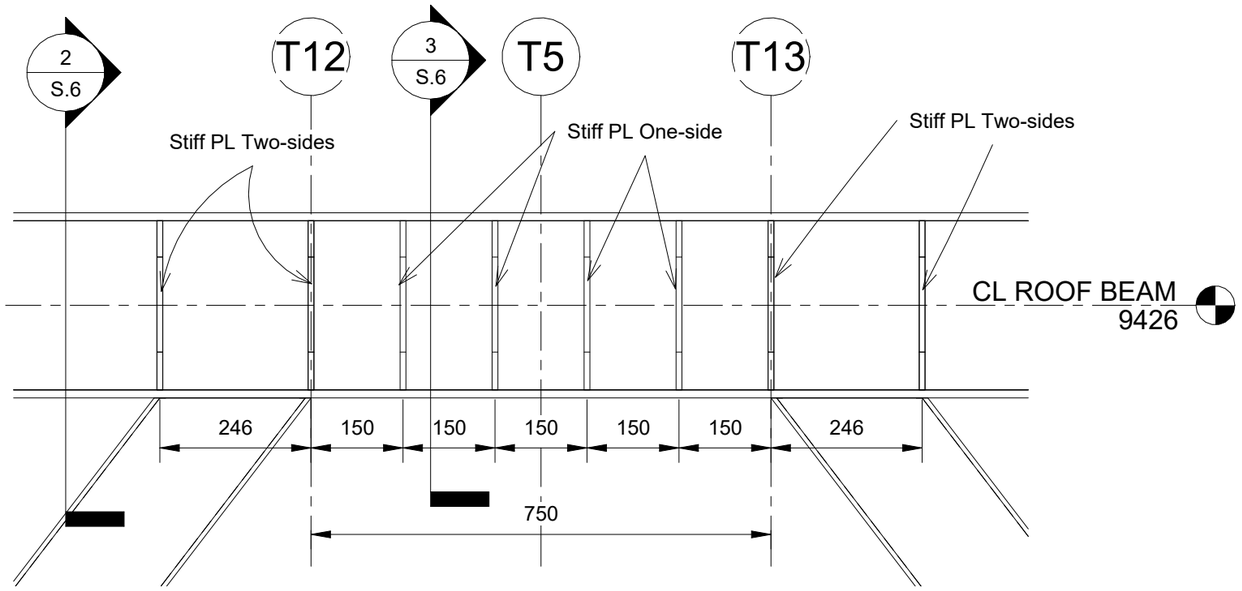

1 LINK STIFFENER-ROOF
1 : 10

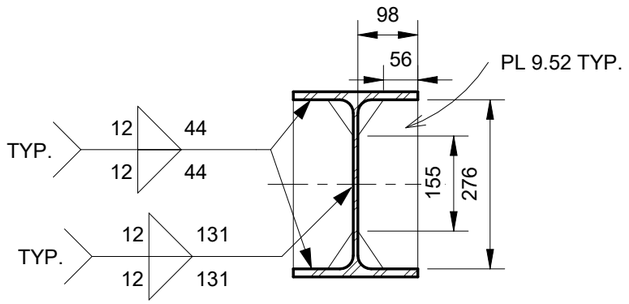

2 LINK STIFFENER SECTION-LINK ENDS
1 : 10

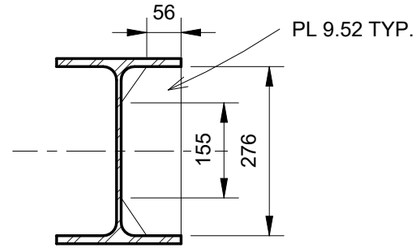

3 LINK STIFFENER SECTION-INTERMEDIATE
1 : 10

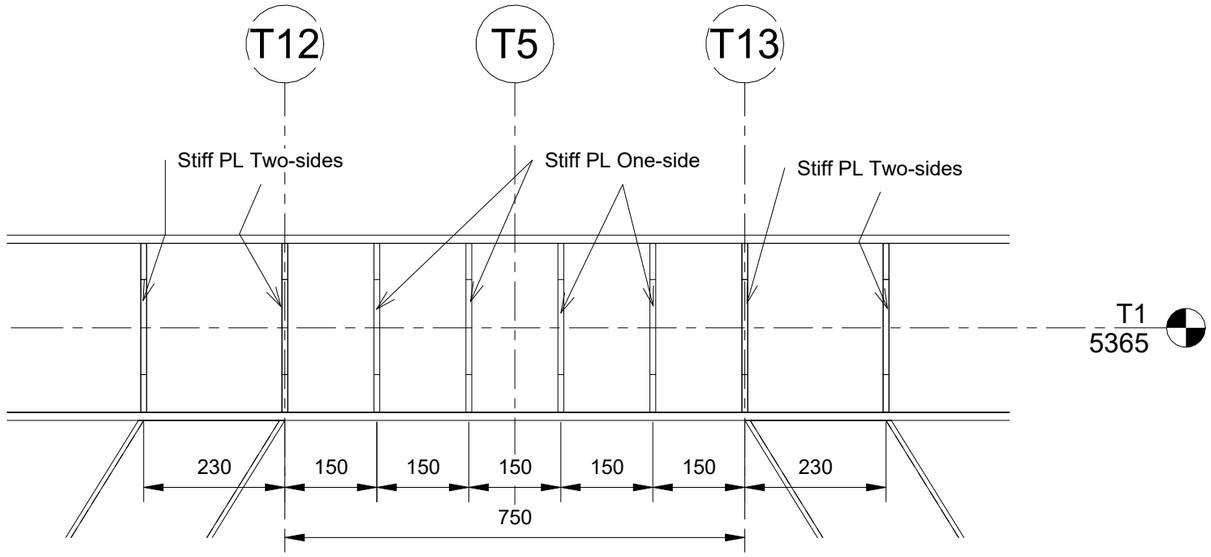

4 LINK ATIFFENER-TIER1
1 : 10

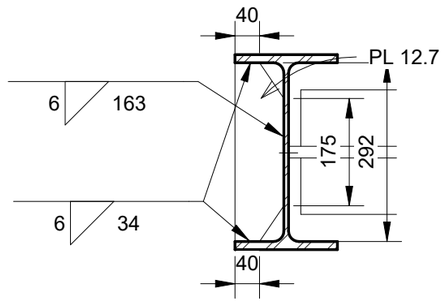

5 COLUMN STIFFENER AT TIER 1
1 : 10

No.	Description	Date

UoA MT-EBFs

SPECIMEN 1

STIFFENER

Project number	EBF
Date	Mar 29, 2022
Drawn by	Author
Checked by	Checker
Scale	1 : 10

S.6

2023-03-19 11:18:44 PM

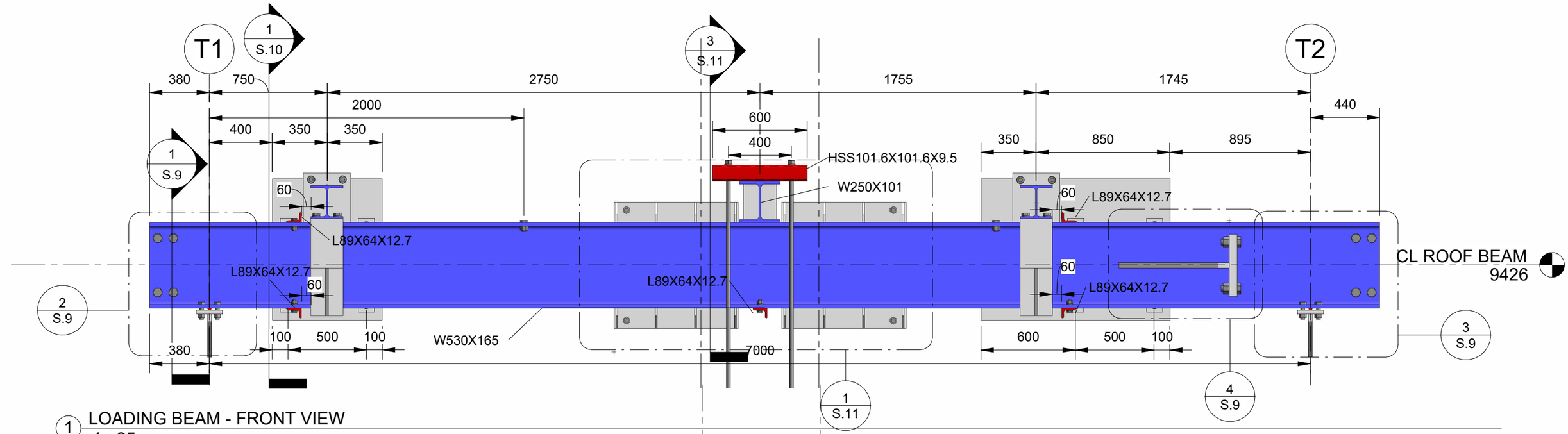

1 LOADING BEAM - FRONT VIEW
1 : 25

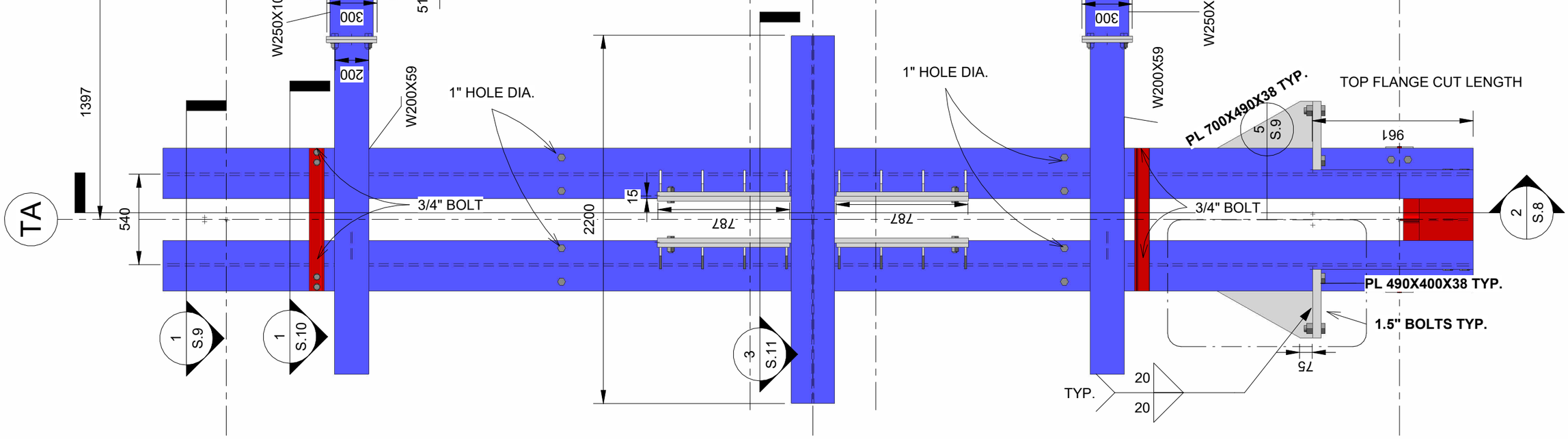

2 LOADING BEAM - PLAN VIEW-TOP
1 : 25

No.	Description	Date

UoA MT-EBFs

SPECIMEN 1

LOADING FRAME

Project number	EBF
Date	Mar 29, 2022
Drawn by	A.A.
Checked by	Checker
Scale	1 : 25

S.7

2023-03-19 11:18:46 PM

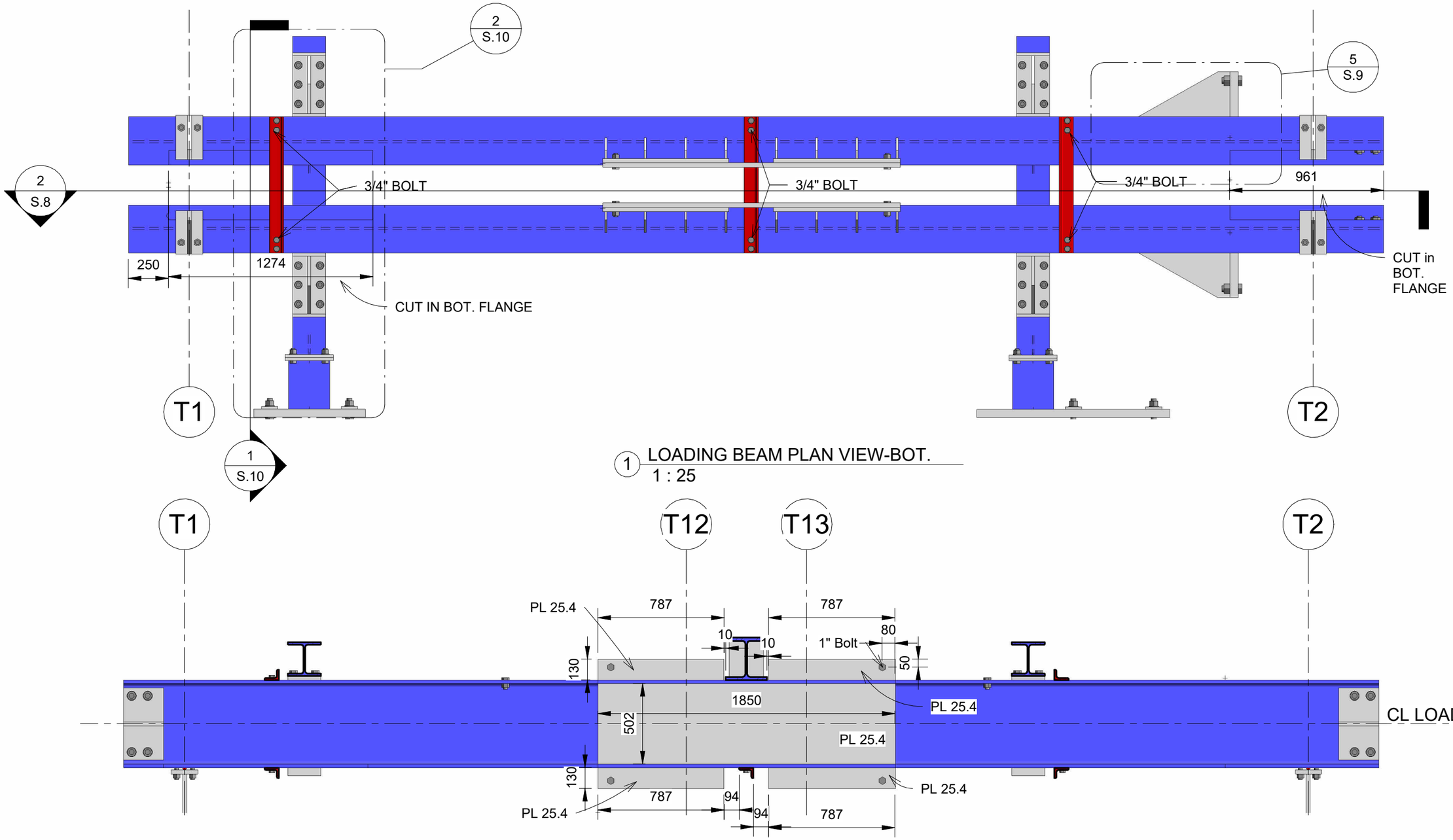

1 LOADING BEAM PLAN VIEW-BOT.
1 : 25

2 LOADING BEAM-INSIDE VIEW
1 : 25

No.	Description	Date

UoA MT-EBFs

SPECIMEN 1

LOADING FRAME2

Project number	EBF
Date	Mar 29, 2022
Drawn by	A.A.
Checked by	Checker
Scale	1 : 25

S.8

2023-03-19 11:18:48 PM

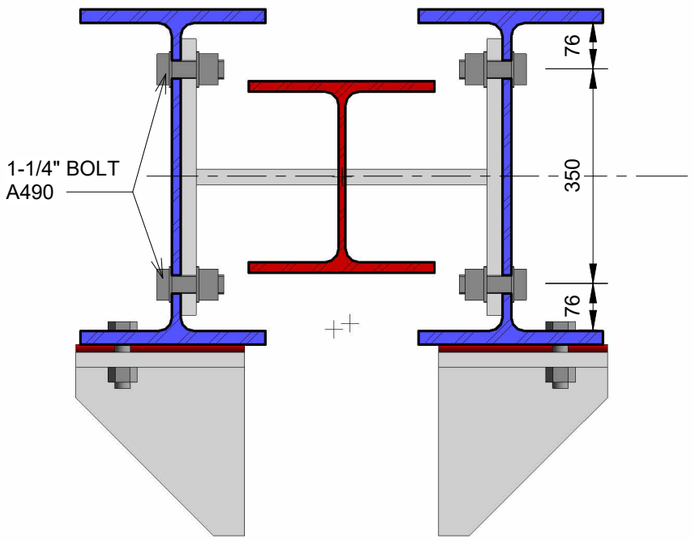

1 LOADING BEAM TO COL. CONNECTION
1 : 10

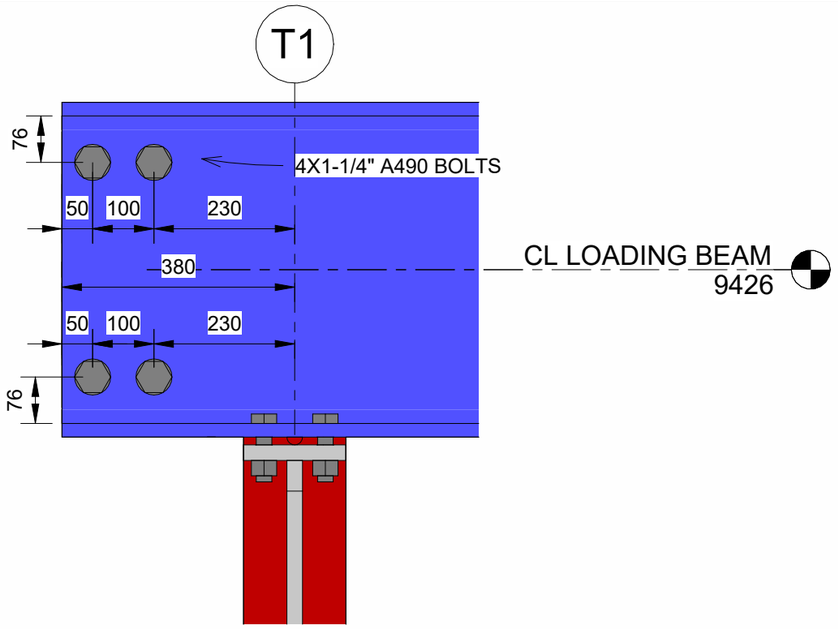

2 LOADING BEAM TO COLUMN CONNECTION - FRONT VIEW
1 : 10

BOLTS BETWEEN PLATE AND LOANDING BEAM LOOSELY TIGHTEN
1" ROUND BAR CUT IN HALF AND WELDED TO PLATE

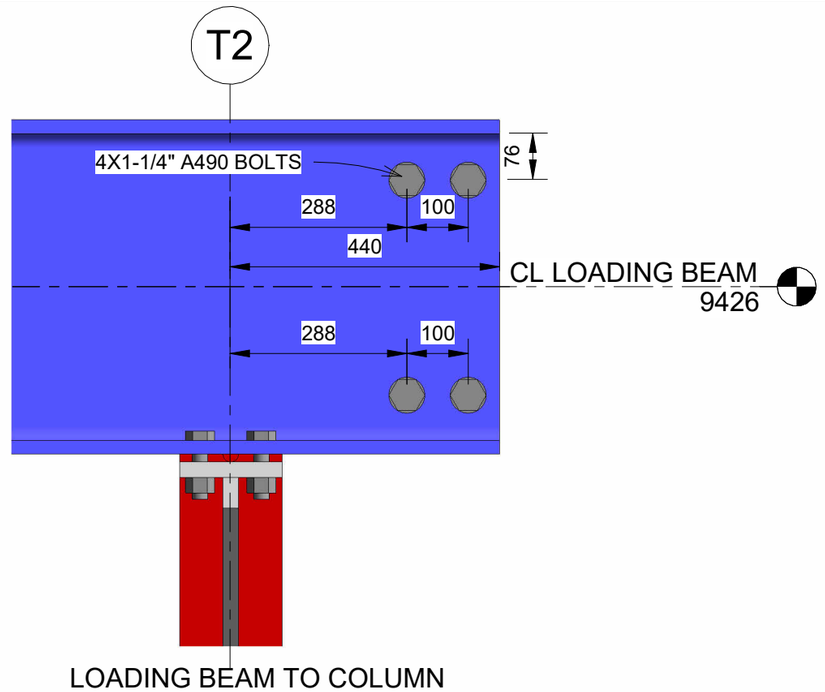

3 LOADING BEAM TO COLUMN CONNECTION-FRONT VIEW-ACTUATOR SIDE
1 : 10

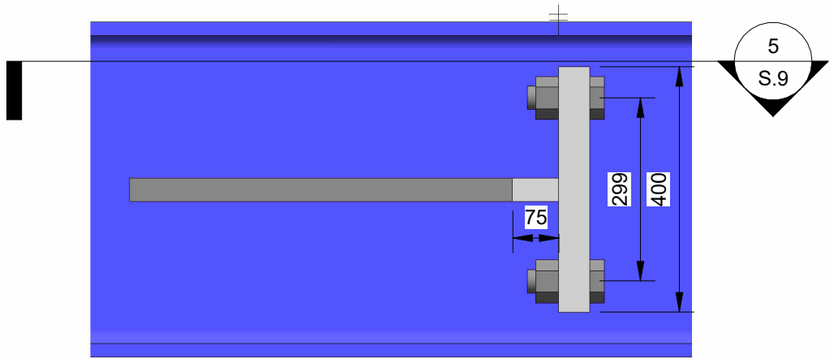

4 LOADING BEAM TO ACTUATOR CONNECTION
1 : 10

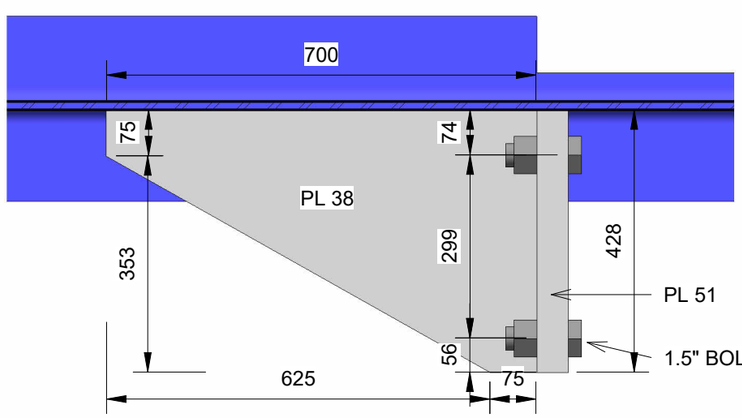

5 LOADING BEAM TO ACTUATOR CONNECTION-TOP VIEW
1 : 10

No.	Description	Date

UoA MT-EBFs

SPECIMEN 1

LOADING FRAME DETAILS

Project number	EBF
Date	Mar 29, 2022
Drawn by	A.A.
Checked by	Checker
Scale	1 : 10

S.9

2023-03-19 11:18:50 PM

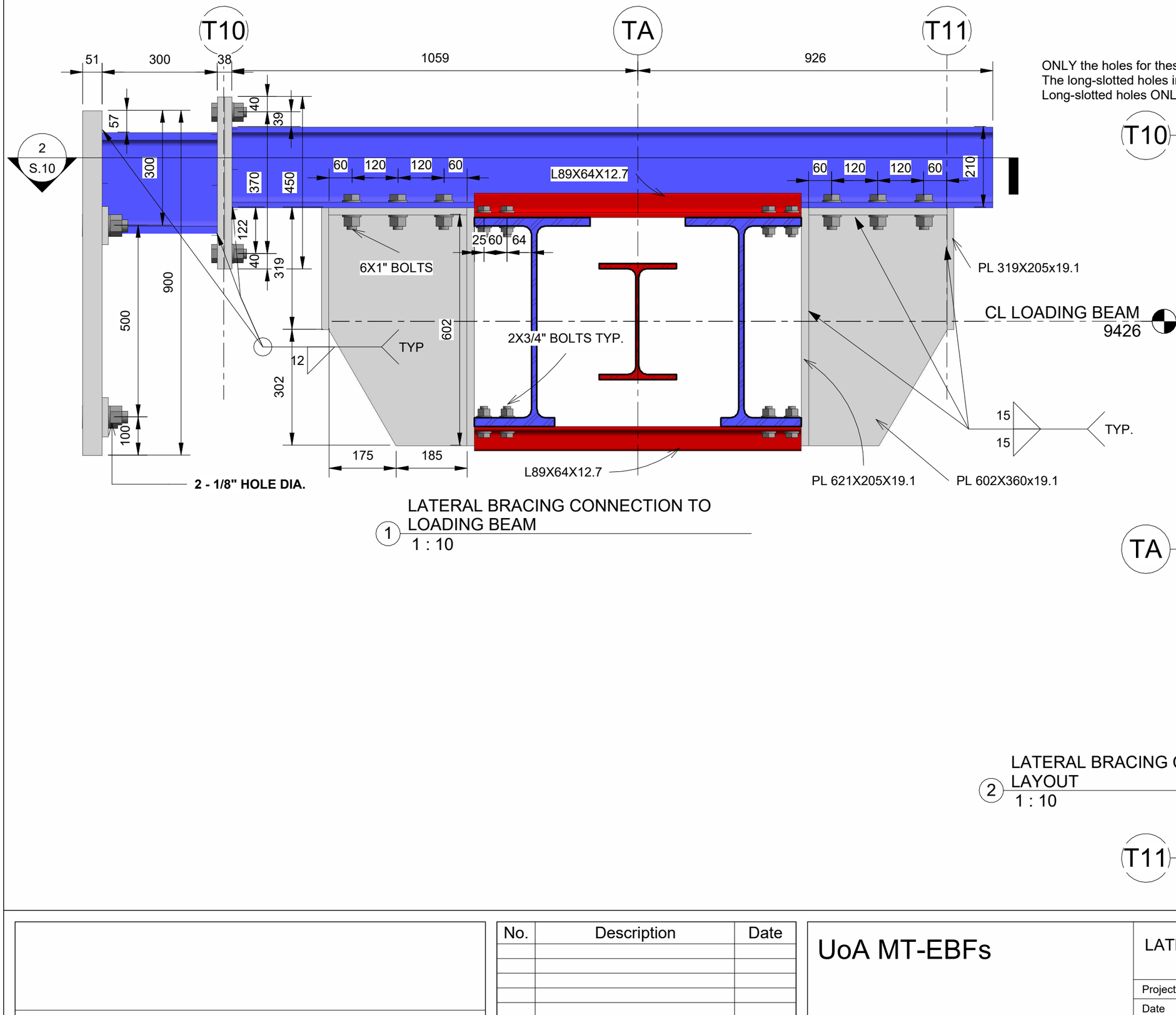

1 LATERAL BRACING CONNECTION TO LOADING BEAM
1 : 10

ONLY the holes for these two bolts (wall-side) need to be long slotted with a 100 mm length
The long-slotted holes in the longitudinal direction of the beam
Long-slotted holes ONLY in the plate

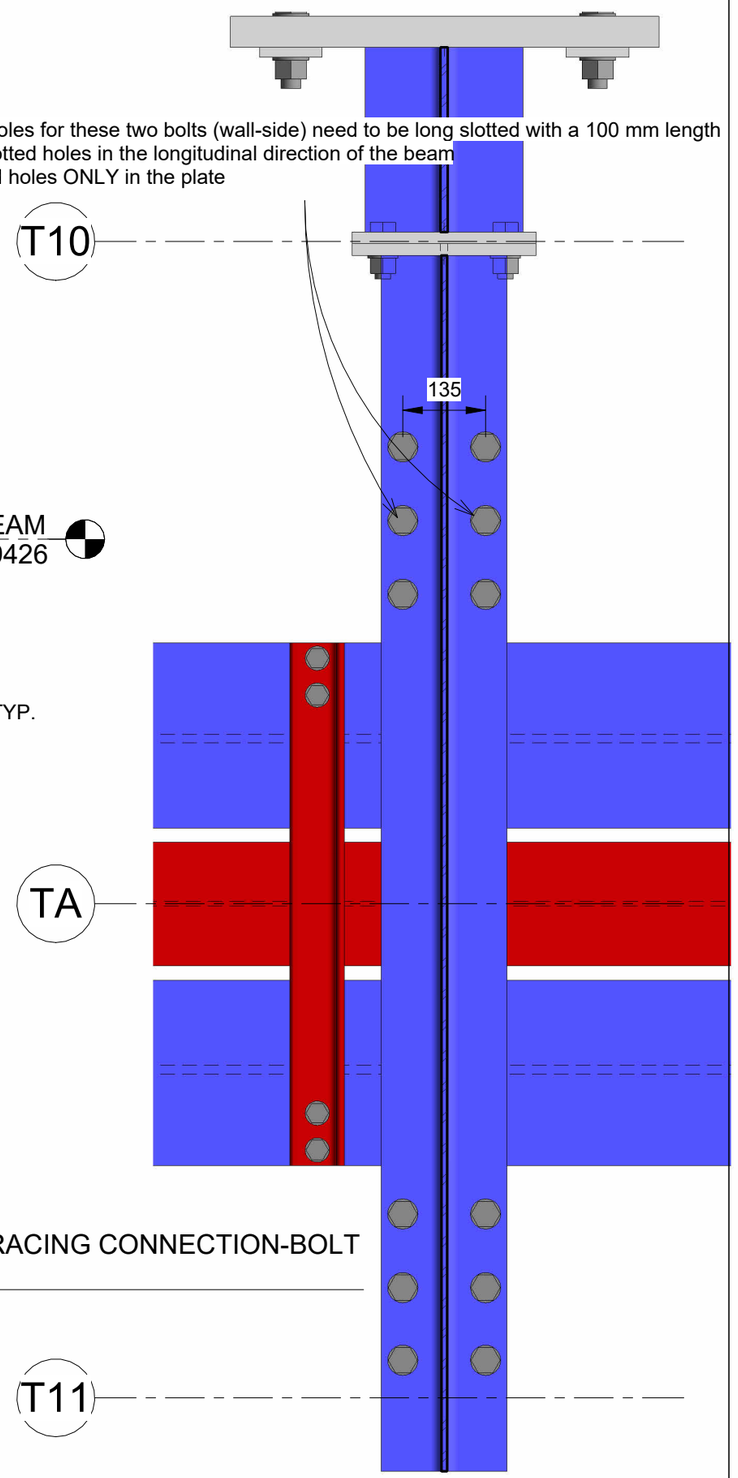

2 LATERAL BRACING CONNECTION-BOLT LAYOUT
1 : 10

No.	Description	Date

UoA MT-EBFs

SPECIMEN 1

LATERAL BRACING

Project number	EBF
Date	Mar 29, 2022
Drawn by	A.A.
Checked by	Checker
Scale	1 : 10

S.10

2023-03-19 11:18:51 PM

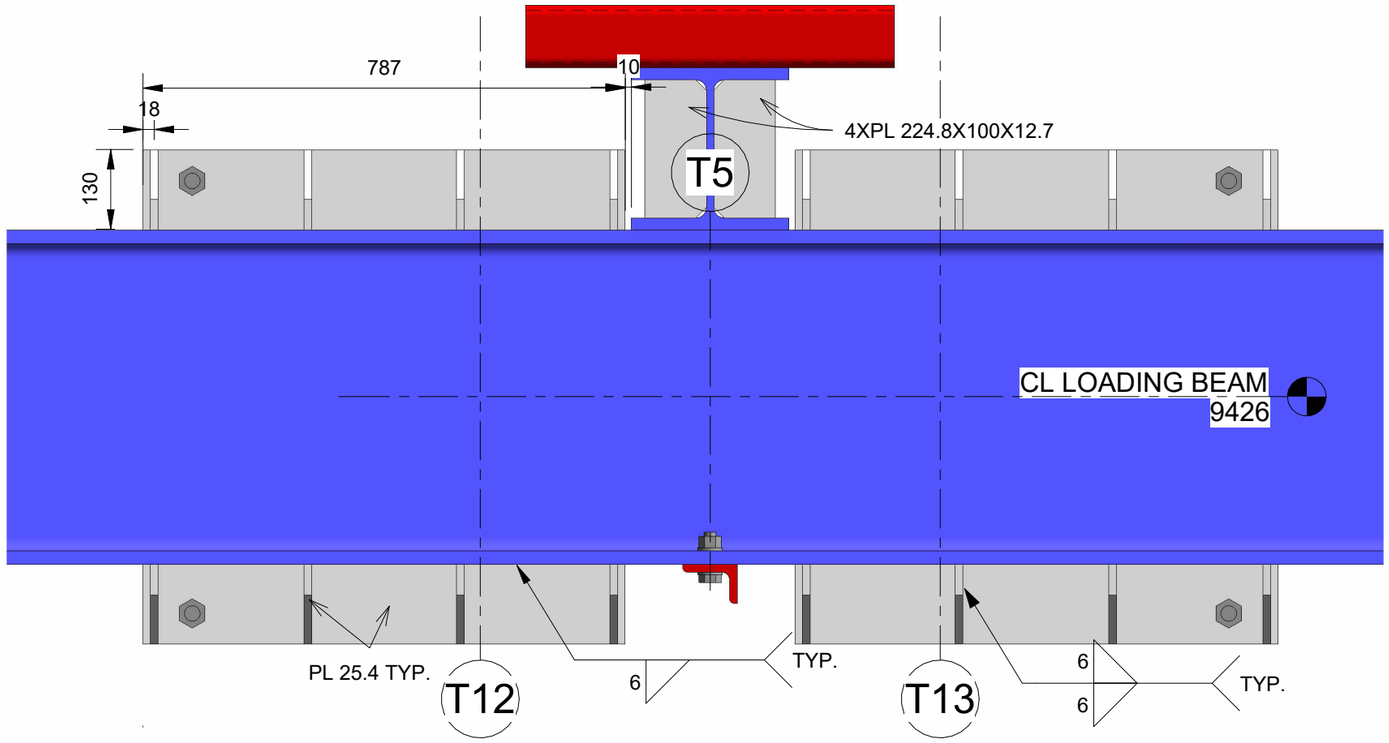

1 LOADING BEAM TO ROOF BEAM CON. - FRONT VIEW
1 : 10

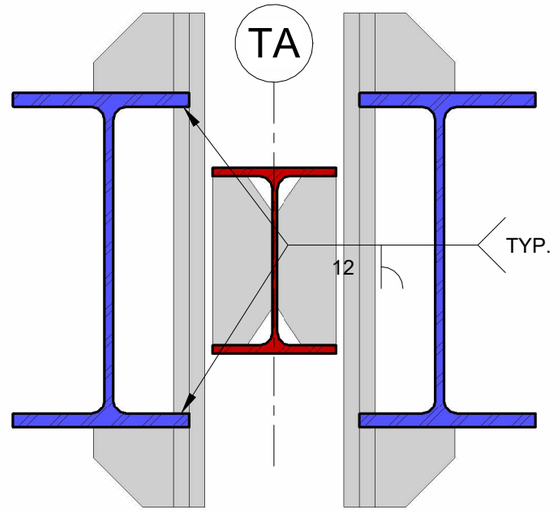

2 LOADING BEAM TO ROOF BEAM CON. - CROSS SECTION
1 : 10

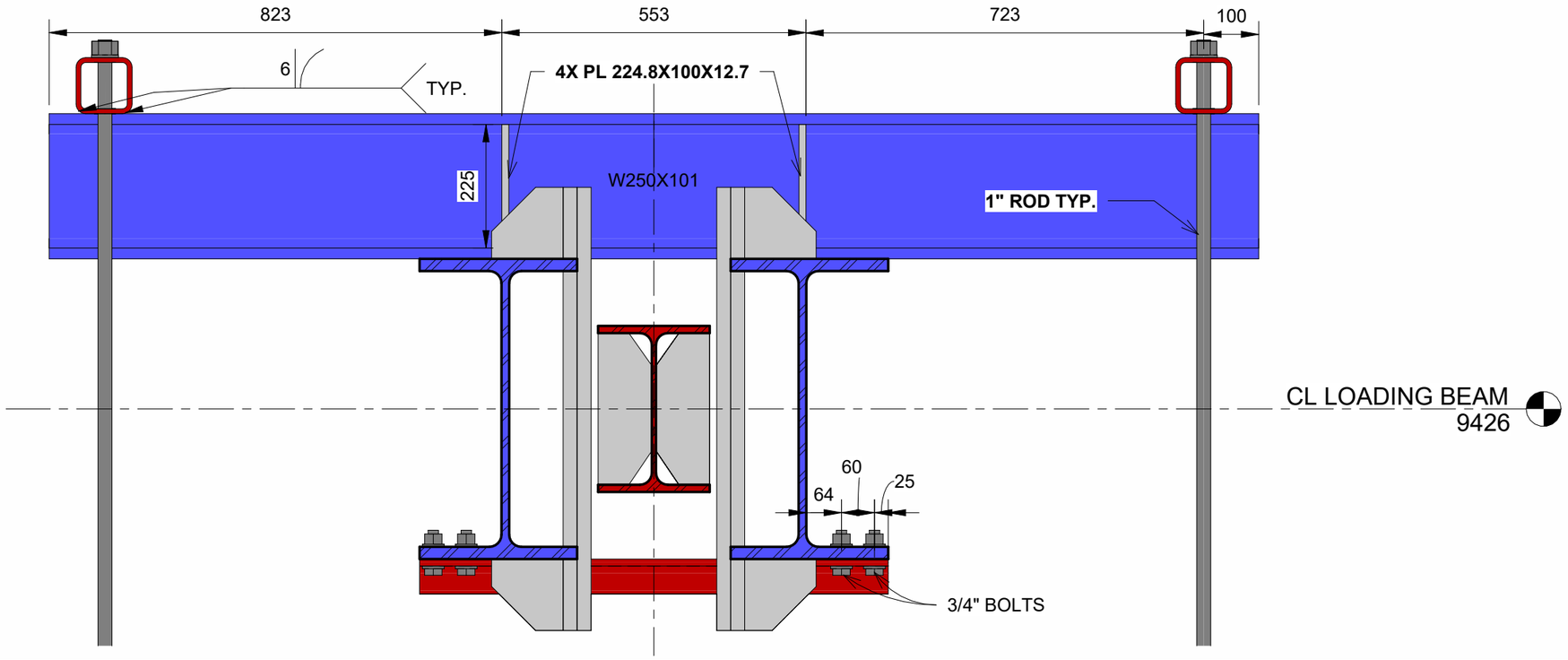

3 GRAVITY BEAM CONNECTION TO LOADING BEAM
1 : 10

No.	Description	Date

UoA MT-EBFs

SPECIMEN 1

LOADING FRAME DETAILS-GRAVITY BEAM

Project number	EBF
Date	Mar 29, 2022
Drawn by	A.A.
Checked by	Checker
Scale	1 : 10

S.11

2023-03-19 11:18:53 PM

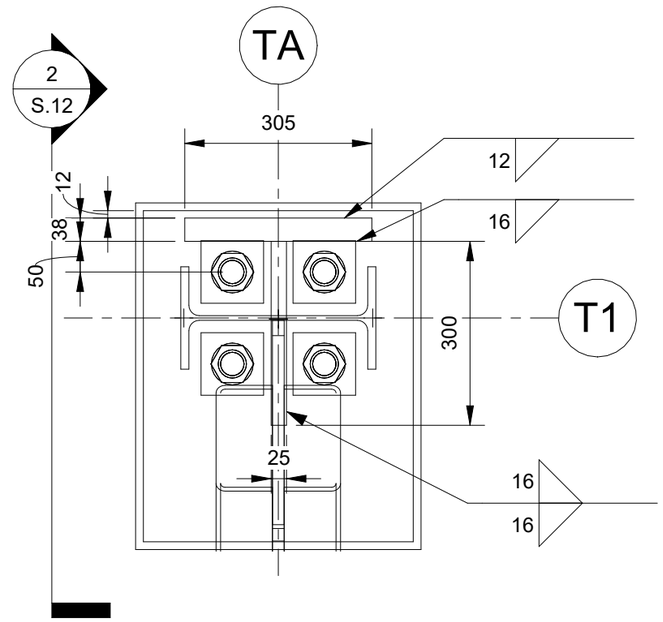

1 F1-F5 SHEAR LUG - PLAN VIEW
1 : 10

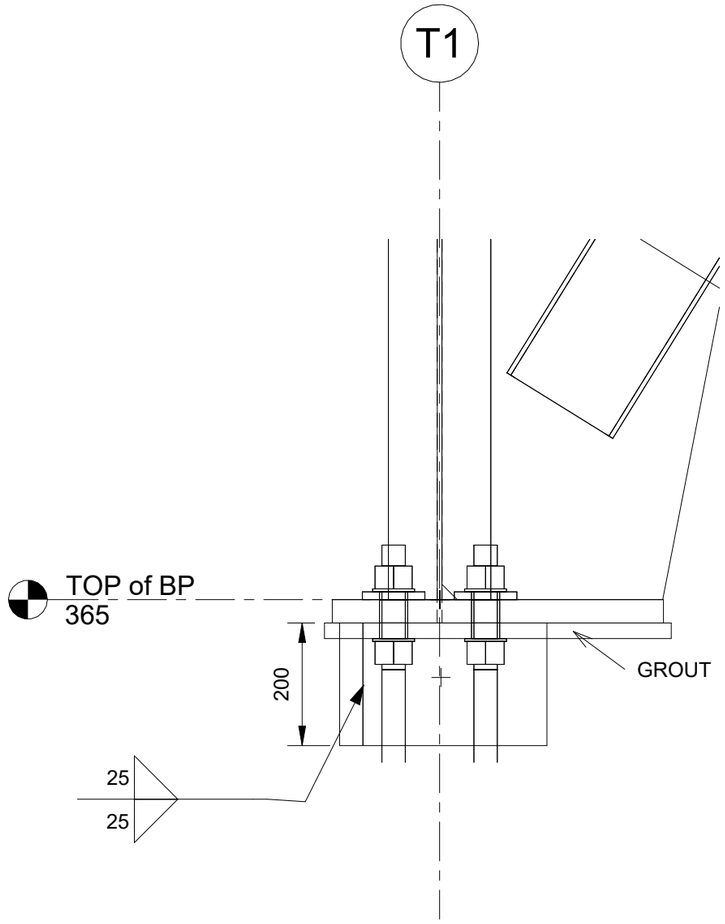

2 F1-F5 SHEAR LUG - SIDE VIEW
1 : 10

No.	Description	Date

UoA MT-EBFs

SPECIMEN 1

SHEAR LUG

Project number	EBF
Date	Mar 29, 2022
Drawn by	A.A.
Checked by	Checker
Scale	1 : 10

S.12

2023-03-19 11:18:54 PM

GENERAL NOTES:

1. ALL DIMENSIONS ARE IN MILLIMETERS UNLESS NOTED OTHERWISE (UNO)
2. FOR ANY CLARIFICATION, CONTACT ABOLFAZL ASHRAFI AT ASHRAFI@UALBERTA.CA OR (780) 566 - 8038
3. PROVIDE A COPY OF MILL TEST REPORT FOR ALL STRUCTURAL STEEL
4. ALL DRAWING TO BE PLOTTED ON A3 PAPER

SCOPE:

1. THREE EXPERIMETAL FRAMES USED TO EXAMINE MULTI-TIERED SPECIAL ECCENTRICALLY BRACED FRAMES (MT-EBFs)
2. ONE LOADING FRAME AND A SET OF CONCRETE FOOTINGS

MATERIALS:

1. COLUMNS: ASTM A992 Fy=345 MPa
2. BEAMS: ASTM A992 Fy= 345 MPa, Fymax=480 MPa
3. BRACES: ASTM A1085 Fy= 345 MPa
4. CONNECTIONS: ASTM A572 Fy=350 MPa
5. ANCHOR RODS: ASTM A193 B7
6. BOLT: ASTM A325 UNO UNLESS NOTED OTHERWISE
7. COLUMNS, BEAMS, AND BRACES SHALL BE MANUFACTURED FROM THE SAME HEAT

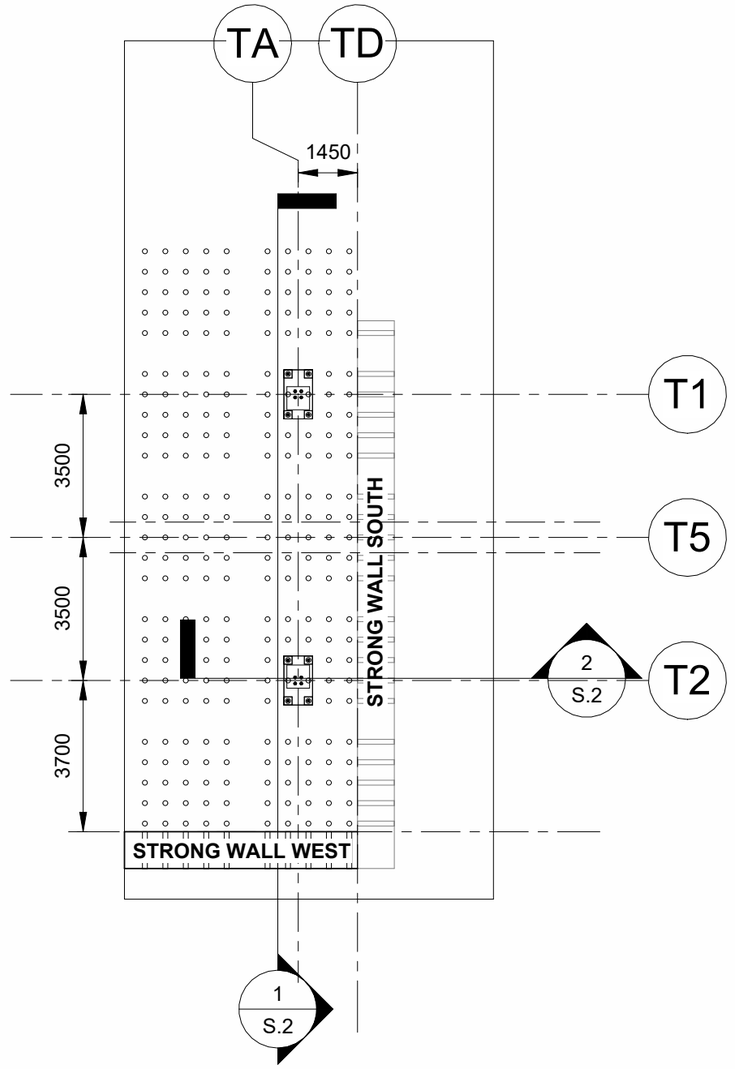

1 TOF
1 : 150

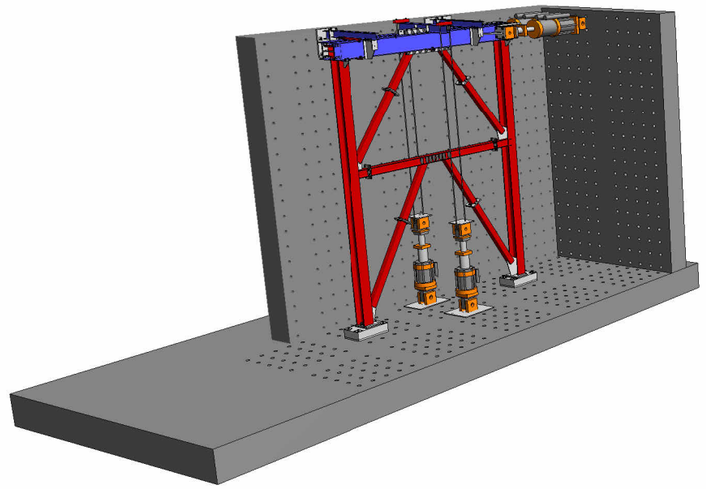

2 3D View 1

No.	Description	Date

UoA MT-EBFs

SPECIMEN 2

GENERAL

Project number	EBF
Date	Mar 29, 2022
Drawn by	A.A.
Checked by	XX
Scale	1 : 150

S.1

2023-03-19 11:20:13 PM

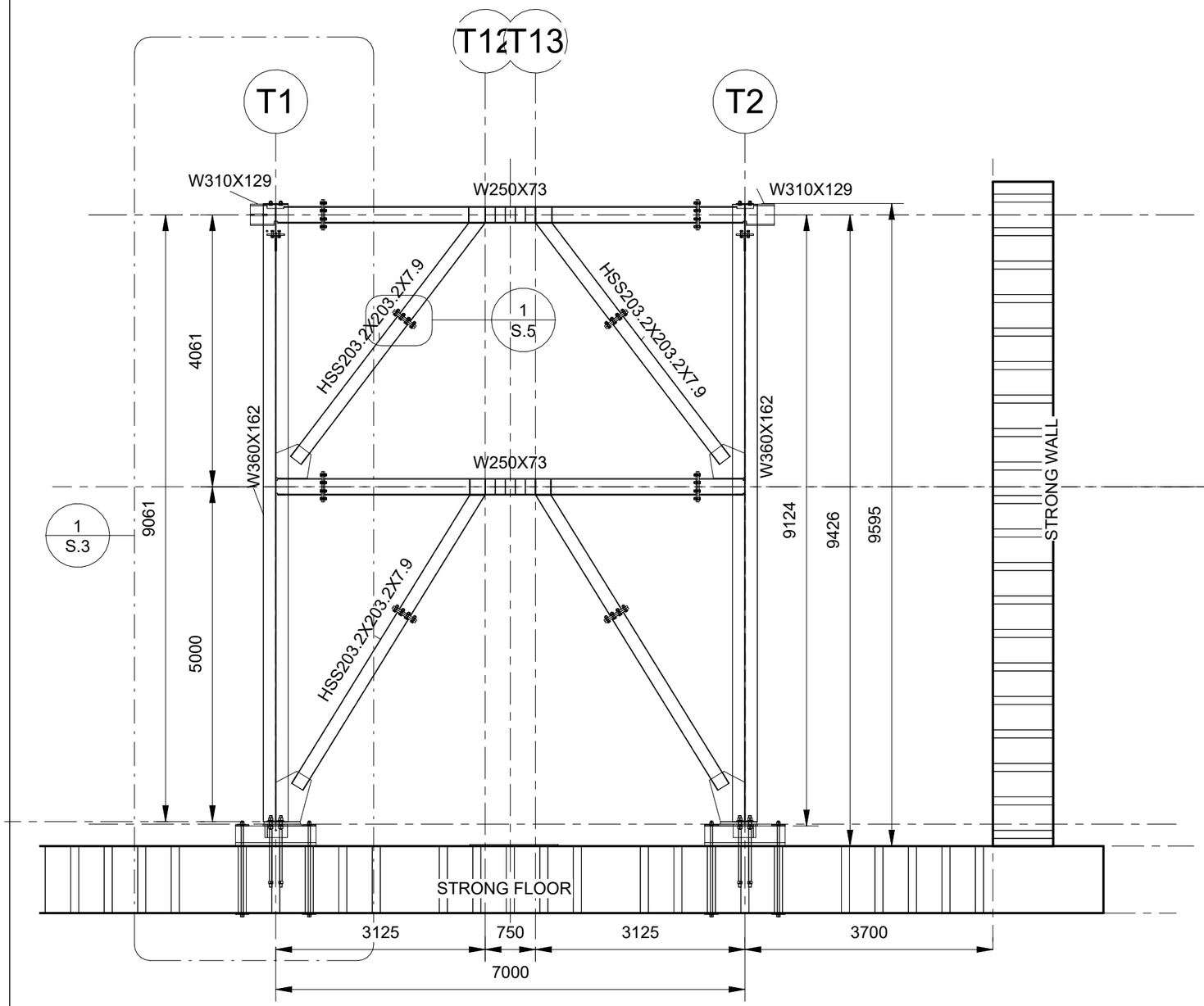

1 FRONT ELEVATION
1 : 75

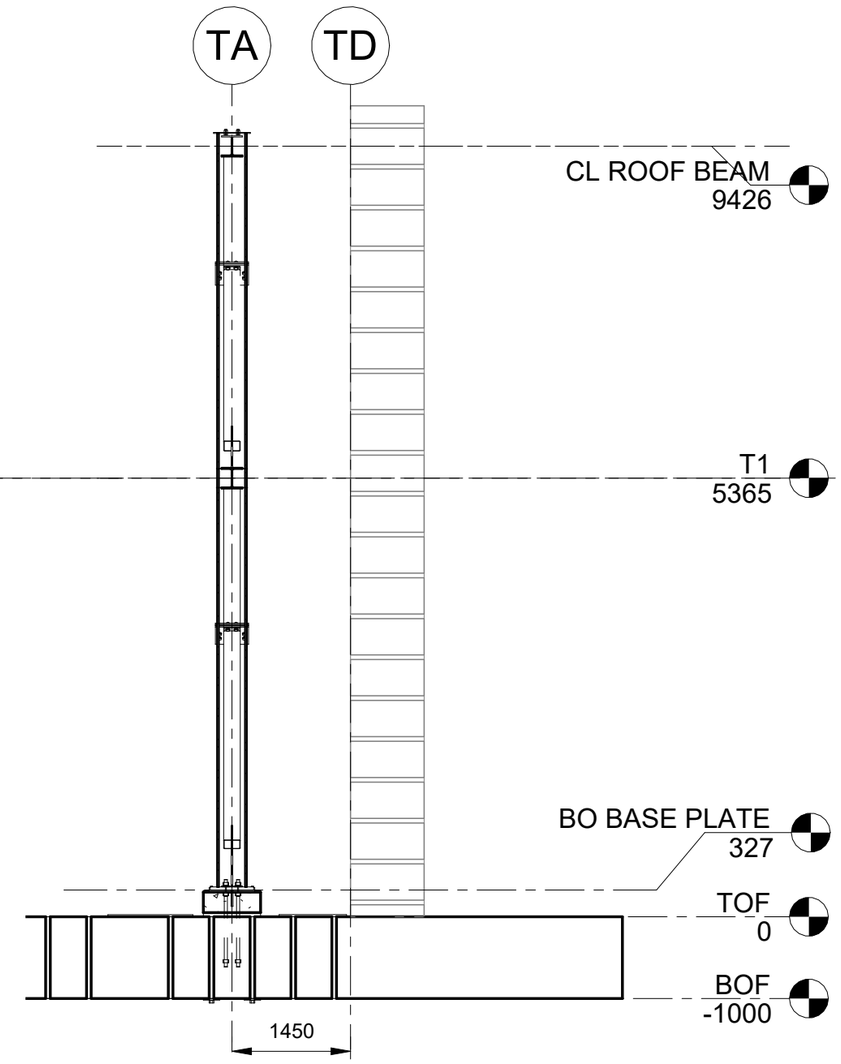

2 SIDE ELEVATION
1 : 75

No.	Description	Date

UoA MT-EBFs

SPECIMEN 2

ELEVATIONS

Project number	EBF
Date	Mar 29, 2022
Drawn by	A.A.
Checked by	Checker
Scale	1 : 75

S.2

2023-03-19 11:20:14 PM

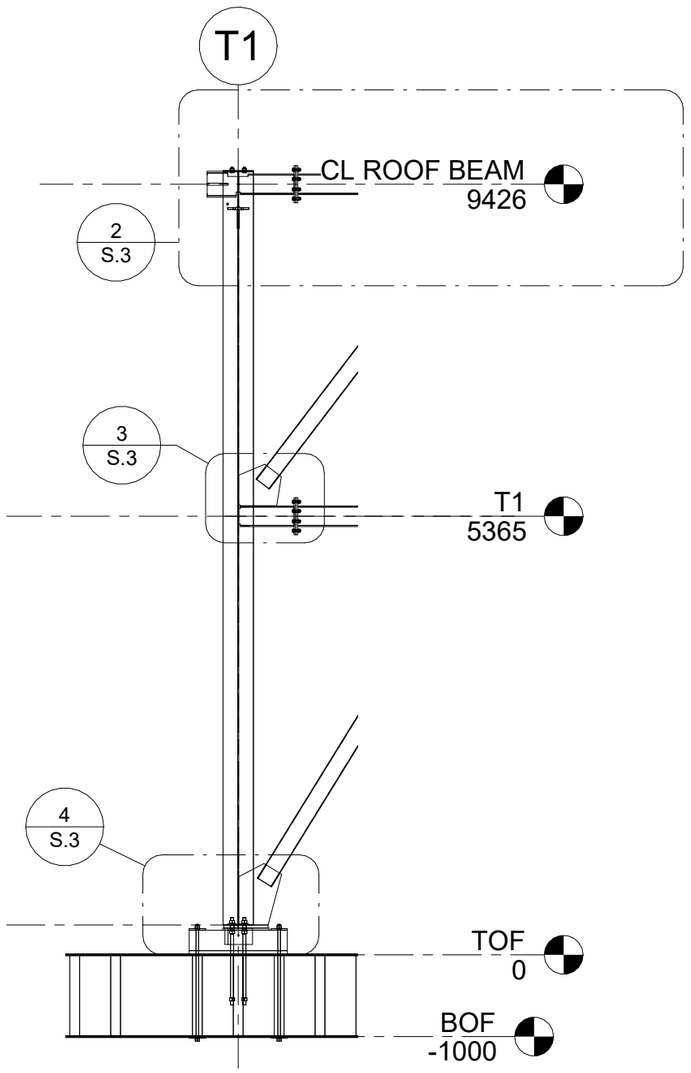

1 FRONT ELEVATION - COLUMN
1 : 75

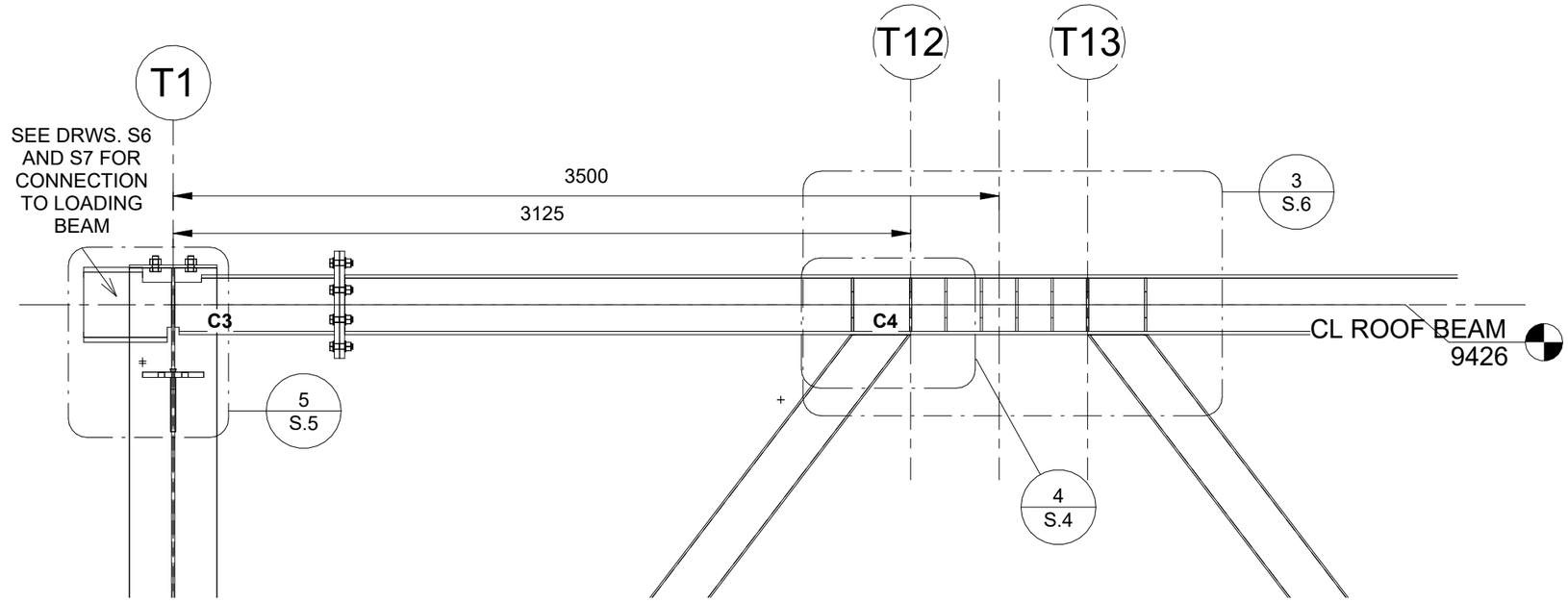

2 FRONT ELEVATION - TOP COLUMN
1 : 25

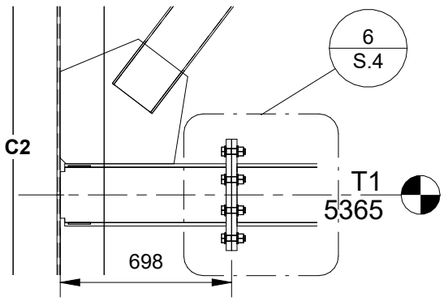

3 FRONT ELEVATION - MIDDLE COLUMN
1 : 25

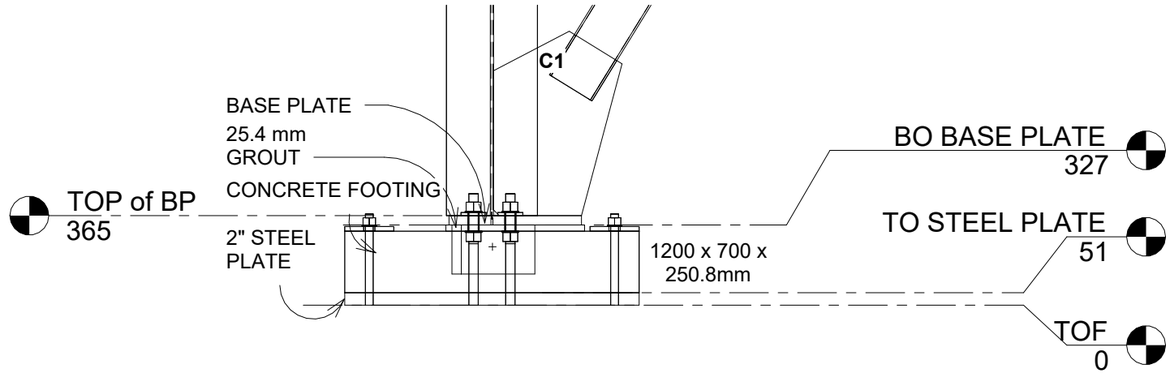

4 FRONT ELEVATION - BOTTOM COLUMN
1 : 25

No.	Description	Date

UoA MT-EBFs

SPECIMEN 2

FRONT ELEVATION DETAILS

Project number	EBF
Date	Mar 29, 2022
Drawn by	A.A.
Checked by	Checker
Scale	As indicated

S.3

2023-03-19 11:20:15 PM

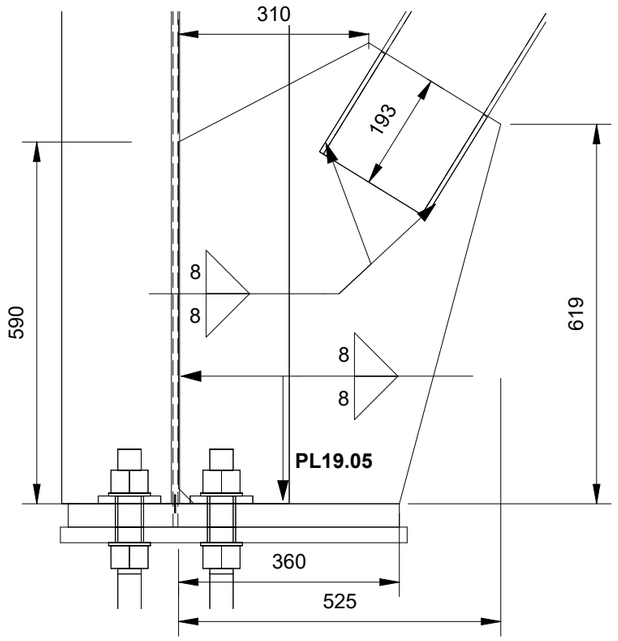

1 CONNECTION DETAIL C1
1 : 10

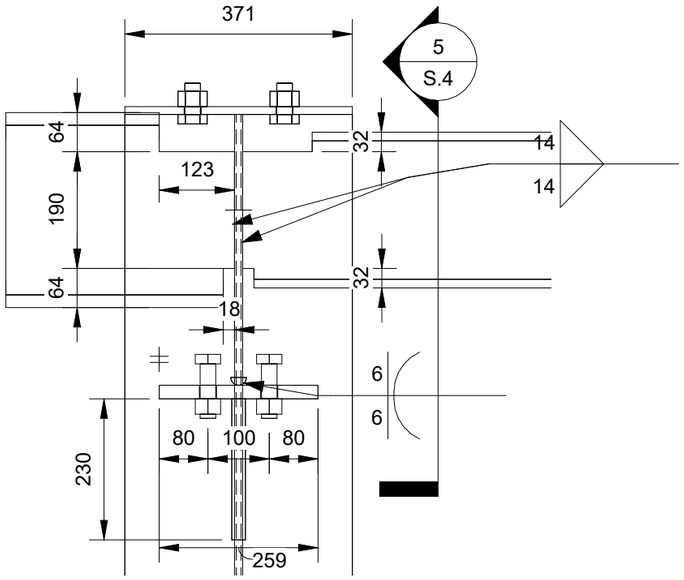

3 CONNECTION DETAIL C3
1 : 10

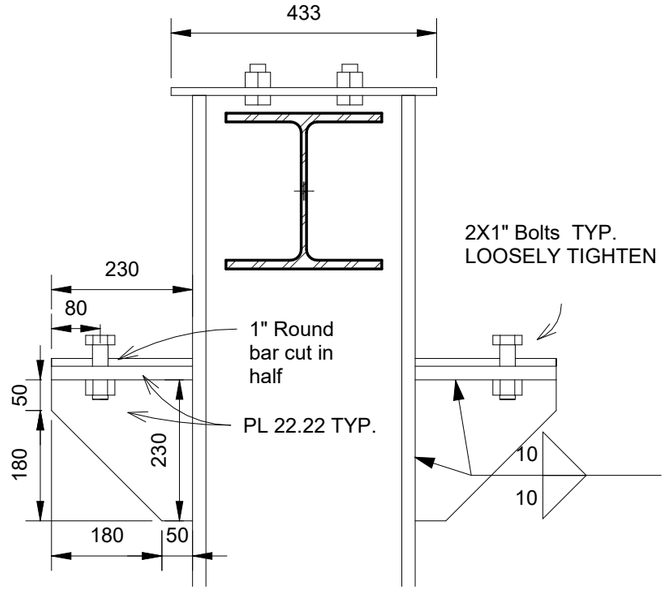

5 CONNECTION DETIAL C3-SIDE VIEW
1 : 10

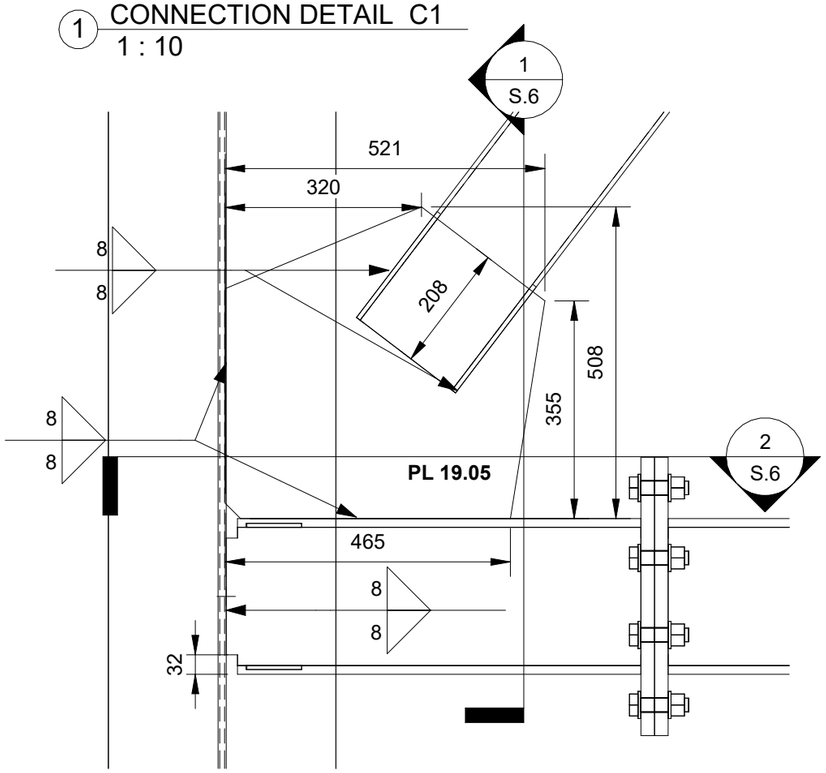

2 CONNECTION DETAIL C2
1 : 10

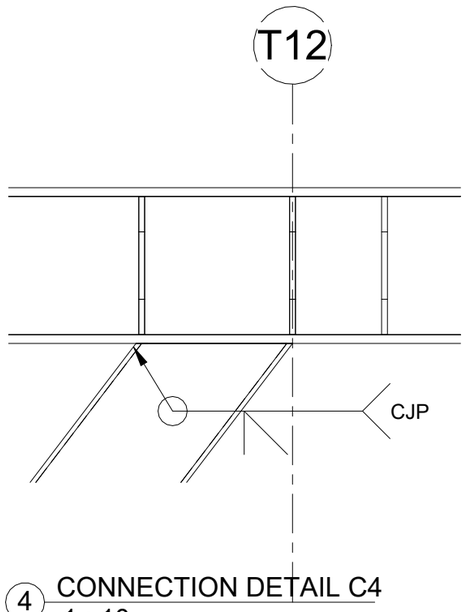

4 CONNECTION DETAIL C4
1 : 10

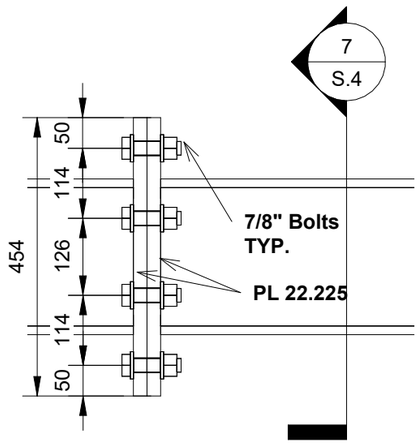

6 BEAM SPLICE TYP.
1 : 10

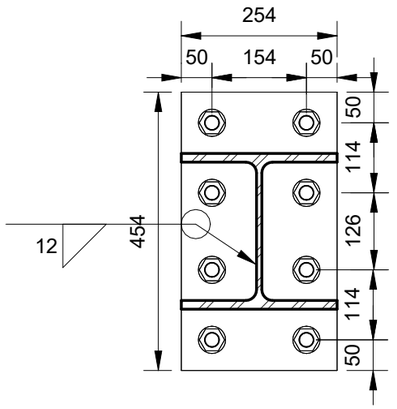

7 BEAM SPLICE TYP. SIDE VIEW
1 : 10

No.	Description	Date

UoA MT-EBFs

SPECIMEN 2

CONNECTION DETAILS

Project number	EBF
Date	Mar 29, 2022
Drawn by	A.A.
Checked by	Checker
Scale	1 : 10

S.4

2023-03-19 11:20:15 PM

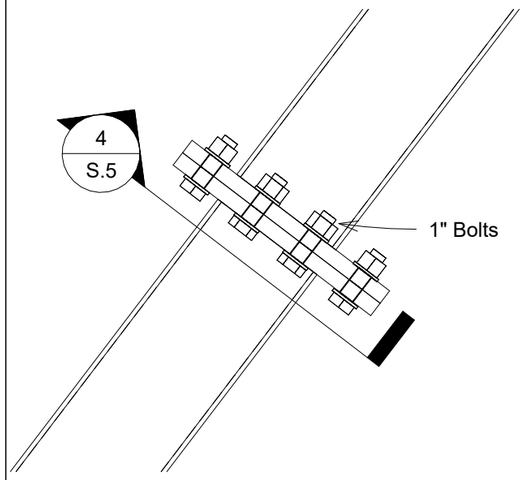

1 BRACE SPLICE-TYP.
1 : 10

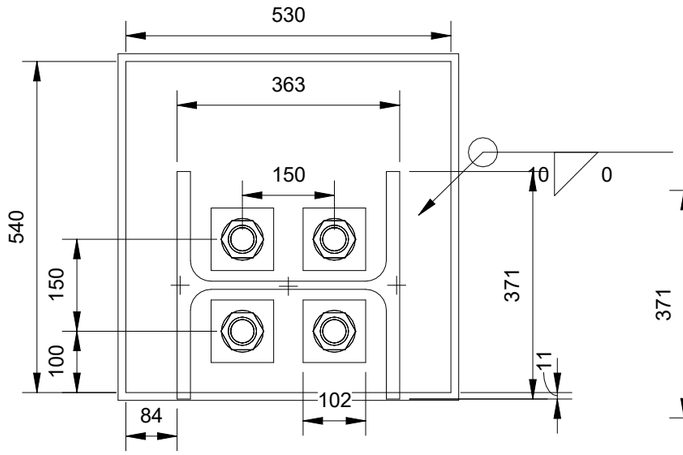

2 BASE PLATE DETAIL
1 : 10

BASE PLATE: 38.1mm THICK
GROUT: 25.4 mm THICK UNDERNEATH
ANCHOR WASHERS: 2.7mm THICK
ANCHORS: 1-1/2" DIAMETER
ANCHORS: 400mm LONG
BASEPLATE AND WASHER HOLE DIAMETER: MIN. 65mm
SHEAR LUG ATTACHED BENEATH BASEPLATE (SEE DRW. S13)

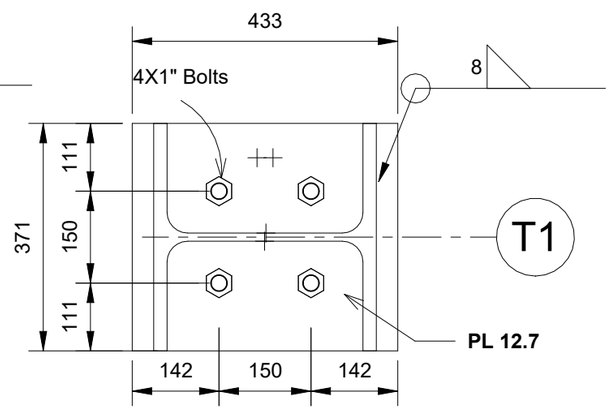

3 ENDPLATE AT COLM. TOP - PLAN VIEW
1 : 10

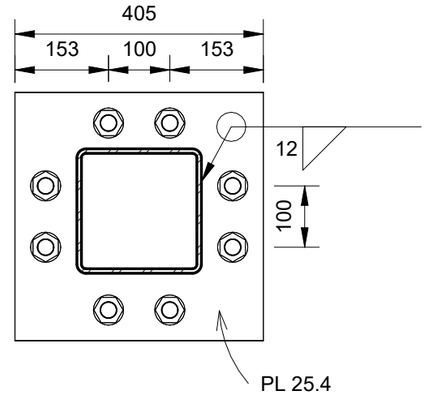

4 BRACE SPLICE TYP.-SIDE VIEW
1 : 10

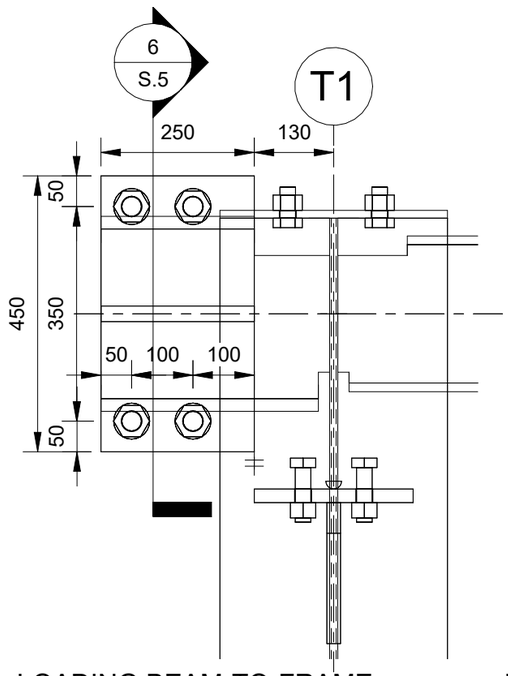

5 LOADING BEAM-TO-FRAME CONNECTION
1 : 10

6 LOADING BEAM-TO-FRAME CONNECTION-SIDE VIEW
1 : 10

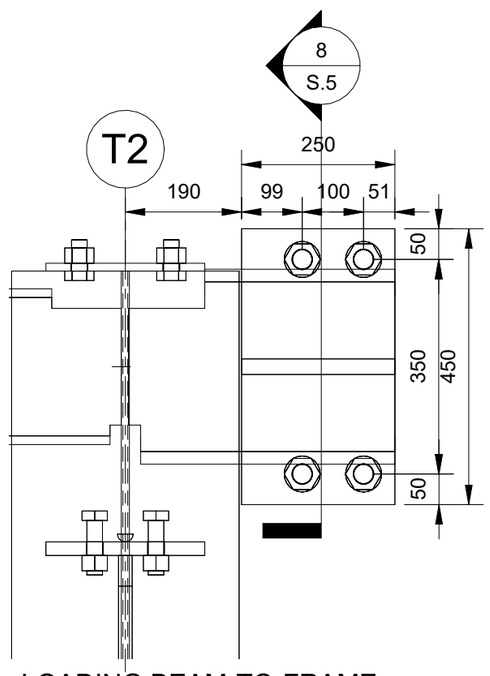

7 LOADING BEAM-TO-FRAME CONNECTION-ACTUATOR SIDE
1 : 10

8 LOADING BEAM-TO-FRAME CONNECTION-ACTUATOR SIDE-SIDE VIEW
1 : 10

No.	Description	Date

UoA MT-EBFs

SPECIMEN 2

CONNECTION DETAILS

Project number	EBF
Date	Mar 29, 2022
Drawn by	A.A.
Checked by	Checker
Scale	1 : 10

S.5

2023-03-19 11:20:15 PM

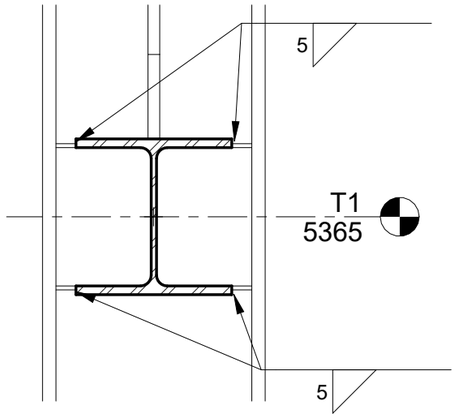

1 BEAM-TO-COLUMN CONNECTION SIDE PLATES
1 : 10

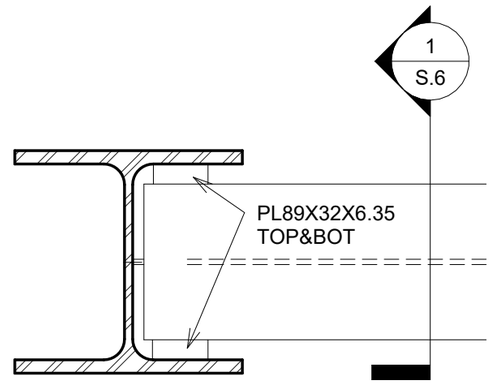

2 BEAM-TO-COLUMN CONNECTION SIDE PLATES-TOP VIEW
1 : 10

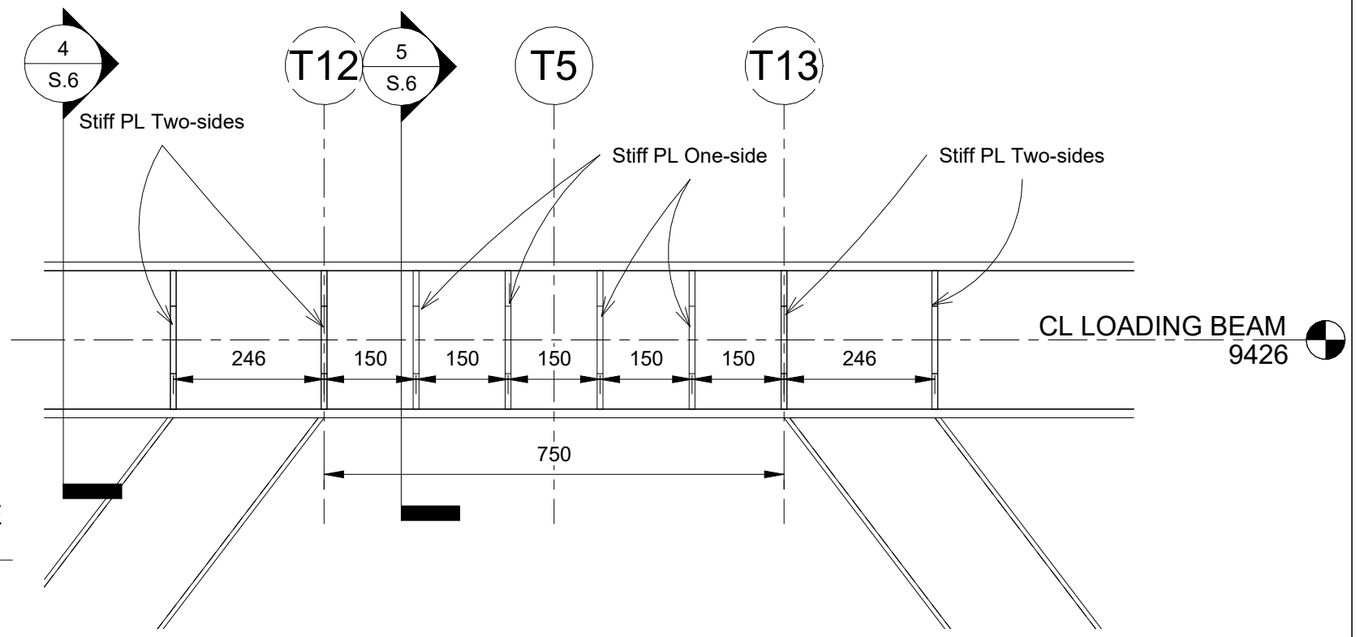

3 LINK STIFFENER-ROOF
1 : 10

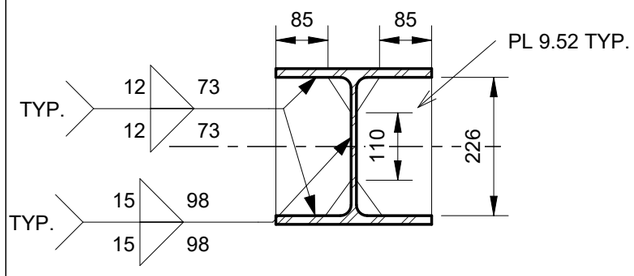

4 LINK STIFFENER SECTION-LINK ENDS
1 : 10

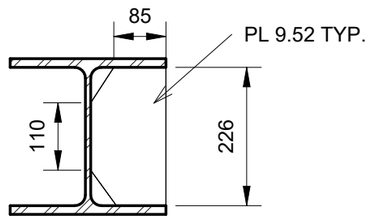

5 LINK STIFFENER SECTION-INTERMEDIATE
1 : 10

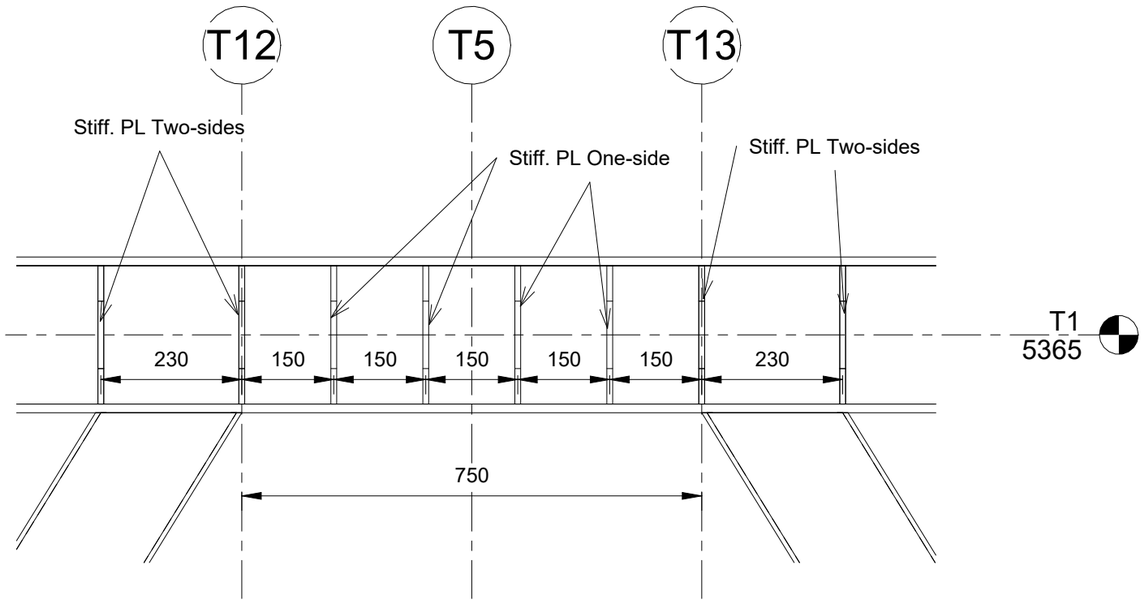

6 LINK STIFFENER-TIER1
1 : 10

No.	Description	Date

UoA MT-EBFs

SPECIMEN 2

CONNECTION-LINK STIFFENER

Project number	EBF
Date	Mar 29, 2022
Drawn by	Author
Checked by	Checker
Scale	1 : 10

S.6

2023-03-19 11:20:16 PM

GENERAL NOTES:

1. ALL DIMENSIONS ARE IN MILLIMETERS UNLESS NOTED OTHERWISE (UNO)
2. FOR ANY CLARIFICATION, CONTACT ABOLFAZL ASHRAFI AT ASHRAFI@UALBERTA.CA OR (780) 566 - 8038
3. PROVIDE A COPY OF MILL TEST REPORT FOR ALL STRUCTURAL STEEL
4. ALL DRAWING TO BE PLOTTED ON A3 PAPER

SCOPE:

1. THREE EXPERIMETAL FRAMES USED TO EXAMINE MULTI-TIERED SPECIAL ECCENTRICALLY BRACED FRAMES (MT-EBFs)
2. ONE LOADING FRAME AND A SET OF CONCRETE FOOTINGS

MATERIALS:

1. COLUMNS: ASTM A992 Fy=345 MPa
2. BRACES: ASTM A1085 Fy= 345 MPa
3. CONNECTIONS: ASTM A572 Fy=350 MPa
4. ANCHOR RODS: ASTM A193 B7
5. BOLT: ASTM A325 UNO UNLESS NOTED OTHERWISE
6. COLUMNS, BEAMS, AND BRACES SHALL BE MANUFACTURED FROM THE SAME HEAT

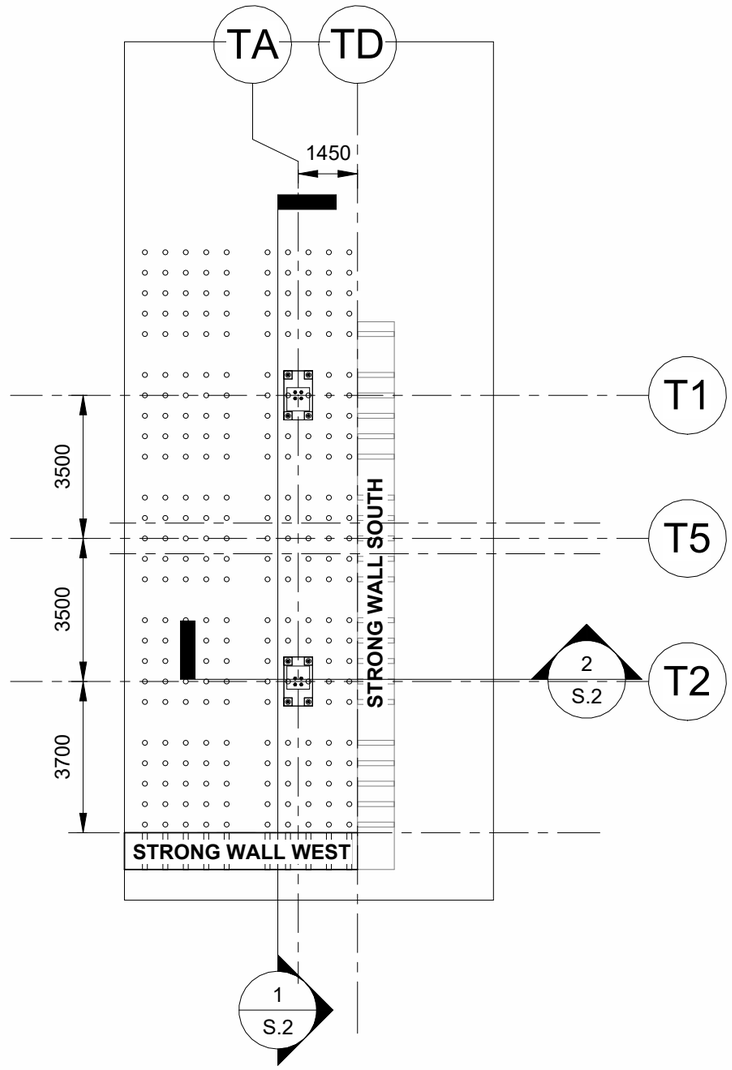

1 TOF
1 : 150

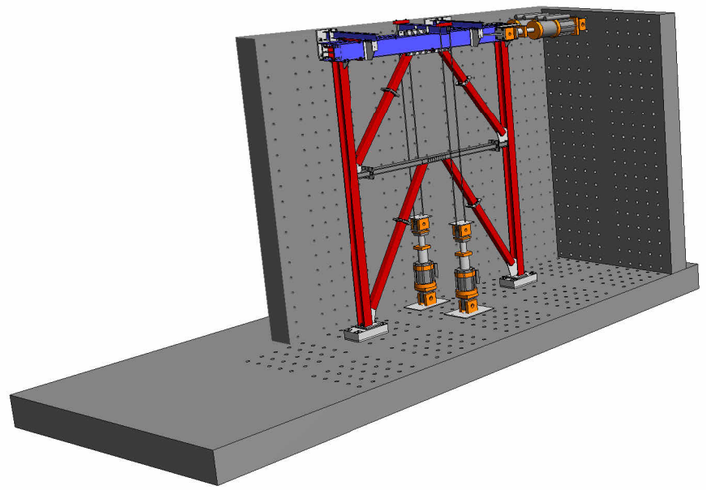

2 3D View 1

No.	Description	Date

UoA MT-EBFs

SPECIMEN 3

GENERAL

Project number	EBF
Date	Mar 29, 2022
Drawn by	A.A.
Checked by	XX
Scale	1 : 150

S.1

2023-03-19 11:16:42 PM

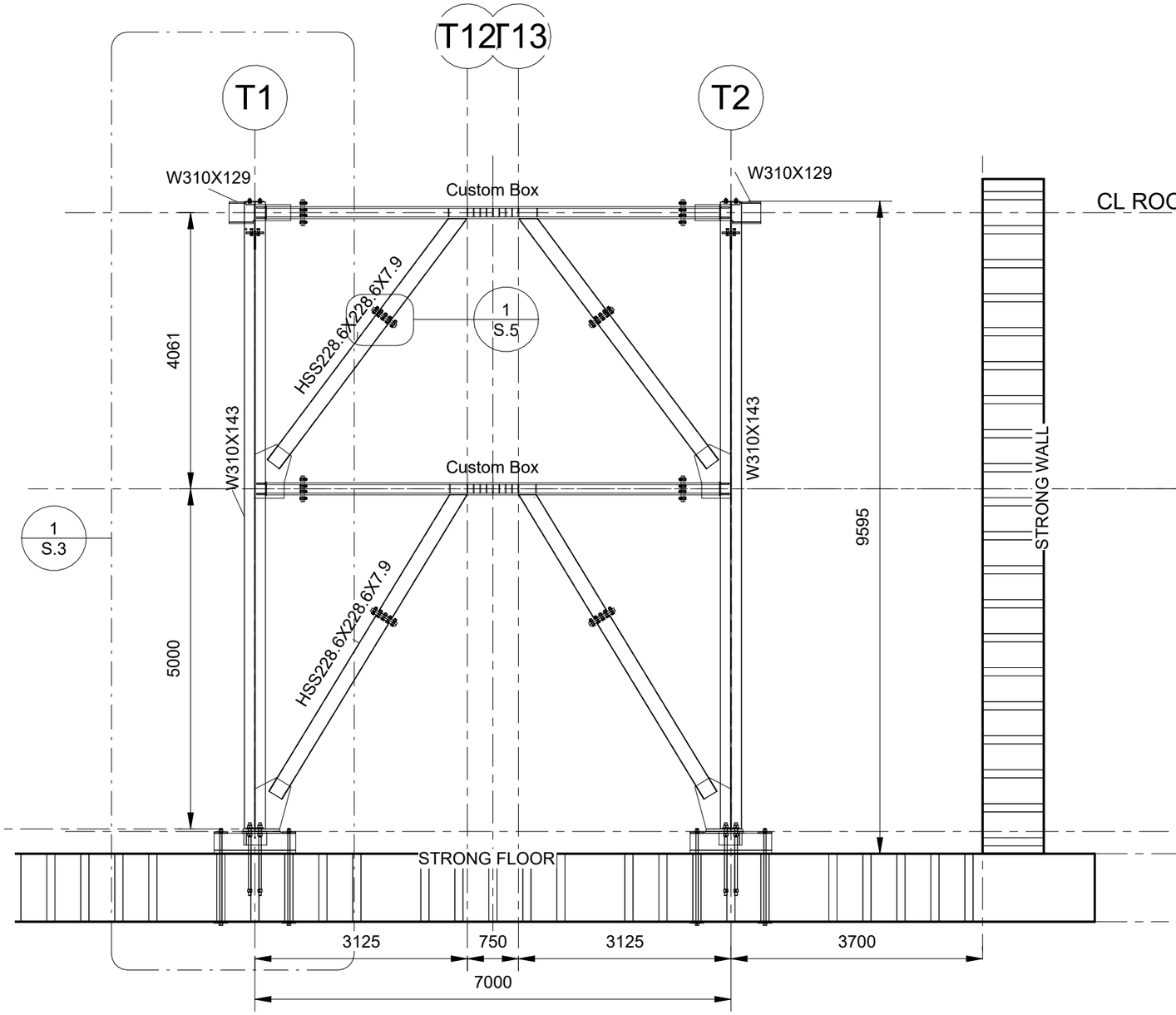

1 FRONT ELEVATION
1 : 75

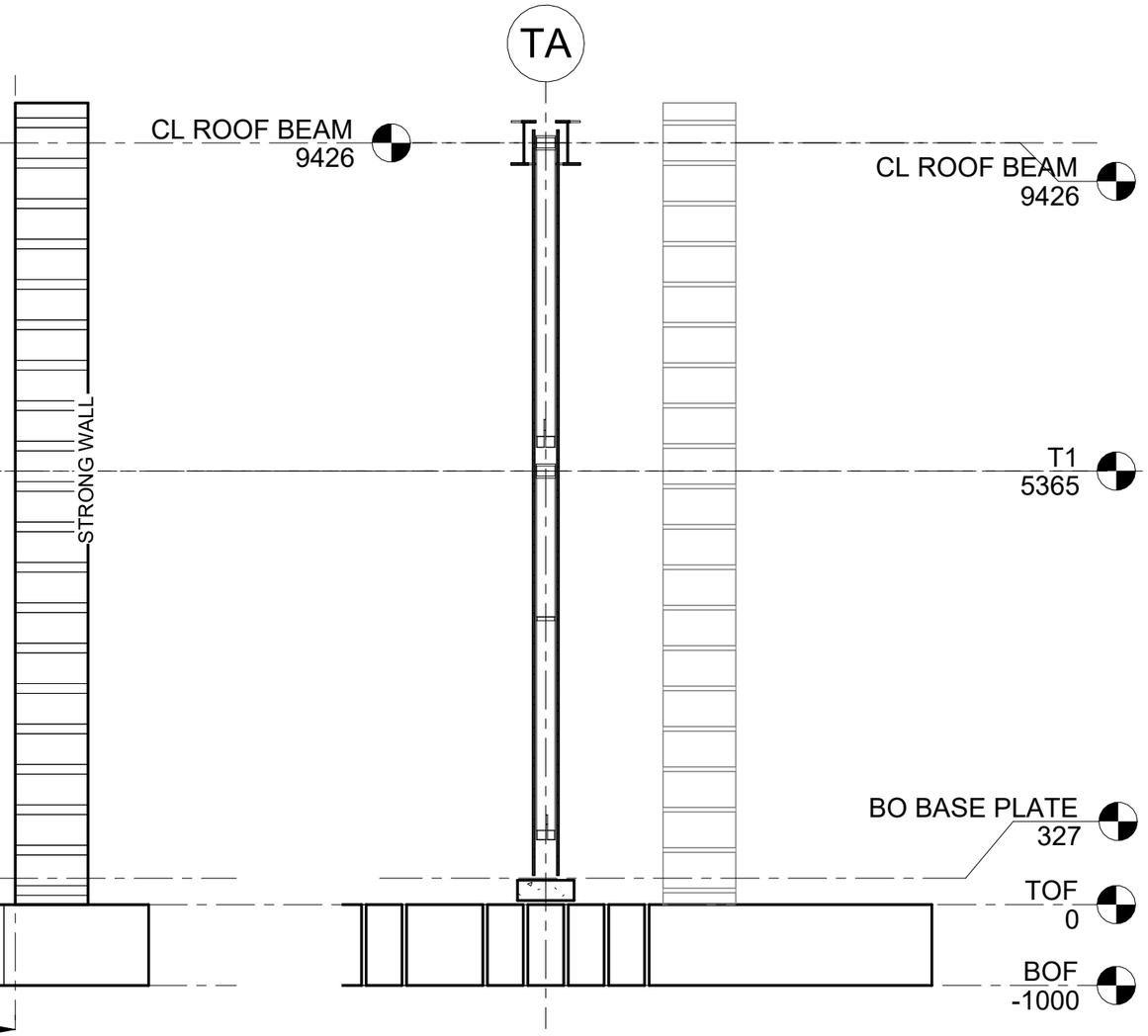

2 SIDE ELEVATION
1 : 75

No.	Description	Date

UoA MT-EBFs

SPECIMEN 3

ELEVATIONS

Project number	EBF
Date	Mar 29, 2022
Drawn by	A.A.
Checked by	Checker
Scale	1 : 75

S.2

2023-03-19 11:16:43 PM

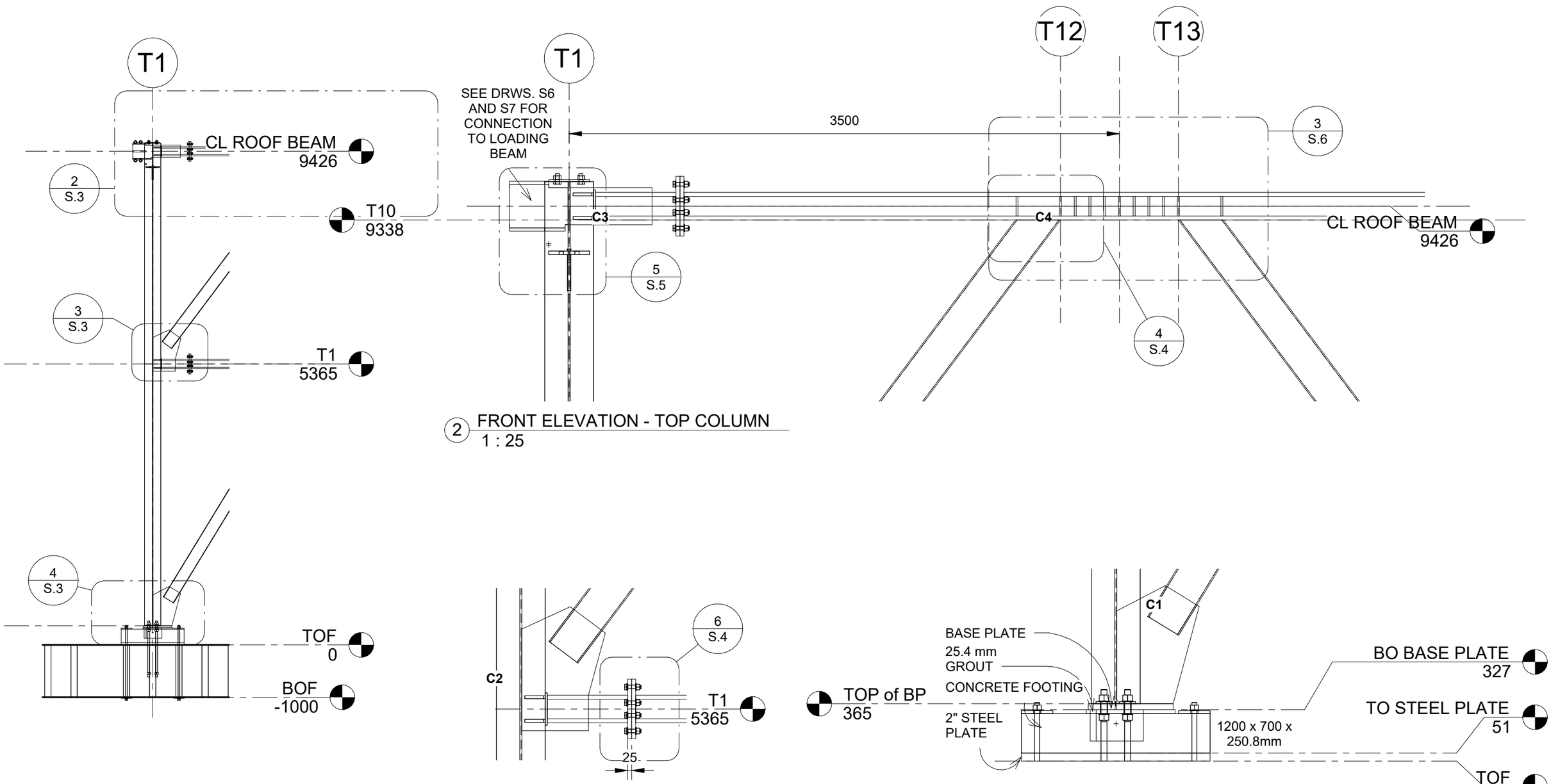

2 FRONT ELEVATION - TOP COLUMN
1 : 25

1 FRONT ELEVATION - COLUMN
1 : 75

3 FRONT ELEVATION - MIDDLE COLUMN
1 : 25

4 FRONT ELEVATION - BOTTOM COLUMN
1 : 25

No.	Description	Date

UoA MT-EBFs

SPECIMEN 3

FRONT ELEVATION DETAILS

Project number	EBF
Date	Mar 29, 2022
Drawn by	A.A.
Checked by	Checker

S.3

Scale: As indicated

2023-03-19 11:16:43 PM

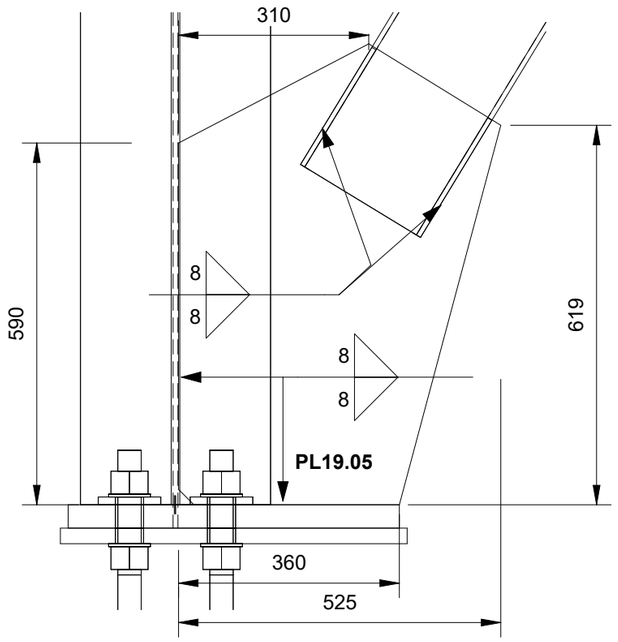

1 CONNECTION DETAIL C1
1 : 10

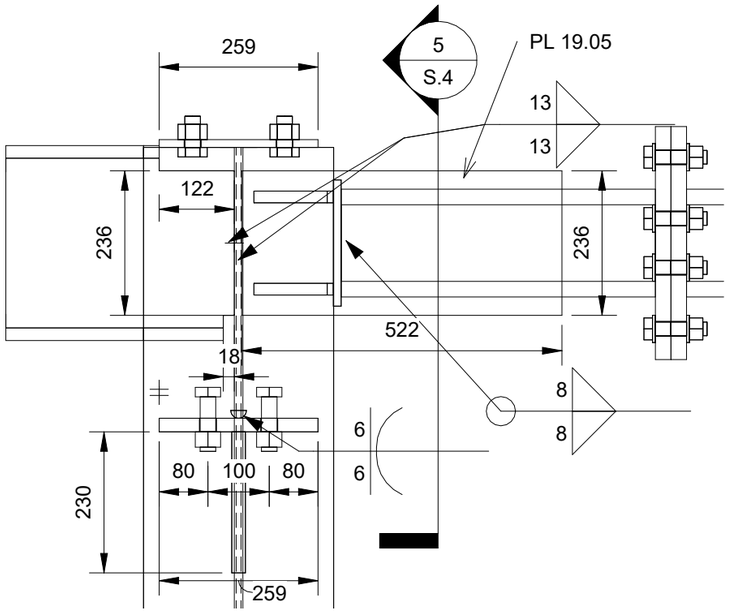

3 CONNECTION DETAIL C3
1 : 10

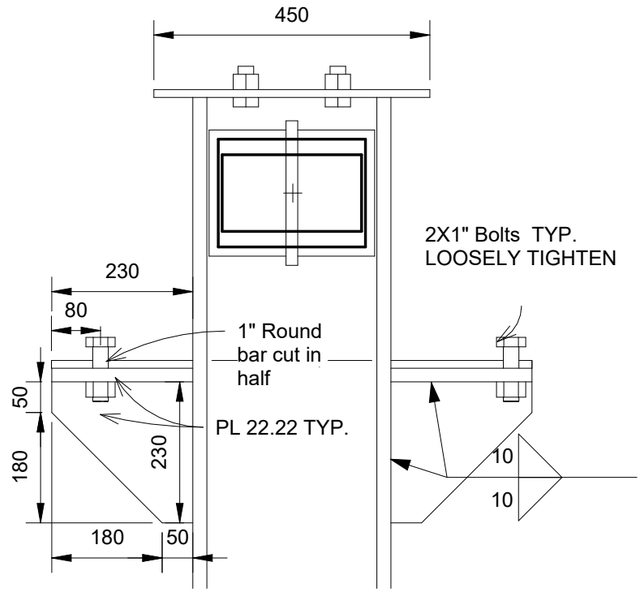

5 CONNECTION DETIAL C3-SIDE VIEW
1 : 10

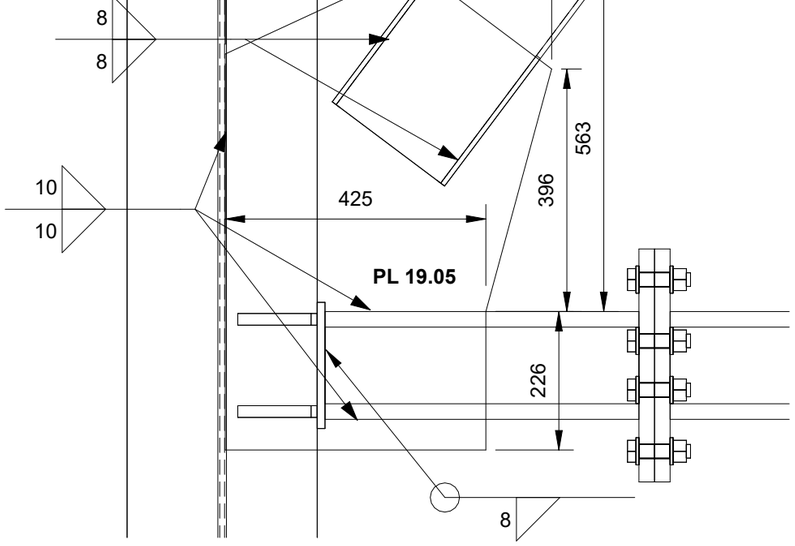

2 CONNECTION DETAIL C2
1 : 10

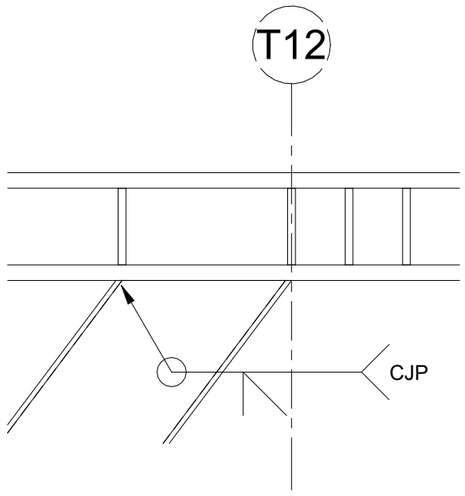

4 CONNECTION DETAIL C4
1 : 10

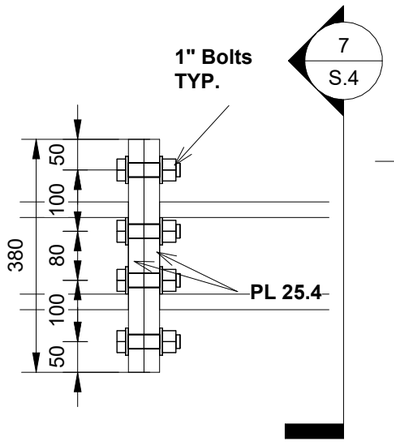

6 BEAM SPLICE TYP.
1 : 10

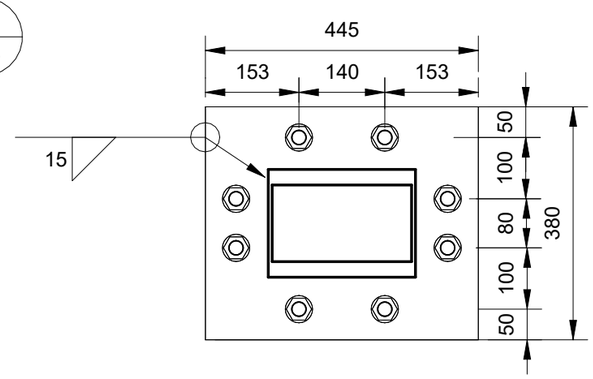

7 BEAM SPLICE TYP. SIDE VIEW
1 : 10

No.	Description	Date

UoA MT-EBFs

SPECIMEN 3

CONNECTION DETAILS

Project number	EBF
Date	Mar 29, 2022
Drawn by	A.A.
Checked by	Checker
Scale	1 : 10

S.4

2023-03-19 11:16:43 PM

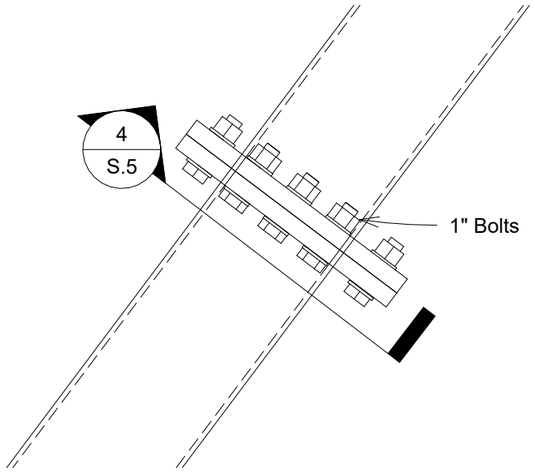

1 BRACE SPLICE-TYP.
1 : 10

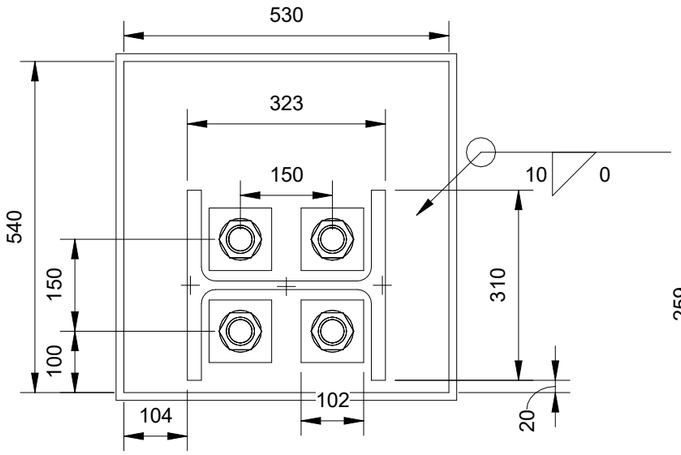

2 BASE PLATE DETAIL
1 : 10

BASE PLATE: 38.1mm THICK
GROUT: 25.4 mm THICK UNDERNEATH
ANCHOR WASHERS: 2.7mm THICK
ANCHORS: 1-1/2" DIAMETER
ANCHORS: 400mm LONG
BASEPLATE AND WASHER HOLE DIAMETER: MIN. 65mm
SHEAR LUG ATTACHED BENEATH BASEPLATE (SEE DRW. S13)

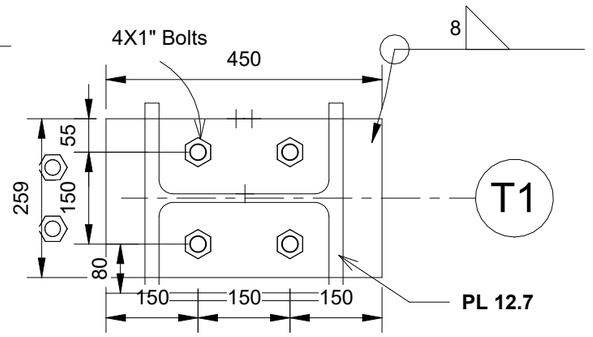

3 ENDPLATE AT COLM. TOP - PLAN VIEW
1 : 10

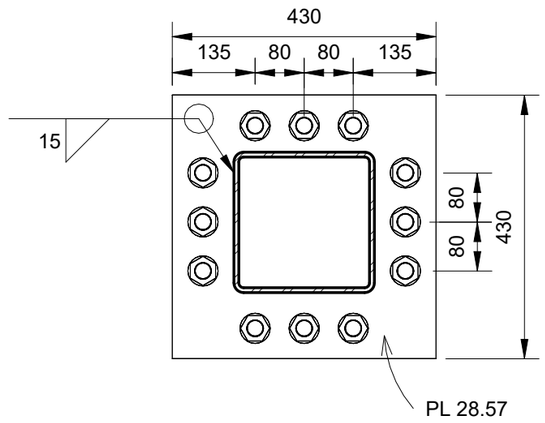

4 BRACE SPLICE TYP.-SIDE VIEW
1 : 10

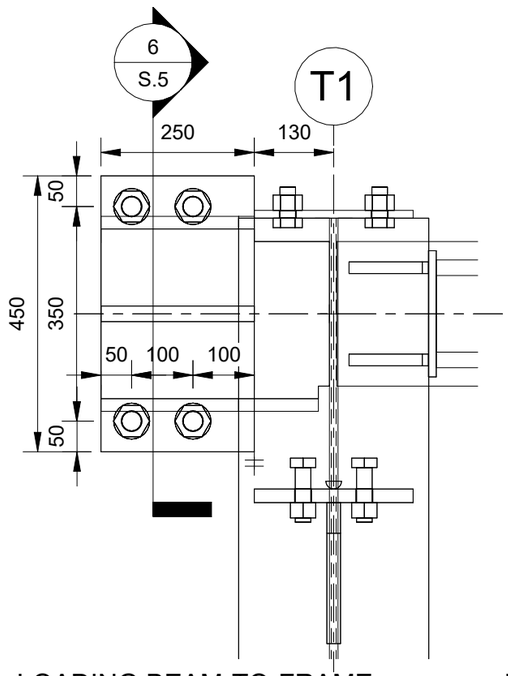

5 LOADING BEAM-TO-FRAME CONNECTION
1 : 10

6 LOADING BEAM-TO-FRAME CONNECTION-SIDE VIEW
1 : 10

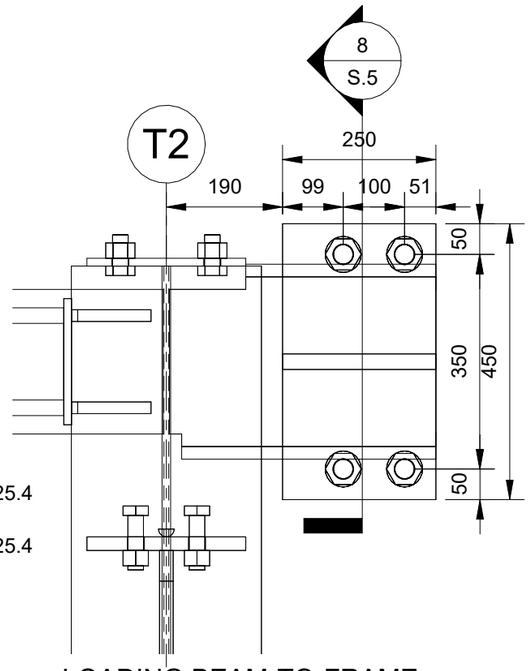

7 LOADING BEAM-TO-FRAME CONNECTION-ACTUATOR SIDE
1 : 10

8 LOADING BEAM-TO-FRAME CONNECTION-ACTUATOR SIDE-SIDE VIEW
1 : 10

No.	Description	Date

UoA MT-EBFs

SPECIMEN 3

CONNECTION DETAILS

Project number	EBF
Date	Mar 29, 2022
Drawn by	A.A.
Checked by	Checker
Scale	1 : 10

S.5

2023-03-19 11:16:44 PM

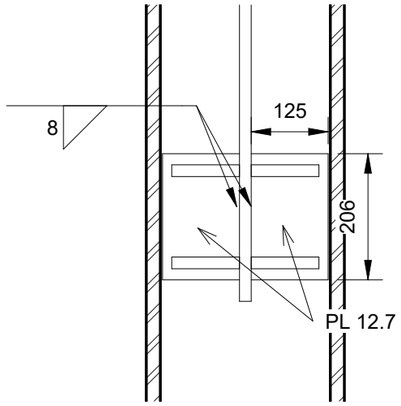

1 BEAM-TO-COLUMN CONNECTION CAP PLATE
1 : 10

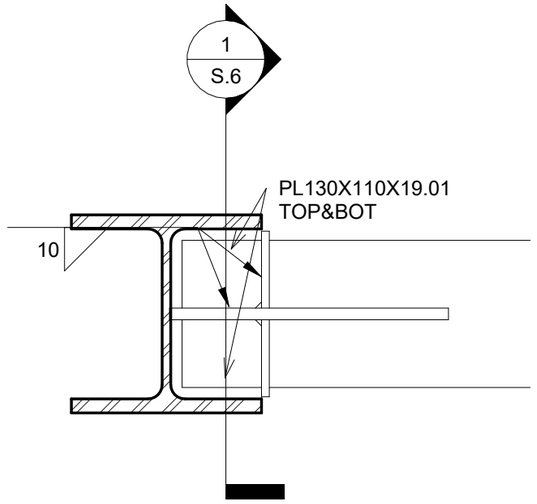

2 BEAM-TO-COLUMN CONNECTION SIDE PLATES-TOP VIEW
1 : 10

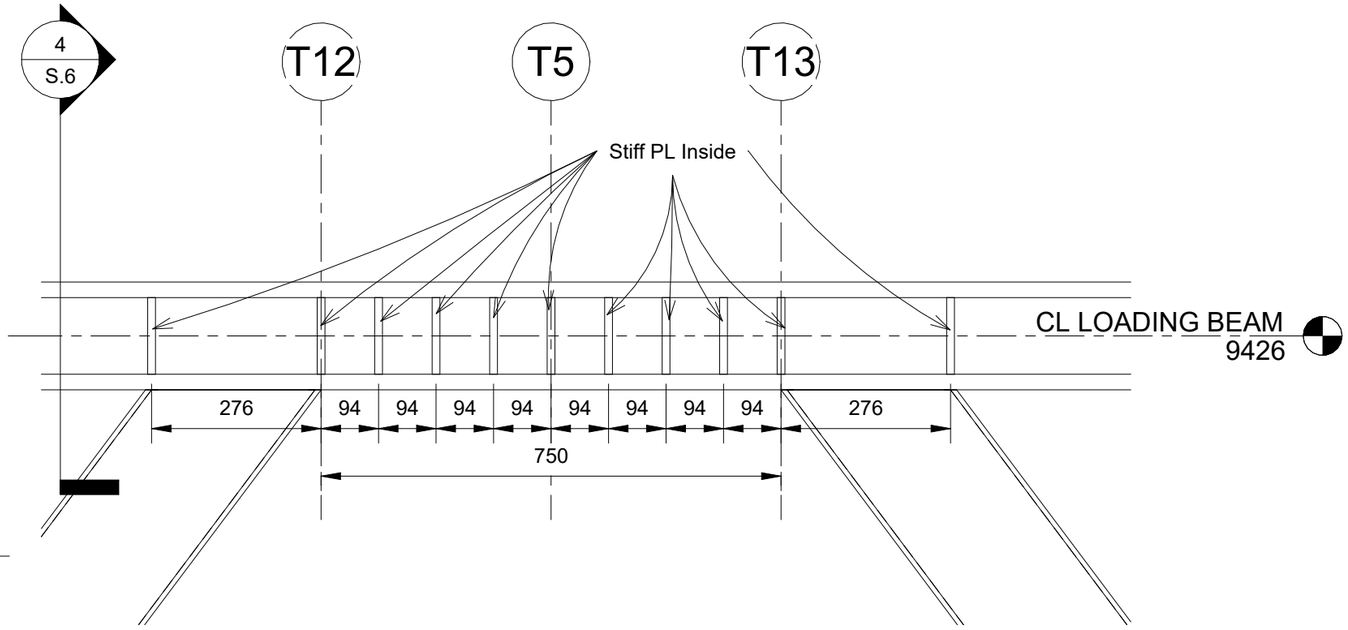

3 LINK STIFFENER-ROOF
1 : 10

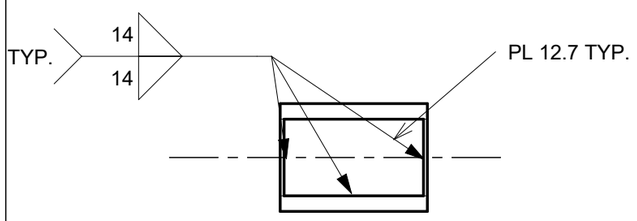

4 LINK STIFFENER SECTION
1 : 10

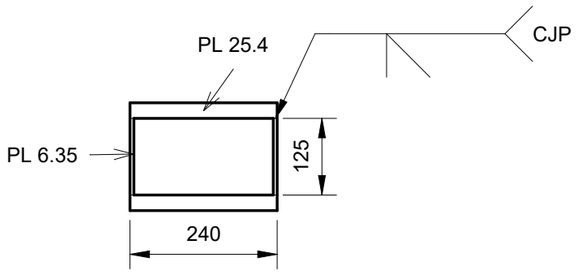

5 CUSTOMIZE BOX
1 : 10

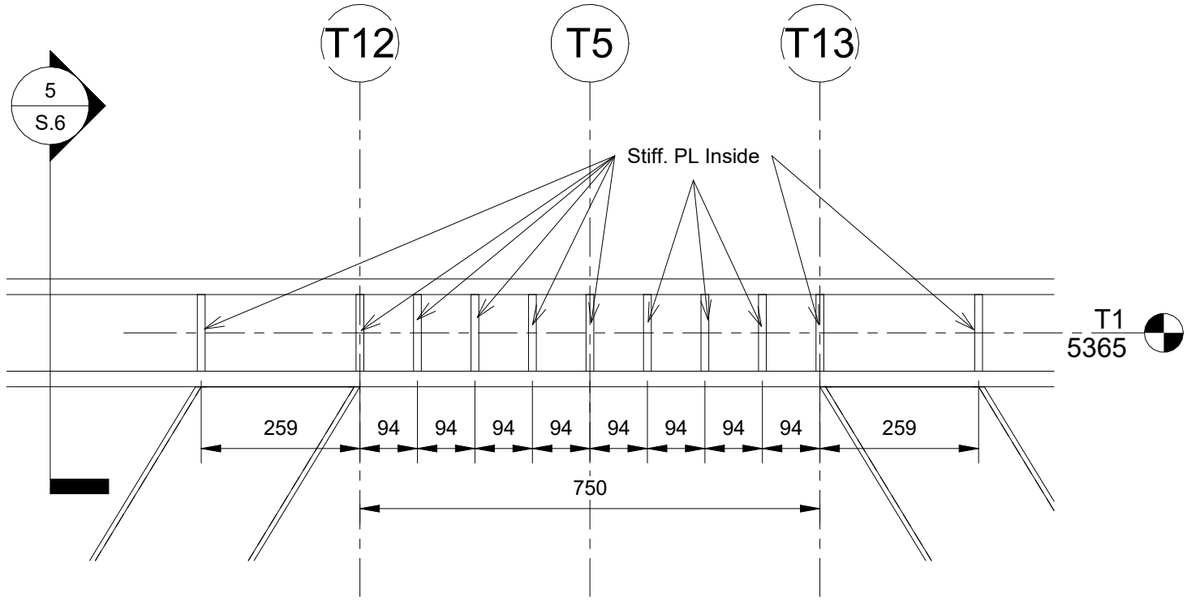

6 LINK STIFFENER-TIER1
1 : 10

No.	Description	Date

UoA MT-EBFs

SPECIMEN 3

CONNECTION-LINK STIFFENER

Project number	EBF
Date	Mar 29, 2022
Drawn by	Author
Checked by	Checker
Scale	1 : 10

S.6

2023-03-19 11:16:44 PM